

**Porous polymer derived ceramic membranes for bioelectricity
generation and wastewater treatment**

Dem Fachbereich Produktionstechnik
der
UNIVERSITÄT BREMEN

zur Erlangung des Grades
Doktor-Ingenieur
genehmigte

Dissertation
von
M.Sc. Vignesh Ahilan

Gutachter:

Prof. Dr.-Ing. Kurosch Rezwan, Prof. Dr. Fabio La Mantia

Tag der mündlichen Prüfung: 26.02.2020

Acknowledgment

I would like to express my sincere gratitude to Prof. Dr.-Ing. Kurosch for giving me the great opportunity to work in Advanced Ceramics laboratory and for his scientific support during the last 3.5 years. I would like to thank Dr. rer. nat. Michaela Wilhelm for all her scientific support, advice during this time. I would like to thank Prof. Dr. Fabio La Mantia from Energy storage and conversion system laboratory to be the co-examiner of my thesis. I would like to thank all my friends and colleagues from Advanced Ceramics lab for all the help, and support which greatly motivated me to reach my research goals. I would like to thank Christian Ellenberg for their help during technical issues in the lab. I would like to thank Christian Nuortila for the engineering works, which supports my research work. I would like to thank Tina Kühn for the lab maintenance. I thank the administrative staff Gabriela Berger for the help in official documents. I would like to thank German Federal Ministry of Education and Research (BMBF) under the framework of INNO INDIGO Partnership Program for the financial support. I would like to thank German Research Foundation (DFG) within the Research Training Group GRK 1860 “Micro-, meso- and macroporous nonmetallic Materials: Fundamentals and Applications” (MIMENIMA). I would like to thank all members of MIMENIMA for their suggestions regarding my research work.

I thank Prof. Dr. Makarand M. Ghangrekar and his student Mr. Gourav Dhar Bhowmick in Indian Institute of Technology, Kharagpur for support in studying microbial fuel cell during my research abroad in India. I would like to thank all Diploma and master students contribute to this work. Their contributions are listed at the end of this work. I would like to thank Dr. Moni Prabu for his help and support during my research work. I would like to thank Thamires Canuto for the help and accompanying as a good friend during research visits and conferences. I would like to thank my family and friends for supporting me all the time during the period of this work.

Contents

Acknowledgment	iii
Zusammenfassung	vii
Abstract	ix
List of Abbreviations	xi
1 Introduction	1
2 State of the art	3
2.1 Microbial fuel cell for energy and wastewater treatment	3
2.1.1 Microbial fuel cell and its components.....	3
2.1.2 Membrane bioreactor	9
2.1.3 Integrated microbial fuel cell-membrane bioreactor (MFC-MBR).....	14
2.2 Requirement and challenges in designing membrane	16
2.2.1 Membrane resistance.....	16
2.2.2 Oxygen diffusion.....	16
2.2.3 Substrate crossover.....	17
2.2.4 Biofouling.....	17
2.3 Membrane for MFC application	19
2.3.1 Polymeric membranes for MFC.....	19
2.3.2 Ceramic membranes for MFC	21
2.3.3 Ion transport mechanism of membrane	27
2.4 Polymer derived ceramic material	30
2.4.1 Processing route.....	32
2.4.2 Polysiloxane.....	35
2.4.3 Tailorable surface characteristics.....	36

2.4.4 Control of porous structure.....	37
3 Aim and approach of the work.....	38
4 Materials and methods.....	40
4.1 Materials.....	40
4.1.1 Required Precursors.....	40
4.1.2 Filler materials.....	40
4.2. Synthesis procedure of PDC membranes.....	42
4.2.1 Polymer derived ceramer and ceramic composite with Montmorillonite and $H_3PMo_{12}O_{40}/SiO_2$	42
4.2.2 Graphitic carbon functionalized polymer derived ceramics.....	43
4.2.3 Polymer derived ceramics composite with hygroscopic filler.....	44
4.4 Characterization methods.....	45
4.4.1 X-ray diffraction.....	45
4.4.2 Scanning Electron Microscopy (SEM)	46
4.4.3 Transmission electron microscopy.....	46
4.4.4 Raman spectroscopy.....	46
4.4.5 Fourier Transform Infrared Spectroscopy (FTIR)	47
4.4.6 Nitrogen adsorption/desorption method.....	48
4.4.7 Mercury Intrusion method.....	48
4.4.8 Water and heptane adsorption.....	48
4.4.9 Acid-base titration method.....	49
4.4.10 Concentration cell test.....	49

4.4.11 Oxygen permeation cell test.....	50
4.4.12 Ring-on-ring bending test.....	51
4.5 Microbial fuel cell and Membrane bioreactor.....	51
4.5.1 Microbial fuel cell setup and operation.....	51
4.5.2 Analytical measurements.....	52
4.5.3 Ultrafiltration setup for MBR.....	53
5 Porous polymer derived ceramic (PDC)-montmorillonite H₃PMo₁₂O₄₀/SiO₂ composite membrane for microbial fuel cell application.....	55
6 Tailoring hydrophilic and porous nature of polysiloxane derived ceramer and ceramic membranes for enhanced bioelectricity generation in microbial fuel cell.....	67
7 Microbial fuel cell performance of graphitic carbon functionalized porous polysiloxane based ceramic membranes.....	82
8 Polysiloxane derived ceramic membrane composite with TiO₂ and SiO₂ filler material for Microbial fuel cell.....	101
9 Polysiloxane derived ceramic membrane for pilot scale model Integrated microbial fuel cell - membrane bioreactor.....	114
10 Conclusion.....	117
11 Outlook.....	119
References.....	121
Appendix.....	141

Zusammenfassung

Die Verschmutzung durch die Nutzung konventioneller Energiequellen stellt eine ernsthafte Bedrohung für das bestehende globale Ökosystem dar, was die kontinuierliche Suche nach alternativen, umweltfreundlichen, biochemischen Energiequellen stimuliert, die in der Lage sind, den zukünftigen Energiebedarf zu decken. Die mikrobielle Brennstoffzellentechnologie (MFC) ist eine dieser alternativen Energiequellen, die das Waste-to-Energy-Prinzip nutzt, das zur Abwasserbehandlung bei gleichzeitiger Rückgewinnung von Bioenergie unter Verwendung von Mikroorganismen als Biokatalysatoren eingesetzt werden kann. Der Membranbioreaktor (MBR) ist eine weitere vielversprechende Technologie zur Abwasserbehandlung, die eine Kombination aus Belebtschlammprozess und Membranfiltration ist. Die Kombination dieser beiden Technologien wird sich als effizient für die Abwasserbehandlung sowie die Biostromerzeugung erweisen. Die Auswahl der protonenleitenden und wasserdurchlässigen Membran sind derzeit die Schlüsselfaktoren, welche die Leistung der mikrobiellen Brennstoffzelle (MFC) bzw. des Membranbioreaktors (MBR) bestimmen. Poröse Membranen aus polymerbasierter Keramik (PDC) wurden durch eine einfache uniaxiale hydraulische Presstechnik unter Verwendung von Polysiloxan als Vorstufe und protonenleitenden Materialien als Füllstoffe hergestellt. Die hergestellten Keramikmembranen weisen anpassbare Oberflächeneigenschaften und eine unimodale Porengrößenverteilung im Bereich zwischen 0,1 und 1 µm auf. Die Membranen sind für MFC- und MBR-Anwendungen konzipiert, bei denen Protonenionendiffusion und Wasserdurchlässigkeit eine wichtige Rolle spielen. Die keramischen Membraneigenschaften wurden durch Zugabe von Füllstoffen wie Kationenaustauschermaterial, Graphitkohle und hygroskopischem Material angepasst. Die Kationenaustauschermaterialien sind Montmorillonit und $\text{H}_3\text{PMo}_{12}\text{O}_{40}/\text{SiO}_2$ -Füllstoff, die im ersten Teilprojekt mit variabler Pyrolysetemperatur (400 bis 1000 °C) verwendet werden. Dies führt zu einer hohen MFC-Leistung unter Verwendung einer funktionalisierten Ceramer-Membran mit Kationenaustauscherfüllstoff (pyrolysiert bei 400 °C). Im zweiten Teilprojekt werden verschiedene Gewichtsprozent von Graphenoxid und mehrwandige Kohlenstoff-Nanoröhrchen bei 1100 °C durch Pyrolyse in eine funktionalisierte keramische Membran überführt. Besonders hohe MFC-Leistungen wurden für die funktionalisierte Keramikmembran mit 0,5 Gew.-% Graphenoxid erhalten. Die hygroskopischen Füllstoffe wie SiO_2 (als Partikel), SiO_2 (abgeleitet von TEOS) und TiO_2 wurden zur Funktionalisierung keramischer Membranen benutzt, die bei 1100 °C pyrolysiert wurde, was zu einer hohen MFC-Leistung und einer guten Wasserdurchlässigkeit für die MBR-Anwendung, insbesondere unter Verwendung einer mit 15

Gew.-% TiO₂ funktionalisierten Keramikmembran, führt. In allen Ansätzen wurden die physikalischen Eigenschaften wie Porosität, Hydrophilie, mechanische Stabilität, Sauerstoffmassentransferkoeffizient der Membranen und Ionenaustauschkapazität gemessen, um die Eignung des Membranmaterials für weitere Tests in MFC- und MBR-Systemen zu ermitteln. Schließlich wurde das integrierte MFC- und MBR-System im 20-Liter-Pilotmaßstab unter Verwendung einer bei 1000 °C pyrolysierten Keramikmembran untersucht und über die Effizienz der Biostromerzeugung und Abwasserbehandlung berichtet.

Abstract

The pollution caused by the use of conventional energy sources represents a serious threat to the existing global ecological system, which stimulates the ongoing search for alternative environmentally safe biochemical energy sources that are able to fulfill the future energy demand. The microbial fuel cell (MFC) technology is one of such alternative energy resources conceptualizing the waste-to-energy principle, which can be used for wastewater treatment with simultaneous recovery of bio-energy using microorganisms as biocatalysts. The Membrane bioreactor (MBR) is another promising technology for wastewater treatment, it is combination of activated sludge process and membrane filtration. The integration of these two technologies will be an efficient one for wastewater treatment and bioelectricity generation. The selection of proton conducting and water permeable membrane are currently the key factors that decide the performance of microbial fuel cell (MFC) and Membrane bioreactor (MBR), respectively. Porous Polymer derived ceramics (PDC) membranes were prepared by a simple uni-axial hydraulic pressing technique, using polysiloxane as a precursor and proton conducting materials as fillers. The ceramic membranes produced have tailorable surface characteristics and uni-modal pore size distribution in a range between 0.1 and 1 μm . These porous ceramic membranes are designed for MFC and MBR applications that involve proton ion diffusion and water permeability. The ceramic membrane properties were tailored by addition of filler materials such as cation exchange material, graphitic carbon and hygroscopic material. The cation exchange materials are montmorillonite and $\text{H}_3\text{PMo}_{12}\text{O}_{40}/\text{SiO}_2$ filler used in the first approach with variable pyrolysis temperature (400 -1000 $^\circ\text{C}$). This results in high MFC performance using cation exchange filler functionalized ceramic membrane (pyrolysed at 400 $^\circ\text{C}$). In the second approach, functionalized ceramic membranes with different weight percentage of graphene oxide and multiwall carbon nanotube pyrolyzed at 1100 $^\circ\text{C}$, were prepared and showed a high MFC performance specially for functionalized ceramic membranes with 0.5 wt.% graphene oxide. Functionalized with ceramic membrane with hygroscopic fillers such as SiO_2 (as particle), SiO_2 (derived from TEOS) and TiO_2 were pyrolysed at 1100 $^\circ\text{C}$, which results in high MFC performance and water permeability for MBR application by using ceramic membrane functionalized with 15 wt% TiO_2 . In all the approaches, the physical characteristics, such as porosity, hydrophilicity, mechanical stability, ion exchange capacity, and oxygen mass transfer coefficient, of the membranes were measured to identify the suitability of the membrane material for further testing in MFC and MBR systems. Finally, the 20 liter capacity

pilot scale integrated MFC and MBR system were studied using a ceramic membrane pyrolysed at 1000 °C and reported the bioelectricity generation and wastewater treatment efficiency.

List of Abbreviations

AEM	Anion exchange membrane
APTES	Aminopropyltriethoxysilane
BET	Brunauer–Emmett–Teller method
BiSA	Bistrimethoxysilylpropyl amine
CE	Coulombic efficiency
CEM	Cation exchange membrane
COD	Chemical oxygen Demand
DO	Dissolved oxygen
GO	Graphene oxide
IEM	Ion exchange membrane
MBR	Membrane Bio Reactor
MFC	Microbial Fuel Cell
MWCNT	Multiwall carbon nanotube
NER	Normalized energy recovery
OCV	Open Circuit Voltage
ORR	Oxygen reduction reaction
OV	Open Voltage
PDC	Polymer Derived Ceramics
PEM	Proton exchange membrane
PMA	$H_3PMo_{12}O_{40}/SiO_2$
SEM	Scanning electron microscopy
TEM	Transmission electron microscopy
TEOS	Tetraethylorthosilicate
XRD	X- ray diffraction

1. Introduction

Renewable energy resources have attracted much attention around the globe since it was found that the use of fossil fuels contributed to the global warming [1]. Another serious issue is the shortage of wastewater treatment facilities, which is often observed in rural areas [2]. Microbial fuel cells (MFCs) represent a possible solution to these problems due to their ability to simultaneously generate green electricity from natural resources and perform wastewater treatment using an eco-friendly approach. Generally, MFCs mimic biological electrochemical systems, in which bacteria catalyze the oxidation of wastewater inside an anaerobic anodic chamber and reduction of oxygen in an aerated cathodic chamber, which results in electricity generation and wastewater treatment [3, 4]. The recent advances in this field include the increase in the power output due to the advancement in the reactor configuration, utilization of inexpensive electrode and catalyst materials, and modification of the operational regime [5-7]. Nevertheless, achieving high energy outputs and large-scale applicability of this technique remain a significant challenge, which can be potentially overcome by replacing the mechanically unstable and expensive polymer-based proton-exchange membrane (PEM) like Nafion with low-cost-efficient membranes [8]. The characteristics criteria of an ideal membrane for MFC consists of high ion exchange capacity, mechanical and chemical stability, and low oxygen permeability and biofouling [9].

Membrane bioreactors (MBRs) are another wastewater treatment equipment that treat wastewater first using a biological treatment, typically an anaerobic digestion tank, followed by membrane filtration, typically with an ultrafiltration (UF) membrane [10]. MBRs provide several advantages such as high mixed/suspended solid concentrations and low sludge output, thus enabling high efficiencies for the removal of chemical oxygen demand (COD) and biological oxygen demand (BOD) [11]. However, membrane fouling and low mechanical stability hinder the widespread application of membrane materials in MBRs [12]. Moreover, large-scale usage of MBRs will require a substantial decrease in membrane prices [13]. An ideal membrane for MBRs should have properties that include a high water permeability, mechanical and chemical stability, and minimal biofouling [14, 15].

Moving these wastewater treatment technologies forward toward realization requires enormous research investigations into membrane materials. In recent years, many research groups have focused on finding new membrane materials for MFC and MBR systems [15-18]. However, no material that can act as an ideal membrane for both approaches has been discovered yet.

Moreover, the integration of both MFC and MBR using a single membrane material would allow efficient wastewater treatment and simultaneous power generation.

The objective of this work was to synthesize and characterize inexpensive porous polymer-derived ceramic (PDC) membranes for MFC and MBR systems with the required properties, as explained in detail in **chapter 3**. For this purpose, pure polysiloxane-based and composite membranes mixed with different proton-conducting fillers were fabricated by simple pressing and pyrolysis techniques, as discussed in **chapter 4**. The surface areas, surface characteristics, pore size distributions, ion exchange capacities (IECs), cation transport numbers, and oxygen diffusion coefficients of the fabricated membranes were measured to determine their suitability for use in an MFC, and their MFC performance was studied as described in **chapters 5 to 7** (the studies are published as research articles), where each chapter reports a different filler type. The applicability of the PDC composites as proton-conducting membranes in an MFC and as a UF membrane in an MBR was studied as described in **chapter 8**. In **chapter 9**, the setup conditions and initial output of a pilot-scale integrated MFC and MBR system using a synthesized PDC membrane are discussed.

2. State of the art

2.1 Microbial fuel cell for energy and wastewater treatment

The electrochemical reaction of bacterial species and a platinum electrode was first observed by Potter in 1911 [19] and later proved by Cohen *et al.* in 1931, who assembled a stacked laboratory-scale MFC and reported a voltage of 35 V at an applied current of 0.2 mA [20]. Later, the National Aeronautics and Space Administration (NASA) space program attempted to recycle human waste for bioelectricity during space journeys using MFC technology [21]. In 1991, Habermann *et al.* operated an MFC for a long-term duration of 5 years using municipal domestic wastewater [22], which represents the first observation of an indirect electron transfer reaction mechanism between a specific bacteria and soluble mediators. Over the subsequent decades, MFCs have been demonstrated as effective for harvesting power on levels from nanowatts to watts per cubic meter of treated wastewater. The innovation and progress of MFC technology continue day-by-day in terms of power production. Logan reported that laboratory-scale MFC systems have achieved a maximum power density greater than 1 kW m⁻³ using anaerobic sludge wastewater [23]. However, the main challenge that remains is to bring this technology from the laboratory scale to industrial bio-power production.

MFC technology is eco-friendly mainly because it can not only generate electricity but also treat wastewater under normal operating conditions [24]. An MFC can operate using only 0.024 kW or 0.076 kW h per kilogram of wastewater, which is 10% less energy consumption than that of the traditional activated sludge process [25]. The treated wastewater is monitored based on chemical oxygen demand (COD), a parameter that clearly indicates the amount of present organic matter [26]. For instance, Mohan *et al.* treated dairy wastewater using an MFC system and achieved a 95% COD removal efficiency [27]. The COD removal efficiency of an MFC depends on the reactor configuration, operation conditions, and materials used in the system [28, 29].

2.1.1 Microbial Fuel Cell and its component

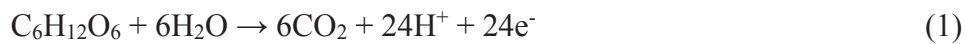
An MFC system consists of an anaerobic anode chamber and aerobic cathode chamber, which are physically separated by a membrane material. In the anode chamber, the active bacterial species present in the wastewater adhere to the anode surface. These species then oxidize the organic matter present in the wastewater and transfer resulting electrons through an external circuit and protons through the membrane to the cathode chamber. The protons and electrons

react in the cathode with the parallel reduction of oxygen to water molecules [30, 31]. A schematic of a typical MFC setup is shown in Figure 1. The active material components of an MFC are as follows:

1. Anode
2. Cathode and its electrocatalyst
3. Membrane

An electrochemical reaction occurs in the anode chamber as shown in equation 1. The microbial species grown on the anode surface degrade organic matter and liberate carbon dioxide, protons, and electrons. The oxygen reduction reaction (ORR) occurs in the cathode chamber as shown in equations 2 (two-electron pathway) and 3 (four-electron pathway). The byproduct formed in the cathode chamber is either H_2O_2 or H_2O from the two- or four-electron pathway, respectively [32, 33]. The reaction mechanism in the cathode chamber completely depends on the cathode material [34].

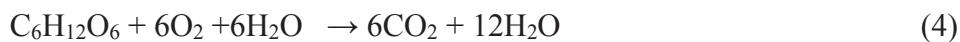
Anodic reaction:



Cathodic reaction:



Overall cell reaction:



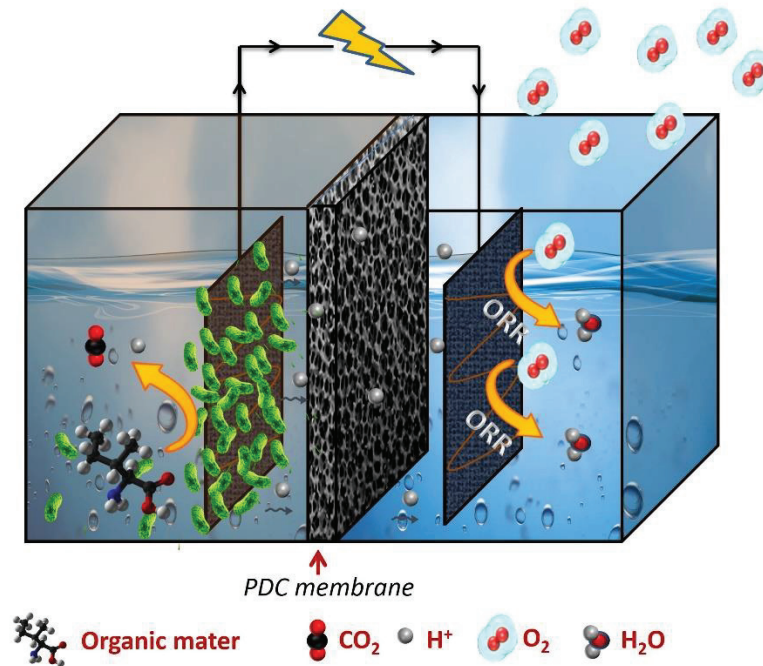


Figure 1. Schematic view of MFC system [35].

Anode electrode

The ideal anode material for an MFC should have an appropriate electrical conductivity, high biocompatibility, large surface area engineered with micro and mesopores, rough surface, suitable mechanical and chemical stabilities, and corrosion resistivity [36, 37]. The mechanism of electron transfer from the bacterial species to the anode material is not a natural phenomenon. The two potential mechanisms are direct and indirect electron transfer between the electrode and bacterial species [38]. In the former, the electrons are directly transferred from the outer cell structure of the bacterial species to the electrode to degrade organic matter. The bacterial species adhere to the electrode surface and transfer electrons using naturally produced electrically conducting nanowires [39]. Up to now, direct electron transfer has been considered the preferable mechanism for efficient power generation in MFC systems. *Shewanella* and *Geobacter* are the two active bacterial species that form electrically conductive nanowires and follow the direct electron transfer mechanism in anode materials [40, 41]. In contrast, in the indirect mechanism, electrons are transferred from the bacteria to the electrode surface with the aid of soluble mediators [42, 43]. These mediators are externally added to or in some cases

naturally produced by bacterial species in the anode chamber. Examples of externally added mediators include thionine neutral red, humic acid, methylene blue, and riboflavin, and many more chemical mediators are under investigation [44-48]. However, externally added chemical mediators followed by indirect electron transfer are unfavorable because of the resulting low power generation and hazards to the environment.

The most common anodes consist of carbon materials including graphite, carbon felt, carbon cloth, carbon paper, and many more as shown in Figure 2 [49-51]. Ahn *et al.* developed a single-chamber MFC with a graphite brush as an anode material and achieved a maximum power density of 422 mW m^{-2} , which was mainly attributable to the high surface area and low electrode resistance of the brush [52]. Wang *et al.* designed a single-chamber MFC with carbon cloth as the anode material and acquired a maximum power density of 483 mW m^{-2} [53]. Nevertheless, the physical and electrical conductivity of these anodes could be improved by the addition of metal nanoparticles such as cobalt, nickel, and iron or by coating with conducting polymers such as poly-3-hydroxyalkanoates and polyaniline [54-58].

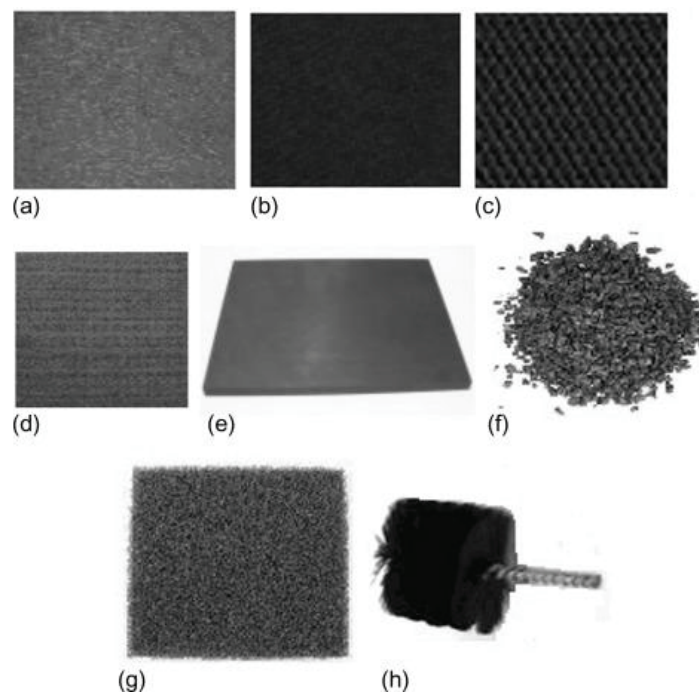


Figure 2. Traditional carbon materials used as MFC anodes. (a) Carbon paper, (b) carbon cloth, (c) carbon mesh, (d) carbon felt, (e) graphite plate, (f) granular graphite, (g) reticulated vitrified carbon, and (h) carbon brush [59].

Cathode and its electrocatalyst

The ideal cathode and corresponding catalyst are necessary for cost efficiency and a high electrocatalytic activity toward the ORR. The essential properties for cathode materials are a high surface area, electrical conductivity, and mechanical and chemical stability [33, 60]. Improving the performance of a cathode material requires an electrocatalyst on its surface, which enhances the overall performance of the MFC. The ORR mechanism in the cathode material follows either two- or four-electron transfer [61, 62]. The two-electron pathway in the cathode produces peroxide, which acts as a disinfecting agent in MFCs to treat wastewater [63]. However, the diffusion of peroxide into the membrane leads to degradation of the material [64, 65]. The four-electron reaction produces H₂O as a byproduct and has a high overpotential, resulting in a high power density in MFC systems [66]. Hence, the four-electron pathway mechanism is preferable. Like in the anode, the reaction mechanism in the cathode mainly depends on the cathode material.

The commonly used cathode materials for MFCs are carbon paper, graphite, and carbon felt [32, 67]. Moon *et al.* developed an MFC with a cathode consisting of platinum incorporated into graphite felt that exhibited a power density of 150 mW m⁻², which is three-fold higher than that of an MFC with pure graphite felt [68]. However, utilization of platinum as a cathode electrocatalyst is not an economically viable option [32]. Increasing the cathode surface area is an effective approach to increasing the performance of MFCs because it enhances the electrochemical active surface area of the material and thus the ORR performance. For instance, an MFC with a stainless-steel brush as a cathode material showed a higher performance than an MFC with graphite felt because of the high surface area [69]. Considering the literature, transition-metal oxide-based cathode electrocatalysts, such as MnO₂, Co₃O₄, NiCo₂O₄, etc., are potential candidates for the ORR because of their variable oxidation states, high oxygen vacancies, and low costs [70] [71, 72]. Various cathode materials and their performances are summarized in Table 1.

Table 1. Some of used electrodes in MFCs with maximum generated power, current and voltage [30].

Cathode	Max. Power density	Max. Current density	Max. Voltage	Reference
Activated carbon fiber	315 mW m ⁻²	1.63 x 10 ⁻³ mA m ⁻²	679 mV	[73]

Pt-coated carbon paper	0.3 W m ⁻³	4.69 mA m ⁻²	644 mV	[73]
Carbon felt	77 mW m ⁻²	6 x 10 ⁻³ mA m ⁻²	573 mV	[73]
Graphite felt	539 mW m ⁻²	3145 mA m ⁻²	742.3 mV	[74]
Plain carbon	67 mWm ⁻²	1.5 mA m ⁻²	598 mV	[73]

Membrane material

The membrane material is one of the most important components in an MFC because it separates the anaerobic anode and aerobic cathode chambers. The function of the MFC membrane is to diffuse the protons produced in the anode chamber to the cathode chamber and prevent the crossover of oxygen from the substrate of one chamber to another [9]. Oxygen crossover inhibits the growth of bacterial species on the surface of the anode, resulting in a decrease in performance [75]. Many research groups have focused on the development of novel membrane materials for MFCs [76, 77]. The ideal membrane should have a high ionic conductivity; low oxygen permeability; high chemical, mechanical, and thermal stabilities; low biofouling; and low cost [9]. Many studies have reported increased current densities for single-chamber MFCs without a membrane [78, 79]. However, the coulombic efficiency (CE) of such MFCs is considerably reduced because of the high oxygen permeability and substrate crossover [80]. Nafion is the current state-of-the-art proton exchange membrane (PEM) material, not only for MFCs but also for PEM fuel cells because of its extraordinary ionic conductivity [80, 81]. The chemical structure of Nafion is a sulfonated tetrafluoroethylene polymer consisting of a hydrophobic fluorocarbon backbone chain (-CF₂-CF₂) to which the hydrophilic sulfonate groups SO³⁻ are attached (Figure 3). The high proton conductivity of Nafion is mainly attributable to these negatively charged sulfonate group [82]. However, the cost, mechanical stability, and biofouling of this material outweigh the performance and durability of the resulting MFC system [83]. The wastewater used in the anode chamber of an MFC contains not only protons but also other cations such as Mg²⁺, Na⁺, Ca²⁺, NH₄⁺, and K⁺, where the cation concentration is 10⁵ higher than that of protons [80]. Huang *et al.* reported the possibility of cation diffusion, particularly of Na⁺ and Ca⁺, from the anode chamber to the cathode chamber through polymeric Nafion membranes, which subsequently reduces the ORR rate and overpotential developed in the cathode. This is mainly because of the selectivity of the Nafion membrane toward all other heavy metal ions, which results in a decrease in the overall MFC performance [84]. Many other alternative membranes are under investigation for this

application. For instance, Yusuf *et al.* developed poly-3-hydroxyalkanoate composites with –COOH-functionalized multiwall carbon nanotubes as a membrane material for MFCs and reported a power output of 361 mW m^{-2} [17]. However, this performance is not higher than that of a commercial Nafion membrane tested under similar conditions. An overview of membrane materials and their classifications is provided in section 2.3.

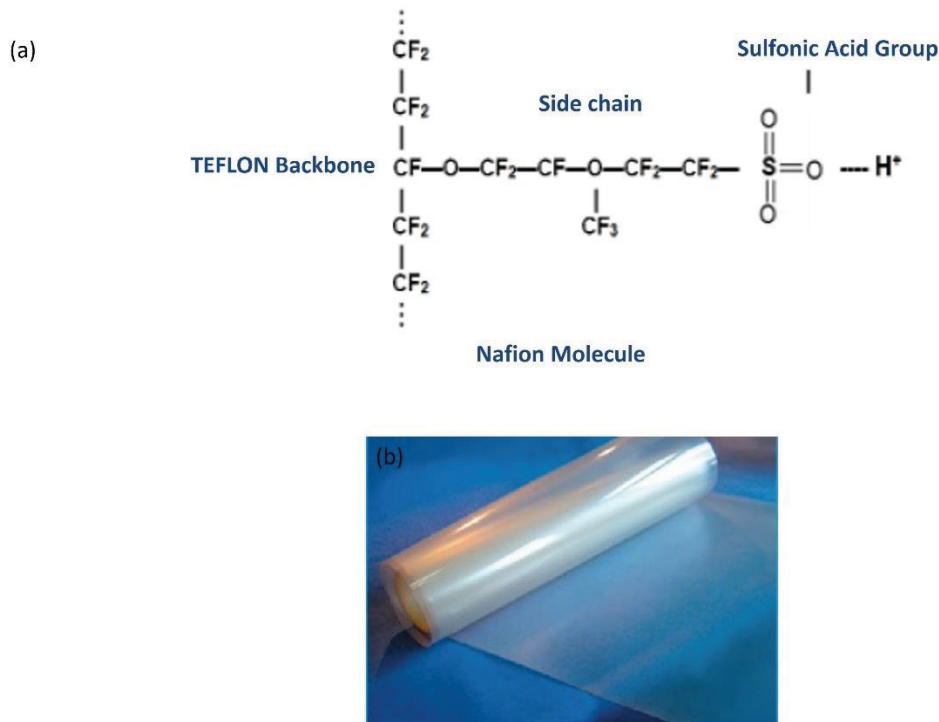


Figure 3. (a) Polymeric chemical structure of Nafion membrane and (b) polymeric nafion membrane sheet [85].

2.1.2. Membrane Bioreactor (MBR)

MBRs combine biological degradation via activated sludge with solid–liquid separation via an ultrafiltration membrane. The activated sludge process is widely used in sewage and industrial wastewater treatment technologies. During this process, the bacterial species present in the wastewater degrade organic matter. The treated wastewater from the activated sludge tank is sent to a filtration tank, where biological solids and other sediments are filtered using a porous membrane [86]. The first application of MBR technology reported by Aileen *et al.* in 1969 employed UF membranes in the filtration tank. The two basic configurations of MBRs are a recirculated configuration with an external filtration tank and a submerged configuration with the membrane immersed in the activated sludge tank. In the second configuration, a suction

pump is used to draw water from the tank through the membrane [87]. Figure 4 shows the two MBR reactor configurations.

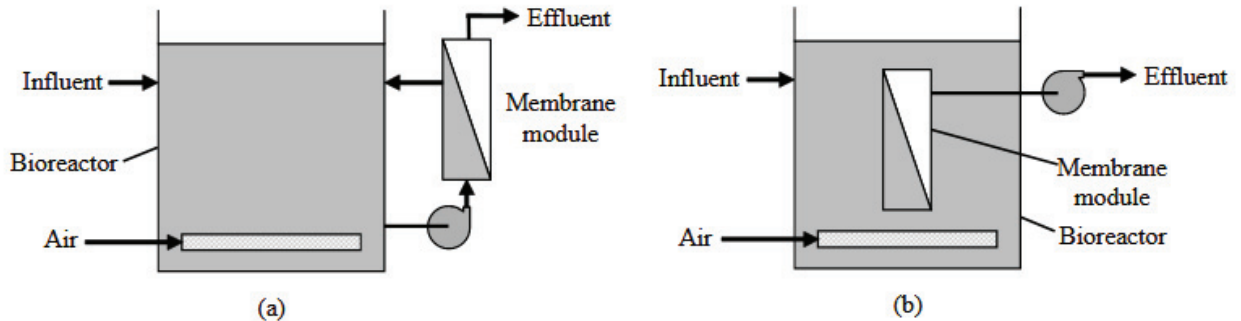


Figure 4. (a) MBR with external membrane module and (b) MBR with immersed membrane module [87].

Furthermore, an MBR is classified into two types based on the environment of the activated sludge process as follows:

1. Aerobic membrane bioreactor
2. Anaerobic membrane bioreactor

Aerobic membrane bioreactor

In an aerobic MBR, the activated sludge tank is aerated with oxygen during operation, and organic matter is metabolized and degraded by bacterial species in the presence of dissolved oxygen for their growth and respiration [88]. Chang *et al.* developed a submerged aerobic MBR with a non-woven fabric membrane material and reported that the COD concentration decreased from 1045 mg L⁻¹ to an average of 90 mg L⁻¹ after 160 days (Figure 5) [89]. Nitrification is another aeration technique in which nitrogen gas is aerated to remove ammonia or nitrogen content from the wastewater. This process is mainly used for wastewater that contains high ammonia and dissolved oxygen concentrations and low organic matter concentrations [90]. Rosenber *et al.* studied the use of an aerobic MBR to treat municipal wastewater for 535 days using a submerged hollow-fiber membrane with a pore size of 0.2 μm and reported COD and nitrogen removal efficiencies of 95% and 82%, respectively (Figure 6) [91]. However, aerobic MBRs are more expensive than anaerobic MBRs because of the costs of aeration and nitrification in the activated sludge process tank [92].

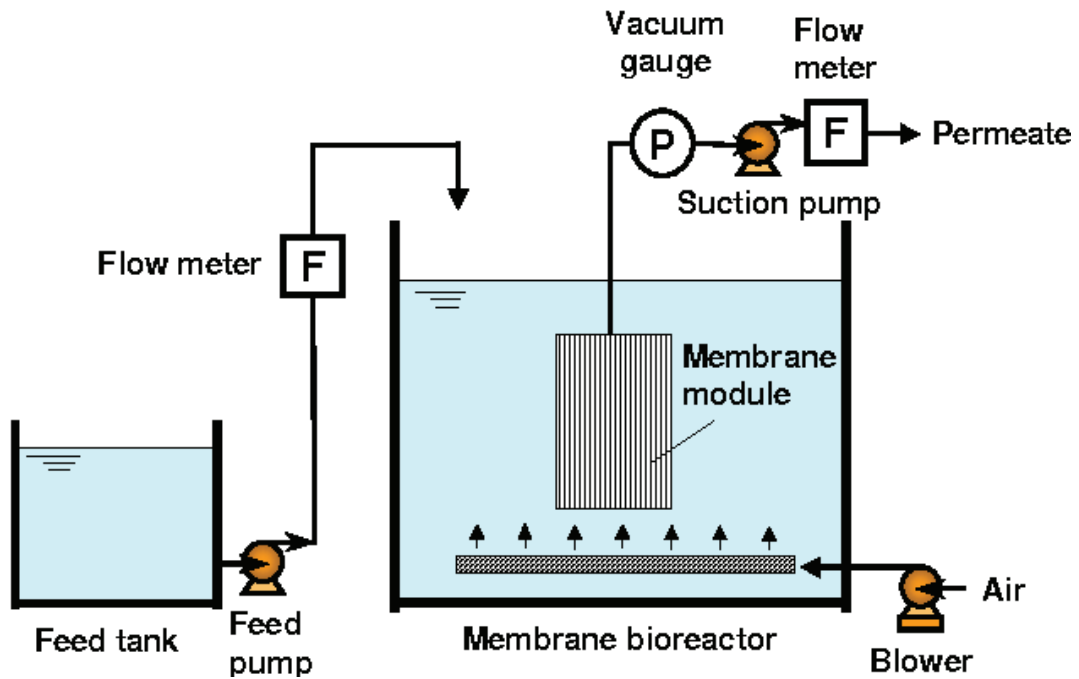


Figure 5. Schematic diagram of aerobic membrane bioreactor using non-woven fabric membrane [89].

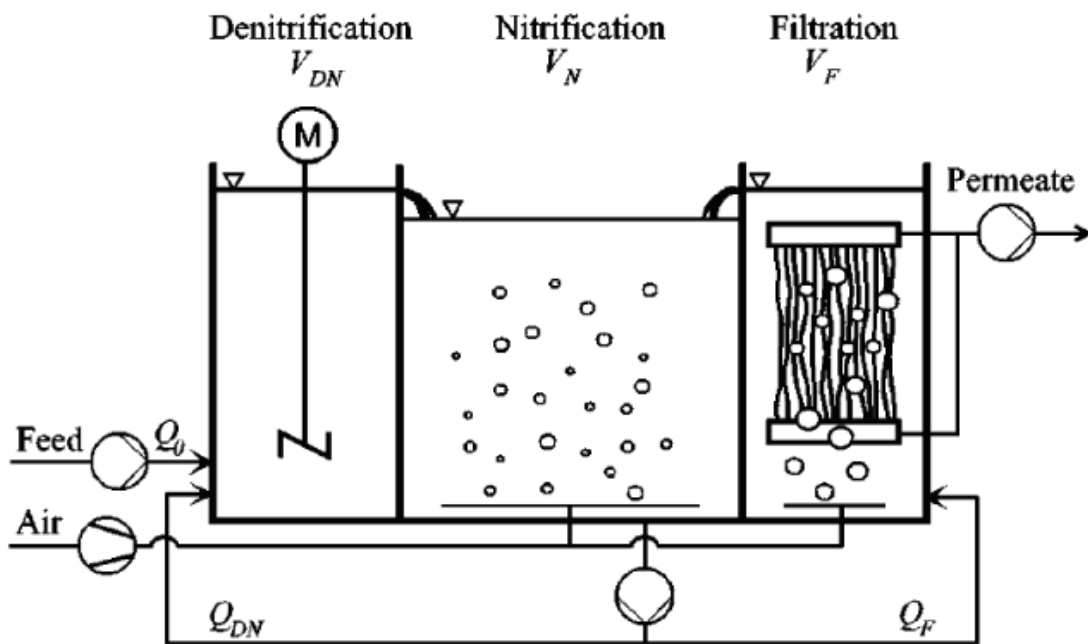


Figure 6. Schematic configuration of membrane bioreactor with nitrification [91].

Anaerobic membrane bioreactor

An anaerobic MBR degrades organic matter into methane and carbon dioxide as byproducts. This process involves the interaction of four different bacterial species—hydrolytic, acidogenic, acetogenic, and methanogenic—with organic matter in the wastewater. The resulting sewage from the anaerobic tank is further treated using an ultrafiltration membrane compartment [93, 94]. Anaerobic MBRs can be configured in multiple manners based on the reactor design and membrane module placement. Some examples of reactor configurations are shown in Figure 7.

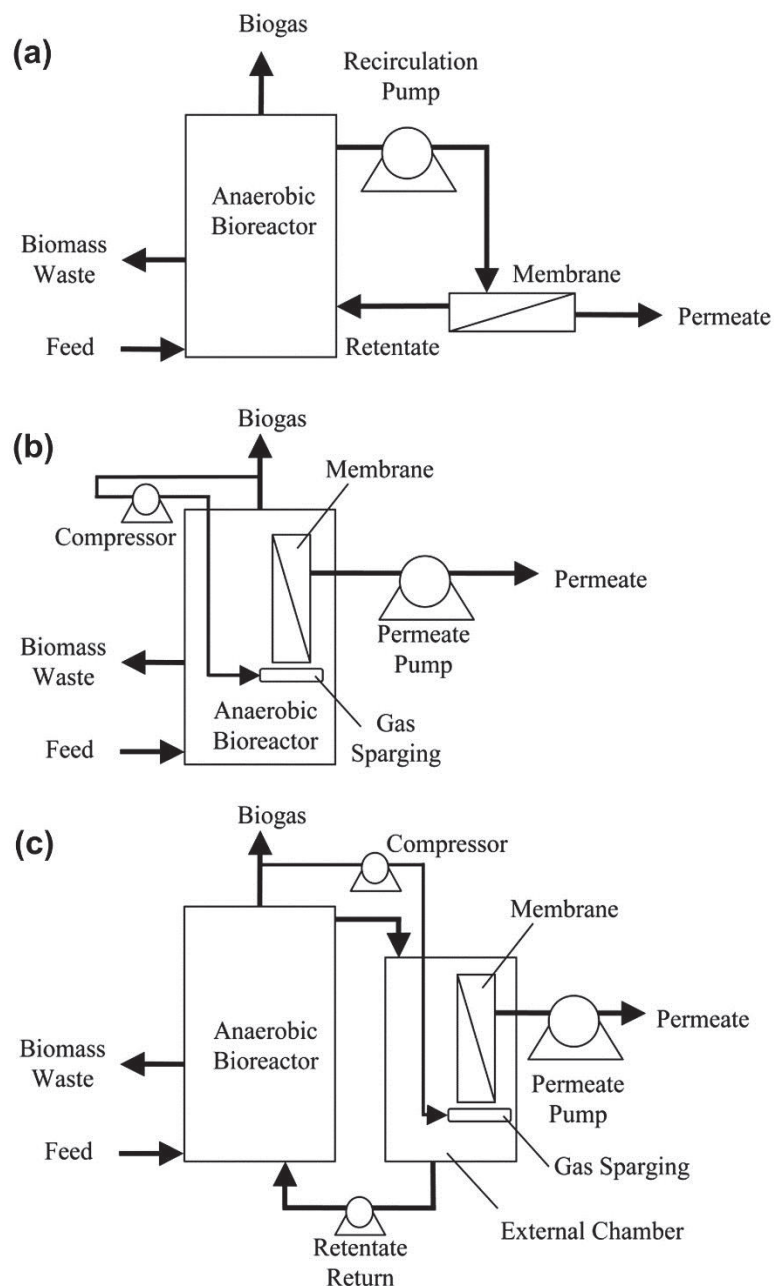


Figure 7. (a) side-stream (external,cross-flow) configuration with pressure-driven membrane,(b) submerged configuration with membrane immersed directly in the reactor -

vacuum-driven membrane, and (c) submerged configuration with membrane in separate chamber - vacuum-driven membrane [92].

The significant advantages of anaerobic MBRs are lower sludge production, ability to treat high organic loads, low costs, and end biogas (CH₄) production [95]. He *et al.* designed an anaerobic MBR with a polyethersulfone ultrafiltration membrane for treating high-concentration food wastewater and reported a COD removal efficiency of 94% with a gas yield of 0.136 m³ kg⁻¹ COD [96]. The main drawback of an anaerobic MBR is the low performance at temperatures below 20 °C. Nevertheless, Smith *et al.* used a submerged anaerobic MBR to treat domestic wastewater at 15 °C and reported a COD removal efficiency of 92%, which was mainly achieved by using a mesophilic bacterial species inoculum in the MBR flocculation tank [97].

Membrane material for MBR

The selection of a membrane material is highly important for improving the wastewater quality in both aerobic and anaerobic MBRs. Membrane material fouling in MBR systems is the major obstacle that slows their commercialization [12]. The membrane material properties such as pore size, porosity, surface charge, roughness, hydrophilicity/hydrophobicity, and other factors have been proven to impact MBR performance, particularly in terms of membrane biofouling [98]. The determination of membrane pore sizes has been extensively investigated by many research groups, and their efforts have shown that pore size distribution is likely an important parameter influencing membrane performance [99]. A membrane with unimodally structured pores showed enhanced water permeability and the highest removal efficiency as reported by Pierre *et al.* [100]. Membranes with hydrophilic properties have an increased water permeability and allow for organic pollutants to adhere to the membrane surface [101]. Membrane mechanical and chemical stability is also a crucial factor for long-term MBR system operation [102]. A narrow pore size distribution would be better to minimize membrane fouling during the MBR and conventional membrane separation processes.

The water permeability, or flux, of the membrane should be high and remain so over time to minimize membrane fouling in MBR systems. According to the literature, available membranes for MBR systems are polyethylene, polyethersulfone, polyvinylidene fluoride, and many more ceramics, metal sheet membranes, etc. [14, 103-105]. Most of these reactors used micro- or ultrafiltration-type membranes with a pore size less than 1 μm [106, 107]. The application of membrane materials with larger pores results in permeation of the bacterial substrate in the

treated wastewater [108]. Zhao *et al.* developed a graphene-oxide-grafted polyvinylidene fluoride composite membrane for MBR applications [14] and observed an average water flux of 48–50 L m⁻² h⁻¹. This high performance mainly depended on the membrane pore size distribution and hydrophilic nature. Another study reported the development of a polysulfone membrane functionalized with titanium oxide nanoparticles for MBR applications. The authors showed that after the addition of titanium oxide nanoparticles, the hydrophilicity and pore size distribution of the polysulfone membrane increased, which in turn resulted in a higher water flux of 98.25 L m⁻² h⁻¹ compared with that of a non-functionalized polysulfone membrane [109].

2.1.3 Integrated Microbial fuel cell - Membrane Bioreactor (MFC-MBR)

MFCs are considered promising devices for wastewater treatment and bioelectricity generation. However, the final treated wastewater effluent from an MFC system is of poor quality for practical usage in terms of recycled industrial and domestic wastewater. Some studies have shown that integrating MFCs with the activated sludge technique by submerging the device in an aeration tank may be a considerable option for wastewater treatment [110, 111]. However, the effluent quality remains poor without a subsequent filtration compartment to remove substrates, and the necessary aeration further reduces the integrated system energy efficiency. Wastewater treatment technologies such as anaerobic MBRs would be the best choice to integrate into an MFC unit, mainly because of the high wastewater treatment efficiency and lack of required aeration in the activated sludge tank [112]. Ren *et al.* demonstrated an MFC with an anaerobic fluidized MBR with a COD removal efficiency of 92% [113]. However, the system was not completely integrated because the two processes were separated within the same system (Figure 8). The idea of integrating an MBR into an MFC system was also reported by Malaeb *et al.*, who submerged an MBR in an MFC system with the cathode in the MFC acting as a filtration unit [114]. The reported energy and COD removal efficiencies of this system were 6.8 W m⁻³ and 97%, respectively (Figure 9).

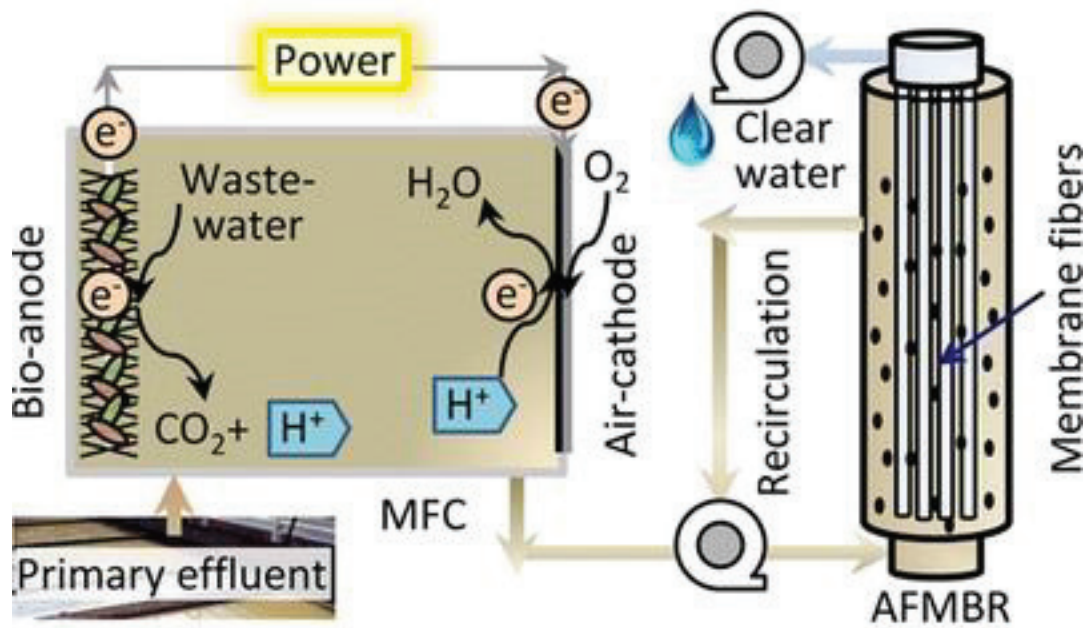


Figure 8. Scheme of two stage MFC combined with Anaerobic fluidized membrane bioreactor [113].

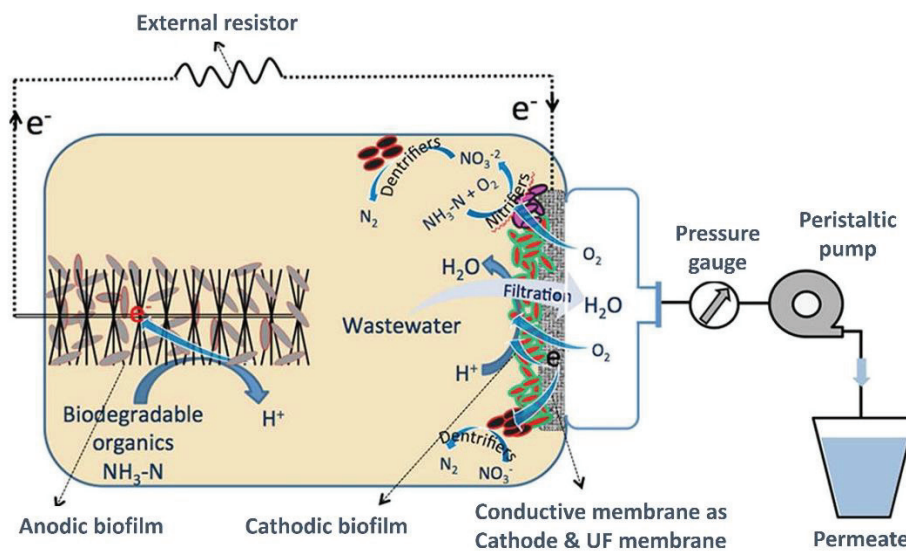


Figure 9. Scheme of submerged MBR in MFC system [114].

2.2. Requirement and challenges in designing membrane

2.2.1 Membrane resistance

The final power output of an MFC system depends on the internal resistance of the individual anode, cathode, electrolyte, and membrane materials. Electrochemical impedance spectroscopy and polarization studies can determine these individual resistances and thus the overall internal resistance of the MFC system [115]. Use of a membrane with a high internal resistance in MFCs results in a decreased overall performance, mainly because the low ion exchange capacity of the membrane material considerably reduces proton diffusion from the anode to the cathode chamber [116]. The membrane resistance depends on numerous factors such as the nature, pH, and concentration of the electrolyte used in the system. A membrane with a low internal electrical resistance would be ideal for MFC systems to afford a high power and current density. One efficient approach to improving MFC performance is to increase the membrane ionic conductivity by tailoring the membrane material via the addition of an external proton-conducting filler materials [117]. Fan *et al.* quantified the internal resistance of an MFC with different anode, cathode, and membrane materials and reported that the membrane resistance has a greater impact on decreasing the MFC performance [118].

2.2.2 Oxygen diffusion

Oxygen diffusion from the aerobic cathode chamber to the anaerobic anode chamber is a significant problem, mainly because of biofilm degradation in the anode resulting from disturbances under anaerobic conditions, which in turn decreases the MFC system performance. Moreover, because oxygen is a more favorable electron acceptor, it competes with the anode material to accept electrons, which further reduces the Columbic efficiency (CE) of the system [119, 120]. Yousefi *et al.* developed a layer-by-layer assembled chitosan/montmorillonite nanocomposite membrane as an oxygen barrier in an MFC system that significantly improved the power generation compared with that of an MFC with a bare membrane [121]. Du *et al.* reported that the CE of a membrane-less MFC was 20% lower than that of an MFC with a membrane because of the lack of physical barriers preventing oxygen permeation into the anode chamber [122]. In fact, the state-of-the-art polymeric Nafion membrane used in MFC systems also has a certain degree of oxygen diffusion [123]. Currently, there are no known membranes that can completely prevent oxygen diffusion. The only means to eliminate the related negative impacts is to use a chemical oxygen scavenger such as cysteine in the anodic chamber, which reacts with oxygen to form disulfides (cystine and cysteine dimers) [119]. Although oxygen

diffusion does not have a permanent impact on MFC performance, it does reduce the voltage output and CE of the system.

2.2.3 Substrate crossover

The ideal membrane material for an MFC should not allow reactants to pass from one chamber to the other. However, substrate crossover occurs because of molecular diffusion and electro-osmosis. Substrates such as bacterial species and organic matter in wastewater may pass through the membrane from the anaerobic anode chamber to the aerobic cathode chamber [124], which occurs more readily in porous membranes than in non-porous polymer membranes [9]. However, negatively charged species such as acetates, butyrates, etc. are assisted by the anion transfer properties of anion exchange membranes (AEMs), and similarly, positively charged species are assisted by cation exchange membranes (CEMs) [125]. During the early stage of MFC research, it was reported that substrate crossover results in the formation of aerobic bacteria on the cathode surface, thereby increasing the ORR activity. However, when the MFC is operated for a long period, this results in a significant decrease in MFC performance because of thickening of the biofilm, which hinders the diffusion of oxygen to the cathode surface [126, 127]. Harnisch *et al.* studied the effect on MFC performance of organic substrate crossover through the membrane and reported that the creation of a mixed potential in the cathode compartment results in a decreased MFC performance. Moreover, the substrates diffuse into the cathode chamber and are oxidized on the cathode electrode surface by aerobic bacteria, which results in an internal short circuit and decreases the CE of the MFC system [127]. Prabhu *et al.* monitored the concentrations of sodium, potassium, magnesium, calcium, and ammonium from diffusion in the cathode chamber and membrane and showed that a lower diffusion of metal species resulted in a higher power density [128]. A membrane with a pore size between 0.1 and 1 μm should minimize the diffusion of bacterial substrates from one chamber to another. The thickness of the membrane may also influence the substrate crossover, where a thinner membrane results in more crossover [121]. Hence, substrate crossover through the membrane results in a decreased MFC system performance.

2.2.4 Biofouling

Biofouling mainly occurs because of the bacterial substrates adhered to the surface of the membrane that faces the MFC anode chamber. The biofilm formed on the membrane surface is inhomogeneous compared with that on the anode surface [129]. Aerobic bacteria form an additional biofilm on the surface of the membrane because of oxygen diffusion from the cathode

to the anode chamber [130]. Moreover, the aerobic bacteria on the membrane surface in the anode compartment consume oxygen from the cathode and encourage oxygen to diffuse through the membrane because of the negative oxygen gradient formed in the anode chamber [131]. The biofilm formed on the membrane hinders proton diffusion from the anode to the cathode, which in turn increases the acidity in the anode chamber and deteriorates biofilm growth on the anode; this results in a significant decrease in MFC performance [129]. Figure 10 shows a scanning electron microscopy (SEM) image of a fouled membrane. Measuring the difference in ion exchange capacity, proton conductivity, and electrical conductivity of the fouled membrane can indicate the effect of membrane deterioration after biofouling. Moreover, membrane biofouling can be determined by measuring the open circuit voltage, power density, and COD removal efficiency after long-term MFC system operation [132]. Ghasemi *et al.* studied the effect of biofouling on a polymeric Nafion membrane and found that the maximum power densities for Nafion and biofouled Nafion were 52.8 and 20.9 mW m⁻², respectively. These studies showed that membrane biofouling is a major obstacle for bioelectricity generation in dual-chamber MFC systems [133]. The internal resistance of an MFC using a biofouled Nafion membrane increased because the bacterial species attack the sulfonic groups of the Nafion backbone, thereby hindering proton conduction [118].

The effective approaches to reducing biofouling effects are to use either an anti-microbial or anti-adhesion approach. In anti-microbial approaches, the membrane is chemically modified to kill the bacterial species adhered to the surface, whereas anti-adhesion approaches chemically modify the membrane to prevent surface adhesion of the biofilm [134]. Anti-microbial approaches include addition or coating of biocide substances such as titanium oxide, silver, copper, etc. onto the membrane composition, which results in decreased biofouling [135, 136]. However, leaching of the anti-microbial substance to the anode chamber results in bacterial growth deterioration in the anode, which significantly reduces the MFC performance [137]. A representative anti-adhesion approach is to alter the surface characteristics of the membrane to a hydrophilic nature, which prevents the growth of a bacterial species substrate [138]. Sun *et al.* modified a polymeric membrane by adding polyethylene glycol, which increased the membrane hydrophilicity to prevent membrane biofouling [139]. Roosjen *et al.* studied the effect of biofouling by modifying membranes with a positively charged or low surface free energy coating to prevent a negatively charged bacterial substrate from adhering to the surface [140]. At present, there are no membrane materials that can completely eliminate biofouling. However, researchers are attempting to reduce the biofouling effect by slight modifications to

membrane materials using either anti-microbial or anti-bacterial approaches. Hence, controlling membrane biofouling is a significant factor in improving the performance of MFC systems.

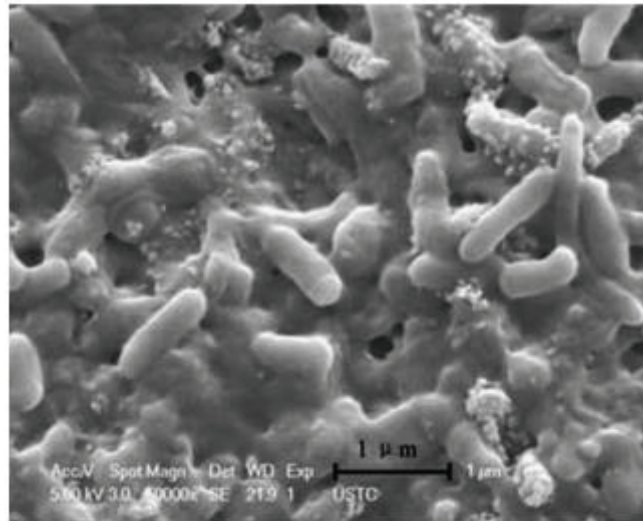


Figure 10. SEM image of polymeric membrane surface that was fouled [132].

2.3. Membrane for MFC application

2.3.1 Polymeric membranes for MFC

The polymeric membrane used in electrochemical applications such as PEM fuel cells, alkaline membrane fuel, batteries, and MFCs should have a high mechanical and chemical stability in harsh oxidative and reductive environments, as well as a suitable ionic conductivity [141-143]. Moreover, the cost of the membrane material should be considered as an important criterion for MFC system commercialization. Polymeric membrane materials are classified based on their ionic selectivity as follows:

1. Cation exchange membrane (CEM)
2. Anion exchange membrane (AEM)

Cation exchange membrane

The most commonly used CEMs for MFCs are perfluorinated or partially fluorinated membranes, namely Nafion. This type of CEM has a high stability in oxidative and reductive environments because of the perfluorinated backbone structure. The high proton conductivity

of Nafion is mainly attributable to the negatively charged end sulfonate groups attached to the polymeric backbone [82]. The negatively charged sulfonate groups are hydrophilic and form a continuous network of proton-conducting aqueous channels, through which cations are transported by mobile, electronegatively charged surfaces [144]. Ghasemi *et al.* studied the MFC performance using a polymeric Nafion membrane and observed a maximum power density of 106.7 mW m^{-2} and COD removal efficiency of 76% [145]. However, polymeric membranes have a tendency to transfer other cations such as heavy metals, which subsequently reduce the overall MFC performance. The performance of Nafion membranes can be further enhanced by adding external fillers such as SiO_2 , TiO_2 , graphene oxide, etc. to the polymeric matrix to achieve a massive increase in power generation [146-148]. The hydrophilic filler material enhances the water holding capacity of the membrane, resulting in an increase in water channels and thus an enhanced membrane ionic conductivity. Other types of CEMs used in MFC systems are polyethylsulfone, sulfonated poly ether ketone, and disulfonated poly (arylene ether sulfone) membranes [149-151]. The sulfonated groups on these polymeric membranes conduct protons in the polymeric chain. However, these sulfonated groups are deactivated by bacterial species after long-term MFC operation, which results in a decrease in performance over time. Non-fluorinated membranes, which are less expensive than fluorinated membranes such as Nafion, consist of aliphatic or aromatic polymers with benzene ring structures in the backbone. Some examples of non-fluorinated membranes are polystyrene, polyvinyl alcohol, and polyvinylbenzene [152-154]. Khilari *et al.* reported the applicability of a polyvinyl alcohol material as a PEM for an MFC system because of its suitable mechanical stability, chemical stability, and hydrophilicity. The ionic conductivity of the polyvinyl alcohol membrane was improved by the addition of silicotungstic acid and graphene oxide as external filler materials [155]. Similarly, as reported by Sivasankaran, the addition of sulfonated SiO_2 to the polymer matrix is an effective means to improve MFC performance using a non-fluorinated membrane such as sulfonated polystyrene ethylene butylene polystyrene [156].

Anion exchange membrane

There has been increasing research interest in the use of AEMs in electrochemical energy storage and conversion systems such as alkaline membrane fuel cells, alkaline membrane electrolyzers, redox flow batteries, electrodialysis, enzymatic fuel cells, and MFCs [157-159]. The ion exchange capacity, water uptake, and mechanical, chemical, and thermal stabilities are significant properties for the application of AEMs in electrochemical devices [160].

AEMs are polymeric membranes that conduct anions, mostly OH^- , since they contain positively charged species bound to an alkyl or aromatic polymeric backbone via extended side chains [161]. The most widely used AEM backbones are polyether ketones, polyether sulfone, poly phenylene oxides, polybenzimidazole, polyvinylbenzyl chloride, and polyvinyl alcohol, among others [162-165]. The bound cationic functional groups for transferring anion species are benzyl-trialkylammoniums, imidazolium, benzimidazoliums, phosphoniums, etc. [166-168]. The characteristics and performance of AEMs are determined by the concentration of cationic species bound to the polymeric backbone. This factor directly depends on the property of ion exchange capacity [169]. One commercially available AEM, Tokuyama A201, is less expensive than Nafion membranes [170]. Non-precious and carbon materials can be used as ORR cathode electrocatalysts in MFCs because of their high corrosion resistance in alkaline environments [171]. Moreover, the most influential factor that affects the MFC performance is the formation of solid metal carbonate precipitates, most commonly Na_2CO_3 , K_2CO_3 , MgCO_3 , and CaCO_3 , in the wastewater. Such precipitates may deposit and thus obstruct the electrolyte-filled electrode pores. This occurs mainly because of carbonate or bicarbonate via the reaction of OH^- ions with CO_2 in the cathode oxidant gas [172]. Pandit *et al.* demonstrated the use of a Ralex AEM in an MFC and reported a maximum power density of 57.8 mW m^{-2} [173]. Similarly, a low-cost surface-modified quaternized poly(ether imide) membrane was used as an AEM in an MFC to study its anti-biofouling properties and internal resistance [174]. The main drawbacks of using AEMs in MFCs are that they are chemically unstable under the low pH conditions of wastewater and their ion conductivity is lower than that of Nafion.

2.3.2 Ceramic membranes for MFC

Ceramic materials are attractive for energy applications because of the various available synthetic approaches; good thermal, chemical, and mechanical stabilities; and most importantly, low costs [175]. Since the invention of the solid oxide fuel cell, ceramic materials have been used as electrodes and membrane materials for such applications [176, 177]. Most recently, MFC technology has used ceramic materials as PEMs because of their excellent properties (Figure 11).

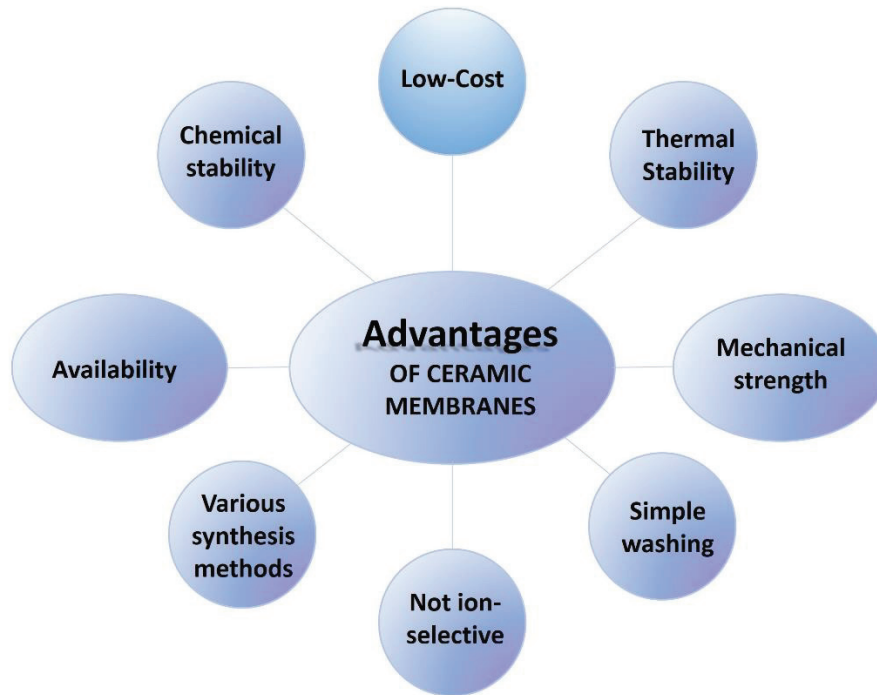


Figure 11. Some important advantages of ceramic membranes [178].

Natural earthenware and its family of ceramic membranes

Natural ceramic materials such as clay, earthenware, terracotta, etc. played a significant role in shaping the culture of ancient civilizations. These natural ceramic materials can be excavated and developed using different methods including clay material digging, mixing with suitable composites, material shaping, drying in sunlight, and finally baking in an oven. The final product is hard and brittle [179]. The use of terracotta natural clay material are among the examples representing the astonishing army of the Chinese emperor 5000 years ago [180]. The application of a ceramic material in the Baghdad battery, invented 2000 years ago, was a stunning discovery for archeologist and electrochemists [181]. The clay composite material accommodated separated copper and iron electrodes, and the container was filled with vinegar as the electrolyte. Moreover, ceramic materials are among the major components of solid oxide fuel cells, particularly as an electrolyte medium for conducting protons. The benefits of using ceramic materials in solid oxide fuel cells are their ability to withstand high operational temperatures and their adjustable porosity and thickness for ion diffusion [182].

Recently, a clayware-type ceramic material was used as a PEM in an MFC application because of its high mechanical and chemical stability, hydrophilic nature, and suitable ion exchange

capacity [183]. Some examples of MFCs with clay-based ceramic membranes studied under different conditions are shown in Table 2. Here, the MFC performance is not directly compared between membranes because of the different operational conditions used in the systems. A clay pot ceramic membrane was developed by Martínez *et al.* to achieve bioelectricity generation, as shown in Figure 12 [184]. Behera *et al.* developed a ceramic pot composed of clay minerals including 58–68% kaolinite, 15–26% illite, and 5–9% smectite. The resulting MFC setup generated a maximum power density of 16.8 W m^{-3} with a CE of 31.3% and was the first work to demonstrate this inexpensive and unique material as a membrane for an MFC system. After this successful result, the same research group used a similar earthenware pot membrane in an MFC system to treat rice mill wastewater and compared the performance to that of a Nafion membrane. The MFC with the earthenware pot membrane showed a power density of 2.3 W m^{-3} , which was nearly four-fold higher than that with a polymeric Nafion membrane [186]. In 2012, a locally purchased terracotta flower pot was used as single-chamber MFC system, and the reported power density was 33.13 mW m^{-2} with a CE of 21% [187].

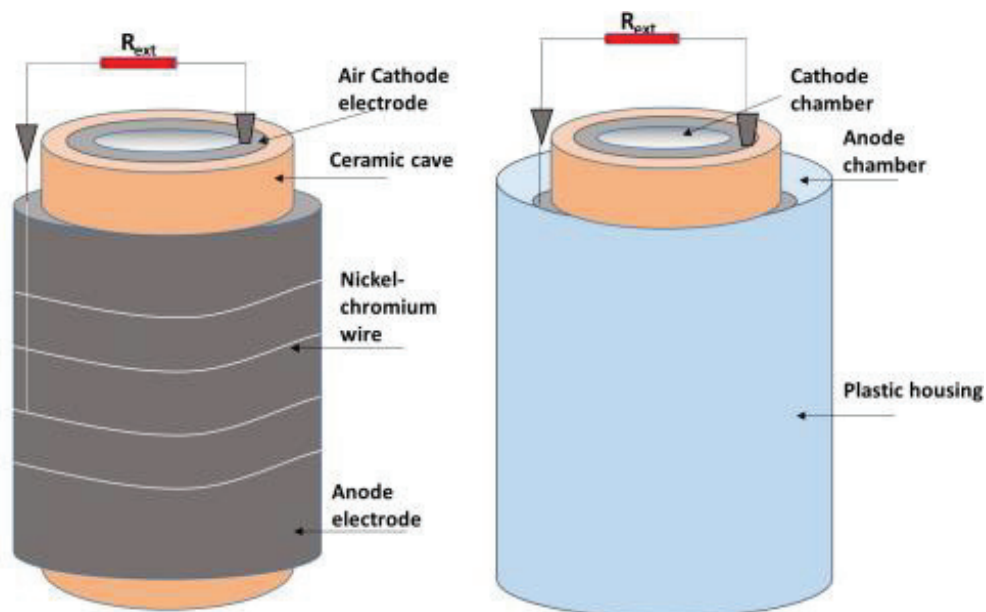


Figure 12. Single chamber ceramic MFC set-up [184].

The thickness of clayware ceramic membranes plays a significant role in proton diffusion from one chamber to another. Behera *et al.* studied the effect of membrane wall thickness on MFC system performance and concluded that a thin membrane was considerably better than a thick membrane [188]. Natural red soil containing alumina and silica and black soil containing calcium, iron, and magnesium were also used as CEMs in an MFC system. The MFC with the

red soil membrane showed a higher power density than the MFC with black soil because of the high cation exchange capacity, low pH, and high ionic conductivity of red soil [189]. Gajda *et al.* studied the scaling up of 560 serial- and parallel-connected miniature MFCs with terracotta membranes (Figure 13) using human urine as a feed anolyte and reported a maximum power density of 25.7 W m^{-3} . The application of low-cost clay ceramic-based MFC systems is particularly suitable for rural applications in developing countries for power generation in sanitation purposes [190]. The aforementioned studies demonstrated that earthenware and clayware membrane materials are a viable choice to replace polymeric ion exchange membranes because they provide a favorable environment for the metabolic reactions of bacterial species present in the chamber.

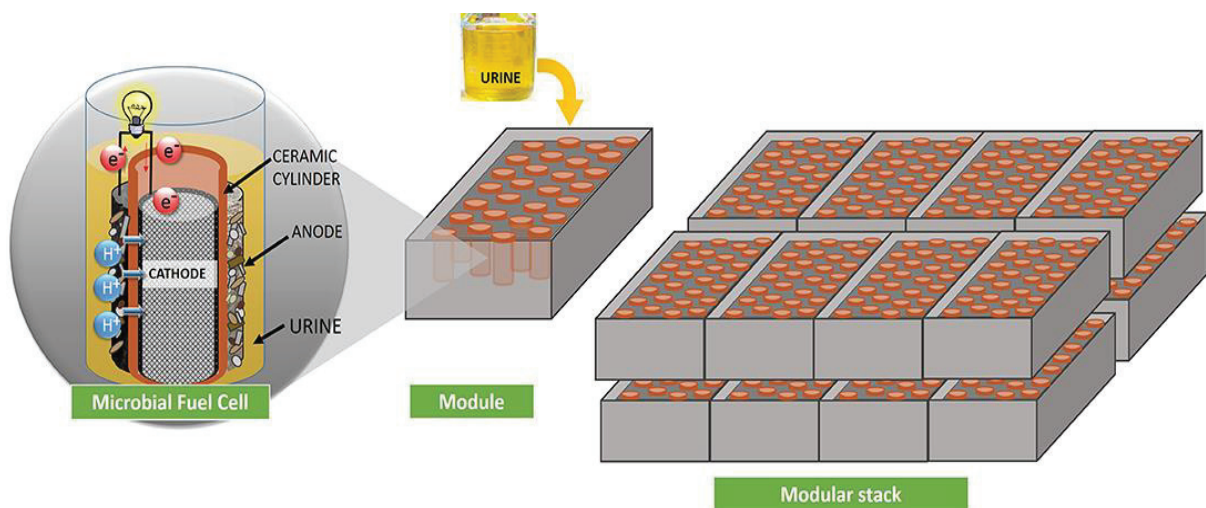


Figure 13. Miniaturized Microbial Fuel Cell in a module and 560-unit modular stack [190].

Table 2. Comparison of ceramic type, MFC configuration and performance [183].

Ceramic type	structure	Thickness (mm)	Anode chamber volume (ml)	Cathode type	Temp.	operation	Feed stock	Max. power density
Earthen [185]	pot	4	400	Aerated	26–34	38 days	Synthetic (acetate)	26.8 m W m^{-2}
Earthen [186]	pot	4	400	Air		70 days	Ricemill wastewater	0.53 W m^{-2}

2. State of the art

Earthen [191]	cylinder	5	600	Perman ganate	24–26		Synthetic (sucrose)	480.18 mW m ⁻²
Teracotta [187]	pot		800	Air	28	14 days	Hay extract	33.13 mW m ⁻²
Teracotta [192]	single chambe r	8	6	Air	22 ± 2	6 weeks	Synthetic (TYE)	2.83 W m ⁻³
Earthenw are [192]	single chambe r	8	6	Air	22 ± 2	6 weeks	Synthetic (TYE)	3.66 W m ⁻³
Clayware [193]	single chambe r		1300	NaClO		20 days	Synthetic (acetate)	6.57 W m ⁻³
Red soil [189]	pot	5	550	Aerated	33–37	22 days	Synthetic (acetate)	51.65 mW m ⁻²
Black soil [189]	pot	5	700	Aerated	33–37	22 days	Synthetic (acetate)	31.2 m W m ⁻²
Clayware [194]	pot	4	450	Air	30	75 days	Synthetic (acetate)	4.21 W m ⁻³
Clayware [195]	pot	8	26	Air	None	14 mon ths	Synthetic (sucrose)	0.74 W m ⁻³ Synthetic (sucrose)
Geothite [196]	cylinder	5	350	Air	27 ± 2	75 days	Synthetic (acetate)	17.1 W m ⁻³
Montmor illonite [195]	two chambe r	4	50	Aerated	30 ± 2	2 mont hs	Synthetic (acetate)	7.55 W m ⁻³
Terracott a [195]	cylinder	3	200	Air	22	14 days	Wastewa ter + acet ate	286 m W m ⁻²
Pyrophyll ite [197]	cylinder	2	6.4	Air	22	100 da ys	Urine	6.93 W/ m ³
Earthenw are [197]	cylinder	3.5	11.4	Air	22	100 da ys	Urine	6.85 W m ⁻³
Terracott a [198]	plates	2.5	variable	Air	22	16 days	Urine	15 W m ⁻³

Oxide ceramic membrane material

Oxide-based ceramics such as Al₂O₃, ZrO₂, TiO₂, SiO₂, etc. are widely used as membranes in electrochemical applications [199]. These membranes are easily fabricated using various methods such as intrusion, tape-casting, pressing, etc. followed by high-temperature sintering [175]. In recent years, oxide ceramic membranes have been extensively employed in wastewater treatment, electrical applications, biotechnology, food and beverage processing, semiconductors, dental applications, etc. [200-202]. Solid electrolyte ceramic materials doped with alumina has been used as an ion-conducting electrolyte for high-temperature fuel cells [203]. Moreover, inorganic materials such as TiO₂ and SiO₂ have been used as additive agents in polymeric membranes to enhance the membrane hydrophilicity, resulting in high fuel cell power generation [156, 204].

Recently, oxide ceramics have been used as membranes in MFC applications (Table 3). For instance, Pasternak *et al.* studied an alumina ceramic membrane for MFCs and achieved a power density of 2.6 W m⁻³. However, this value is less than that obtained with earthenware- and mullite-based natural ceramic membranes, mainly because of the low open porosity (< 1%) of the alumina membrane [197]. Yang *et al.* compared MFCs with zirconia and alumina membranes purchased from Sterlitech and Anodisc, respectively. Although the zirconia membrane had less oxygen and substrate diffusion, during operation, the power density of the MFC with the alumina membrane was higher than that obtained with the zirconia membrane. This was largely attributable to the smaller thickness and cylindrical microstructural pores of the alumina membrane, which led to high proton diffusion and low charge and diffusion resistances [205]. Daud *et al.* studied the long-term performance of MFCs containing zirconia ceramic membranes with different pore sizes (0.14, 0.015, and 0.0005 μm). Among them, the membrane with a pore size of 0.0005 μm resulted in the highest power density, which was attributed to its high proton conductivity and hydrophilic nature [206]. Hence, the aforementioned studies clearly demonstrated the application of oxide ceramics as membrane materials in MFC applications.

Table 3. Comparison of ceramic type, MFC configuration and performance.

Ceramic type	structure	Thickness	Anode chamber volume (ml)	Cathode type	Temp. (°C)	operation	Feed stock	Max. power density

Alumina [197]	Flat sheet	3 mm	11.4	Aerated	26–34	32 days	Anaerobic sludge	2.06 W m ⁻²
Alumina [205]	Flat sheet	63.5 μm	130	Phosphate buffer	25	60 days	Anaerobic sludge	0.12 W m ⁻²
Zirconia [205]	Flat sheet	2.6 mm	130	Phosphate buffer	25	60 days	Anaerobic sludge	0.01 W m ⁻²
Zirconia (pore size -0.14 μm) [206]	Flat sheet	2.5	16	Phosphate buffer	28	8 months	Anaerobic sludge	1.6 W m ⁻²
Zirconia (pore size -0.015 μm) [206]	Flat sheet	2.5	16	Phosphate buffer	28	8 months	Anaerobic sludge	2.0 W m ⁻²
Zirconia (pore size -0.015 μm) [206]	Flat sheet	2.5	16	Phosphate buffer	28	8 months	Anaerobic sludge	2.8 W m ⁻²

2.3.3 Ion transport mechanism of membrane

Ion transport mechanism in polymeric membrane

Polymeric membranes transport ions by means of functional groups bound to the polymer backbone. Proton diffusion proceeds favorably via either the Grotthuss or the vehicular mechanism [207].

As proposed by Theodor von Grotthuss in 1804, protons are transported in a polymeric membrane via a hopping mechanism through chains of hydrogen-bonded water molecules. This hopping or tunneling of protons from one molecule to another results in a high proton mobility of $3.6 \times 10^{-3} \text{ cm}^2 \text{ s}^{-1} \text{ V}^{-1}$. In the Grotthuss mechanism (Figure 14), a proton ion hops from one

hydronium molecule to another by the exchange of hydrogen bonds with covalent bonds via the reorientation of water molecules and hydronium ions [208]. The vehicular mechanism, on the other hand, involves protons diffusing together with H_5O_2^+ (Zundel cation), H_9O_4^+ (Eigen cation), and several water molecules [209]. These two mechanisms are examples of structural diffusion, and most polymeric membranes for proton exchange use them for proton conduction [210]. Petersen *et al.* theoretically and experimentally modeled the Grotthuss shuttling mechanism of proton transport using a perfluorinated sulfonic acid membrane (Nafion). Furthermore, some polymeric membranes use both the Grotthuss and vehicular mechanisms to transport protons [211]. For instance, a previously reported metal–organic framework composite with a polyvinylpyrrolidone membrane used both proton conduction mechanisms, and the framework aids in holding water molecules in the polymeric structure (Figure 15). This was also proved by theoretical modeling experiments [212].

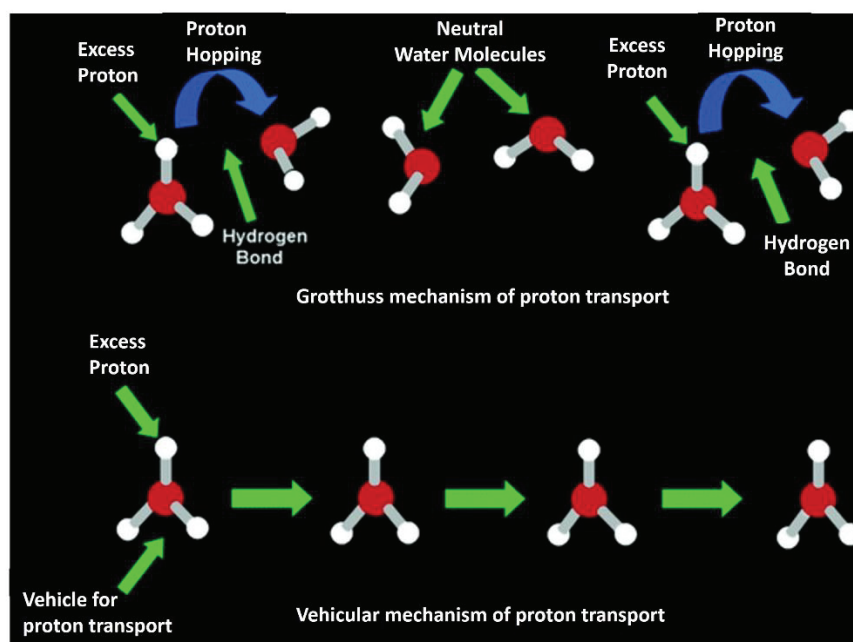


Figure 14. Proton transport mechanism (a) Grotthuss mechanism (b) vehicular mechanism [213].

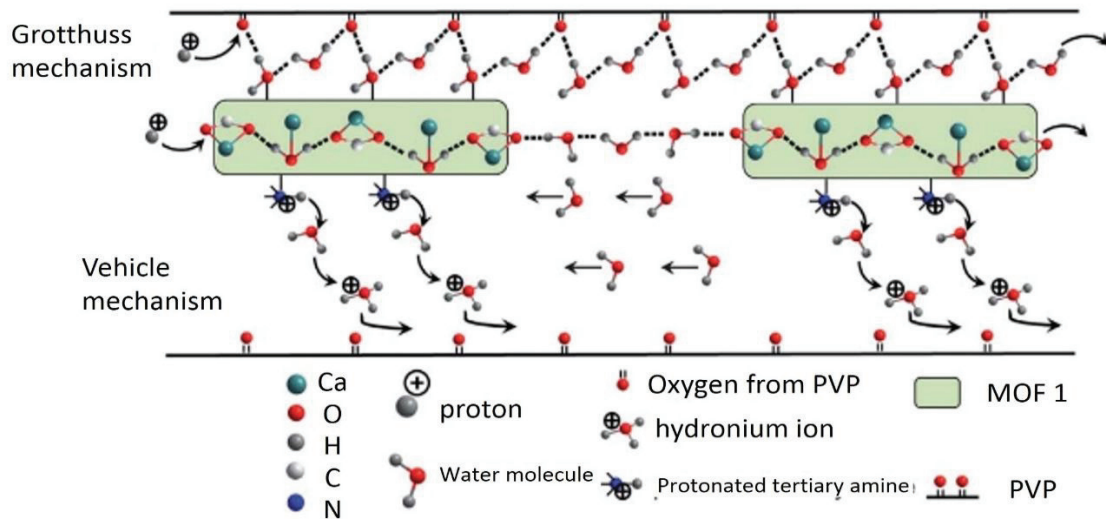


Figure 15. Combination of Grotthuss and vehicular mechanism in metal organic frame work composite with polymeric matrix [212].

Ion transport mechanism of porous ceramic membrane

Ceramic membranes transport protons from the anode to the cathode chamber by their porous structure. There are three mechanisms involved in ceramic ion transport: (1) convection, i.e., ion transport via electrolyte mechanical motion; (2) electric migration, i.e., ion transport via an electric potential developed in the anode and cathode; and (3) diffusion, i.e., ion transport via a concentration gradient developed in the anode and cathode chambers (Figure 16) [9]. The ion transport mechanism occurring in porous ceramic membranes is determined by the membrane surface characteristics, pore size, and thickness [206]. Porous membranes have no ion selectivity, and thus they freely transport protons through the pores. The membranes adsorb water molecules in the porous structure, and protons are transferred via migration and diffusion. However, the exact mechanism of proton transfer through ceramic membranes has not been studied in detail [121].

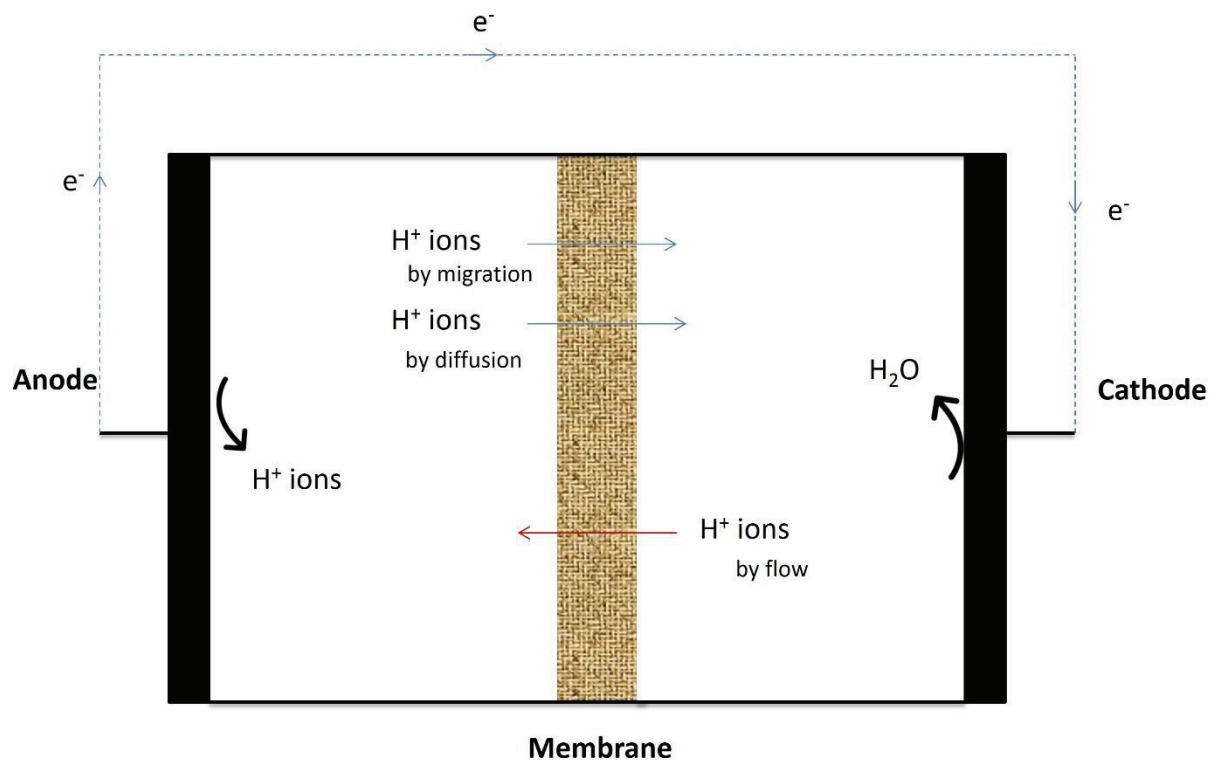


Figure 16. Ion transfer in porous membrane.

2.4 Polymer derived ceramic material

To meet the aforementioned requirements, polymer-derived ceramics (PDCs) have been found as suitable membrane materials for MFC and MBR applications. The term PDC indicates that the ceramic material was synthesized via the controlled pyrolysis of a polyorganosilicon compound [214]. Verbek *et al.* developed the first practical experimental procedure for ceramic materials derived from polyorganosilicon precursors in the early 1970s. The research group primarily fabricated non-oxide ceramics like silica carbide and silica nitride monoliths starting from polymeric precursors such as polysiloxanes, polycarbosilanes, and polysilazanes, which led to a polymer-to-ceramic transformation [215].

Polyorganosilicon precursors are potential candidates for various applications such as membranes for electrochemical devices, anticorrosion protective coatings, biomedical applications, etc. [216-218]. An increasing interest over the last few decades in developing new polymeric precursors for ceramics has led to a broad range of developed precursors [214].

Preceramic polymers are classified based on their chemical composition, with an organosilicon as the backbone with side functional groups (Figure 17).

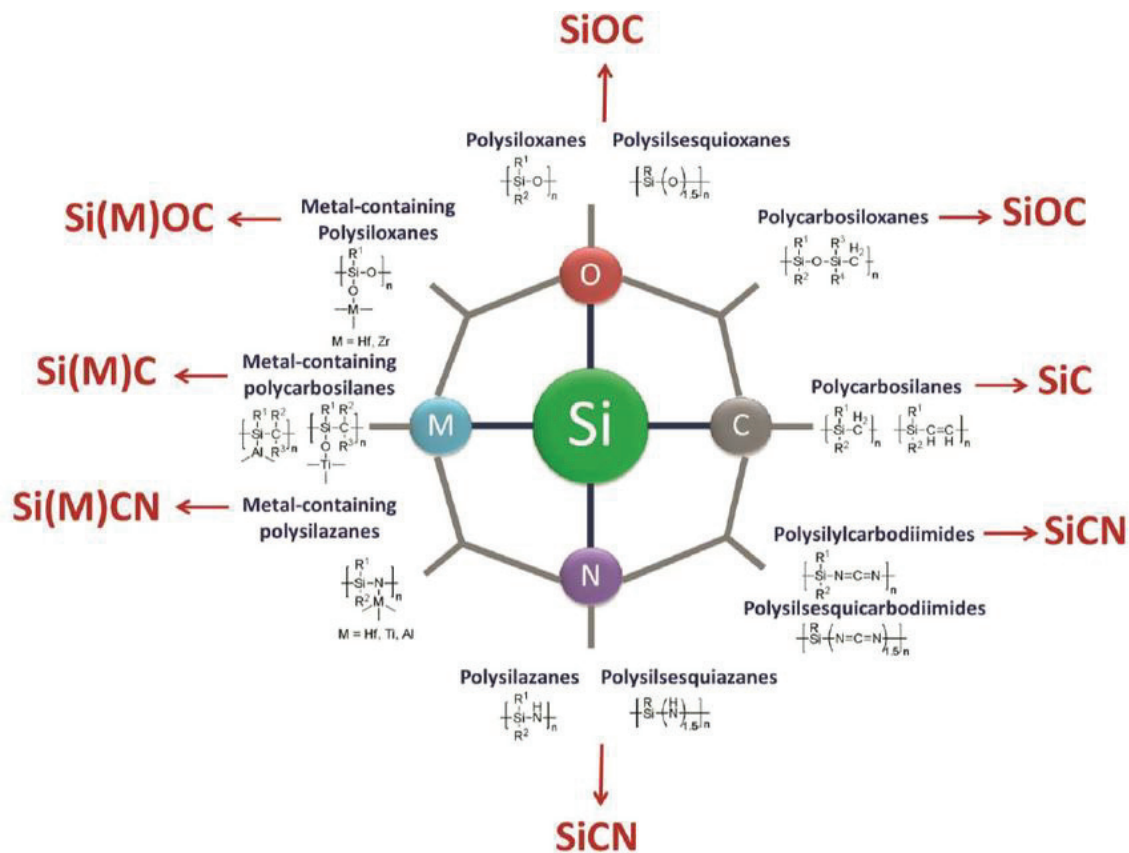


Figure 17. Overview over the main classes of silicon-based preceramic polymers [219].

Therefore, the different constituent atoms determine the final polymer classification of precursors, namely polysilanes (Si-Si), polysiloxanes (Si-O-Si), polycarbosilanes (Si-CH₂-Si), polysilazanes (Si-NH-Si), polysilylcarbodiimides (Si-N=C=N-Si), and polyborosilanes (Si-O-Si-B-Si). Each polymeric precursor has its own functionalities [220]. For instance, ceramics derived from polyborosilane precursors have a high mechanical and thermal stability due to the extraordinary creep and stress resistance of the boron-doped ceramic material [221]. Similarly, polysilazane-derived ceramics have been studied as porous ceramic supports at elevated temperatures. These materials have a high thermal stability in oxidizing and inert atmospheres over long periods of operation, with no significant changes observed in their microstructure. This is mainly because of the strong bonding nature of the final ceramic material [222].

2.4.1 Processing route

Cross-linking

Cross-linking is a mandatory step to produce a stable green body during the polymer-to-ceramic conversion process [219]. The condensation or polymerization reaction below 200 °C occurs by incorporating suitable functional groups such as vinyl or hydroxyl groups [223]. Catalyst materials have been used in the polymerization reaction to reduce the cross-linking temperature [224]. The cross-linking of the polymeric precursor after polymerization results in a mechanically stable ceramic structure due to the strong bonding [225]. Moreover, this process can yield a highly branched structure with a high molecular weight and thus increase the yield of the final ceramic material [226]. The release of gaseous molecules such as water or ethanol may occur depending on the curing mechanism during the cross-linking phase, which results in the formation of inhomogeneous structures such as bubbles and closed pores inside the polymeric material [227]. Ceramics can be formed as either dense or porous, crack-free macrostructural materials by controlling this cross-linking process [228]. Other lithographic cross-linking treatments aside from thermal such as ultraviolet radiation, X-ray irradiation, plasma irradiation, electron beams, etc. have also been used to cross-link polymeric precursors [229].

Shaping

The geometrical structure of green body were fabricated in the shapping step. The sample viscosity can be changed by melting in organic solvents, a polymer as a starting precursor material is an advantage of PDCs. This material allows for the use of various shaping techniques to obtain controlled geometric structures [230]. In addition to basic shaping methods such as pressing, tape-casting, coating, and injection molding, more advanced formation methods such as extrusion, spin-coating, and chemical vapor deposition can be used. Complicated geometrical structures can also be fabricated by fiber drawing, infiltration, electrospinning, and lithographic techniques [231]. Some examples of shaping techniques are shown in Figure 18.

Of the various shaping methods, powder pressing is one of the major techniques for fabricating ceramic materials, although tape-, slip-, and freeze-casting are also notable examples [232]. There has been growing interest in pressing for two reasons. First, many large-volume applications for structural ceramics such as wastewater filtration membranes will only be realized with low-cost products, which will likely necessitate pressing techniques [233].

Second, there is a demand for an increased quantity of products such as flat sheet membranes and tiles that are manufactured by pressing and have been in production for many years [233].

The porous structure of a pyrolyzed packed powder depends on the yield obtained from the green body, which in turn majorly depends by the behavior of the particles during packing. For the pressing technique, the powder should freely flow into and uniformly pack in the die mold [234]. In addition, homogeneous microstructures can be formed by the uniform packing of powder particles. The powder used for pressing is first uniformly ball-milled for a certain period. The packing density, particle size, and compressibility of this ball-milled powder decide the micro/meso/macrostructure and porosity of the resulting ceramic material [235]. The pressing method has been successfully used to produce silica oxycarbides, silica carbides, oxide ceramics, and silica nitrides [236-238]. In many cases, the green body fabricated *via* pressing has a higher density than those produced with other methods. This is mainly due to plastic deformation of the polymer material, which partially eliminates the porosity of the green body by mutual sliding of polymer particles and viscous flow [230]. In PDC materials, the formation of cracks during pyrolysis is less extensive, and thus there is no need for a binder. Such benefits arise from the formation of chemical bonds between individual polymer particles and the polymer itself acting as a binder during pressing [230].

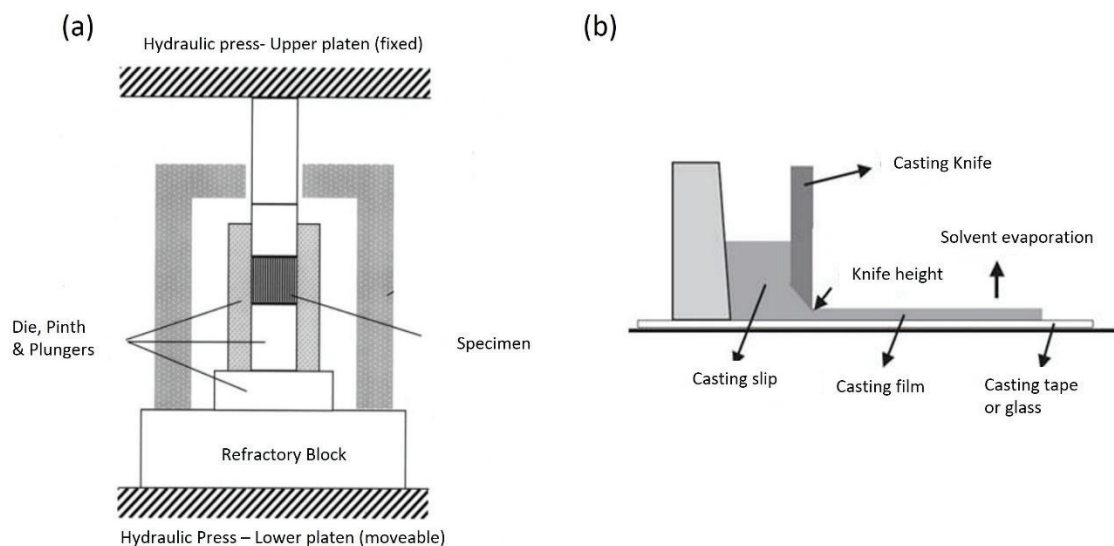


Figure 18. Shaping techniques for ceramic material (a) powder pressing (b) tape-casting technique.

Pyrolysis

The most significant step in the polymer-to-ceramic conversion process is thermal pyrolysis under inert conditions to produce a totally inorganic and non-volatile ceramic component. This step is rather complicated and can be divided into several temperature phases. Water and other solvents evaporate in the pyrolysis temperature range below 250 °C, followed by the decomposition of additional volatile oligomer molecules up to 400 °C [214]. Decomposition of the polymeric material begins at pyrolysis temperatures above 400 °C, and further increases in temperature result in structural deformation of the organosilicon polymeric precursor and the breaking of chemical bonds such as Si-H, Si-C, and C-H. Subsequently, gaseous products such as hydrogen and volatile hydrocarbons are released, and organic functional groups such as phenyl and methyl groups decompose. Finally, the decomposition of functional groups results in the formation of an open micro and mesoporous structure. Materials pyrolyzed between 400 and 800 °C, called hybrid ceramics or ceramers, have the properties of both the polymer and the ceramic materials [223].

The collapse of the micro and mesoporous structure begins in the pyrolysis temperature range between 800 and 1000 °C. The resulting ceramic material has an amorphous structure after complete transformation of the polymer to a ceramic, the covalent bonding structure of which depends on the polymeric precursor [239]. Pyrolysis temperatures above 1000 °C result in slight conversion of the amorphous phase to crystalline with a dense morphological structure [219]. These ceramics have high chemical, mechanical, and thermal stabilities due to the strong covalently bonded matrix between Si-C, Si-N, Si-B-C, etc., the nature of which again depends on the precursor [214]. The polymer-to-ceramic transformation over the range of pyrolysis temperatures is shown in Figure 19.

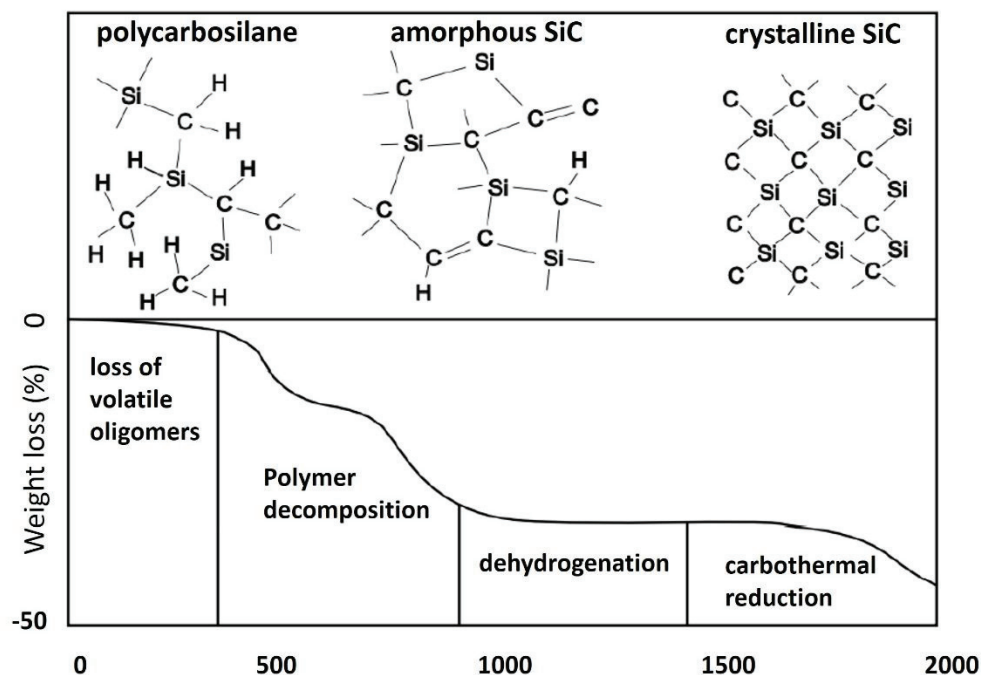


Figure 19. Weight loss and change of structure over temperature for a polycarbosilane [240].

2.4.2 Polysiloxane

Silicon-based polymeric precursors, which are classified as polysilanes, polysilazanes, polycarbosilanes, polysiloxanes, etc. [219], can be used to prepare a range of ceramic components for various applications. The ceramic materials are prepared by the controlled pyrolysis of the polymeric precursor to eliminate organic molecules, break C–H bonds, and release H₂, CH₄, or other volatile compounds [241]. The obtained ceramic materials are either crystalline or uniquely amorphous with a free-carbon phase from the preceramic polymers, which completely depends on the pyrolysis conditions [242, 243]. Among polymeric precursors, polysiloxanes are superior in terms of chemical and thermal resistance. Therefore, silicone-based materials are used as sealants, electric insulator coatings, surface treatments for glass materials, heat-resistant material, and chemically stable elastomers [244]. Jeske *et al.* developed a polysiloxane material functionalized with sulfonic acid as a proton-conducting membrane for a high-temperature fuel cell and reported that the membrane proton conductivity did not decrease even at high operating temperature, clearly illustrating the thermal stability of polysiloxane membranes for proton-conducting applications [245]. A polysiloxane precursor was synthesized *via* a traditional reaction of chloro (organo) silanes with water [214]. The

intrinsic property of the silicone material such as the viscoelastic liquid nature is within a wide range of temperature. Polmanteer *et al.* reported that the glass transition temperatures of polymethylphenylsiloxane and polydimethylsiloxane are -86 and -127 °C, respectively [246]. Cross-linked polysiloxane materials can better withstand high temperatures without forming cracks compared with other PDC materials such as polycarbosilanes, polysilanes, and polysilazanes. This specific property is helpful for shaping the precursor material into desired forms *via* casting, molding, and extrusion [244]. Other advantages of using a polysiloxane precursor for ceramics are storage and handling (no protective atmosphere required); low ceramization temperature (1000–1200 °C); and excellent chemical, mechanical, and thermal stabilities [247-249]. Polysiloxane materials can be processed using various synthetic methods to obtain porous ceramic materials with properties tailored for specific applications

2.4.3 Tailorable surface characteristics

The surface characteristics of PDCs mainly refer to the hydrophilicity/hydrophobicity, where surfaces that attract water are hydrophilic and surfaces that repel water are hydrophobic. Highly hydrophilic PDC materials have a great number of applications in various sectors which includes filtration, gas transportation, catalyst supports, biomedical applications, etc. [250-252]. Preceramic polysiloxanes are organic–inorganic polymers whose backbones usually contain Si atoms with phenyl and methyl groups, which provide highly hydrophobic characteristics during the cross-linking stage [253]. The polymer to ceramic conversion is achieved by thermal pyrolysis technique by conventional oven annealing, microwave, or laser heating, normally by processing in an inert atmosphere. The PDC surface characteristics can also be modified by the choice of precursor or by surface modification. There are a few techniques for surface modification, such as plasma, which is often used to modify the surface characteristics of preceramic polymers [254]. However, the surface characteristics of the resulting ceramics are particularly affected by the plasma technique. Prenzel *et al.* reported that pyrolyzing a methyl polysiloxane precursor at temperatures below 630 °C resulted in a hydrophobic surface, whereas pyrolyzing at 700 °C resulted in further decomposition of the hydrophobic organic moieties, leading to a more hydrophilic surface [255]. Zhang *et al.* reported that PDC surface characteristics can be modified to a greater extent by using more hydrophilic materials such as silica, titanium oxide, zeolites, etc. and adjusting the pyrolyzing temperature [256].

2.4.4 Tailorable porous structure

Controlled pore formation in ceramics can be achieved using several synthetic approaches. Material pores can be classified based on their size as micropores (< 2 nm), mesopores (2–50 nm), or macropores (> 50 nm) [257]. For MFC applications, a ceramic membrane with a porous structure facilitates the transfer of protons from the anode to the cathode chamber. However, a pore size larger than 1 μm must be avoided to prevent diffusion of the bacterial substrate through the membrane, which would limit the performance of the MFC [119].

PDCs can be fabricated with high specific surface areas and microporous structures *via* pyrolysis. Different precursors decompose and are pyrolytically converted at different temperatures, resulting in microporosity from the pyrolytic cleavage of organic groups and the pathways of the released gaseous pyrolysis products [117, 118]. Optimally high specific surface areas are typically observed at intermediate temperatures (500–700 °C) [258, 259]. Pore collapse will occur during pyrolysis above the glass transition temperature because of viscous flow [260]. Pyrolysis byproducts can block pore entrances, which also results in a loss of specific surface area. Loss of micro and mesoporosity during pyrolysis at higher temperatures can be diminished using low heating rates. Surfactants are also often used to afford mesoporous structures by directed assembly at the molecular level and subsequent surfactant removal *via* thermal decomposition or solvent extraction [261]. Strengthening of the gel network and directed assembly *via* surfactants are the major approaches for mesopore formation reported in the literature [262]. However, these approaches are expensive and result in cracks because of surfactant bubbling. Using the powder pressing technique, macroporous ceramics with a controlled pore size and porosities up to 60% can be prepared [175].

3. Aim of the work

Along with a general trend towards technological advancement, an integrated system of MFC and MBR has become increasingly popular as an alternative energy conversion system for generating bioenergy from wastewater. As a bioelectrochemical hybrid system, MFCs involved in generating electricity and wastewater treatment provide a wide range of benefits, including nutrient recovery, energy conservation, reduced sludge generation, and energy conversion. However, achieving high-energy efficiency and large-scale applicability using this technique remains a significant challenge, which could potentially be overcome by replacing the mechanically unstable and expensive polymer proton-exchange Nafion membranes of MFCs with low-cost, efficient, ceramic membranes.

Aim of this work is to produce porous ceramic membrane with proton conducting property for MFC application and additionally explore the possibility to use them as ultrafiltration membrane material for MBR application. To satisfy the demands of this application, the membrane needs a specific array of characteristics, such as hydrophilicity, chemical stability in wastewater, controlled porosity (from 20 to 40% open porosity), and pore size distribution (from 0.1 to 1 μm) that enables proton diffusivity and water permeability, while simultaneously requiring minimal oxygen diffusion. PDCs are remarkable materials with desirable properties like tailorable porous structure and surface characteristics, and improved mechanical and chemical stability as compared to those of polymeric material. Therefore, PDCs should be a suitable membrane material for MFC and MBR.

To prepare a uni-modal pore structured ceramic membrane with a pore size smaller than 1 μm , the uni-axial hydraulic pressing approach was adopted to synthesize flat sheet PDC material. Moreover, the following approach will help to produce crack free ceramic membranes with proton conducting property.

The different weight percentage of montmorillonite and $\text{H}_3\text{PMo}_{12}\text{O}_{40}/\text{SiO}_2$ fillers should act as cation exchange filler material to enhance the proton conducting property of polymer derived ceramics. Furthermore, the functional property of PDC composite membrane should be tailored by varying pyrolysis temperature from 400 to 1000 $^\circ\text{C}$. The best PDC composite membrane will be studied for MFC application

Secondly, the influence of graphitic filler material like graphene oxide and multiwall carbon nanotubes in PDC membranes pyrolysed at 1100 $^\circ\text{C}$ should be studied. The incorporation of

graphene oxide and multiwall carbon nanotube to PDC should tailor the physical properties of the composite membrane such as ion exchange capacity and mechanical stability of the membrane. The composite material will be physically characterized and the membrane performance in MFC system will be studied.

Thirdly, the PDC membrane should be functionalized with hygroscopic fillers such as TiO_2 , SiO_2 , and Tetraethylorthosilicate (TEOS) material and pyrolysed at $1100\text{ }^\circ\text{C}$. The hygroscopic filler material should increase the hydrophilic property of the PDC composite membrane. The physical characteristics, MFC performance, and water permeability in MBR applications of the composite membrane will be studied.

Finally, the PDC membrane prepared at $1000\text{ }^\circ\text{C}$ will be used as proton conducting and ultrafiltration membranes for an integrated MFC-MBR system and the generation of electricity and efficiency of wastewater treatment will be studied.

4. Materials and methods

4.1. Materials

4.1.1 Required Precursors

Commercial hydrophobic oligomeric methyl-phenyl polysiloxane powder (silres®H44, wacker chemie AG), monomeric aminopropyltriethoxysilane (APTES, ABCR Dr. Braunagel GmbH & Co. KG), Bis(trimethoxypropyl)silyl amine (BISA, ABCR Dr. Braunagel GmbH & Co. KG), ethanol solvent, ammonia solution, and deionized (DI) water. The chemical formula of some precursors are shown in Figure 20.

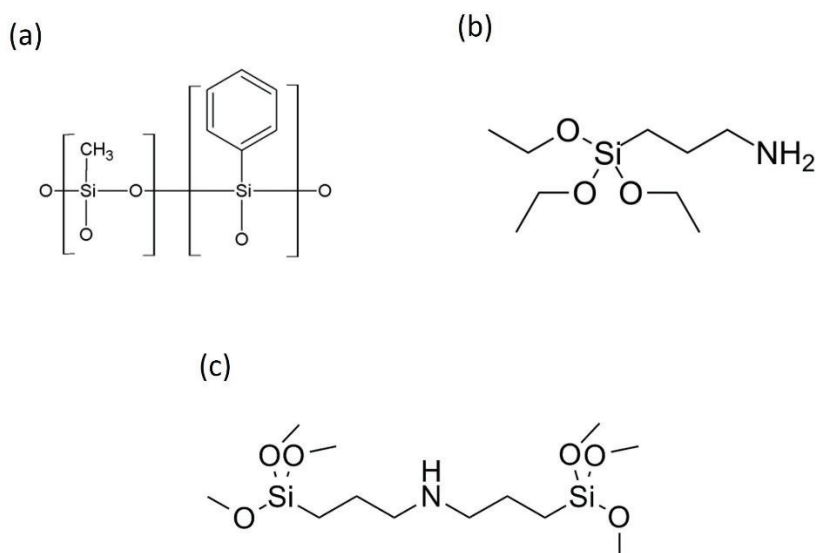


Figure 20. Structural chemical formula of precursors (a) methyl-phenyl polysiloxane (b) aminopropyltriethoxysilane (c) Bis(trimethoxypropyl)silyl amine.

4.1.2 Filler materials

Montmorillonite K10 (sigma aldrich), phosphomolybdenic acid hydrate ($\text{H}_3\text{PMo}_{12}\text{O}_{40} \cdot x\text{H}_2\text{O}$, alfa aesar), tetraethylorthosilicate (TEOS, sigma aldrich), Graphene oxide, and Multiwall carbon nanotubes (MWCNT, nanochem), Titanium oxide (TiO_2 , alfa aesar), Silica oxide (SiO_2 , sigma aldrich), quaternary dodecyltrimethylammonium chloride (alfa aesar), Potassium permanganate (KMnO_4 , sigma aldrich), Hydrogen peroxide (30 wt% H_2O_2 , sigma aldrich),

Hydrochloric acid (37 % HCl, sigma aldrich), Sulfuric acid (conc. H₂SO₄, sigma aldrich). Some of the structural chemical formula of filler material shown in Figure 21.

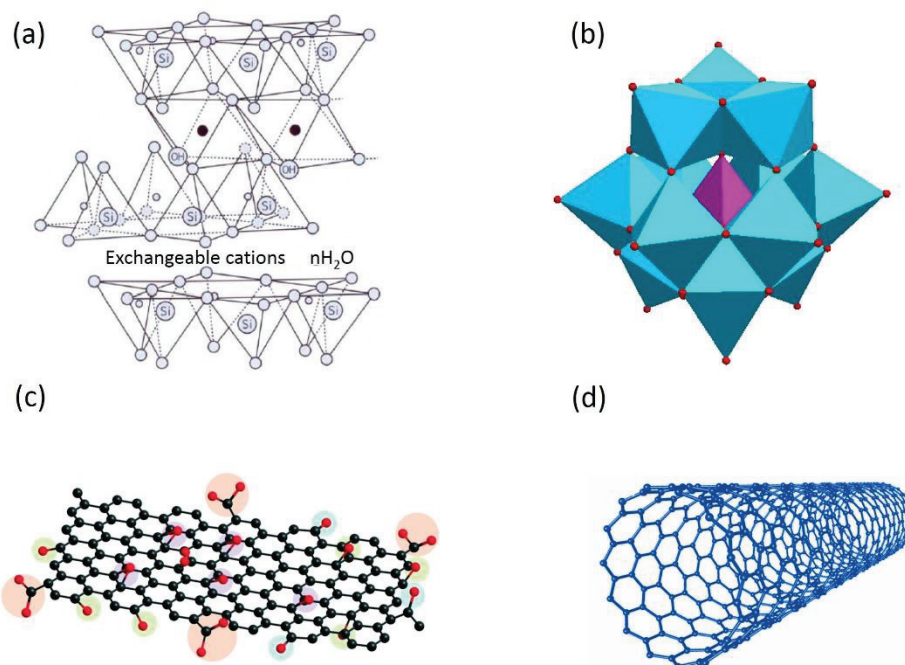


Figure 21. Structural chemical formula of precursors (a) Montmorillonite (b) Phosphomolybdic acid (c) Graphene oxide (d) multiwall carbon nanotube.

Synthesis of H₃PMo₁₂O₄₀/SiO₂ (PMA) filler

The filler material was prepared using a method previously developed by Li *et al.* [263] with minor modifications. First, 1.99 g of quaternary dodecyltrimethylammonium chloride was dissolved in 200 mL of 2.5 M HCl aqueous solution in a 250-mL conical flask followed by the addition of 17.83 mL of TEOS and 4.69 g of H₃PMo₁₂O₄₀·H₂O under stirring at a speed of 800 rpm for 1 h. After that, the mixture was aged at room temperature for 4 h, separated by filtration, thoroughly washed with ethanol, and dried inside an oven at a temperature of 80 °C for 24 h.

Synthesis of Graphene oxide filler

GO was produced from graphite powder using a modified Hummers method. Briefly, 3 g of graphite powder was added to 70 mL of concentrated H₂SO₄ and well agitated for several minutes followed by the addition of 9 g KMnO₄ using an ice bath. The solution was transferred to a flask containing 150 mL of deionized (DI) water and then placed in an oil bath at 40 °C under stirring. After vigorously stirring for 15 min, the oil temperature increased to 95 °C, after

which the reactants were stirred for 15 more minutes. Subsequently, 500 mL of DI water were added to the reaction mixture followed by the slow addition of 15 mL H₂O₂ (30 %) and overnight stirring at room temperature. After that, the liquid was washed with concentrated HCl and DI water until its pH reached 7 and then ultrasonically agitated for 30 min. At this point, the aqueous dispersion contained two different materials: GO and non-exfoliated graphite oxidized to graphite oxide, which were easily separated by centrifugation.

Pretreatment of multiwall carbon nanotube filler

Functionalization of MWCNT is performed using mixture of HNO₃ and H₂SO₄ acids in a molar ratio of 1:3 to create a solution with a final volume of 20 ml. 100 mg of pristine MWCNTs are added to this solution and the mixture is treated by magnetic stirring vigorously for 3 h at room temperature. The functionalized MWCNTs are then purified by extraction from the residual acids by dilution with distilled water and centrifuge filtration the solutions until the pH is approximately 6. After the purification process, the oxidized samples are dried at 80°C for overnight [264].

4.2. Synthesis procedure of PDC membranes

4.2.1. Polymer derived ceramer and ceramic composite with montmorillonite and H₃PMo₁₂O₄₀/SiO₂

A scheme of the synthesis procedure is shown in Figure 22a. The as-prepared PMA composite or montmorillonite filler was dispersed in ethanol for 30 min *via* ultrasonication followed by the addition of a mixture of H44 and APTES with the subsequent polymerization for 3 d under reflux at a temperature of 70 °C (a solution containing 3.27 mL of NH₃ in 3 mL of water was used as a catalyst). After removing the solvent, drying, cross-linking in air at 200 °C for 2 h, and grinding using a high-energy ball mill, the resulting fine powder was pressed to a monolithic membrane. The fabricated membranes were pyrolyzed at temperatures of 400, 500, 600, and 1000 °C under nitrogen atmosphere (see Figure. 22b).

Sample notation

Sample nomenclature was based on the notation PDC:PMA_{xx}:M_{yy}-*zzz*, where PDC represents SiOC, PMA stands for H₃PMo₁₂O₄₀/SiO₂ with weight fraction *xx*, M denotes montmorillonite with weight fraction *yy*, and *zzz* is the pyrolysis temperature (in °C). The sample compositions and their nomenclatures are listed in Table A1 in appendix.

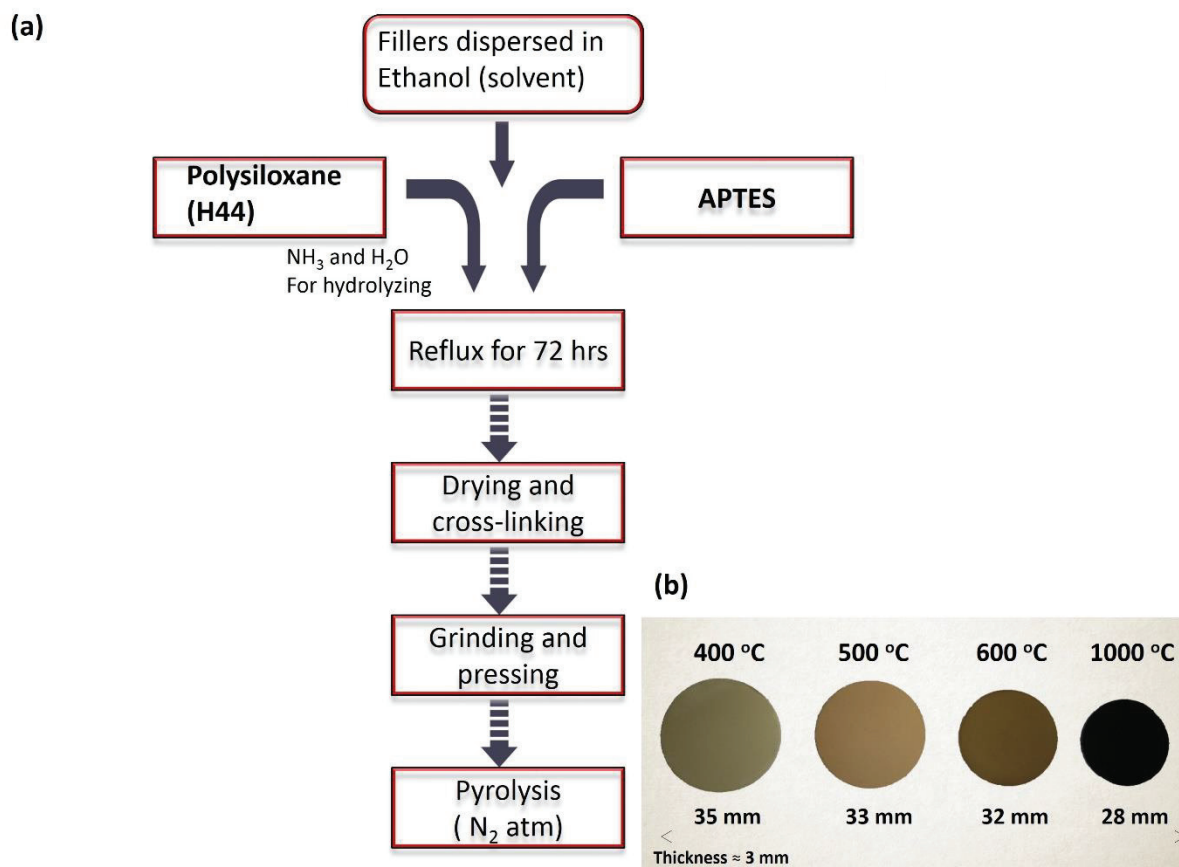


Figure 22. (a) Process scheme of PDC membranes, (b) synthesized PDC membranes at different pyrolysis temperature.

4.2.2 Graphitic carbon functionalized polymer derived ceramics

In this synthesis, an equimolar ratio of methyl-phenyl polysiloxane (H44) and bistrimethoxysilylpropylamine (BISA) (1:1) was dissolved in the ethanol dispersion of a filler material inside the round bottom flask placed in an oil bath at 70 °C under stirring. Subsequently, 3.27 mL of ammonia and 3 mL of distilled water were slowly added to the reaction mixture. The reaction was performed under reflux until a stable polymeric solid material was obtained. After that, the solvent was removed by drying and cross-linking in air – first at 140 °C for 1 h and then at 200 °C for 2 h. The cross-linked PDC sample was ground to fine powder *via* high-energy ball milling and pressed to a monolithic structure. The produced membranes were pyrolyzed at 1100 °C for 4 h under nitrogen atmosphere. The schematic representation of the synthesis procedure is shown in Figure 23.

Sample notation

Sample nomenclature was based on the notation PDC:xGO-zzz and PDC:yCNT-zzz, where PDC represents SiOC, GO stands for Graphene oxide with weight fraction x in the starting material, CNT denotes multiwall carbon nanotube with weight fraction y , and zzz is the pyrolysis temperature. The sample compositions and their nomenclatures are listed in Table A2 in appendix.

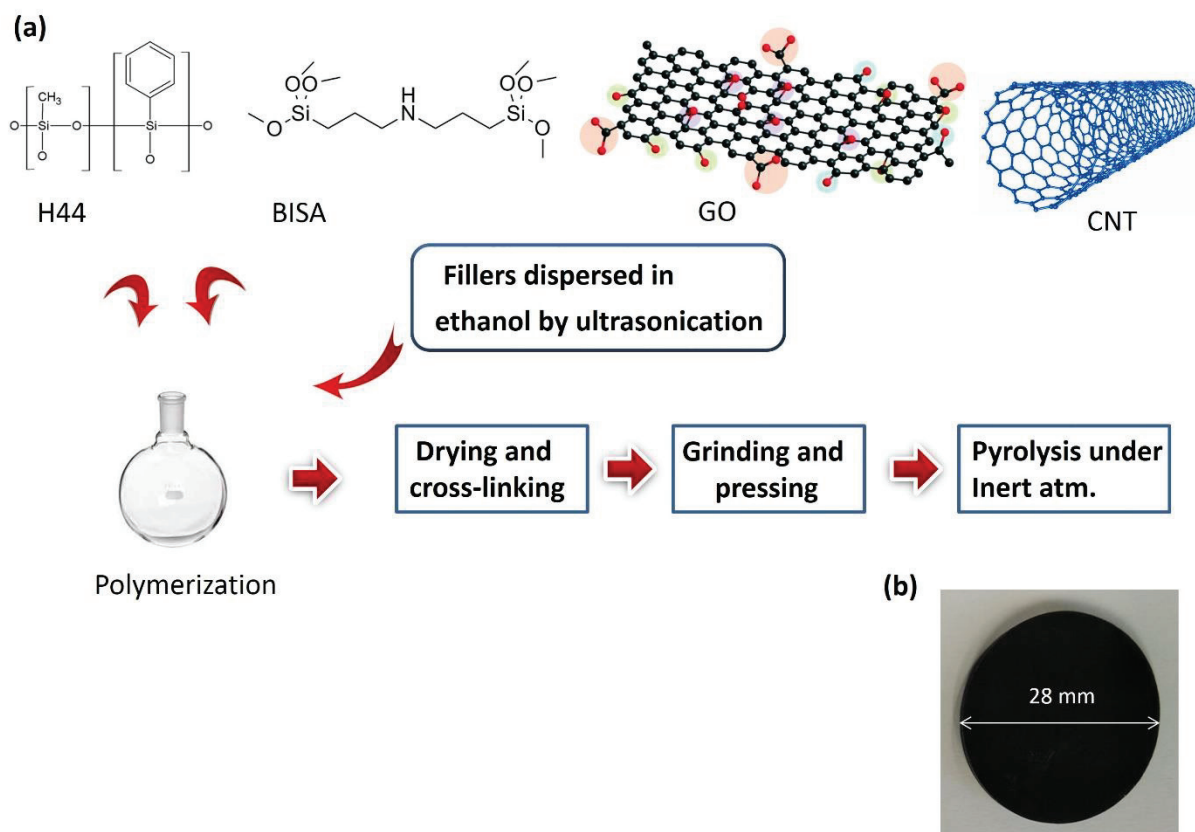


Figure 23. (a) Synthesis flowchart of PDC composite membrane (b) Sample prepared at 1100 °C.

4.2.3. Polymer derived ceramics composite with hygroscopic filler

The hygroscopic filler dispersed in ethanol solvent and the mixture was ultrasonicated for 30 minutes, and agitated using a vortex device. Once the flask reached 70 °C, 10.87 g of Methylphenyl polysiloxane (H44), 23.49 ml of Aminopropyltriethoxysilane (APTES), 3.27 ml of ammonia, 3 ml of demineralized water, and the correspondent wt% of the additional precursor (15 wt% of TEOS) or filler (15 wt% of SiO₂ or TiO₂) were added to the flask, for the bare sample only H44 and APTES were used as precursors. Following, the reaction was left stirring at 70 °C, under refluxing conditions, for 72 hours [19]. After removal of the solvent, drying,

cross-linking in air at 200 °C for 2h, followed by grinding to fine powder using high energy ball milling, and pressing the sample into a monolith, the membranes were pyrolysed at 1100 °C under nitrogen atmosphere.

Sample notation

Sample nomenclature was based on the notation PDC:TiO₂-zzz, PDC:SiO₂-zzz and PDC:TEOS-zzz, where PDC represents SiOC, TiO₂ stands for Titanium oxide, SiO₂ stands for silica oxide and TEOS stands for SiO₂ derived from Tetraethyl orthosilicate and zzz is the pyrolysis temperature. The sample compositions and their nomenclatures are listed in Table A3 in appendix.

4.4. Characterization

4.4.1 X-ray diffraction

X-ray diffraction (XRD), is a technique that measures the three dimensional structure of crystalline samples. XRD is used in various fields, from biochemistry to materials science. Briefly, X-rays - electromagnetic radiation with wavelengths between 0.01 to 10 nm is pass onto the material, and the waves interact with the atoms in the sample and are reflected in a characteristic manner [265]. The result is a diffraction pattern that depends on the size and position of the atoms in the sample; subsequently, the molecular structure of the substance can be deduced. The minimal distance between two signals or reflections that can still be resolved approximately resembles half the wavelength of the radiation, small distances between atoms can be distinguished. For analysis, the material is mounted on a platform within the X-ray diffraction machine and illuminated using a monochromatic beam of X-ray radiation of one specific frequency [266]. This yields a two dimensional diffraction pattern; illuminating the crystal from various different angles yields a collection of these patterns, which can then be translated into a three dimensional crystal structure using Fourier transformation, a mathematical analysis method [267].

For XRD measurements, the samples were finely grounded into powder. The powder is compacted in the sample holder of the diffractometer (SEIFERT XRD 3003). The device uses Cu-K α radiation with a wavelength of 0.154 nm at 40 kV and 40 mA. The Data is recorded starting from 10 to 80 °C in 0.025 °C steps. The software package X'pert HighScore and the database PDF-2 (JCPDS) were used for analysing the observed data.

4.4.2 Scanning electron microscopy (SEM)

To obtain images of the material macrostructure, the scanning electron microscope is used to detect surface morphology, pore structure, defects, phases, and nanoparticles. Through the composition of the precursors, differences in the macro and microstructure are expected to be found, these variances are projected to help explain changes in the functional properties of distinctive samples [268]. The SEM is a resourceful device that allows a sample to acquire surface morphology. It produces an interaction between the electron beam and the sample atoms by using a high-energy electron beam centered on the sample surface under high vacuum circumstances. The detector therefore identifies the reflection of components of the beam electrons (back-scattered electrons) and sample electrons emission (secondary electrons) [269]. To samples were analysed by using the instrument model Camscan Series 2, Obducat CamScan Ltd was used. Before starting the study, the samples were sputtered with gold. Images with magnifications ranging from 25000x to 100000x have been obtained with distinct compositions for both the monolith surface and powder.

4.4.3. Transmission electron microscopy (TEM)

The transmission electron microscopy is used to identify the surface morphology of the material and dispersion of nanoparticles. This technique uses a thin film of the sample irradiated by a beam of electron in a uniform current density. The energy of electron use in the instrument is 60 – 150 keV. The irradiated electron distributed behind the sample and observed the image with four-stage lens system on a fluorescent screen. This technique mainly used for detecting the materials in nano dimensional range. A TEM model Titan 80-300 ST, FEI Instrument was used for analysis. The sample was prepared by dispersed the sample in ethanol, placing a drop of solution in copper grid coated, and then drying under open air condition. The copper grid were mounted in the high vacuum chamber TEM instrument for analysis.

4.4.4 Raman spectroscopy

Raman spectroscopy can be used to analyze the structure of a compound, especially vibrations and rotations on the molecular level. A highly focused laser beam, the frequency of which can cover the ultraviolet to infrared spectrum is shone onto the sample and interacts with various molecular vibrational states; as a result, the reflected laser beam has a different energy from the incident beam, which can then be analyzed using a detector. Raman spectroscopy is built on the principle of inelastic scattering. Instead of simply bouncing off a molecule, if an incoming photon from the laser beam provides the energy that correlates to the difference between the

ground state and an excited stage of a molecule, the photon will be absorbed by the molecule, which acquires a temporary activated stage [270, 271]. When relaxing back into the ground state, a photon will be emitted with a different energy. Hence, the original laser photon interacts with the molecule and changes its wavelength, i.e. energy, in the process. The change of energy and wavelength is also called Stokes shift. The more polarizable a molecule is along its vibrational axis, the stronger the signals that can be detected with Raman spectroscopy. Thus, Raman spectroscopy allows us to gain insight into the vibrational states of the molecules and therefore lets us analyze its molecular structure [272].

Raman spectra were recorded at ambient condition on a LabRam ARAMIS (Horiba Jobin Yvon) Micro-Raman spectrometer equipped with a laser working at 785 nm and less than 20 mW. The usage of a 50x objective (Olympus) with a numerical aperture of 0.75 provides a focus spot of about 2 μm diameter when closing the confocal hole to 200 μm . The spectra were collected in the range from 800 cm^{-1} to 2000 cm^{-1} with a spectral resolution of approximately 1.2 cm^{-1} using a grating of 1800 grooves/mm and a thermoelectrically-cooled CCD detector (Synapse, 1024 x 256 pixels). Each spectrum was baseline corrected with the 'LabSpec' software (Horiba Jobin Yvon).

4.4.5 Fourier Transform Infrared Spectroscopy

Fourier-transform infrared spectroscopy (FTIR) is a method to analyze the structure of compounds in various disciplines. The basic operating principle of a spectrometer is that the sample is illuminated by radiation of a certain wavelength; the sample will interact with the electromagnetic radiation in a specific way, depending on its properties, and reflect it in a characteristic way; the reflected light is then detected, and the difference between the original electromagnetic beam and the beam that arrives at the detector can then be used to get information about the sample [273]. In an FTIR, the original infrared beam is split between a moving mirror and a stationary mirror in a so-called Michelson Interferometer. This produces a characteristic interference pattern, which will be modulated after interacting with a sample based on the wavelength of light that the sample absorbs. The important feature of an FTIR is that it used polychromatic radiation to interact with the sample; the combined information will then be analyzed and split in its basic elements, which can then be analyzed, using Fourier Transformation [274]. FTIR can be used to analyze the structure of a compound, detect impurities, elucidate whether material has deteriorated, and many other properties.

For our measurement, we use Bruker equinox 55 with ATR unit. The samples were ground into fine powder, and it compacted in the sample holder and irradiate the radiation through diamond crystal and observed the spectrum.

4.4.6 Nitrogen adsorption/desorption

The nitrogen adsorption porosimetry was used to study the micro and mesoporosity of the samples in different compositions. It was possible to determine the specific surface area, and to generate the adsorption-desorption graph, which states the micro (Pore size < 2nm), meso (Pore size < 2 – 50 nm) and macroporus (Pore size > 50 nm) structure of the material [275].

The equipment used was the Belsorp II Mini - Bel Japan, Inc. The temperature of liquid nitrogen is approximately -196 °C, and the amount of adsorbed nitrogen was calculated by measuring the change of the gas pressure. The Brunauer-Emmett-Teller (BET) theory was used to analyse the specific surface area of the material. Before analysis the samples remained in vacuum conditions for three hours at a temperature of 120 °C, this pre-treatment aimed to remove all water content in the samples.

4.4.7 Mercury Intrusion method

The mercury intrusion was carried out to quantify the open porosity of samples in all the various compositions. At the same time, the distribution of pore size, the average pore size and the total open porosity percentage could be determined. This was the only characterization that also tested the pressing pressure of 191 MPa in order to evaluate the pressure influence in these characteristics. The size of the pore is determined by the pressure needed to penetrate liquid mercury into the material pores. Because larger pores require less pressure to be filled with mercury, they are first filled, therefore the pressure applied during the experiment rises to fill the lower pores. Because of its un wetting nature, mercury is the preferred liquid [276]. The device used was POROTEC GmbH, Mercury Porosimeter Pascal 140 and 440, which allows the measurement of pores below 200 micrometers, up to 4 nanometers. For the narrower pores, this device utilizes a maximum pressure of 4000 bar. Total porosity, average pore size, and distribution of pore size were evaluated in each composition's tiny cylindrical samples.

4.4.8 Water and heptane adsorption

The surface characteristics of the material tells the hydrophilic and hydrophobic nature of the material by using water and n-heptane as polar and non-polar adsorption solvent, respectively [256]. The surface characteristics of the materials were analyzed by placing the 0.5 g of dried

PDC powder composite material inside a closed Erlenmeyer flask filled with the solvent (water or heptane, respectively) in equilibrium with its vapor phase at room temperature. Samples were weighed at the start and end of a 24 h measurement period in order to determine the vapor adsorption of the material. Later, the adsorption of solvent was recalculated into mmol/m² using the BET specific surface of the materials. The results were optimized based on water and heptanes ratio factor. When the water/heptane ratio is higher than one, the studied material is assumed to possess hydrophilic properties or else material tends to hydrophobic nature.

4.4.9 Acid and base titration method

This method determines the Ion exchange capacity (IEC) of the membrane. The IEC states the amount of protons exchanged per gram of material [277]. First, the membrane was equilibrated by soaking in 100 mL of 1 M HCl solution for 72 h, after which it was rinsed with D.I. water to remove the adsorbed ions from the membrane surface and transferred to 50 mL of 1 M NaCl solution for 24 h to exchange H⁺ and Na⁺ ions during equilibration. Finally, the membrane was removed from the reaction system, and the remaining medium was titrated with 0.005 M NaOH solution to determine the amount of H⁺ ions present. The IEC obtained was expressed in milliequivalents of H⁺ per gram of dry membrane as per Equation (5).

$$\text{IEC} = (V_{\text{NaOH}} \times M_{\text{NaOH}})/W_{\text{dry}} \quad \dots (5)$$

Where, V_{NaOH} – Volume of the NaOH solution consumed;

M_{NaOH} – Molarity of NaOH (0.005 M);

W_{dry} – Weight of the dry sample.

4.4.10 Concentration cell test

The concentration cell method were used to determine the cation transport number of the membrane. The cation transfer number determines the fraction of the cations transferred through membrane from one chamber to other by a specified ion. The cation transport number (t^+) was estimated using a dual-chamber tank, whose anode and cathode chambers were filled with 0.5 and 0.005 M NaCl solutions, respectively, to create an osmotic drag concentration gradient. Two identical Ag/AgCl reference electrodes were used to monitor the potential difference between the closest points of the membrane sides over time. The commercial Ag/AgCl reference electrode (saturated with 3M KCl) purchased from Sigma Aldrich were used for this study. The value of t^+ was estimated using Equation (6).

$$E_v = \frac{RT}{F} (2t - 1) \ln \left(\frac{C_1}{C_2} \right) \quad (6)$$

Where,

E_v – Potential difference at the nearest point of the membrane (mV);

R – Gas constant; F – Faraday constant ($C \text{ mol}^{-1}$)

T – Temperature (K); t^+ – Cation transport number

C_1 – Anode chamber concentration (0.5 M)

C_2 – Cathode chamber concentration (0.005 M).

4.4.11 Oxygen permeation cell test

The concentration of oxygen diffusion from one chamber to another through membrane were measured using oxygen permeability method. The high diffusion of oxygen from cathode to anode decreases the MFC performance, so the ideal membrane should have low oxygen permeability. The oxygen diffusion coefficients of the produced membranes were measured by filling the chamber 1 with D.I. water and purged with N_2 gas for 30 min to reach the anaerobic state with an oxygen concentration of $< 0.02 \text{ mg L}^{-1}$, whereas chamber 2 (also filled with D.I. water) was aerated continuously to maintain a near-saturation level of dissolved oxygen (DO). The oxygen concentration in the chamber 1 chamber was monitored at regular intervals of 15 min using a DO probe, and the oxygen mass transfer and diffusion coefficients were estimated using Equation (7) and (8), respectively.

$$k_o = -\frac{v}{At} \ln \frac{C_{oc} - C_{oa}}{C_{oc}} \quad (7)$$

$$D_o = K_o * L_{th} \quad (8)$$

Where,

v – Volume of the chamber (cm^3)

A – Area of the membrane (cm^2)

t – Time (s)

C_{oc} – Oxygen concentration at chamber 2

C_{oa} – Oxygen concentration at chamber 1

K_o – Oxygen mass transfer coefficient

D_o – Oxygen diffusion coefficient

L_{th} – Thickness of the membrane

4.4.12 Ring-on-Ring bending test

The mechanical stability of the membrane determines how strong the membrane is for MFC and MBR application to withstand the hydraulic pressure of water in the chamber. According to German Standard Code DIN 52 292, ring-on-ring bending test is carried out to measure the bending strength of the ceramic membrane. The test samples, with a radius r_3 and a thickness S , were placed on a supporting ring while the force was applied with a load ring perpendicular to the sample surface. A Zwick/Roell material-testing machine type Z005 (Zwick/Roell GmbH, Ulm, Germany) equipped with a 5 kN load cell was used to measure the maximum force F at the moment of failure. The ratio $r_1 : r_2$ between the radius of the load ring r_1 and the supporting ring r_2 was set to 1:5. The initial load was set to 0.5 N, the test velocity to 0.5 mm/min and the number of trial samples was three. For all samples, the Poisson's ratio of $\mu = 0.12$ was assumed. The bending strength σ in mega pascal (MPa) was calculated followed the equation 9.

$$\sigma = \frac{3(1+\mu)}{2\pi} \left[\ln \frac{r_2}{r_1} + \frac{(1-\mu)}{(1+\mu)} \cdot \frac{r_2^2 - r_1^2}{2r_3^2} \right] \cdot \frac{F}{S^2} \quad (9)$$

4.5. Microbial fuel cell and Membrane bioreactor

4.5.1 Microbial fuel cell setup and operation

MFCs were fabricated by 30 mm thick poly-(methyl-methacrylate) fiber sheet with certain working volume for the anodic and cathodic chambers. The Nafion membrane (Fuel cell store, USA) was used as a PEM for the control MFC after pre-treating with 3% H_2O_2 solution for one hour followed by dipping in D.I. water for 2 h. The pieces of carbon felts used as the anode and cathode were pre-treated by a sequence of washing with 1 N HNO_3 , 30% ethanol, and D.I. water until reaching the neutral pH, followed by drying in a hot air oven at 100 °C. The dried carbon felt pieces were subjected to thermal treatment in a muffle furnace at 400 °C for 30 min and then stored in vacuum desiccators for further use after cooling. The anode and cathode were

connected with concealed copper wires, and the membranes were glued to a Teflon gasket sheet using specified proportions of water-resistant resin and glue.

The operating voltage (OV) was measured over a 100 Ω external resistance. The MFCs were inoculated with anaerobic mixed consortia collected from a septic tank at the Indian Institute of Technology, Kharagpur after heat pre-treatment (100 °C for 15 min) with volatile and total suspended solids concentrations of 19.9 and 30.2 g L⁻¹, respectively. Synthetic wastewater with sucrose as a carbon source was supplied as the feed for all MFCs. The feed composition was adopted from the work of Jadhav *et al.* with an organic matter concentration of around 3 g of COD L⁻¹ supplemented with trace nutrients and having pH of 7.4. [278]. The feed composition of synthetic wastewater was prepared by adding 900 mg/l sucrose, 1500 mg/l NaHCO₃, 318 mg/l NH₄Cl, 27 mg/l K₂HPO₄, 9 mg/l KH₂PO₄, 250 mg/l CaCl₂.2H₂O, and 64 mg/l MgSO₄.7H₂O. Trace metals like Fe, Ni, Mn, Zn, Co, Cu, and Mo were added and its compositions are 10 mg/l FeSO₄.6H₂O; 0.5 mg/l NiSO₄.6H₂O; 0.5 mg/l MnCl₂.4H₂O; 0.106 mg/l ZnSO₄.7H₂O; 0.106 mg/l H₃BO₃; 50 μ g/l CoCl₂.6H₂O; 50 μ g/l (NH₄)₆Mo₇O₂₄.4H₂O and 4.5 μ g/l CuSO₄.5H₂O. The DI water were used as catholyte in the cathode chamber of the MFCs. All MFCs were operated in an open environment with ambient temperature of 28 \pm 2 °C. MFCs were operated under batch mode at a fresh feeding frequency of 3 days and to verify the precision of the results each MFC was operated for 15 feed cycles to achieve representative performance results.

4.5.2 Analytical measurements

The potential values and generated currents were measured using a digital multi-meter with a data acquisition unit (Agilent Technologies, Malaysia). Polarization was performed by varying the external resistances from 10,000 to 10 Ω using a variable resistance box (GEC 05 R Decade, Renown Systems, Kolkata, India), and the corresponding stable voltages at all external resistances were recorded at 30-min time intervals using a data acquisition unit connected to a personal computer. Normalized volumetric power density was expressed with respect to the volume of anodic chamber according to Equation (10).

$$P_{V,\max} = \frac{V^2}{Rv_{an}} \quad (10)$$

Where, $P_{V,\max}$ is the volumetric power density (W m⁻³); V is the acquired voltage (V); R is the external resistance (Ω); and v_{an} is the volume of anodic chamber (m³).

The total internal resistance of the MFC was estimated from the slope of the linear portion of the polarization plot (voltage vs. current density). Columbic efficiency (CE) was calculated by integrating the measured current over time with respect to the maximum available coulombs associated with the organic matter *via* Equation (11) [279].

$$CE = \frac{M_s \int_0^t I dt}{F b_{es} V_{An} \Delta COD} \quad (11)$$

Where, M_s is the molecular weight of the substrate (g mol^{-1}), ΔCOD is the change in the substrate concentration over a batch cycle (g L^{-1}), V_{An} is the liquid volume of the anodic chamber (L), F is Faraday's constant (96485 C mol^{-1}), and b_{es} is the molar amount of electrons generated during the oxidation of one mole of substrate ($\text{mol of e}^- \cdot \text{mol of substrate}^{-1}$). For the samples collected from the anodic chamber of MFCs at regular time intervals Chemical oxygen demand (COD) values were estimated by a closed reflux method according to the procedure described in Standard Methods [280]. Normalized energy recovery (NER) was also assessed and expressed based on the volume of wastewater treated over time (kWh m^{-3}) as per Equation (12) [281]

$$NER [\text{kWh/m}^3] = \frac{\text{Energy output}}{\text{Treated wastewater volume}} \quad (12)$$

The power recovery from MFCs using different membranes was analysed in terms of the corresponding power/cost ratio as per Equation (13) [282]

$$\text{Power recovery} = \frac{P_s \left(\frac{\text{mW}}{\text{m}^2} \right)}{\text{Cost} \left(\frac{\text{€}}{\text{m}^2} \right)} \quad (13)$$

Where,

P_s is the power density (based on membrane surface area) of the *MFC*,

Cost is the cost per unit area of the membrane.

4.5.3 Ultrafiltration setup for MBR

The water permeability experiments were measured using the setup shown in Figure 24. The membrane was inserted in the setup with effective filtration area of 3.5 cm^2 . All experiments were measured at ambient temperature and the water permeability tests experiments were conducted for consecutive three times. All the values in this study are calculated mean. Furthermore, standard deviation was calculated for experimental filtration data. The transmembrane pressure were varied from 2 to 5 bar to measure the water permeability. The

permeate flux and the permeability were calculated by using the following equations (14) and (15).

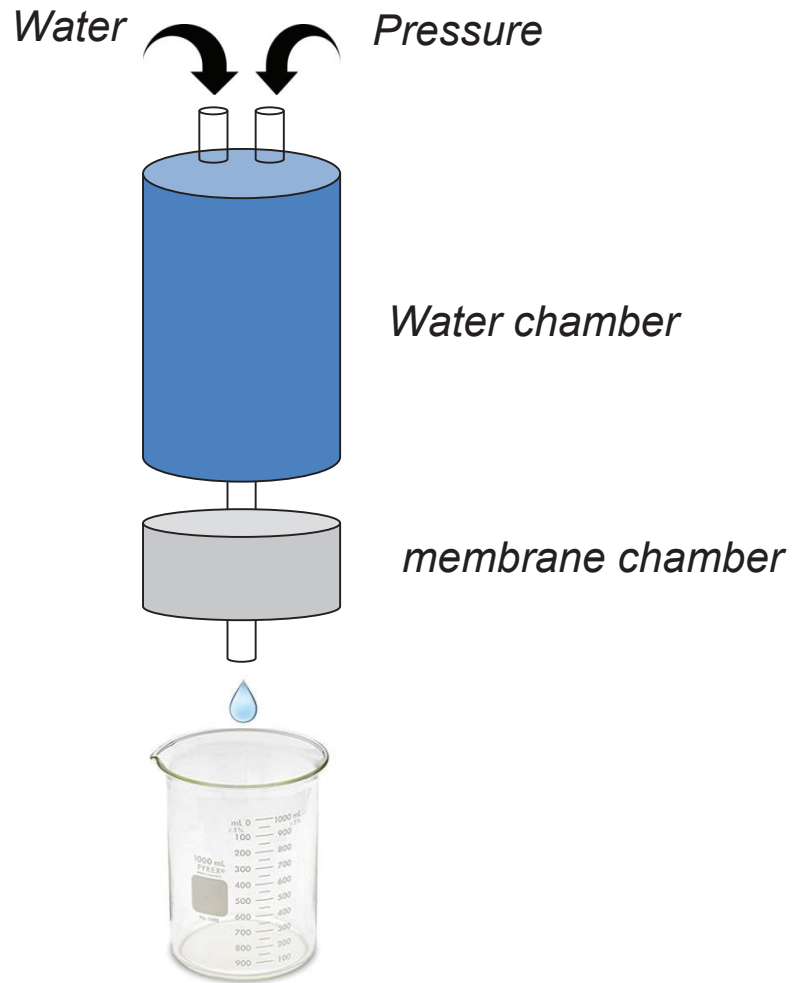


Figure 24. Schematic setup of ultrafiltration

$$F = \frac{V}{A.t} \quad (14)$$

$$L_p = \frac{F}{\Delta P} \quad (15)$$

Where,

V (L) is the permeate volume and

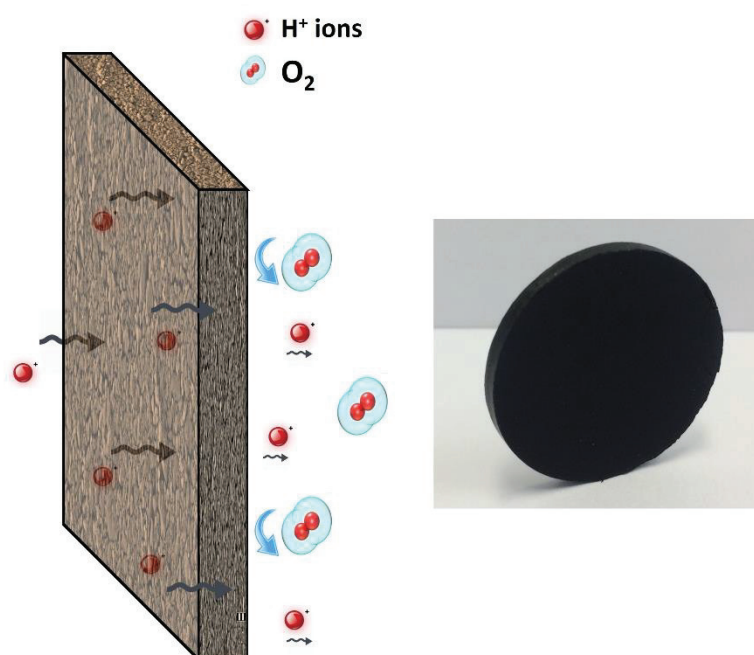
t (h) is filtration time.

5. Porous polymer derived ceramic (PDC)-montmorillonite- $\text{H}_3\text{PMo}_{12}\text{O}_{40}/\text{SiO}_2$ composite membranes for Microbial Fuel Cell (MFC) application

5. Porous polymer derived ceramic (PDC)-montmorillonite- $\text{H}_3\text{PMo}_{12}\text{O}_{40}/\text{SiO}_2$ composite membranes for Microbial Fuel Cell (MFC) application

Objective

The objective of this part of the work was to synthesis and characterize inexpensive porous PDC membranes for MFCs with good proton exchange properties. For this purpose, pure polysiloxane-based and composite membranes blended with different proton conducting fillers (including montmorillonite and $\text{H}_3\text{PMo}_{12}\text{O}_{40}/\text{SiO}_2$ (PMA)) were fabricated by simple pressing and pyrolysis techniques and it showed in section 4.2.1. In this study, the physical characterization of the as-prepared membranes were evaluated namely phase analysis, micro-/meso-/macro porous structure, surface area, and surface characterization and functional properties of the membrane were evaluated inside a dual chamber tank, and their oxygen diffusion coefficients, mass transfer coefficients, and cation transport numbers were determined and compared with those of the commercial polymeric Nafion 117 membrane examined under the same conditions. This study was published as an article in Ceramics international journal [283].



5. Porous polymer derived ceramic (PDC)-montmorillonite- $\text{H}_3\text{PMo}_{12}\text{O}_{40}/\text{SiO}_2$ composite membranes for Microbial Fuel Cell (MFC) application

Scheme 1. Schematic view of a membrane for proton conducting, but oxygen rejecting MFC and synthesized PDC membrane.

Results and Discussion

Phase analysis

XRD patterns of the prepared membranes were recorded to analyse their crystalline phases obtained at different pyrolysis temperatures as shown in Figure 25a. The XRD pattern of the montmorillonite K10 mineral indicates that it belongs to the smectite group of aluminosilicates containing some impurities such as quartz, cristobalite, and feldspar, as previously reported in detail by Varadwaj *et al.* [284]. Figure 25a demonstrates that the membranes formed at 400 and 500 °C have the stable structure of a smectite mineral. When the temperature was further increased to 600 °C and 1000 °C, partial and complete decompositions of this structure were observed, respectively, followed by the formation of a stable silicate phase. The layered smectite structure contains aluminate and silicate species with interlayer spacing [285], as shown in Figure 25b. The obtained XRD patterns reveal that PDC-based materials are amorphous in nature due to the presence of amorphous carbon and silica in the Si–O–C matrix (even at the pyrolysis at a high temperature of 1000 °C). The amorphous structure of Si–O–C is composed of tetrahedrally coordinated $\text{SiO}_{4-x}\text{C}_x$ ($x = 1-4$) structural units containing SiO_2 - and C-enriched regions, as previously observed by other research groups [286, 287]. In a similar way, the XRD patterns of the PDC:PMA10:M10 based materials show that the SiOC matrix and PMA filler are amorphous compounds, whereas the montmorillonite phase still retains its crystalline structure (Figure A1a in appendix). Zhao *et al.* found that the addition of SiO_2 filler increased the thermal stability of the $\text{H}_3\text{PMo}_{12}\text{O}_{40}$ structure in the temperature region up to 550 °C [263]. The FTIR spectrum of PMA is displayed in Figure A1b. It shows the four characteristic bands between 1100 and 700 cm^{-1} (indicating the presence of a Keggin-type structure) that are centered at 1079 cm^{-1} (P–O stretching in the central PO_4 tetrahedron), 957 cm^{-1} (terminal Mo=O groups of the exterior MoO_6 octahedron), 881 cm^{-1} , and 796 cm^{-1} (Mo–O_b–Mo and Mo–O_c–Mo bridges, respectively). In Figure A2 visualizes the surface morphology of PDC-1000 membrane and indicates that this ceramic membrane is porous in nature. This porous nature of the ceramics improves the efficiency of proton transfer through the membrane in the MFC system.

5. Porous polymer derived ceramic (PDC)-montmorillonite- $\text{H}_3\text{PMo}_{12}\text{O}_{40}/\text{SiO}_2$ composite membranes for Microbial Fuel Cell (MFC) application

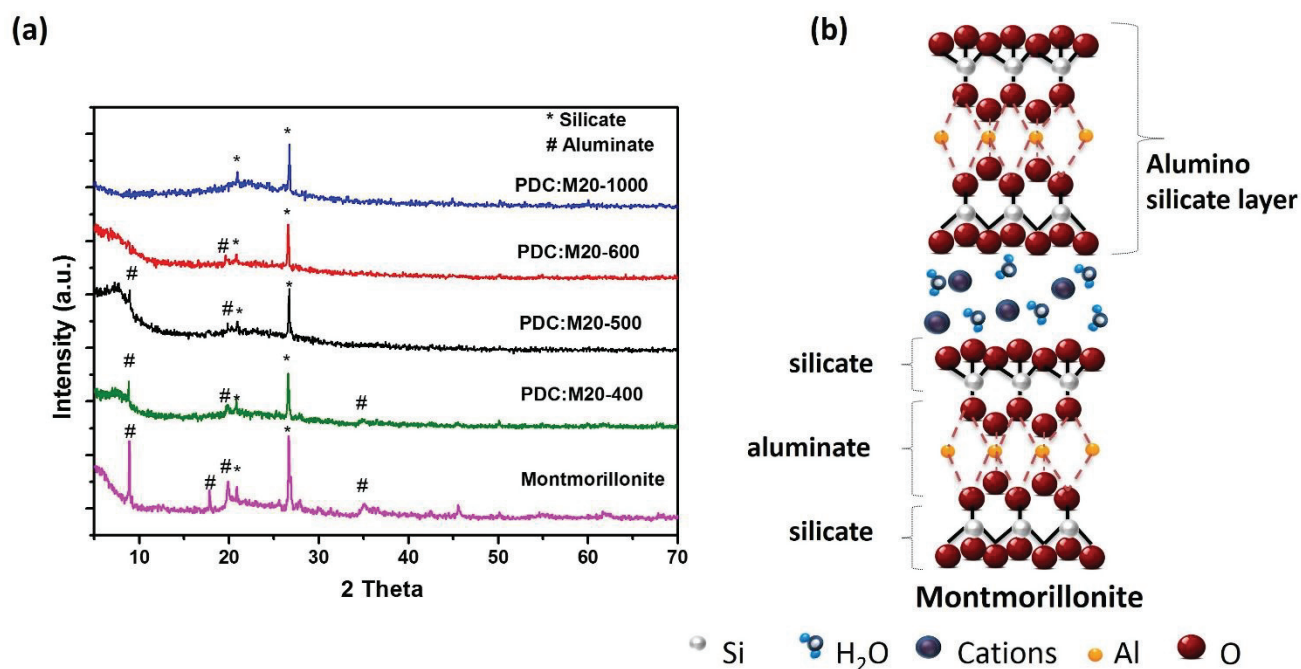


Figure 25. (a) XRD image of PDC:M20 based membranes with respect to pyrolysis temperature (b) Structure of montmorillonite clay mineral.

Porosity and pore size distribution

The pore sizes of the prepared membranes determined by an Hg intrusion technique varied from 0.1 to 1 μm , while their degrees of porosity ranged from 25 to 40% depending on the pyrolysis temperature and filler composition (see Figures 26a–d). The average pore sizes of the pure PDC membranes decrease with decreasing particle size of the pre-pyrolyzed material, as shown in Appendix Table A4. Moreover, the pore size of the membrane first increases with increasing pyrolysis temperature to 600 $^{\circ}\text{C}$, but then decreases at a higher pyrolysis temperature of 1000 $^{\circ}\text{C}$. This phenomenon is often attributed to the shrinkage of particles and decomposition of organic molecules present in the polysiloxane matrix [288, 289]. The PDC:M20-400 membrane exhibits an average pore size of 410 nm, which is smaller than that of the PDC-400 membrane (620 nm) due to the smaller particle size distribution of PDC:M20 pre-pyrolyzed powder. On the other hand, the PDC:PMA10:M10-400 based material has an average pore size of 260 nm, which is much lower than those of the other PDC membranes, owing to the further addition of PMA filler, which decreases the average particle size of the pre-pyrolyzed membrane. In addition, the formation of mesopores ($x = 2$ to 50 nm) was observed for the PDC:PMA10:M10 based membranes, but not for the bare PDC and PDC:M20 ones due to the presence of micro-

5. Porous polymer derived ceramic (PDC)-montmorillonite-H₃PMo₁₂O₄₀/SiO₂ composite membranes for Microbial Fuel Cell (MFC) application

and mesopores in the PMA structure. The membranes containing macropores with sizes as high as 250 nm are most suitable for MFC applications because of their limited oxygen permeability and good ionic transport properties. Similarly, Li *et al.* concluded that the performance of porous membranes for MFCs was strongly dependent on their oxygen transfer, cation transfer, and proton diffusion characteristics, which drastically affected the columbic efficiency and power density of the resulting MFC systems [111]. A porous ceramic membrane promotes proton transfer due to its high porosity rather than good ionic conductivity, as previously observed by Winfield *et al.* [290].

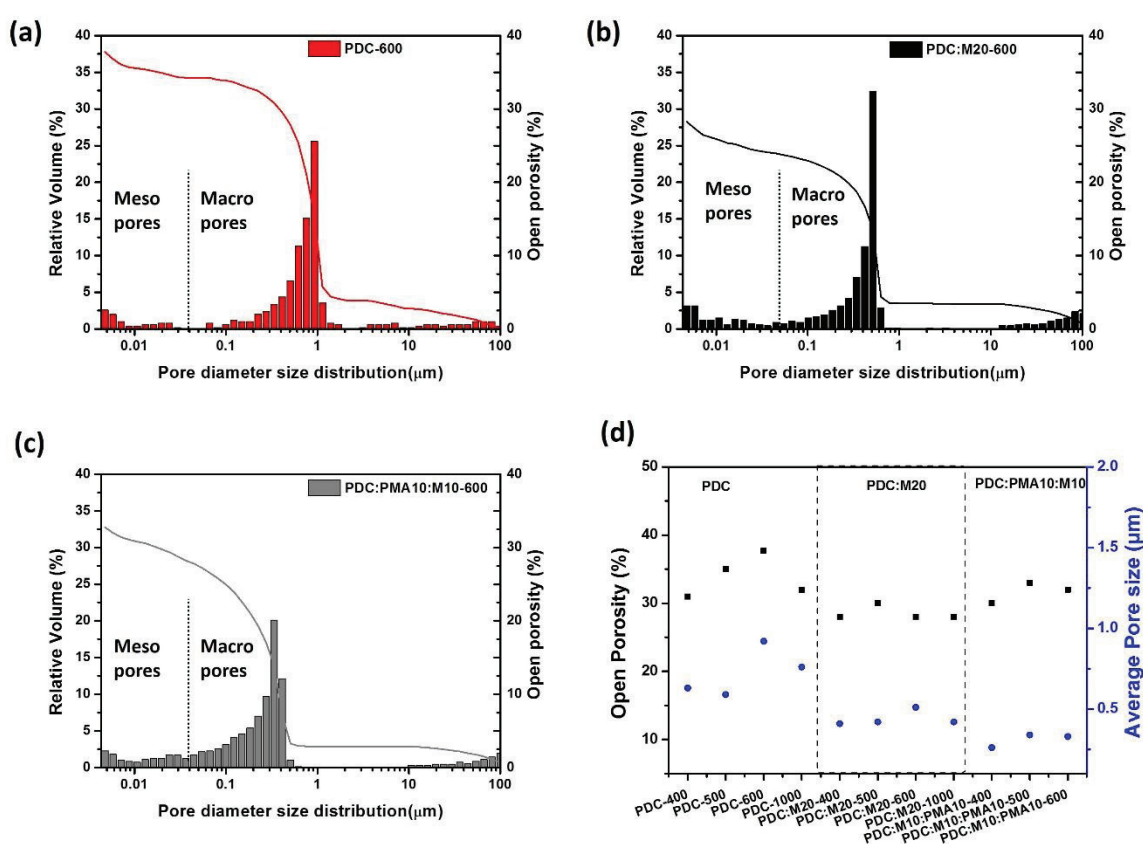


Figure 26. (a-c) Pore size distribution versus relative pore volume and open porosity curves obtained from Hg-porosimetry histogram of pyrolyzed samples (d) Average pore size and open porosity versus as prepared PDC membrane plots. From these diagrams no significant difference in mesopore content can be seen.

Specific surface area

N₂ adsorption/desorption isotherms were obtained to identify the type of the membrane pore structure and determine its specific surface area. Figure 27a–b show the Brunauer–Emmett–

5. Porous polymer derived ceramic (PDC)-montmorillonite-H₃PMo₁₂O₄₀/SiO₂ composite membranes for Microbial Fuel Cell (MFC) application

Teller (BET) isotherms recorded for all the as-prepared PDC materials. The PDC and PDC:M20 based membranes pyrolyzed at 400, 500, and 600 °C exhibit type I isotherms typical for microporous structures (according to the classification of the International Union of Pure and Applied Chemistry). The sample pyrolyzed at 1000 °C has no micropores, and its specific surface area is low because of the collapse of pores caused by the viscous flow at pyrolysis temperatures greater than 500 °C [258]. The surface area of the PDC-400 material is about 2.5 m²/g, whereas that of PDC:M20-400 equals 112 m² g⁻¹, which can be explained by the presence of the layered montmorillonite structure in the PDC matrix (the surface area of pure montmorillonite is 250 m² g⁻¹). After pyrolyzing the montmorillonite-functionalized PDC material at 500 °C, its surface area increased to 428.83 m² g⁻¹. The further increase in the pyrolysis temperature to 600 °C slightly lowered the surface area due to the partial decomposition of the montmorillonite structure, as confirmed by the XRD spectra. On the other hand, the surface area of the PDC material functionalized with both montmorillonite and PMA ranged between 88 and 300 m² g⁻¹ at pyrolysis temperatures from 400 to 600 °C due to the presence of microporous and mesoporous structures identified by the type IV isotherms depicted in Figure 27c. Between 500 and 600 °C, the PMA filler starts to decompose simultaneously with the PDC matrix, leading to a slight decrease in the surface area.

PDC and its composites typically contain micro-, meso-, and macropores, which strongly influence the proton transfer properties of the produced membranes. Xu *et al.* reported that the presence of mesopores in a material enhanced its proton conduction characteristics as compared to those of non-porous membranes [291]. However, the formation of highly ordered narrow pores also increases the flux of water molecules and promotes the diffusion of oxygen species, which negatively affects the long-term performance of MFC systems. Since the ceramic membranes produced in this work contain a mixture of micro/meso- and macropores in the SiOC structure, they represent a potential solution to these problems. The smooth surface characterized by irregular or non-linear pores that decrease the permeability of oxygen gas and water from one chamber of the MFC system to another exhibits good diffusion properties [292].

5. Porous polymer derived ceramic (PDC)-montmorillonite- $H_3PMo_{12}O_{40}/SiO_2$ composite membranes for Microbial Fuel Cell (MFC) application

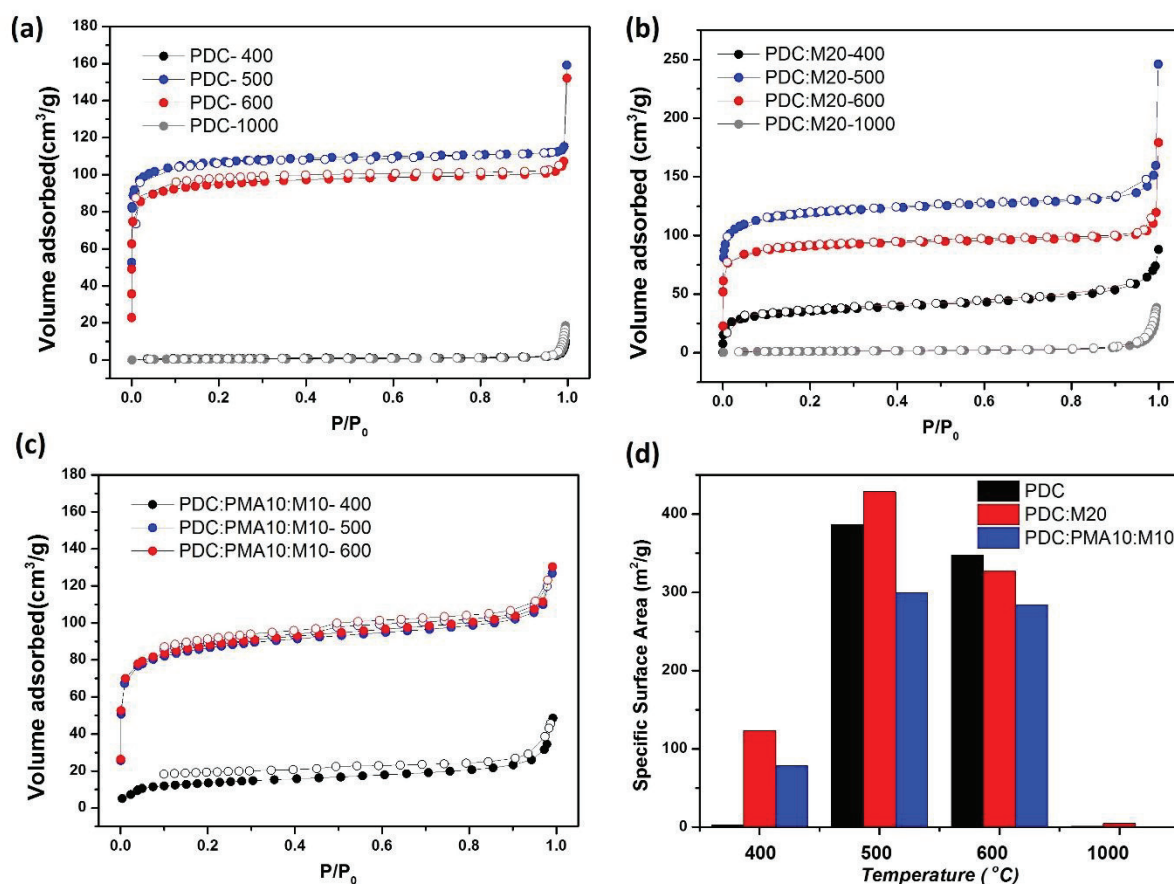


Figure 27. (a-c) Nitrogen adsorption/desorption isotherms of PDC and composite membranes, pyrolyzed at 400, 500, 600 and 1000 °C (d) Specific surface areas of pyrolyzed (400/500/600/1000 °C) membranes as determined by nitrogen adsorption isotherm.

Surface characteristics (hydrophilicity/hydrophobicity)

The surface characteristics of the prepared membrane materials for MFC applications (including their degrees of hydrophilicity) were analyzed by n-heptane and water vapor adsorption methods, and the obtained results are shown in Figure 28a. The amounts of adsorbed vapors (in mmol m⁻²) were determined from the changes in the specific surface area measured by recording N₂ adsorption-desorption isotherms. When the water/heptane ratio is higher than one, the studied material is assumed to possess hydrophilic properties (see Figure 28b). The PDC-based materials exhibit a higher degree of hydrophilicity with increasing pyrolysis temperature due to the decomposition of the hydrophobic methyl and phenyl groups of the polysiloxane (H44) matrix [256]. Prenzel *et al.* found that increasing the APTES content in the polysiloxane precursor made the final pyrolysed PDC material more hydrophilic due to the lower temperature stability of the propylamino chains of the APTES groups [293].

5. Porous polymer derived ceramic (PDC)-montmorillonite- $H_3PMo_{12}O_{40}/SiO_2$ composite membranes for Microbial Fuel Cell (MFC) application

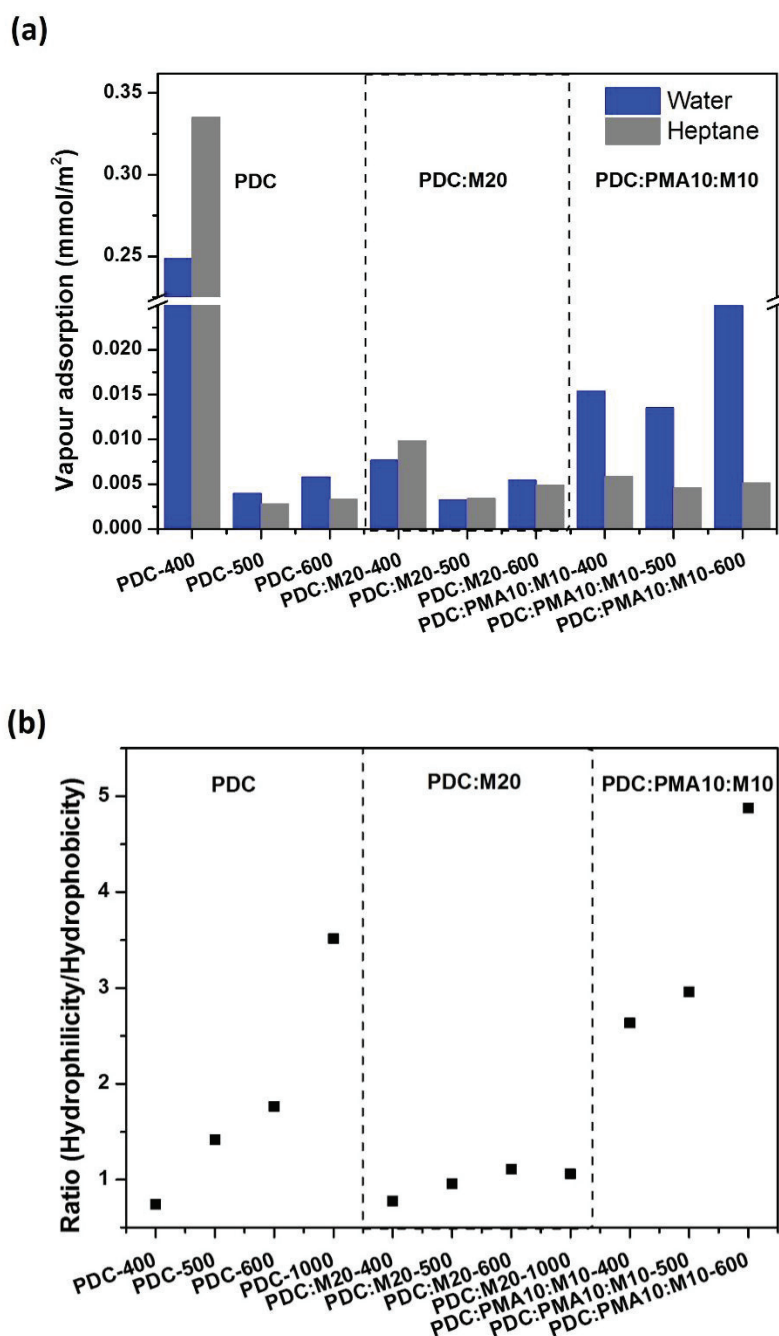


Figure 28. (a) Water and n-heptane vapor adsorption at 25 °C for as prepared membrane materials. (b) Ratio of hydrophilic and hydrophobic nature for all membranes as prepared.

The water/heptane ratio slightly decreased after the functionalization of the synthesized PDC materials with montmorillonite, due to its hydrophobic nature [294, 295]. However, its ratio greater than one were obtained for PDC:M20-600 and PDC:M20-1000, while their degrees of hydrophilicity were smaller than those of the PDC-based materials. The PDC:PMA10:M10

5. Porous polymer derived ceramic (PDC)-montmorillonite- $\text{H}_3\text{PMo}_{12}\text{O}_{40}/\text{SiO}_2$ composite membranes for Microbial Fuel Cell (MFC) application

material exhibited a similar hydrophilic nature, while the samples pyrolyzed at 500 °C and 600 °C were characterized by the highest water/heptane ratios as compared to those of the other specimens due to the alignment of the Keggin $\text{H}_3\text{PMo}_{12}\text{O}_{40}$ structure. The utilized filler possessed the ability to retain water molecules inside its micro- and mesopores, which was consistent with the types of the N_2 adsorption isotherms recorded.

Ion exchange capacity

The IEC values (Figure 29) of the PDC:M20 based materials obtained using a back titration method were higher than those measured for the PDC-based materials. In contrast, the IEC of the sample pyrolyzed at 1000 °C was relatively low because of the decomposition of its layered montmorillonite structure containing aluminates and silicates. Moreover, for the PDC:M20-600 sample, a dramatic increase in IEC value was observed as compared to that of the PDC-600 sample due to the existence of the montmorillonite structure with negative charges. On the other hand, the specimens containing montmorillonite and PMA fillers exhibited a tremendous increase in IEC after the pyrolysis at 400 °C and 500 °C, whereas the PDC:PMA10:M10-600 membrane showed a drop in IEC as compared to the values obtained for the PDC-600 and PDC:M-20-600 samples, owing to the thermal instability of the PMA filler.

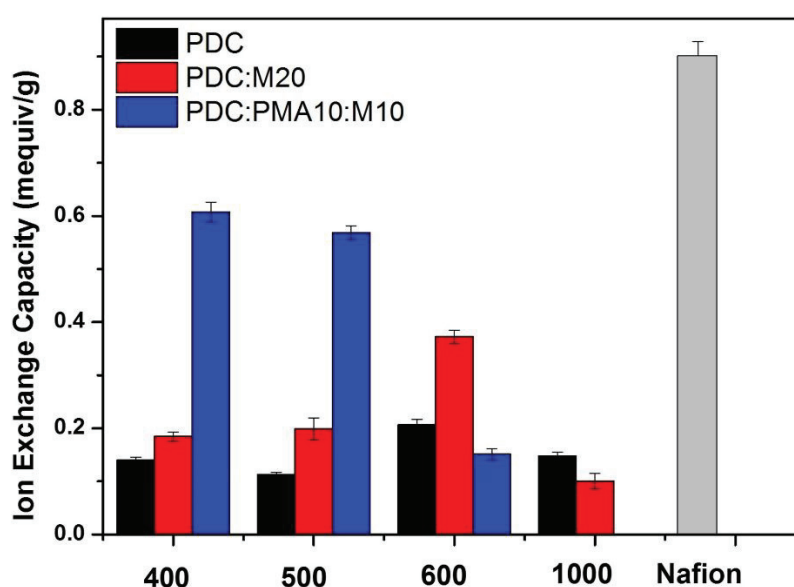


Figure 29. Ion exchange capacity measured for as prepared ceramic membrane compared with nafion

5. Porous polymer derived ceramic (PDC)-montmorillonite- $\text{H}_3\text{PMo}_{12}\text{O}_{40}/\text{SiO}_2$ composite membranes for Microbial Fuel Cell (MFC) application

The IEC magnitudes of the PDC:PMA10:M10-400 and PDC:PMA10:M10-500 membranes were five and six times higher than those of the PDC-500 and PDC-400 samples, respectively, and were equal to almost 68% of the IEC of the polymeric Nafion membrane. The ion transfer in ceramic membranes is realized *via* the hopping of protons between the hydroxyl groups and water molecules adsorbed on the porous PDC surface, whereas the addition of montmorillonite and PMA fillers facilitates the transfer of protons by the presence of charged ions in their structures [296].

Cation transport number

The functionalization of PDC with montmorillonite slightly increases its cation transport number (Figure 30) as compared to those of the bare PDC and PDC: M20 materials pyrolyzed at 400, 500, and 600 °C. At a pyrolysis temperature of 1000 °C, its magnitude decreases due to the complete decomposition of the aluminate layer in the montmorillonite structure. In addition, the presence of micro- and mesopores in the membrane provides better pathways for the diffusion of ions from one chamber to another. Many researchers concluded that the diffusion of ions through porous membranes represented a classical problem of diffusion chemistry [290, 291]. The presence of SiOC species in the montmorillonite structure along with aluminate and silicate species leads to optimal surface characteristic for MFC applications, which are also assumed to promote the diffusion of ions through the membrane body. The adsorption of water molecules on the ceramic surface is enhanced by the negatively charged sites of the layered montmorillonite structure, which promotes the ion transfer from one MFC chamber to another. The PDC: PMA10:M10 based membrane exhibits a higher cation transport number as compared to those of the other membranes, due to the incorporation of PMA filler into the Keggin structure. According to Wang *et al.*, this material possesses the ability to retain water molecules in its mesoporous structure and acts as a proton-conducting filler even for polymeric Nafion-based membranes [297]. The higher cation transport number obtained for the sample pyrolyzed at 400 °C resulted from the alignment of the Keggin shape and mesoporous structure of the PMA filler. However, PMA decomposes at temperatures above 550 °C (even under inert atmosphere), leading to a sharp decrease in the cation transfer number of the PDC: PMA10:M10-600 sample. The destruction of the PMA Keggin structure observed at 600 °C and the beginning of the transformation of the $\alpha\text{-MoO}_3$ phase decreased the number of mesopores and thus negatively affected its water-retaining ability [263]. The cation transport number of the composite membrane with montmorillonite and PMA fillers pyrolyzed at 400 °C

5. Porous polymer derived ceramic (PDC)-montmorillonite-H₃PMo₁₂O₄₀/SiO₂ composite membranes for Microbial Fuel Cell (MFC) application

is equal to 72 % of that of the polymeric Nafion membrane, which represents a relatively high value for MFC ceramic membranes. This phenomenon can be attributed to the smallest average pore size (260 nm) and highly hydrophilic surface of this membrane, which presumably promote the transfer of protons *via* a proton hopping mechanism, as previously reported by Nogami *et al* [298].

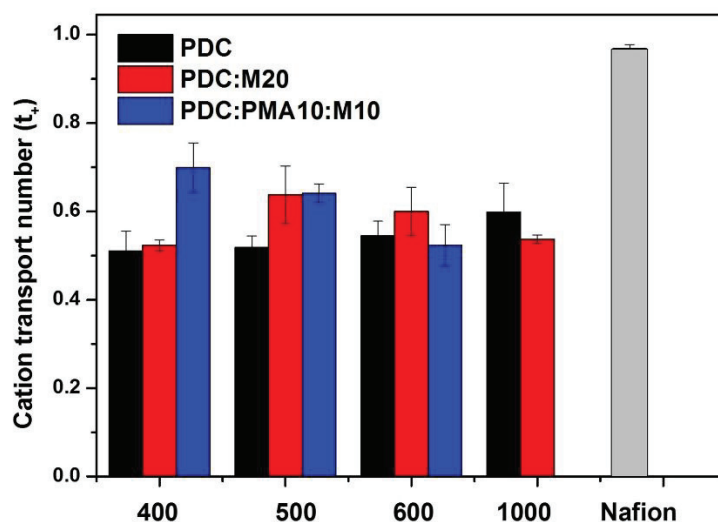


Figure 30. Cation transport number of ceramic membrane compared with nafion.

Diffusion of dissolved oxygen

One of the major purposes of using membranes in MFCs is to prevent the leakage of oxygen molecules from the aerobic cathode chamber to the anode chamber and maintain its anaerobic conditions. In this work, the diffusion of dissolved oxygen species through the PDC membranes was compared with their diffusion through the commercial polymeric Nafion membrane. This process can be suppressed by tailoring the average membrane pore size since its degree of porosity strongly affects the oxygen diffusion coefficient [111]. The PDC-600 membrane exhibits a degree of porosity and an average pore size of 920 nm. These values are higher than the values obtained for the other membranes synthesized in this study. As a result, its oxygen diffusion coefficient of $7.06 \times 10^{-4} \text{ cm}^2 \text{ s}^{-1}$ is noticeably higher than that of the PDC:M20-600 membrane ($6.86 \times 10^{-4} \text{ cm}^2 \text{ s}^{-1}$), owing to the presence of montmorillonite in the SiOC matrix, which decreases its porosity degree to 28% and to an average pore size of 510 nm. The pyrolysis temperature also produces a significant effect on the degree of porosity and average pore size

5. Porous polymer derived ceramic (PDC)-montmorillonite-H₃PMo₁₂O₄₀/SiO₂ composite membranes for Microbial Fuel Cell (MFC) application

of the membrane that decreases the amount of diffused oxygen. For instance, the diffusion coefficient of dissolved oxygen obtained for the PDC-400 membrane is $2.41 \times 10^{-4} \text{ cm}^2 \text{ s}^{-1}$, and that of the material pyrolyzed at 1000 °C (PDC-1000) is equal to $1.93 \times 10^{-4} \text{ cm}^2 \text{ s}^{-1}$ due to the increase in porosity and average pore size of the ceramic membrane with increasing pyrolysis temperature. On the other hand, the PDC: PMA10:M10 based membrane pyrolyzed at 500 °C is characterized by the smallest oxygen diffusion coefficient of $1.68 \times 10^{-4} \text{ cm}^2 \text{ s}^{-1}$ (as compared to those of the PDC and PDC:M20 based membranes), owing to the changes in the average pore size and degree of porosity as well as the presence of the PMA Keggin structure. The mass transfer coefficient of dissolved oxygen through the polymeric Nafion membrane is equal to $3.06 \times 10^{-4} \text{ cm s}^{-1}$, which is very close to the value of $5.45 \times 10^{-4} \text{ cm/s}$ obtained for the PDC:PMA10:M10-500 membrane in this work. The oxygen diffusion coefficient mainly depends on the membrane thickness; therefore, its value determined for the thin polymeric Nafion 117 membrane (with a thickness of 170 μm) was 2 orders of magnitude smaller than those of the ceramic membranes with thicknesses of 3–4 mm. The oxygen mass transfer and diffusion coefficients of the membranes prepared in this work are listed in Table 4.

Table 4. Physical characterization of as prepared PDC and composite ceramic membranes.

Membranes	Ko (cm s ⁻¹)	Do (cm ² s ⁻¹)	t+	IEC (mequiv g ⁻¹)	Pore size (nm)
PDC-400	7.56×10^{-4}	2.41×10^{-4}	0.5104	0.1402	630
PDC-500	7.21×10^{-4}	2.23×10^{-4}	0.5185	0.1131	590
PDC-600	7.06×10^{-4}	2.11×10^{-4}	0.5447	0.2068	920
PDC-1000	7.15×10^{-4}	1.93×10^{-4}	0.5985	0.1483	760
PDC:M20-400	5.54×10^{-4}	1.77×10^{-4}	0.5233	0.1844	410
PDC:M20-500	5.23×10^{-4}	1.50×10^{-4}	0.6378	0.1989	420
PDC:M20-600	6.86×10^{-4}	2.18×10^{-4}	0.5999	0.3723	510
PDC:M20-1000	8.20×10^{-4}	1.97×10^{-4}	0.5371	0.1006	420
PDC:M10:PMA10-400	5.62×10^{-4}	1.79×10^{-4}	0.6988	0.6072	260
PDC:M10:PMA10-500	5.45×10^{-4}	1.68×10^{-4}	0.6405	0.5686	340
PDC:M10:PMA10-600	6.88×10^{-4}	2.06×10^{-4}	0.5234	0.1516	330
Nafion	3.06×10^{-4}	5.45×10^{-6}	0.9680	0.9026	-

5. Porous polymer derived ceramic (PDC)-montmorillonite- $\text{H}_3\text{PMo}_{12}\text{O}_{40}/\text{SiO}_2$ composite membranes for Microbial Fuel Cell (MFC) application

Summary

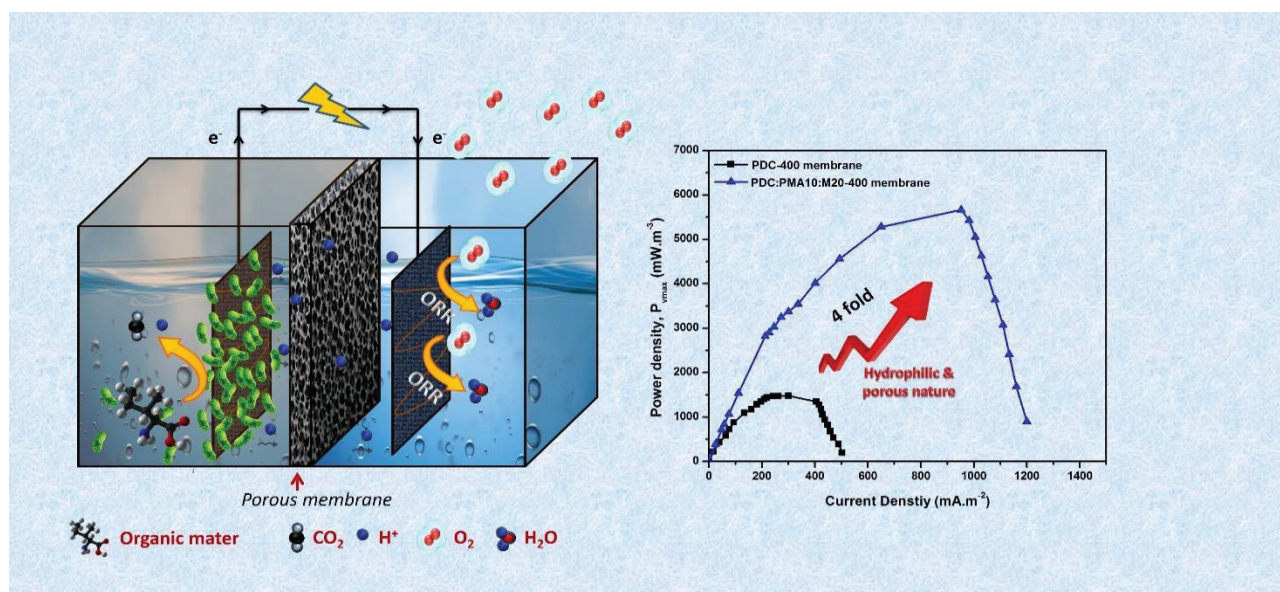
In this study, PDC composite membranes were synthesized from polysiloxane precursor mixed with the montmorillonite and PMA proton-conducting filler materials, and their IEC values, cation transport numbers, oxygen mass transfer coefficients, and diffusion coefficients were determined. The obtained results revealed that the PDC:M20-600 and PDC:PMA10:M10-400 based membranes exhibited better performances as compared to those of the other PDC membranes, while the IEC value and cation transport number of PDC:PMA10:M10-400 were equal to 67% and 68% of the magnitudes obtained for the commercial polymeric Nafion membrane, respectively. Similarly, a small oxygen diffusion coefficient of $1.79 \times 10^{-4} \text{ cm}^2 \text{ s}^{-1}$ was observed at an average membrane pore size of 260 nm, which was very close to that of the Nafion 117 membrane. Therefore, the as-prepared PDC composite ceramic membranes can be potentially utilized as the separators in MFC systems. Testing the real-scale performance and wastewater treatment efficiency of the MFCs fabricated from PDC composite membranes will be conducted in the following chapter.

6. Tailoring hydrophilic and porous nature of polysiloxane derived ceramer and ceramic membranes for enhanced bioelectricity generation in microbial fuel cell

6. Tailoring hydrophilic and porous nature of polysiloxane derived ceramer and ceramic membranes for enhanced bioelectricity generation in microbial fuel cell

Objective

In this study, PDC membranes were modified with proton-conducting montmorillonite and $H_3PMO_{12}O_{40}/SiO_2$ (phosphomolybdic acid with silica – PMA) fillers at various concentrations and pyrolyzed at 400 and 1000 °C to produce ceramer (PDC:M10–400 and PDC:PMA10:M20–400) and ceramic (PDC:M10–1000) composites, respectively. The surface area, surface characteristics, pore size distributions, IEC, cation transport number, and oxygen diffusion coefficient of the fabricated membranes were measured and compared with those of the materials studied in the previous chapter to determine their suitability for applications in MFC. The influential properties of ceramic membrane were investigated for enhanced performance of MFC and evaluated in terms of the generated power density, internal resistance of the MFC, coulombic efficiency (CE), chemical oxygen demand (COD) removal efficiency, and cost comparison analysis. Finally, the performance of MFC with the porous PDC ceramer and ceramic membranes were compared with that of the conventional Nafion membrane under the same operating conditions. This study was published as research article in Ionics journal [35].



Scheme 2. MFC with porous membrane and its performance.

6. Tailoring hydrophilic and porous nature of polysiloxane derived ceramer and ceramic membranes for enhanced bioelectricity generation in microbial fuel cell

Results and Discussion

Micro-/meso- and macro pore structure

The physical characteristics of PDC:M10–400 and PDC: PMA10:M20–400 ceramers and the PDC:M10-1000 ceramic membranes synthesized in this study were examined and compared with those of the materials discussed in our previous study. The macropore sizes of the membranes and their distributions determined by the mercury intrusion method are shown in Figure 31a and b. The fabrication of membranes with pore sizes smaller than 1000 nm is beneficial for preventing the migration of bacterial substrate from the anodic to the cathodic chamber. The resulting membrane pore sizes ranged between 100 and 1000 nm depending on the material composition, for instance, the ceramer-based samples exhibited average pore sizes ranging from 200 to 650 nm, whose magnitudes decreased with increasing contents of montmorillonite and PMA fillers. Similarly, the average pore size of the PDC ceramic membrane decreased from 760 to 420 nm after the addition of 20 wt.% montmorillonite (PDC:M20–1000), owing to the decrease in the particle sizes of the pre-pyrolyzed powders (Table 1). Meanwhile, the average pore size of PDC: PMA10:M20–400 ceramer was equal to 316 nm, and its open porosity was 39%. Higher value of the open porosity of a hydrophilic membrane helps to retain a large amount of water molecules, which enhance the proton transfer characteristics of the MFC.

The BET specific surface areas of the resulting ceramers were strongly affected by the micro- and mesoporous structures of montmorillonite and PMA fillers. The nitrogen adsorption-desorption isotherm curves shown in Figure 31c. In particular, PDC:PMA10:M20–400 ceramer was characterized by the highest specific surface area of $124 \text{ m}^2 \text{ g}^{-1}$ as compared to the values obtained for the other tested materials and bare PDC ceramer membrane (Figure 31d). These results suggest that the ceramer containing both montmorillonite and PMA fillers exhibits a hierarchical (micro-/meso-/macro) pore structure. Xu *et al.* found that the formation of mesopores in metal organic framework and covalent organic framework materials enhanced their proton conductivity properties as compared to those of non-porous membranes [299]. Moreover, the presence of a hierarchical (micro/meso/macro) pore structure in the membrane material inhibits the migration of dissolved oxygen (DO) from the cathodic to the anodic chamber, which improves its overall efficiency. However, all ceramic membranes (pyrolyzed at 1000 °C) investigated in this study do not have any micro- or mesopores (including the PDC:

6. Tailoring hydrophilic and porous nature of polysiloxane derived ceramer and ceramic membranes for enhanced bioelectricity generation in microbial fuel cell

M20–1000 ceramic membrane with a specific surface area of $4.2 \text{ m}^2 \text{ g}^{-1}$), which could be explained by the collapsing of the layered aluminosilicate montmorillonite structure and complete transformation of organic molecules to SiOC species at high pyrolysis temperatures. Hence, the ceramic SiOC membranes possess only macroporous structures, which can also promote proton diffusion from one chamber to the other.

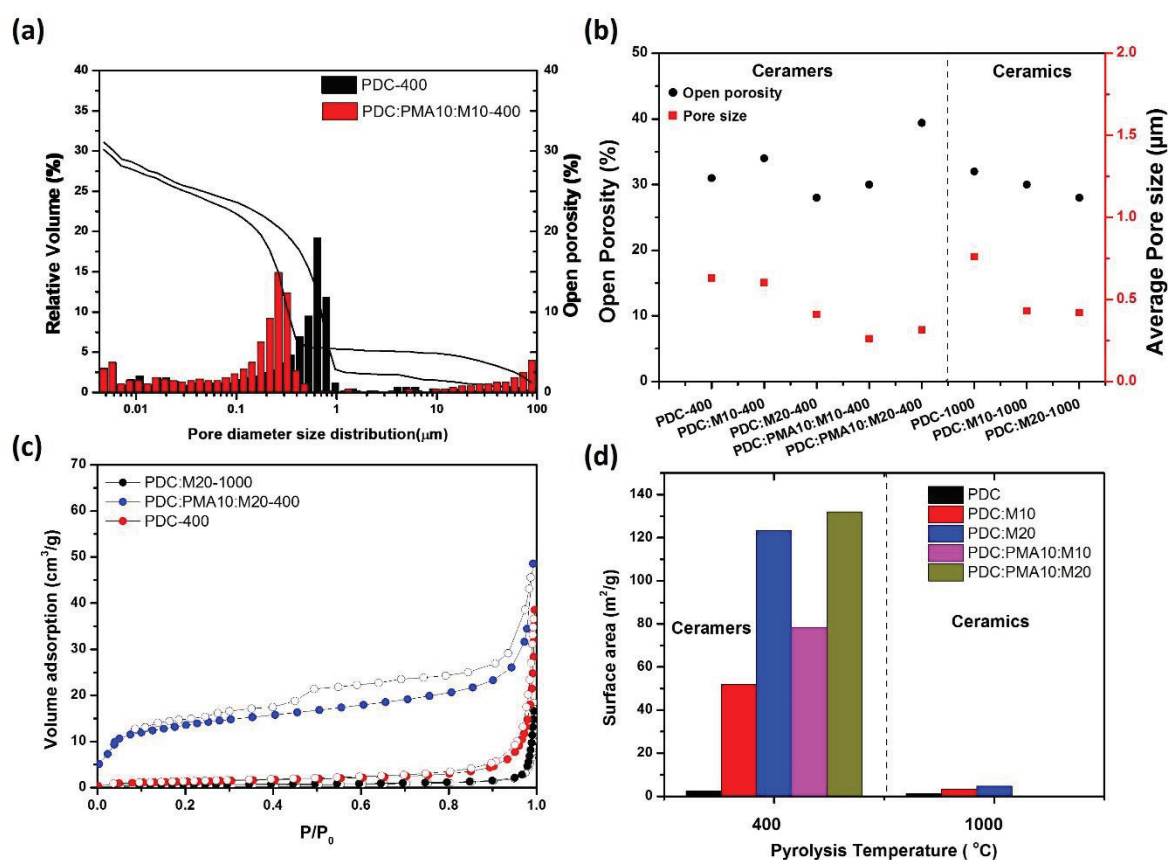


Figure 31. (a) Pore size distribution versus relative pore volume and open porosity curves obtained from Hg-porosimetry histogram of pyrolyzed samples, (b) Average pore size and open porosity versus as prepared PDC membranes plot, (c) Nitrogen adsorption-desorption isotherms of montmorillonite and $\text{H}_3\text{PMo}_{12}\text{O}_{40}/\text{SiO}_2$ functionalized PDC membranes, pyrolyzed at 400 and 1000 $^{\circ}\text{C}$ (d) Specific surface areas of pyrolyzed (400 and 1000 $^{\circ}\text{C}$) membranes as determined by nitrogen adsorption/desorption isotherm.

Hydrophilic/hydrophobic characteristics

The water and heptane adsorption characteristics of the prepared membranes were examined to elucidate their hydrophilic/hydrophobic properties (Figure 32a and b). The obtained adsorption capacities were found to be dependent on the specific surface areas of the studied materials and

6. Tailoring hydrophilic and porous nature of polysiloxane derived ceramer and ceramic membranes for enhanced bioelectricity generation in microbial fuel cell

determined by recording nitrogen adsorption–desorption isotherms. The degree of hydrophilicity of a material is correlated with the water/heptane adsorption ratio; when its magnitude is greater than one, it is considered hydrophilic despite its intrinsic hydrophobicity.

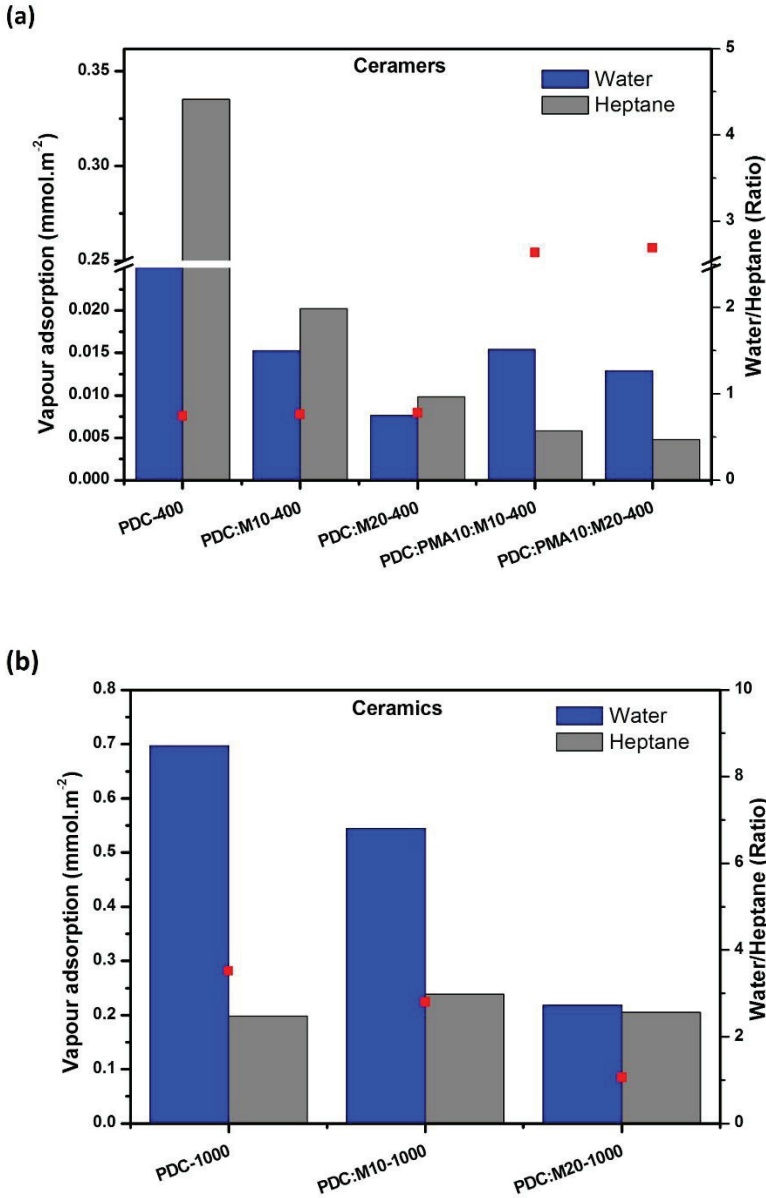


Figure 32. Water and n-heptane vapor adsorption at 25 °C and ratio of hydrophilic and hydrophobic nature: (a) ceramer membranes, (b) ceramic membranes.

The observed hydrophobic behavior of the produced ceramer membranes can be attributed to the partial decomposition of methyl and phenyl functional groups in the H44 polysiloxane matrix. In this study, the addition of montmorillonite to the PDC matrix did not apparently affected the water/heptane adsorption ratios of the ceramer membranes. However, the addition

6. Tailoring hydrophilic and porous nature of polysiloxane derived ceramer and ceramic membranes for enhanced bioelectricity generation in microbial fuel cell

of PMA filler led to the formation of the highly hydrophilic PDC: PMA10:M10–400 and PDC:PMA10:M20–400 ceramer structures, owing to the hygroscopic nature of PMA that was capable of retaining water molecules inside its micro- and mesopores. The PDC–1000, PDC:M10–1000, and PDC:M20–1000 ceramic materials exhibited hydrophilic properties because of the complete decomposition of their methyl and phenyl functional groups into SiOC species during pyrolysis at 1000 °C. Such hydrophilic behavior helps to retain water molecule in the membrane structure, which promotes the transfer of protons from the anode to the cathode chamber.

Ion exchange capacity

The IEC values of the ceramer membranes demonstrated stepwise increases with the addition of montmorillonite to the PDC matrix (Figure 33) due to the presence of a charged interlayer between the aluminate and silicate layers in the montmorillonite structure. Moreover, the addition of both PMA and montmorillonite fillers to PDC dramatically increased the IECs of the ceramer membranes by a factor of six. The ion transfer process in the membrane structure was caused by the proton hopping between various hydroxyl groups or water molecules adsorbed on the porous membrane surface.

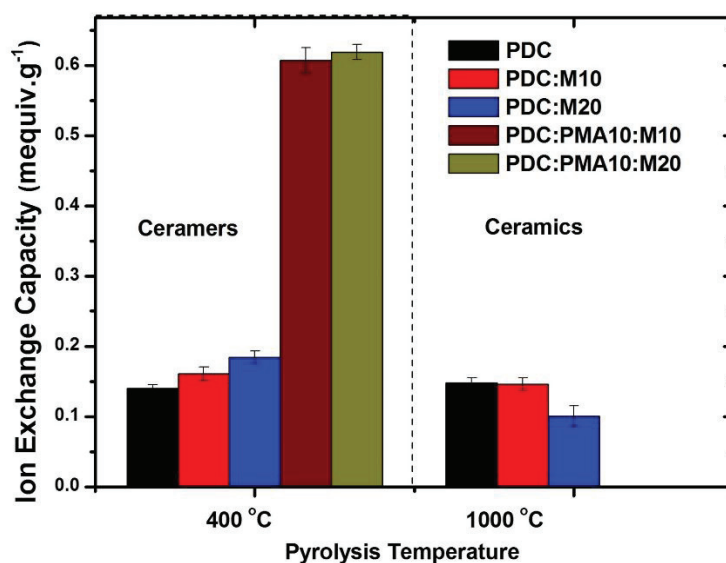


Figure 33. Ion exchange capacity measured for as prepared ceramer and ceramic membranes

6. Tailoring hydrophilic and porous nature of polysiloxane derived ceramer and ceramic membranes for enhanced bioelectricity generation in microbial fuel cell

Meanwhile, the addition of montmorillonite and PMA fillers facilitated the proton transfer by charged ions in the membrane structure. However, the ceramic membranes exhibited completely different behavior: their IEC values decreased with increasing montmorillonite content, which resulted not only from their lower degrees of hydrophilicity, but also from the collapse of the charged interlayer structure of montmorillonite filler after the pyrolysis at 1000 °C [283].

Cation transport number

The cationic transport number (Figure 34) of PDC and montmorillonite-modified PDC ceramers is comparable to each other because both materials exhibit hydrophobic properties. The addition of PMA and montmorillonite fillers to the PDC matrix dramatically increased the cation transport number of the membrane due to the mesoporous structure of PMA. Higher cation transport numbers were obtained for the PDC:PMA10:M20–400 (0.7028) and PDC:PMA10:M10–400 (0.6928) ceramer membranes because of their good hydrophilic properties and smaller pore sizes. Daiko *et al.* elucidated the ion transport mechanism in hydrophilic porous structures by adsorbing water molecules, which formed passages for ion hopping at low activation energies and high ionic conductivity [298].

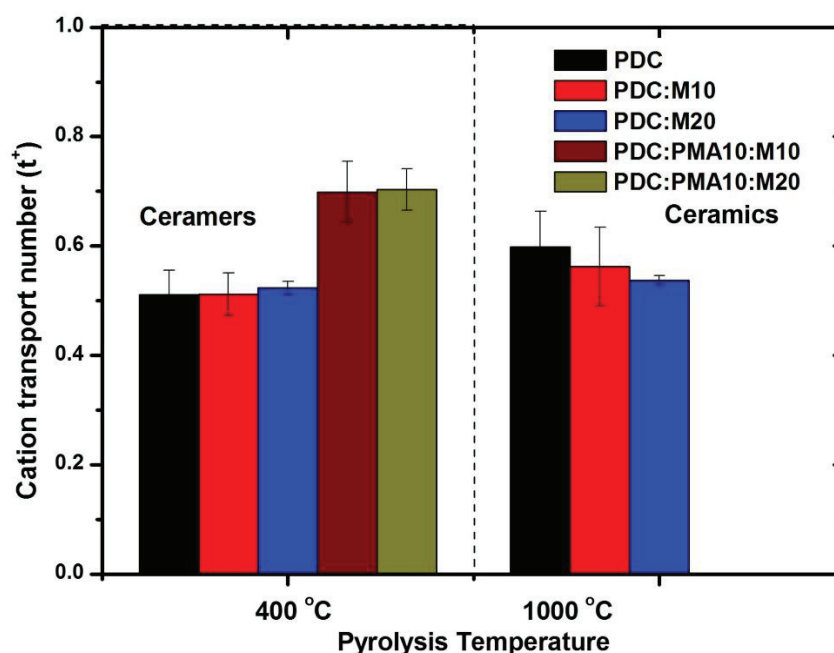


Figure 34. Cation transport number of ceramic membrane.

6. Tailoring hydrophilic and porous nature of polysiloxane derived ceramer and ceramic membranes for enhanced bioelectricity generation in microbial fuel cell

The cation transport number of the fabricated ceramic membranes was observed to be in the decreasing order as PDC–1000, PDC:M10–1000, and PDC:M20–1000, owing to the gradual changes of their hydrophilic properties.

Oxygen Permeability

Presence of separator in MFC prevents the diffusion of DO from the aerobic cathodic chamber to the anaerobic anodic chamber. The oxygen diffusion coefficients of the membranes fabricated in this study are shown in Figure 35. According to Li *et al.*, pore structure and open porosity of the membrane significantly influence the diffusion of DO in the MFC systems [300]. The PDC ceramer membrane investigated in this work was characterized by the average pore size of 630 nm and oxygen diffusion coefficient of $2.41 \times 10^{-4} \text{ cm}^2 \text{ s}^{-1}$, which decreased to $1.77 \times 10^{-4} \text{ cm}^2 \text{ s}^{-1}$ after the addition of 20 wt. % montmorillonite due to the reduction of the average pore size of the SiOC matrix to 410 nm. Furthermore, after the addition of both PMA and montmorillonite fillers, the PDC:PMA10:M20–400 ceramer membrane exhibited the minimal oxygen diffusion coefficient of $1.72 \times 10^{-4} \text{ cm}^2 \text{ s}^{-1}$ and average pore size of 316 nm while retaining the open porosity of 39%, which could be mainly attributed to the mesoporous Keggin structure of PMA.

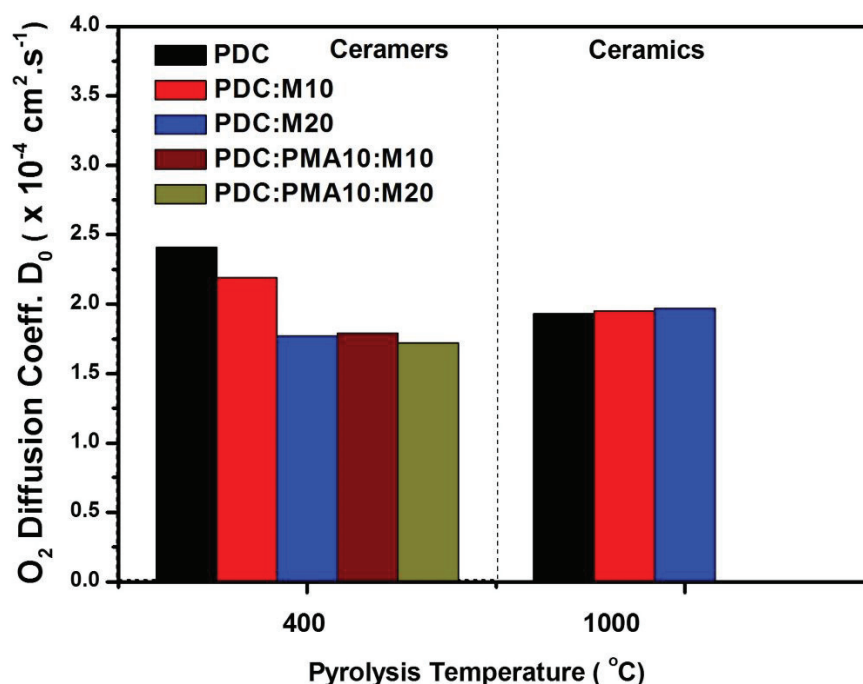


Figure 35. Oxygen diffusion coefficient of PDC membranes.

6. Tailoring hydrophilic and porous nature of polysiloxane derived ceramer and ceramic membranes for enhanced bioelectricity generation in microbial fuel cell

The observed low degree of oxygen permeation through the PDC: PMA10:M20–400 ceramer membrane might be due to the presence of a randomly oriented micro/mesoporous structure in the macropore architecture. Meanwhile, the minimal DO diffusion coefficient was obtained for the PDC ceramic membrane (as compared to that of PDC:M20–1000 ceramic), because of the surface characteristic of the PDC:M20–1000 membrane was less hydrophilic and possessed higher oxygen permeability, owing to the nonpolar nature of oxygen molecules. Similarly, Atwater *et al.* reported that the hydrophilic properties of the membrane inhibited the permeation of DO through the membrane due to their non-polar characteristics [301].

Power generation

Three ceramer and two ceramic membranes were selected based on their physical properties such as surface area, water/heptanes ratio, IEC, cation transport number, and oxygen permeability. In particular, the hierarchical (micro/meso/macro) pore structured PDC:M10:PMA10–400 and PDC:M10:PMA20–400 ceramer membranes exhibited high degrees of hydrophilicity, IECs, and cation transport numbers as well as low oxygen permeabilities as compared with those of the other ceramer membranes pyrolyzed at 400 °C. Meanwhile, the macropore structured PDC-400 ceramer, PDC–1000 and PDC:M20–1000 ceramic membranes were also studied as membrane materials for MFCs to understand the significance of membrane hydrophilic and porous structural properties.

The electrical performance of the fabricated MFCs was evaluated in terms of generated voltages and power density. Their magnitudes were determined by measuring the OV and open-circuit voltage (OCV) from the day of activation of MFC confirming the presence of active electrogenic bacteria in the septic tank mix consortia. The operating voltage was measured over a 100 Ω external resistance. Six MFCs with PDC-400, PDC:PMA10:M10–400, PDC:PMA10:M20–400, PDC–1000, PDC:M20–1000, and Nafion PEM were labeled as MFC–1, MFC–2, MFC–3, MFC–4, MFC–5, and MFC-6 respectively using the reactor shown in Figure A3 (appendix). The average OV of 224.5 ± 6.5 mV was achieved for the MFC-3 with PDC:PMA10:M20–400 membrane under steady-state operating conditions corresponding to an external resistance of 100 Ω , which exceeded the values obtained for the MFC–1 with the PDC–400 membrane (86.3 ± 3.4 mV) and MFC–6 with a polymeric Nafion membrane (186.0 ± 6.5 mV). The internal resistances of the MFCs resulting from the overpotential losses of their electrodes as well as because of the ohmic resistances of the membrane–electrolyte interfaces

6. Tailoring hydrophilic and porous nature of polysiloxane derived ceramer and ceramic membranes for enhanced bioelectricity generation in microbial fuel cell

was measured from the slopes of the linear portions of the voltage versus current curves. The MFC-3 was characterized by the lowest internal resistance of 138 Ω followed by the MFC-2 (142 Ω) and MFC-4 (151 Ω) (Figure 36a), which mainly dependent on the ion transport capability of the membrane. In addition, polarization was conducted for MFCs containing different membranes to compare their overall volumetric power densities. Among various MFCs with the as-synthesized and commercial membranes, MFC-3 demonstrated the best performance corresponding to the maximum volumetric power density ($P_{V,max}$) of 5.66 $W\ m^{-3}$, which was 4 fold higher than MFC-1 with PDC-400 ceramer membrane. On the other hand, the OV and $P_{V,max}$ of 157.7 ± 5.61 mV and 5.10 $W\ m^{-3}$ were achieved for the MFC-4 with PDC-1000 membrane material; these values were 24.4 and 21.6 % higher than that obtained for MFC-5 with the PDC:M20-1000 membrane, respectively. Moreover, the current density of the MFC-4 (1013 $mA\ m^{-2}$) was 1.6 times greater than that of the MFC-5 with PDC:M20-1000 membrane. The maximum volumetric power and current densities obtained for the fabricated MFCs can be ranked as follows: MFC-3 > MFC-6 > MFC-2 > MFC-4 > MFC-5 > MFC-1 (Figure 36b).

From these results, it can be concluded that the MFC-3 with the PDC:PMA10:M20-400 ceramer membrane exhibit the highest power generation proficiency as compared to those of the other membranes due to its highly hydrophilic properties that facilitates capturing water molecules in the membrane structure. These water molecules act as carriers for protons diffusing from the anodic to the cathodic chamber in the form of hydronium (H_3O^+) clusters under the action of osmotic and electroosmotic drag forces. In addition to that, the presence of hierarchical (micro/meso/macro) pores in the PDC:PMA10:M20-400 and PDC:PMA10:M10-400 ceramer membranes inhibit the migration of oxygen molecules from the cathodic to the anodic chamber. On the other hand, MFC-1 with PDC-400 ceramer membrane showed the lowest power generation among all other MFCs. This is due to the hydrophobic characteristics and bigger pore size that lead to diffusion of higher concentration of oxygen to the anodic chamber, which significantly reduces the performance of MFC. Meanwhile, the MFC-4 with PDC-1000 membrane generated higher power and current densities as compared to that of the MFC-5 with PDC:M20-1000 membrane. This is mainly because of higher hydrophilicity behavior of PDC-1000 ceramic membrane.

6. Tailoring hydrophilic and porous nature of polysiloxane derived ceramer and ceramic membranes for enhanced bioelectricity generation in microbial fuel cell

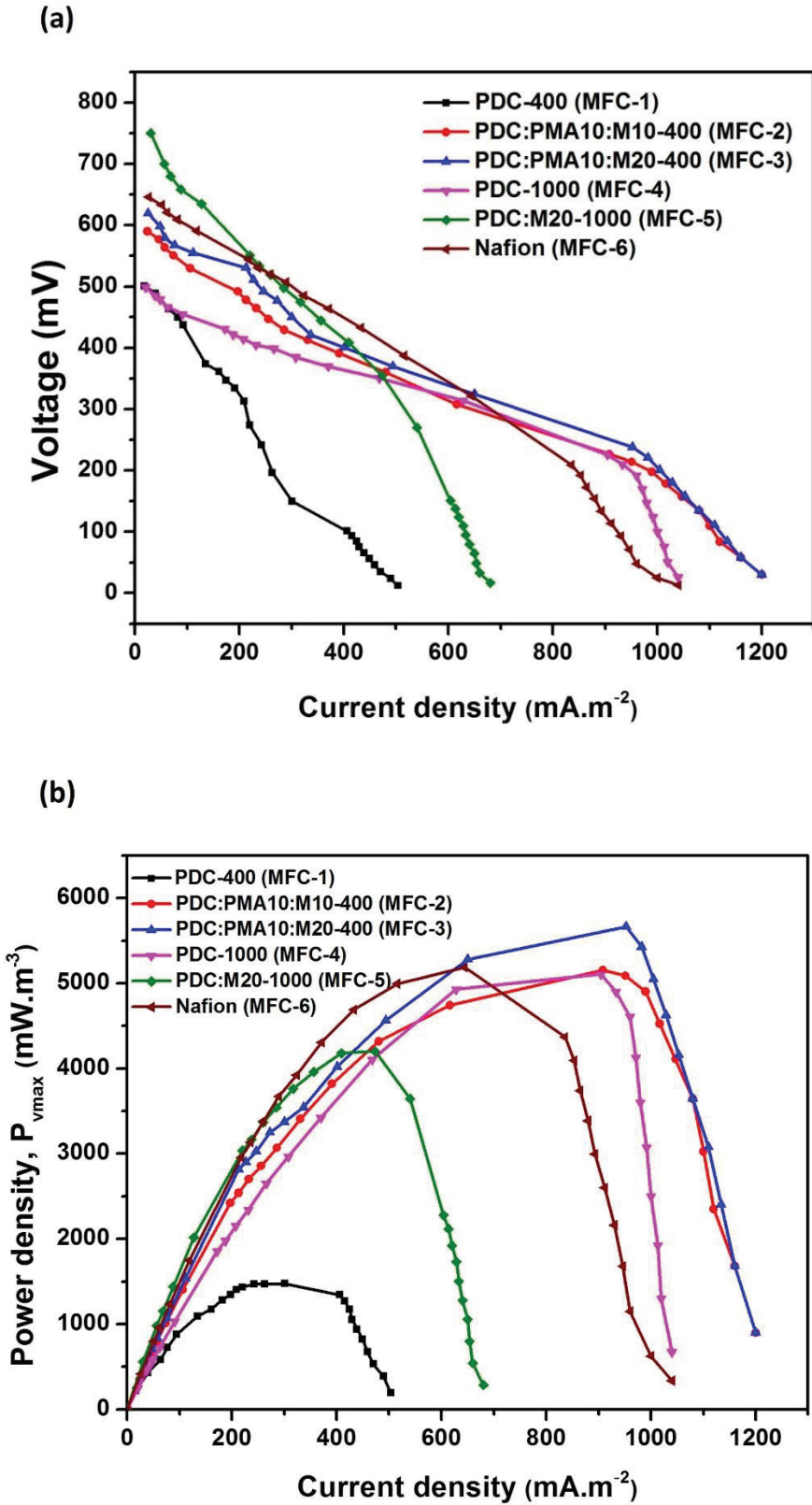


Figure 36. (a) Polarization curve and (b) power density curves.

6. Tailoring hydrophilic and porous nature of polysiloxane derived ceramer and ceramic membranes for enhanced bioelectricity generation in microbial fuel cell

Although the hydrophilicity of the PDC-1000 ceramic membrane is higher than that of the PDC:PMA10:M20-400 ceramer membrane, the power generation of the MFC-4 with PDC-1000 is lower than that of the MFC-3 with PDC:PMA10:M20-400 because of the presence of a hierarchical pore structure in PDC:PMA10:M20-400, which inhibits the permeation of oxygen molecules through the membrane. The physical characteristics of the prepared membrane materials, including their surface areas, pore structures, hydrophilic properties, IECs, cation transport numbers and oxygen diffusion coefficients were in good agreement with the performance results of MFCs.

Wastewater treatment

Wastewater contains complex macromolecules, which are easily degraded in the presence of various bacteria in the anaerobic inoculum. The electrogenesis step of the wastewater treatment procedure is preceded by fermentation, during which complex macromolecules such as polysaccharides undergo fermentation and are ultimately reduced to simpler carbon chain compounds. A fraction of the reduced substrate is consumed by microbes, while the rest is converted into electrons and protons, leading to power generation. During the stable phase of operation, all MFCs demonstrated COD removal efficiencies ranging from 72 to 92 %. In particular, specific COD removal efficiency values of 72.3 ± 1.1 , 90.7 ± 1.3 , 91.4 ± 1.4 , 88.0 ± 1.1 , 90.0 ± 1.0 , and 91.1 ± 1.7 % were achieved by the MFC-1, MFC-2, MFC-3, MFC-4, MFC-5, and MFC-6, respectively (Figure 37). Highest COD removal was observed for the MFC-3, which could be attributed to the large IEC value, good pore size distribution, and other physical characteristics of the PDC:PMA10:M20-1000 ceramer membrane, which preserved the microenvironment in the vicinity of the anode by promoting the scavenging of electrons and protons from the anodic chamber of MFC to the cathodic chamber.

The CE of the MFC-3 (25.1 ± 0.8 %) was also substantially higher than other MFCs, including the MFC-6 containing a commercial polymeric Nafion membrane (Figure 38), indicating that a larger fraction of organic matter was effectively consumed by the electrogenic bacteria during oxidation in the MFC-3. This phenomenon can be explained by the porous structure of the ceramer membrane and its superior physical properties, such as the relatively high IEC and cation transfer number and low oxygen permeability coefficient. Overall, the MFC-3 containing a PDC:PMA10:M20-400 ceramer separator exhibited the highest power density and

6. Tailoring hydrophilic and porous nature of polysiloxane derived ceramer and ceramic membranes for enhanced bioelectricity generation in microbial fuel cell

better organic matter removal efficiency as compared to the values obtained for the other four MFCs used in this investigation (Table 5).

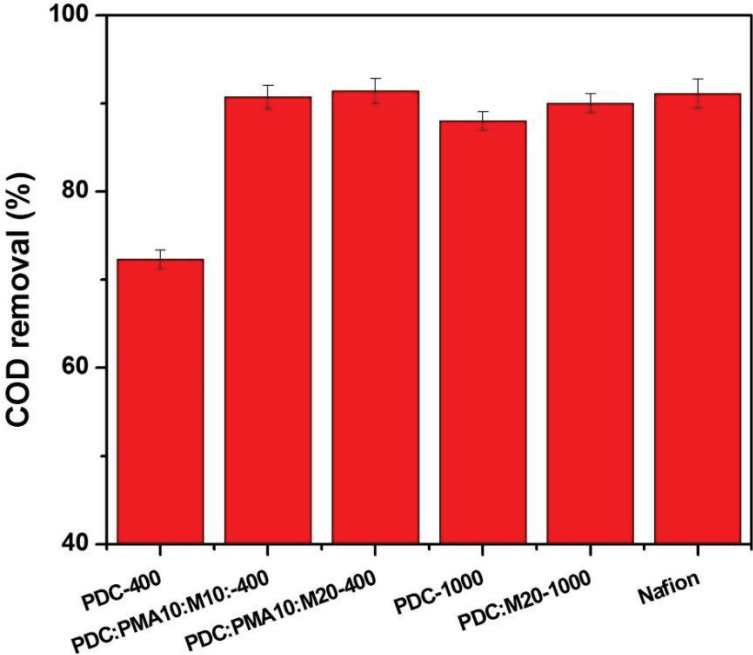


Figure 37. Chemical oxygen demand (COD) removal efficiency of MFCs.

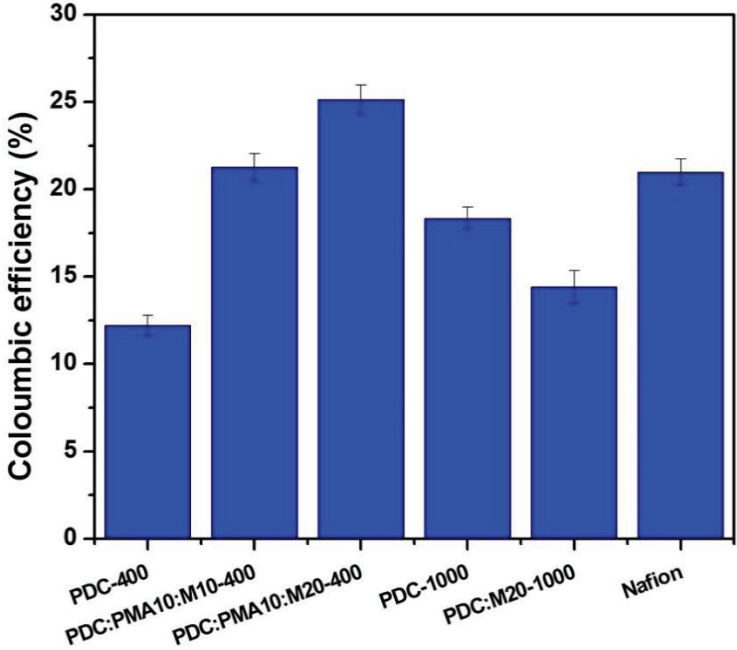


Figure 38. Coloumbic efficiency (CE) of MFCs.

6. Tailoring hydrophilic and porous nature of polysiloxane derived ceramer and ceramic membranes for enhanced bioelectricity generation in microbial fuel cell

Cost analysis

The cost comparison of the polymer derived ceramer and ceramic membranes with the commercial Nafion membrane was done based on retail market price of the raw materials in Germany. In order to compare the performance of MFCs in terms of power and cost, the specific power recovery per unit cost were estimated based on Equation 13 in materials and method section. PDC ceramer and ceramic membranes exhibited net power recovery ranging from 0.28–1.09 mW €⁻¹ with PDC:PMA10:M20-400 ceramer based MFC being the best with net power recovery of 1.09 mW €⁻¹ than commercial Nafion membrane (0.54 mW €⁻¹). Hence, the net power recovery seems to be in favour of the PDC membranes developed in this work towards scaling up of MFC.

Table 5. Performance comparison of PDC membranes with polymeric and ceramic membranes

Membranes	Anode	Cathode	Power density, $P_{V,max}$ (mW m ⁻³)	Membrane cost (€ m ⁻²)	Power recovery (mW € ⁻¹)	Coulombic efficiency (%)	NER (kWh m ⁻³)	COD removal (%)
PDC-400 (MFC-1)	Carbon felt	Carbon felt	1479.2	1066.8	0.282	12.2	0.106	72.3
PDC:PM A10:M10-400 (MFC-2)	Carbon felt	Carbon felt	5152.9	1112.9	0.944	21.2	0.371	90.7
PDC:PM A10:M20-400 (MFC-3)	Carbon felt	Carbon felt	5664.4	1015.54	1.09	25.1	0.407	91.4
PDC-1000 (MFC-4)	Carbon felt	Carbon felt	5107.6	1066.8	0.97	18.3	0.367	88.0
PDC:M20-1000 (MFC-5)	Carbon felt	Carbon felt	4200.8	984.6	0.87	14.4	0.302	90.0

6. Tailoring hydrophilic and porous nature of polysiloxane derived ceramer and ceramic membranes for enhanced bioelectricity generation in microbial fuel cell

Nafion (MFC-6)	Carbon felt	Carbon felt	5184.2	1943	0.54	20.9	0.373	91.1
PVA-STA/GO [155]	Carbon cloth	Carbon cloth/Pt-C	1190	-	-	3.3	-	83.7
Polybenzimidazole/SBA15 [302]	Carbon paper	Carbon cloth	1521.0	-	-	-	-	78.0
Mullite [197]	Carbon veil	Carbon veil	4980.0	-	-	-	-	41.5
Alumina [197]	Carbon veil	Carbon veil	2600.0	-	-	-	-	49.4
Earthenware [303]	Graphite plate	Stainless steel mesh	3800.0	-	-	19.8	-	-
Coconut shell [304]	Carbon felt	Carbon felt	3200	-	-	16.5	-	66.0
Nylon (10 μm pore size) [17]	Carbon cloth	Carbon cloth	769 ± 65 mW m ⁻²	-	-	55	-	-
Glass fiber filter (1 μm pore size) [17]	Carbon cloth	Carbon cloth	716 ± 60 mW m ⁻²	-	-	60	-	-

Summary

The study investigated the polysiloxane derived ceramer and ceramic composite membranes as separator material for MFC. The addition of 20 wt. % montmorillonite and 10 wt. % H₃PMo₁₂O₄₀/SiO₂ to polysiloxane derived ceramer (PDC:PMA10:M20-400) increased its hydrophilic nature and formation of hierarchical pore structure so as to cause considerable improvement of physical properties including high IEC and cation transport number and relatively low oxygen permeability coefficient. The MFC with hierarchical pore structured PDC:PMA10:M20-400 ceramer membrane generated the maximum volumetric power density of 5.66 W m⁻³ and CE of 25.1 \pm 0.8%, which was 4 and 2 fold higher than that obtained for the

6. Tailoring hydrophilic and porous nature of polysiloxane derived ceramer and ceramic membranes for enhanced bioelectricity generation in microbial fuel cell

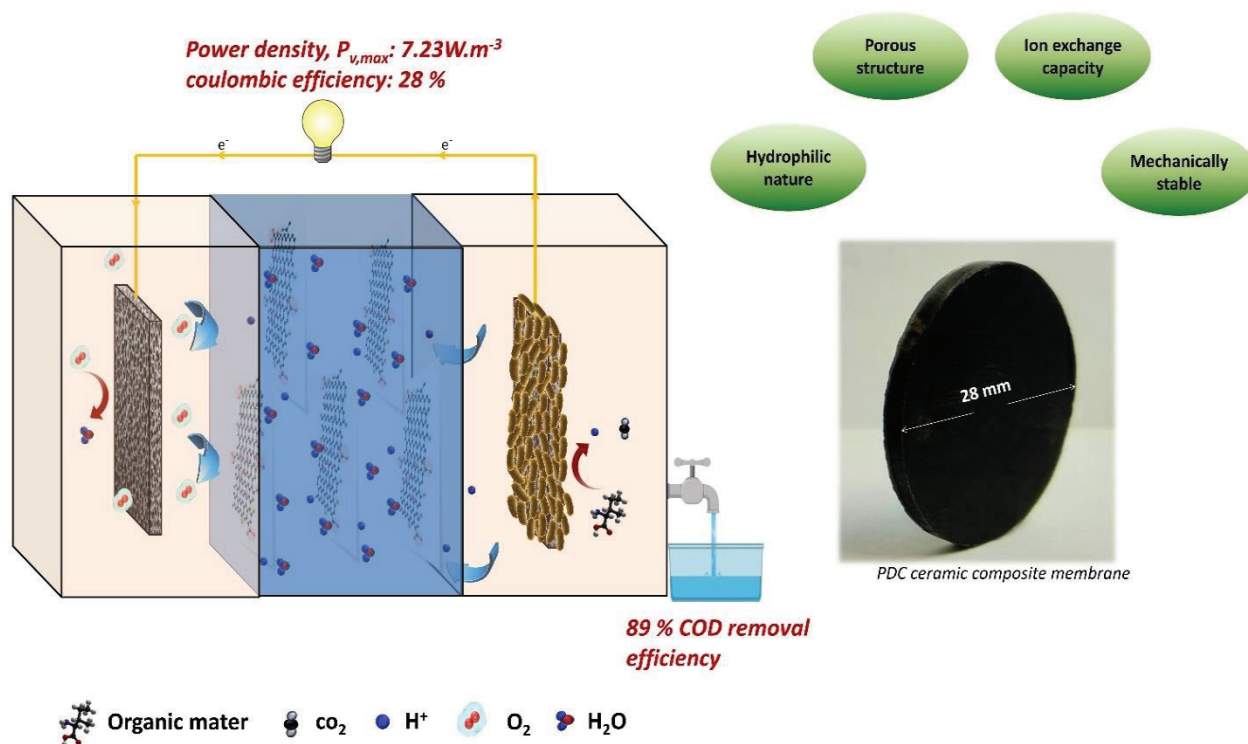
MFC with PDC-400 ceramer membrane, respectively. In addition to that, power recovery per unit cost for MFC with PDC:PMA10:M20-400 ceramer membrane was double as compared with MFC having Nafion membrane. Current density of the MFC with macropore structured PDC-1000 ceramic membrane (1013 mA m^{-2}) was 1.6 times greater than that of the macropore structured PDC:M20-1000 ceramic membrane (633 mA m^{-2}), owing to the poor hydrophilic properties of the latter. This shows that the hydrophilic and porous nature could be a decidable factor for choosing proper separator material for MFC and PDC:PMA10:M20-400 ceramer being an better alternative to the commercially available Nafion membrane for its field scale applications.

7. Microbial fuel cell performance of graphitic carbon functionalized porous polysiloxane based ceramic membranes

7. Microbial fuel cell performance of graphitic carbon functionalized porous polysiloxane based ceramic membranes

Objective

In this study, porous PDC composite membrane modified with GO and functionalized multi-wall carbon nanotube (MWCNTs) were evaluated for their potential as the separator material for application in MFC. First, a series of composite PDC membranes with different contents of GO and MWCNTs were synthesized through a facile pressing technique. The fabricated membranes were characterized in terms of their pore size distributions, surface characteristics, ion exchange capacities, oxygen permeability and mechanical stability, which were compared with the parameters of the standard commercial polymeric Nafion membrane. Furthermore, the performance of MFCs using PDC and its composite membranes was evaluated in terms of the power density, internal resistance, COD removal efficiency and coulombic efficiency (CE). This study was published as research article in Bioelectrochemistry journal [305].



Scheme 3. Schematic view of MFC and membrane.

7. Microbial fuel cell performance of graphitic carbon functionalized porous polysiloxane based ceramic membranes

Results and discussion

Phase analysis

XRD was used to study the phase evolution of PDC membrane pyrolyzed at 1100 °C. The XRD pattern is shown in Figure A4 (appendix), the observation of broad peaks between 20 and 30 °C significantly shows that SiOC is amorphous in nature. Such amorphous SiOC network can be generated by the substitution of two divalent oxygen ions by one tetravalent carbon atom within the SiO₂ network. The composition of a stoichiometric SiOC, consisting solely of Si–O, Si–C bonds and some excess free carbon, this clearly explained by H. J. Kleebe *et al* [306]. We studied the Raman spectroscopy to understand the graphitic nature of carbon present in the SiOC and in the filler materials (Figure 39). The Raman spectrum of graphitic carbon shows the usual three bands at around 1340, 1582 and 2717 cm⁻¹, which are designated as the D, G, and 2D bands, respectively. However, the Raman spectrum of these samples displays only two major peaks at 1343 and 1585 cm⁻¹ in the range from 800 to 2000 cm⁻¹, corresponding to the D band due to structural defects and the G band representing the degree of order of graphene structure, respectively [307]. In detail, The G-band is attributed to the first order scattering of the E 2g phonon of the sp² carbon-carbon bond; while the D-band represents the defect sites associated with vacancies and grain boundaries [308]. The carbon with sp² hybridization such as graphene or graphite has lower ID/IG ratio, which tells lower the defect concentration. However, GO is not a purely sp² system but a highly disordered one with a significant sp³ content. So, contrary to the standard sp² materials, the increase of defects in GO would produce a decrease of the ID/IG ratio. This is because there would be more sp² carbon atoms surrounding the defects [309].

The observed D and G band of PDC-1100 sample show a ratio of 1.06, which significantly shows the presence of free carbon in the SiOC matrix. The I_D/I_G intensity ratio increases from 0.96 of PDC:0.5GO-1100 to 1.02 of PDC:2GO-1100. It suggests a decrease in the average size of the sp² domains upon reduction of the GO phase in the PDC:2GO-1100 sample[310]. This shows that GO presence in PDC:0.5GO-1100 is comparatively stable probably due to grafting of graphene oxide functional group with the SiOC matrix. A similar effect was observed by Y. Lou *et al.* in a research study on ceramic supported graphene oxide composite membrane[311]. Further addition of 2 wt % of GO results in segregation of GO along with the graphitic free carbon in the PDC Matrix, which results in partially reduced graphene oxide during pyrolysis

7. Microbial fuel cell performance of graphitic carbon functionalized porous polysiloxane based ceramic membranes

at 1100 °C. On the other hand, I_D/I_G ratio of PDC:0.5CNT-1100 and PDC:2CNT-1100 material is 1.02 for both. This shows graphitic carbon nature with increased band ratio of above 1, due to the segregation of multiwall carbon nanotube along with free carbon presence in the PDC matrix[307]. The Raman spectrum of Graphene oxide and multiwall carbon nanotube materials are shown in appendix Figure A5. The I_D/I_G of GO pyrolysed at 1100 °C increased, which clearly shows the transformation of GO to reduced graphene oxide.

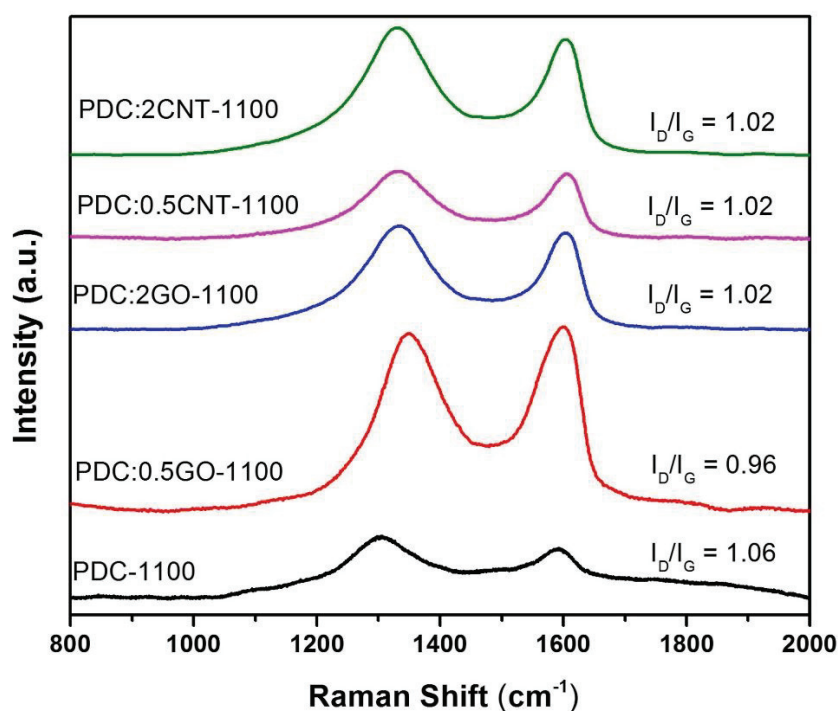


Figure 39. Raman spectroscopy of PDC and its composite membrane pyrolysed at 1100 °C.

Specific surface area

Unlike the polymeric membranes whose ion transfer properties depend on the presence of functional groups, porous ceramic membranes are not ion-selective and transport ions through their porous structures when the membrane surface is hydrophilic[121]. Therefore, studying the micro-, meso and macroporous structural properties of PDC membranes are very important for determining their suitability for application in MFCs. In this work, the micro-meso-porosity of the prepared samples were characterized by recording nitrogen adsorption-desorption isotherms (Figure 40a).

7. Microbial fuel cell performance of graphitic carbon functionalized porous polysiloxane based ceramic membranes

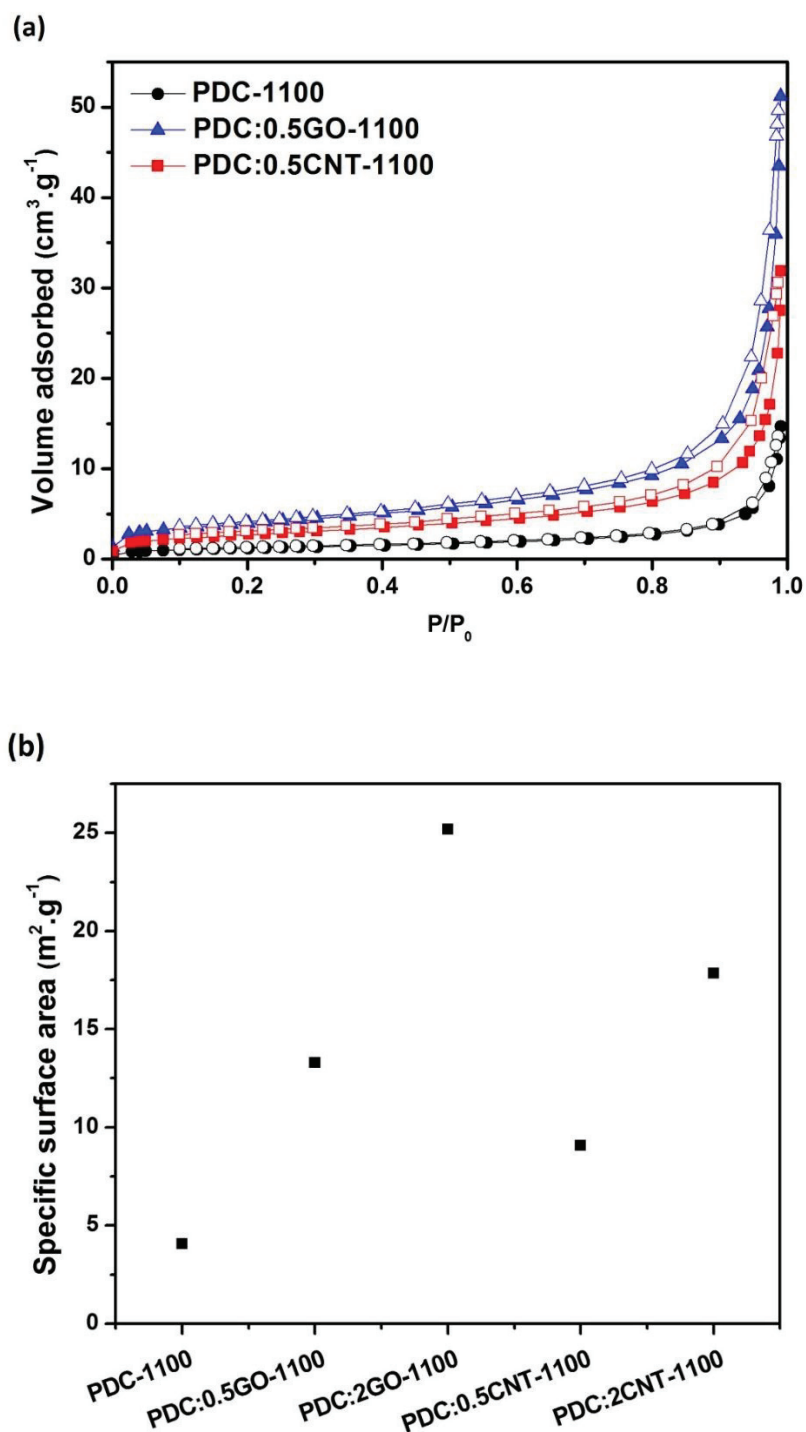


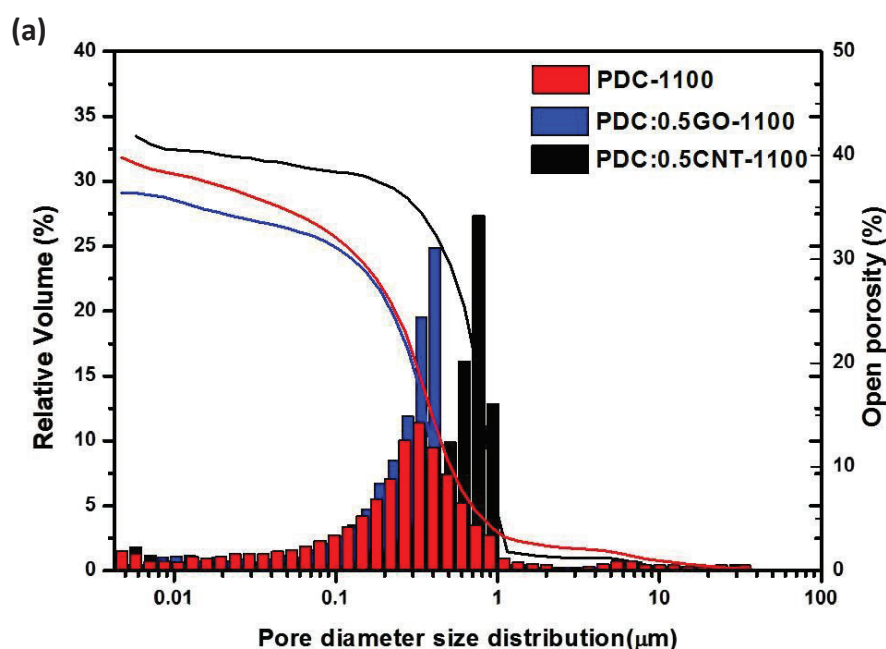
Figure 40. (a) Nitrogen adsorption/desorption isotherms of PDC membranes pyrolysed at 1100 °C (b) Specific surface areas of pyrolyzed membranes calculated (BET) from nitrogen adsorption isotherm.

7. Microbial fuel cell performance of graphitic carbon functionalized porous polysiloxane based ceramic membranes

According to the IUPAC classification, the shapes of the isotherm curves obtained for the sample pyrolyzed at 1100 °C correspond to type III isotherms, indicating that the material has only a macroporous structure. The incorporation of GO and MWCNTs (with contents of 0.5 and 2 wt.%, respectively) into the PDC matrix increased its specific surface area due to the presence of high surface area fillers[312]. The BET specific surface area (Figure. 40b) increased in the order of PDC-1100 < PDC:0.5CNT-1100 < PDC:0.5GO-1100 < PDC:2CNT-1100 < PDC:2GO-1100 from 4 up to 25 m² g⁻¹.

Pore size and its distribution

Macroporous size distributions and open porosities of the membranes were determined by mercury intrusion porosimetry (the histograms are shown in Figure 41a). The pore size distribution in the PDC membranes did not change significantly with addition of GO filler material. The average pore size of PDC-1100, PDC:0.5GO-1100 and PDC:2GO-1100 are 325 nm, 407 nm and 344 nm, respectively. On the other hand, the opposite trend was observed for PDC composite with multiwall carbon nanotube since the average pore size of PDC:0.5CNT-1100 and PDC:2CNT-1100 membrane is 735 nm and 619 nm, respectively (Figure 41b).



7. Microbial fuel cell performance of graphitic carbon functionalized porous polysiloxane based ceramic membranes

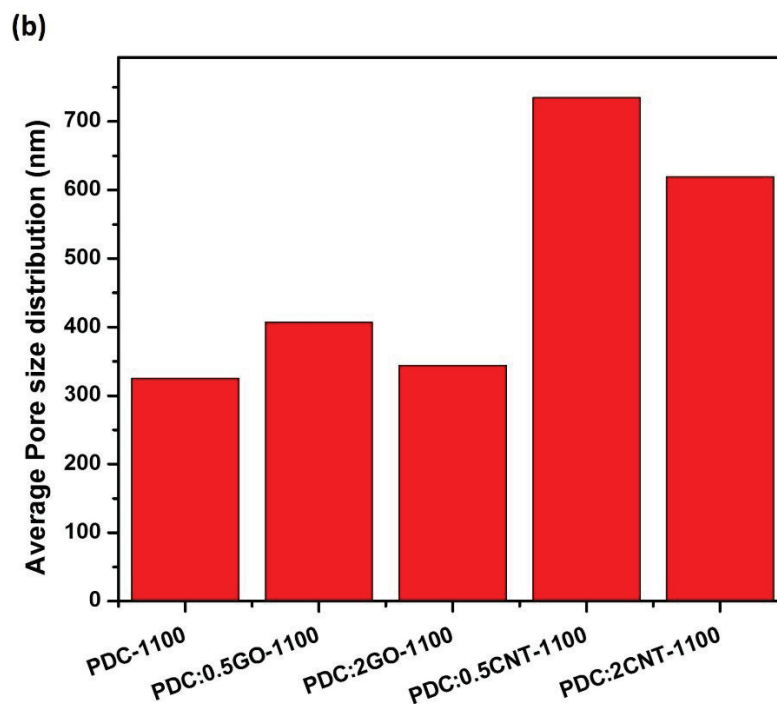


Figure 41. (a) Pore size distribution versus relative pore volume and open porosity curves obtained from Hg-porosimetry histogram of pyrolyzed samples, and (b) Average pore size of prepared PDC membranes.

This phenomenon might be caused by the partial decomposition of MWCNTs at 1100 °C leading to the evolution of carbon-containing gases and formation of large voids and defects in the membrane structure due to the dispersion of MWCNTs across the polysiloxane matrix during synthesis (MWCNTs easily agglomerate, bundle, and entangle in a polymer matrix, which can produce defects such as large pores[313, 314]). In addition, all PDC and composite membranes prepared in this study exhibited open porosities between 31 and 43 %, which were suitable for application in MFCs and facilitated the diffusion of protons from one chamber to another by the osmotic and electro-osmotic drags [315].

Hydrophilic characteristics

The hydrophilic properties of the membrane promote the adsorption of water molecules in its porous structure that act as proton transfer carriers [316]. Since an accurate water contact angle is difficult to measure for a porous structure, the adsorption of polar and non-polar solvent vapors at the pore walls (such as water and n-heptane) was performed to examine the

7. Microbial fuel cell performance of graphitic carbon functionalized porous polysiloxane based ceramic membranes

hydrophobic/hydrophilic behavior of the samples tested (Figure 42). The amount of adsorbed vapors (in mmol m^{-2}) were related to the specific surface area measured by recording N_2 adsorption-desorption isotherms. In the samples pyrolyzed at $1100\text{ }^\circ\text{C}$, most of the hydrophobic methyl and phenyl groups of the pre-ceramic polymers (H44 and BISA) were decomposed increasing their degrees of hydrophilicity[317]. Although all the membrane samples were hydrophilic in terms of the water-to-heptane ratio (> 1), the specimens without fillers were clearly less hydrophilic than other samples due to the presence of hydrophilic functional property of the filler materials. The phenomenon was observed for the PDC-1100 and PDC:0.5GO-1100 specimens, which demonstrated an increment of 91.1% after the addition of 0.5 wt.% GO. The presence of the GO network across the PDC matrix led to strong hydrophilic behavior. Similarly, Ganesh *et al.* reported that the GO-modified polysulfone membrane exhibited hydrophilic properties because of the negatively charged surface of the GO filler [317]. This is mainly because of oxidized graphene sheets (or ‘graphene oxide sheets’) having their basal planes decorated mostly with epoxide and hydroxyl functional groups, in addition to carbonyl and carboxyl functional groups located presumably at the edges (Lerf–Klinowski model). These oxygen functionalities render the graphene oxide layers of GO hydrophilic and water molecules can readily intercalate into the interlayer galleries. GO can therefore be also thought of as a graphite-type intercalation compound with both covalently bound oxygen and non-covalently bound water between the carbon layers.

The strong bonding of GO functional group across the free carbon presence in the PDC matrix led to prevent the reduction of graphene oxide for 0.5 wt % GO loading [318]. However, further addition of 2 wt.% GO into the PDC membrane resulted in a slight decrease in the water-to-heptane ratio, which might be related to the existence of reduced graphene oxide in the SiOC matrix and this inhibited the adsorption of water molecules in its structure. Due to the high loading of GO in the PDC matrix leads to segregation of graphene oxide filler material without bounding with free carbon presence in the PDC matrix. This segregated graphene oxide thermally reduced to reduced graphene oxide during pyrolysis, which shown in raman spectrum. The presence of reduced graphene oxide in the PDC:2GO-1100 membrane makes less hydrophilic nature compared to PDC:0.5GO-1100 membrane. Similarly, G. Stankovich *et al.* reported that the transformation of graphene oxide to reduced graphene oxide tends to hydrophobic nature due to the absence of hydrophilic functional sites [318]. On the other hand,

7. Microbial fuel cell performance of graphitic carbon functionalized porous polysiloxane based ceramic membranes

samples prepared with MWCNT (PDC:0.5CNT-1100 and PDC:2CNT-1100) exhibited water-to-heptane ratios of 4.36 and 4.18, which were 34 % and 28 % higher than the values obtained for bare PDC-1100, respectively. The surface characteristics of PDC:0.5CNT-1100 and PDC:2CNT-1100 is almost similar. This is because of the tendency of MWCNT didn't change gradually with increase in filler content, that evidently shown in Raman spectrum. However, these increments were not significantly higher than the magnitudes determined for the GO-modified PDC membranes.

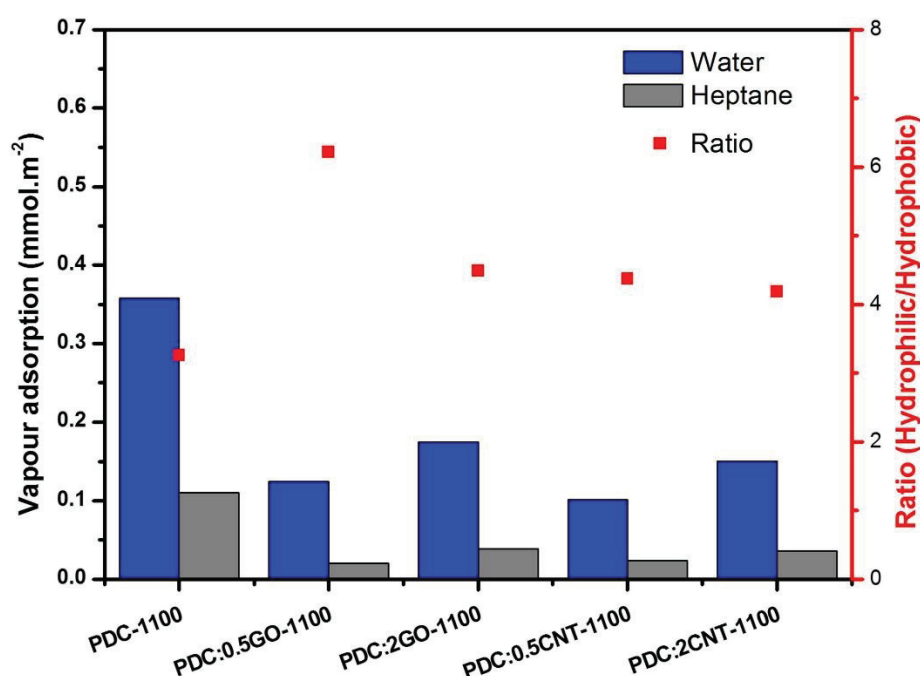


Figure 42. Water and n-heptane vapor adsorption at 25 °C for as prepared membrane materials at 1100 °C.

Ion exchange capacity

The IEC values of the PDC composite membranes (Figure 43) were obtained by a back titration method. Their magnitudes determined for the PDC:0.5GO-1100 and PDC:2GO-1100 membranes were 9 and 6 fold higher than the IECs of PDC-1100, owing to the proton-conducting nature of the well dispersed GO network in the PDC matrix [319]. The decrease in

7. Microbial fuel cell performance of graphitic carbon functionalized porous polysiloxane based ceramic membranes

IEC value of PDC:2GO-1100 membrane due to the existence of reduced graphene oxide in the matrix, which lead to less hydrophilic property. Similarly, for the PDC:0.5CNT-1100 and PDC:2CNT-1100 specimens, the corresponding IEC magnitudes increased dramatically to 0.33 and 0.28 meq g⁻¹, respectively. K. J. Lee *et al.* found that the addition of graphene oxide in nafion membrane results in increased ion conducting property and similarly Zhu *et al.* found that the presence of tubular channels in the MWCNT enhanced their ionic conduction properties [320, 321]. Moreover, high loading of graphitic filler material to PDC material are lead to high electrical conductivity, which results in decrease in ionic conductivity [312]. The observed IEC value of PDC:0.5GO-1100 and PDC:0.5CNT-1100 is almost half and one third of polymeric nafion IEC value.

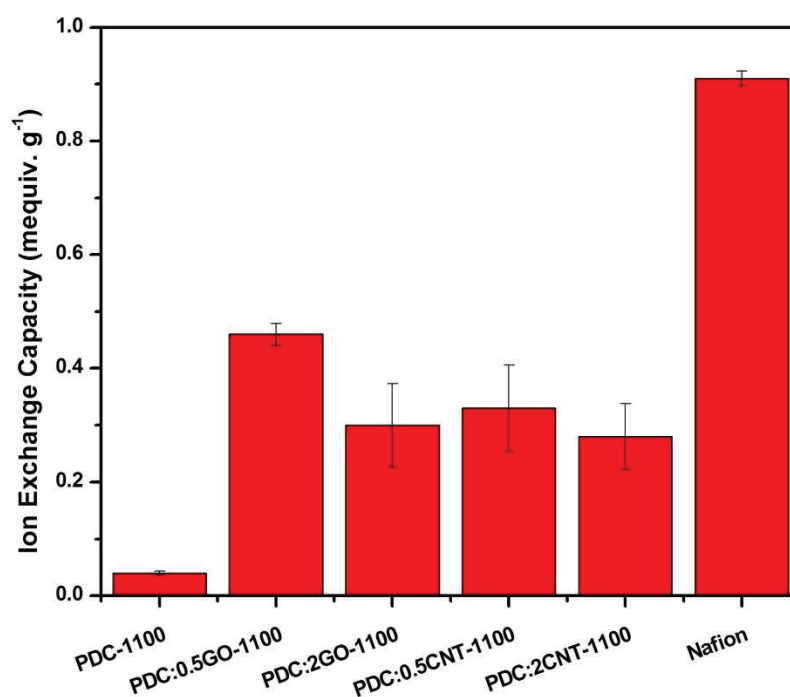


Figure 43. Ion exchange capacity measured for as prepared membranes compared with Nafion.

Oxygen permeability

The oxygen permeability of the membrane is an important factor that directly affects the efficiency of MFC. The diffusion of oxygen through the membrane from the cathode to the anode leads to the creation of a mixed potential in the anodic chamber and disturbs its anaerobic condition because oxygen molecules act as electron acceptors and inhibit the reaction at the

7. Microbial fuel cell performance of graphitic carbon functionalized porous polysiloxane based ceramic membranes

anode for thermodynamic reasons[322]. The measured oxygen mass transfer coefficients of the membranes are shown in Figure 44. Since the oxygen mass transfer and diffusion coefficients of the materials for application in MFCs should be as small as possible, the PDC:0.5GO-1100 composite membrane demonstrated the best performance with the corresponding values equal to $6.37 \times 10^{-4} \text{ cm s}^{-1}$ and $1.91 \times 10^{-4} \text{ cm}^2 \text{ s}^{-1}$, respectively. This phenomenon is mainly because high hydrophilic nature and small pore size results in low oxygen diffusion. Even though, PDC:0.5GO-1100 and PDC:2GO-1100 membranes has almost similar pore size but the hydrophilic property of PDC:0.5GO-1100 membrane is much higher than PDC:2GO-1100 membrane. For instance, Atwater *et al.* reported that the hydrophilic properties of the membrane inhibited the permeation of Dissolved Oxygen molecules through the membrane due to their non-polar characteristics [301].

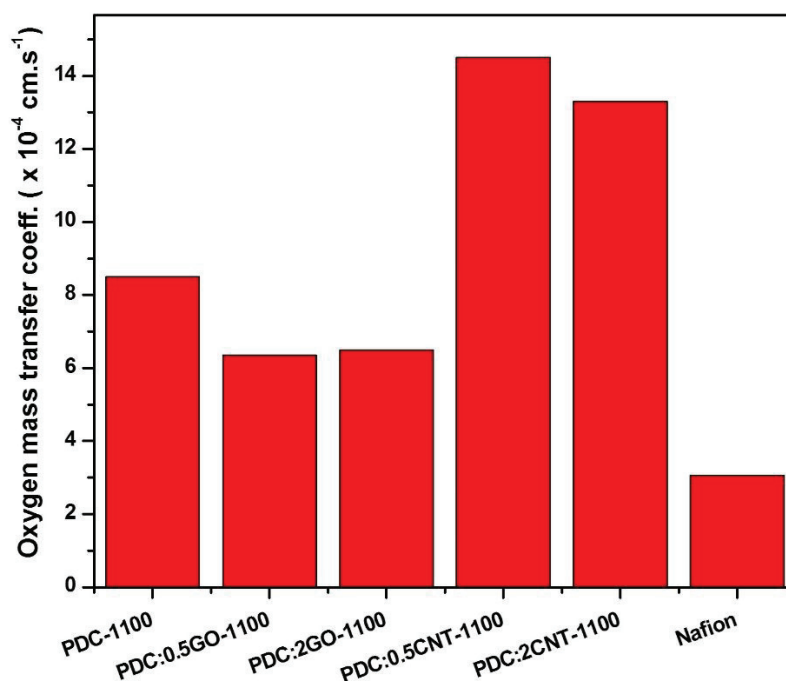


Figure 44. Oxygen mass transfer coefficient of PDC membranes.

On the other hand, the samples containing 0.5 and 2 wt. % of CNTs pyrolyzed at 1100 °C exhibited higher oxygen mass transfer and diffusion coefficients as compared to those of the PDC-1100 samples. Usually, the incorporation of MWCNTs decreases these parameters since the introduction of nanocomposites tends to block the diffusion paths for oxygen permeation.

7. Microbial fuel cell performance of graphitic carbon functionalized porous polysiloxane based ceramic membranes

However, the PDC:0.5CNT-1100 and PDC:2CNT-1100 membranes possessed the large pore sizes of 735 nm and 619 nm, respectively, which resulted in high oxygen mass transfer and diffusion coefficients. This factor tremendously affects the final power production of MFCs.

Mechanical properties

The flexural strength of a membrane is one of the most important parameters of the MFC separator. In this study, ring-on-ring ball bending tests were performed to evaluate the effects of the pyrolysis temperature and addition of GO and MWCNTs on the flexural strengths of the PDC composite membranes (Figure 45). The flexural load-displacement curves indicate nearly elastic deformation followed by a stage, during which the flexural strength increases until rupture. It is also evident that the flexural strength increases with the addition of graphitic filler material to ceramic matrix, which can be attributed to strong interfacial bonding between the graphitic filler and the ceramic matrix [323].

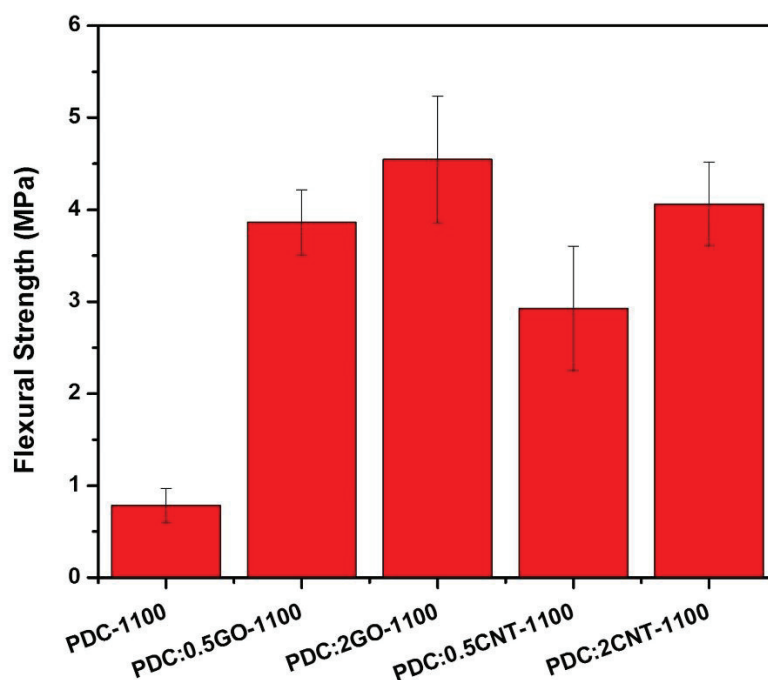


Figure 45. Flexural strength of the PDC membranes.

7. Microbial fuel cell performance of graphitic carbon functionalized porous polysiloxane based ceramic membranes

The membrane containing 0.5 wt. % GO in the SiOC matrix demonstrated a significant increase in the flexural strength from 0.782 to 3.862 MPa at a pyrolysis temperature 1100 °C, respectively. This effect is very likely resulted from the cross-linking of the polysiloxane matrix with functional groups of GO above 200 °C, which reduced the curing temperature [324]. The further increase in the GO loading to 2 wt. % produced very small flexural strength increments of only 17 % compared to 0.5 wt. % loaded PDC membrane. This phenomenon might be due to the saturation limit of filler in the PDC matrix. Similar to the GO filler, MWCNTs were composite with the polysiloxane matrix, which increased its mechanical strength as compared to that of the bare SiOC membrane. Thus, the flexural strengths of SiOC loaded with 0.5 wt.% MWCNTs and pyrolyzed at 1100 °C was 2.926 MPa, respectively. After increasing the MWCNT content to 2 wt. % MWCNT, the flexural strength of the membrane were increased, which was similar to the effect observed after GO addition.

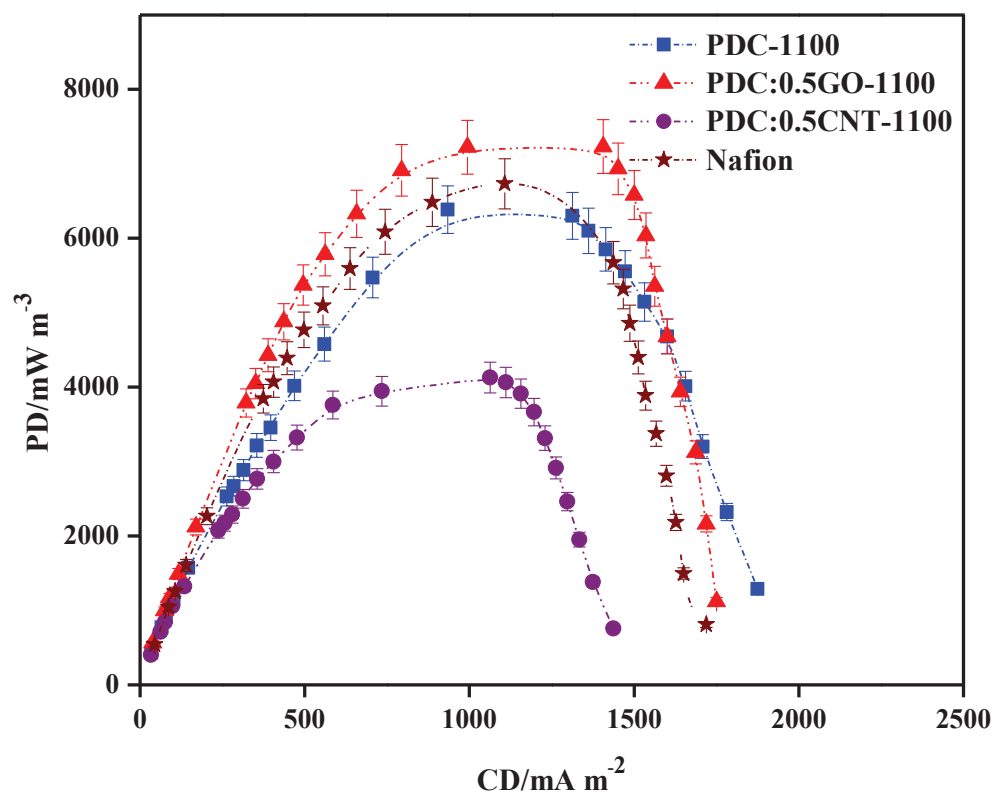
Power generation and polarization curves

The bare PDC membranes and membranes containing 0.5 wt. % graphitic fillers prepared at 1100 °C were selected as the separator materials for MFC and performance difference was evaluated because of differences in physical properties of the separators, such as IEC, mechanical stability, oxygen permeability, and water-to-heptane adsorption ratio. The PDC:0.5GO-1100 membranes exhibited higher water-to-heptane adsorption ratios, IEC values, and mechanical stability and low oxygen permeability as compared to that of the PDC-1100 samples, respectively. On the other hand, the oxygen permeability of the PDC:0.5CNT-1100 membrane was higher than the magnitudes obtained by the other membranes, which can significantly deteriorate the performance of MFC. However, the other physical properties of these two membranes were noticeably better than that of PDC-1100 membrane. Evaluating the performance of MFCs utilizing PDC-1100, PDC:0.5GO-1100, and PDC:0.5CNT-1100 membranes could thus provide the information on the most influential physical property for selecting a suitable membrane separator.

The operating voltage was measured over a 100 Ω external resistance. Four MFCs with PDC-1100, PDC:0.5CNT-1100, PDC:0.5GO-1100, and Nafion PEM were studied using the reactor shown in Figure A6 (appendix). During the first 20 days of operation of MFC, an electroactive biofilm grew on the anode surface, which ultimately caused voltage fluctuations due to the

7. Microbial fuel cell performance of graphitic carbon functionalized porous polysiloxane based ceramic membranes

immature biofilm. After five feed cycles, the MFCs were able to generate stable OV and OCV values. The MFC containing PDC:0.5GO-1100 produced an OV of 245 ± 3.46 mV, which exceeded the values obtained for PDC-1100 and the polymeric Nafion membrane by 15% and 35%, respectively. On the other hand, the MFC with the PDC:0.5CNT-1100 membrane exhibited an OV of 170.2 ± 4.56 mV, which was significantly lesser than that of the bare PDC-1100 membrane. This decrement was mainly influenced by the high oxygen permeability between the cathode and the anode caused by the larger pore sized membrane. Furthermore, the internal resistance of the MFCs was strongly affected by the overpotential losses at anode and cathode as well as by the ohmic resistance of the membrane–electrolyte interfaces. In this work, the MFC containing the PDC:0.5CNT-1100 membrane had an internal resistance of 141Ω , which was clearly higher than those of the MFCs with the PDC-1100 (137Ω) and PDC:0.5GO-1100 (123Ω) membranes. The polarization was conducted after achieving a stable OV (Figure 46). The MFC performance in terms of the power density resembled the trends observed for OV and OCV.



7. Microbial fuel cell performance of graphitic carbon functionalized porous polysiloxane based ceramic membranes

Figure 46. Power density vs. current density curves obtained for MFC with different ceramic membranes and compared with commercial Nafion membrane.

The power density of the MFC with the PDC:0.5GO-1100 membrane was found to be 7.23 W m^{-3} , which was nearly 1.15 times higher than those of the MFCs containing PDC-1100 membranes. Moreover, the power density obtained in MFC using PDC:0.5GO-1100 membrane was 53% higher than the power density produced by the MFC using Nafion membrane. The anode and cathode polarization curves suggested that there is hardly any variation in anode and cathode potential trends for all the MFCs, which further emphasize the change in the performance of MFC was mainly due to membrane properties not because of other influences (Figure 47).

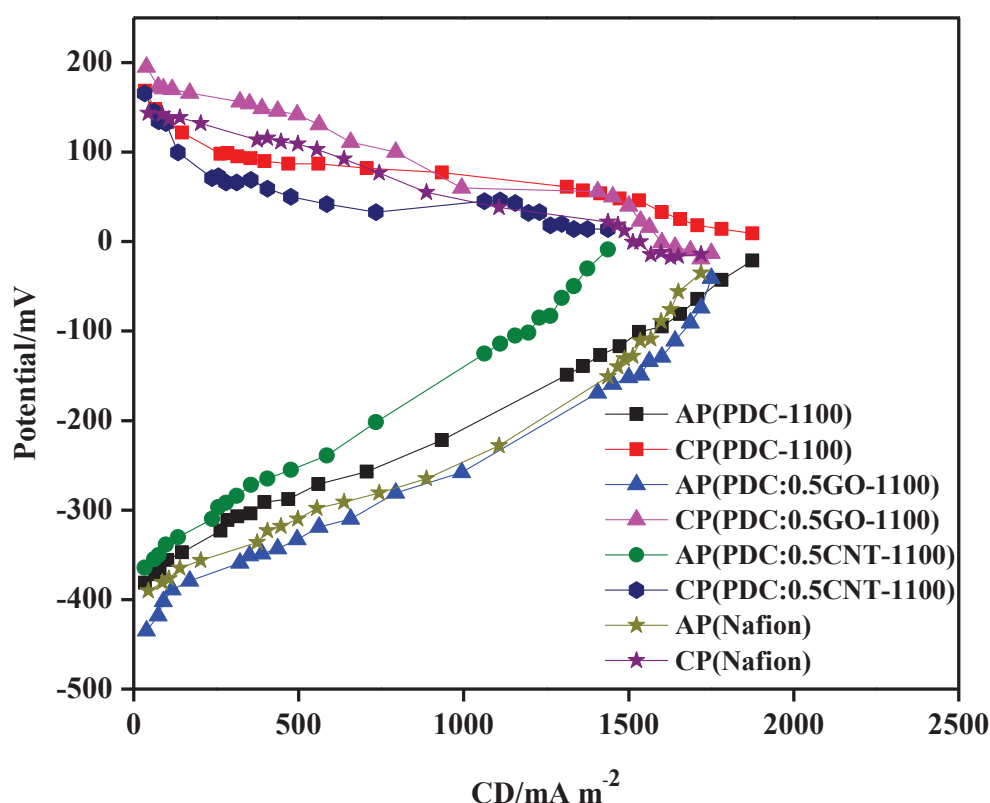


Figure 47. Anode potential and cathode potential curves for the MFCs.

Although the polymeric Nafion membrane exhibits higher ion exchange capacity and lower oxygen permeability, its performance in MFC was slightly inferior than MFC with

7. Microbial fuel cell performance of graphitic carbon functionalized porous polysiloxane based ceramic membranes

PDC:0.5GO-1100 membrane, which gave the best performance among all. The Nafion membrane transports protons due to the presence of a negatively charged sulfonic acid in the polymeric backbone. However, the long-term operation of the MFC containing the Nafion membrane causes deactivation of proton-exchange sulfonic acid groups, which deteriorates its performance. Another possible explanation is that the transportation of other cations through Nafion membrane (K^+ , Na^+ , Mg^+ , Ca^+) through electro-dialysis process rather than proton driven by the concentration gradient [325]. In an investigation, it was found that the number of cations flowing through Nafion membrane from anodic to cathodic chamber was almost the same as the number of electrons transferred through the external circuit, which may drastically affect the performance of MFC [326]. Recently, Flimban *et al.* demonstrated that the biofouling of the polymeric Nafion membrane observed during the long-term operation of the MFC system is a major factor affecting the MFC characteristics[129].

On the other hand, possible proton-conduction mechanisms have not been extensively studied for porous ceramic membranes. However, it is likely that these mechanisms involve the osmotic and electro-osmotic drag forces. Many researchers claimed that the vehicle mechanism of the proton conductivity in porous ceramic membranes was the most probable one [209]. In this mechanism, the membrane adsorbs water molecules that are further protonated to form ionic clusters such hydronium ions (H_3O^+), which penetrate through the medium *via* molecular diffusion causing proton transfer. These water molecules adsorb in the porous channels of the ceramic membrane further promoting the molecular diffusion of H_3O^+ ions from the anode to the cathode.

The water movement through the ceramic membrane of the MFC can proceed *via* two different routes. The first route corresponds to the active transport due to the electro-osmotic drag force in the closed circuit mode (under load), which is linearly related to the current generated by MFC. The second route is the passive transport induced by the osmotic pressure gradient between the dissimilar solutions in the anodic and cathodic chambers, which is dominant under open circuit conditions. The MFC utilizing macroporous PDC:0.5GO-1100 membrane generated relatively high power and current density at a low internal resistance because of its high water-to heptane ratio (hydrophilicity) as compared to those of all other PDC membranes prepared in this work. These hydrophilic characteristics, as well as the porous structure of the membrane, promote the adsorption of water molecules in its pores. Furthermore, the ion

7. Microbial fuel cell performance of graphitic carbon functionalized porous polysiloxane based ceramic membranes

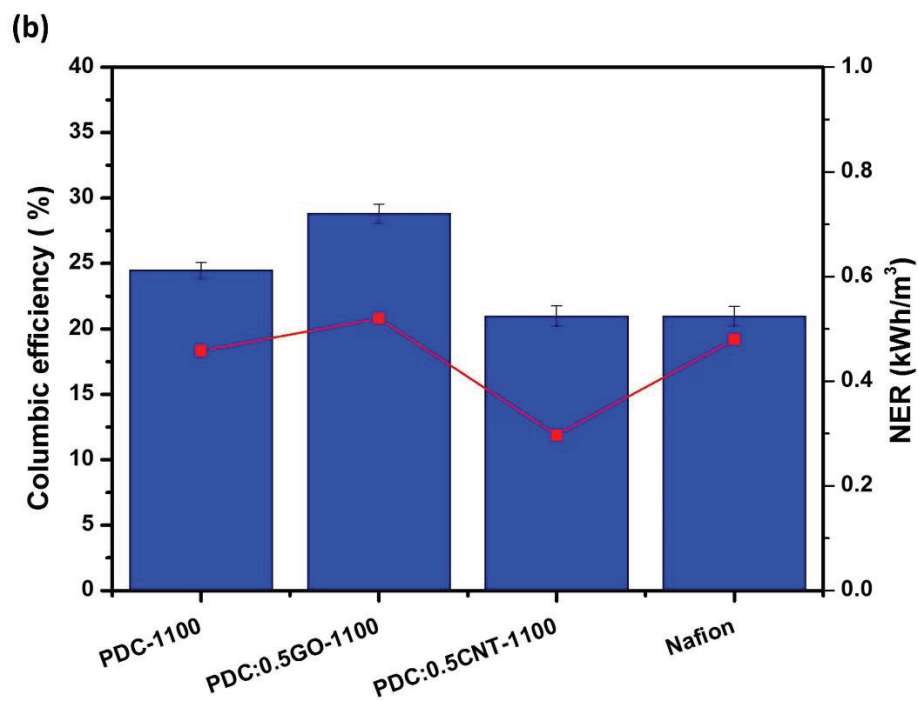
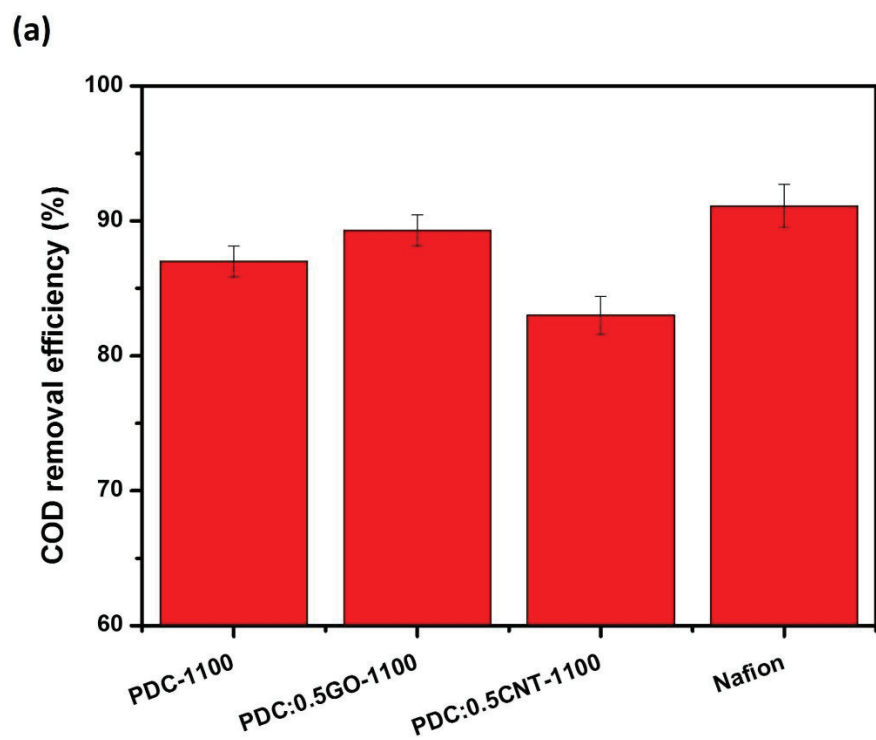
conduction in the membrane is enhanced demonstrated by its high IEC value. These physical properties of the membrane (such as its hydrophilic characteristics, porous structure, and IEC) facilitate the proton transfer from the anode to the cathode chamber.

Although PDC-1100 membrane exhibits similar porous structure, its hydrophilic characteristics are less than the PDC:0.5GO-1100 membrane, which inhibit the adsorption of water molecules and limit the diffusion of hydronium ions. On the other hand, the PDC:0.5CNT-1100 membrane has higher water-to-heptane ratio and IEC as compared to those of the PDC-1100 membrane. However, the performance of MFC using PDC:0.5CNT-1100 membrane was considerably weaker than that of the PDC-1100 membrane due to the high permeability of oxygen from the cathode to the anaerobic anode chamber. This phenomenon reduced the performance of MFC, because of the voltage loss caused by the increase in redox potential due to either substrate consumption or the loss by aerobic oxidation rather than anaerobic fermentation. Moreover, since oxygen is a strong electron acceptor, it competes with the anode during the electron accepting process, negatively affecting the performance of MFC. Overall, the high power output observed from MFC using PDC:0.5GO-1100 shows that, the properties like hydrophilic characteristics and oxygen permeability could be the influential parameter for membrane performance in MFC system.

Wastewater treatment and coulombic efficiency

The wastewater treatment efficiency in terms of COD removal was monitored for 10 batch cycles with the retention time of 3 days. After the stable phase of operation, all MFCs demonstrated COD removal efficiencies in the range of 87–91% (Figure 48a). The average COD removal efficiencies of the MFCs containing the PDC-1100, PDC:0.5GO-1100, and PDC:0.5CNT-1100 membranes were $89 \pm 1.14\%$, $87 \pm 1.25\%$, and $83.00 \pm 1.41\%$, respectively. The high COD removal efficiency suggests slight improvement in the kinetics of anodic oxidation caused by the rapid scavenging of protons through the porous ceramic membrane[304]. Moreover, the stacking of protons in the anodic chamber increases the acidity value, which decreases the microbial catalysis kinetic activity in the anodic chamber. The COD removal efficiency of the MFC with the Nafion membrane was equal to $90.8 \pm 1.86\%$, which was comparable with the MFC containing the PDC ceramic membranes prepared at 1100 °C.

7. Microbial fuel cell performance of graphitic carbon functionalized porous polysiloxane based ceramic membranes



7. Microbial fuel cell performance of graphitic carbon functionalized porous polysiloxane based ceramic membranes

Figure 48. (a) Average COD removal efficiency of MFC; (b) Average columbic efficiency and Normalized energy recovery of MFC using ceramic membranes and polymeric Nafion membrane.

The MFC operated with the PDC:0.5GO-1100 membrane demonstrated CE of 28.8 ± 0.73 %, which was 1.18 time higher than that of MFCs containing the PDC-1100 membrane (Figure 48b). The CE value of the MFC with the Nafion membrane was 20.48 ± 0.64 %, which was 29 % lower than that of the MFC containing the PDC:0.5GO-1100 membrane. The NER studies also followed almost the same trend with PDC:0.5GO-1100 being the highest followed by PDC-1100 > Nafion > PDC:0.5CNT-1100 (Table 6). Thus, the performance evaluation demonstrated that PDC:0.5GO-1100 membrane exhibits superior proton conducting properties and can be a potential candidate to be used as an alternative to the extensively used Nafion 117 membrane for large scale MFC applications.

Table 6. Electrochemical analysis data for all the MFCs

Parameter s	PDC-1100	PDC:0.5GO-1100	PDC:0.5CNT-1100	Nafion	Mullite [197]	Alumina [197]	Earthenware [197]
OV (mV)	213.60 ± 2.67	245.00 ± 3.46	170.20 ± 4.56	181.80 ± 3.51	-	-	-
OCV(mV)	621.70 ± 4.32	636.80 ± 3.19	546.90 ± 4.20	586.70 ± 2.66	519.8 \pm 13 .1	474.6 \pm 7.7	529.0 \pm 2 .4
MPD (mW m ⁻³)	6300	7232	4128	6733	4980.0	2600	6850
Internal Resistance (Ω)	137	123	141	160	500	2000	304
COD removal efficiency (%)	87.00 ± 1.15	89.30 \pm 1.15	83.00 \pm 1.41	90.80 \pm 1.86	41.5 \pm 5.9	49.4 \pm 7. 3	50.2 \pm 3. 7
CE (%)	24.47 ± 0.31	28.81 \pm 0.73	20.98 \pm 0.77	20.48 \pm 0.64	-	-	-

7. Microbial fuel cell performance of graphitic carbon functionalized porous polysiloxane based ceramic membranes

NER (kWh m⁻³)	0.45	0.52	0.29	0.48	-	-	-
-------------------------------------	------	------	------	------	---	---	---

Summary

Graphitic carbon modified PDC composite membranes were synthesized using a polysiloxane precursor and graphitic carbon fillers such as GO and MWCNTs. The PDC-based samples prepared in this study exhibited a porous structure with an open porosity ranging from 31% to 43%. The mechanical stability and IEC of the PDC matrix were considerably improved by the incorporation of GO and MWCNT species. The samples containing 0.5 wt. % of GO and MWCNTs featured a high mechanical stability, corresponding to 5-fold and 4-fold increase in the flexural strength of the bare PDC membrane pyrolyzed at 1100 °C. The PDC:0.5GO-1100 membrane possessed the highest water-to-heptane ratio and an IEC value of 0.46 meq g⁻¹, which was equal to 50% of the magnitude obtained for the Nafion membrane. Moreover, the oxygen diffusion coefficient was decreased from 4.03×10⁻⁴ cm² s⁻¹ for the PDC-1100 membrane to 1.91×10⁻⁴ cm² s⁻¹ for the PDC:0.5GO-1100 membrane. Owing to the superior hydrophilic characteristics and minimal oxygen permeability of the PDC:0.5GO-1100 membrane, the corresponding MFC exhibited coulombic efficiency values that was much higher than those of the MFC with the polymeric Nafion membrane. Therefore, the as-prepared PDC composite ceramic membranes can be potentially utilized as the membrane materials for large scale MFC applications.

8. Polysiloxane derived ceramic membrane composite with TiO₂ and SiO₂ filler material for Microbial fuel cell (MFC) and membrane bioreactor (MBR)

8. Polysiloxane derived ceramic membrane composite with TiO₂ and SiO₂ filler material for Microbial fuel cell (MFC) and membrane bioreactor (MBR)

Objective

The aim of this part of the work is to demonstrate the capability of porous PDC membranes as an inexpensive proton exchange membrane for MFC and MBR application. With this purpose, the chemical composition of the polysiloxane-based precursors were altered by the addition of filler material like SiO₂ (as particle), SiO₂ (derived from TEOS), TiO₂ to the pre-ceramic polymer. The functional properties of as-prepared membranes were evaluated in a dual chamber tank in terms of ion exchange capacity, oxygen diffusion, and mass transfer coefficient in comparison with commercial polymeric Nafion 117 membrane. Applicability of these ceramic membranes in MFCs were investigated in terms of power density, wastewater treatment, normalized energy recovery, and coulombic efficiency (CE), by comparing these ceramic membrane performance with the MFC having polymeric nafion under same conditions. Furthermore, the water permeability tests were carried out to determine the membrane capability for ultrafiltration application in MBR system.

Results and Discussion

Surface morphology

The SEM analysis shows the surface morphology of the PDC membrane (Figure 49 a-d). The bare PDC ceramic membrane has smooth surface when compared to all other membrane. The highly dispersed SiO₂ as particles observed in PDC:SiO₂-1100, whereas SiO₂ derived from TEOS source (PDC:TEOS-1100) has no silica particles. This could be due to insitu formation of silica with PDC matrix while cross-linking step. Similarly, TiO₂ particle is also dispersed throughout the PDC membrane. From the TEM image observed that the TiO₂ particles were dispersed in the PDC matrix (Figure 49 e).

8. Polysiloxane derived ceramic membrane composite with TiO₂ and SiO₂ filler material for Microbial fuel cell (MFC) and membrane bioreactor (MBR)

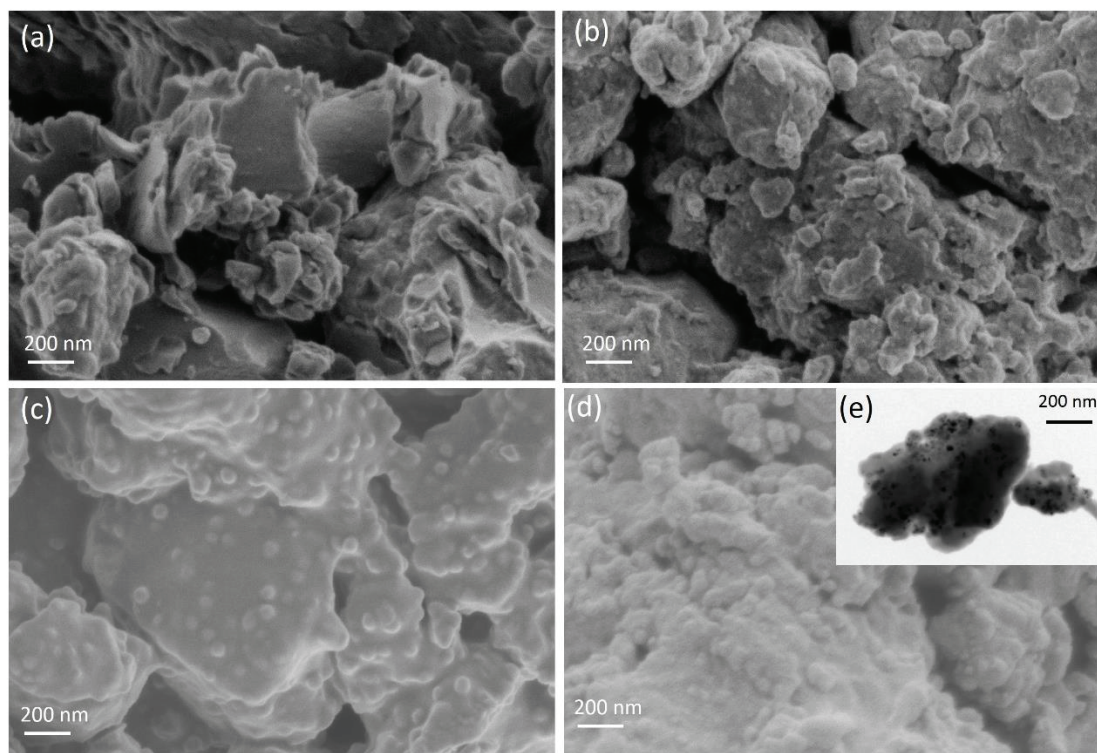


Figure 49. SEM morphology of samples (a) PDC-1100 (b) PDC:TEOS-1100 (c) PDC:SiO₂-1100 (d) PDC:TiO₂-1100 (e) TEM morphology of PDC:TiO₂-1100

Pore size distribution and porosity

The pore size distribution and porosity (Figure 50) of the as-synthesized ceramic membranes are analyzed by the mercury intrusion method. The pore sizes of the membranes are distributed in the range 100–1000 nm and change significantly based on the material compositions. For instance, the bare ceramic membranes have mean average pore sizes of 300 to 770 nm, with decreasing pore size upon the incorporation of TiO₂, SiO₂ (as particle) and SiO₂ (derived from TEOS) filler material. Meanwhile, the PDC:TiO₂-1100 ceramic shows the lowest average pore size of 348 nm.

The porosity of the ceramics arise from the macro structures of the material. The PDC:TiO₂-1100 ceramic shows a higher porosity of 37 % compared to the other materials tested here. This value is significantly higher than that of the bare PDC ceramic membrane, as are shown in Figure 49. From this result, the ceramic functionalized with hygroscopic fillers has a highly porous structure. Hong *et al.* reported that the presence of highly porous structures enhance the water flux and permeability compared to that shown by non-porous membranes [27].

8. Polysiloxane derived ceramic membrane composite with TiO₂ and SiO₂ filler material for Microbial fuel cell (MFC) and membrane bioreactor (MBR)

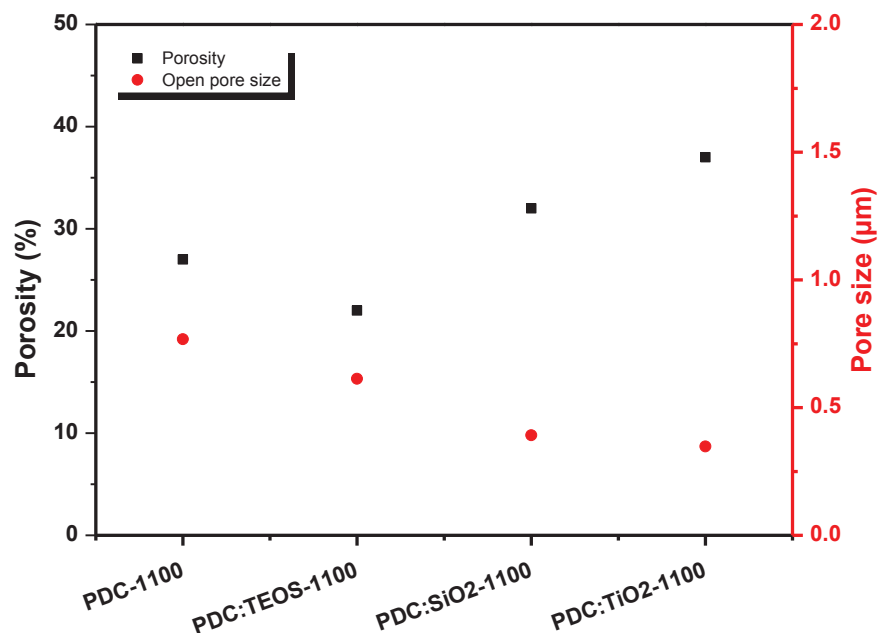


Figure 50. Average poresize and open porosity of PDC membranes.

Surface characteristics

The water and heptane adsorption characteristics are examined to understand the hydrophilic and hydrophobic behaviors of the materials, as shown in Figure 51. The vapor adsorption is related to the specific surface area obtained from the nitrogen gas adsorption–desorption isotherm (Surface area). The material nature is classified by the ratio of water to heptane vapor adsorption; for a ratio >1 , the material is hydrophilic. Prenzel *et al.* reported that the addition of APTES with polysiloxane caused increased hydrophilicity in the pyrolyzed ceramic materials [18]. In this experiment, the addition of hygroscopic filler to the PDC matrix pyrolyzed at 1100°C influence the water/heptane adsorption ratios of the ceramic membranes. Specifically adding TiO₂ to the PDC matrix, a transformation to higher hydrophilic/hydrophobic ratio occurs for the PDC:TiO₂-1100 ceramic membrane. This is because of the hygroscopic nature of TiO₂, which can hold water molecules in its porous structure. The PDC:SiO₂-1100 membrane hydrophilic nature is comparatively higher than PDC:TEOS-1100. This could be due to SiO₂ exposed as particle in the PDC matrix, which shown in surface morphology section. Meanwhile, all the PDC ceramic materials in this study show hydrophilic behaviour because of the complete decomposition of the methyl and phenyl functional groups to SiOC structures at 1100 °C.

8. Polysiloxane derived ceramic membrane composite with TiO₂ and SiO₂ filler material for Microbial fuel cell (MFC) and membrane bioreactor (MBR)

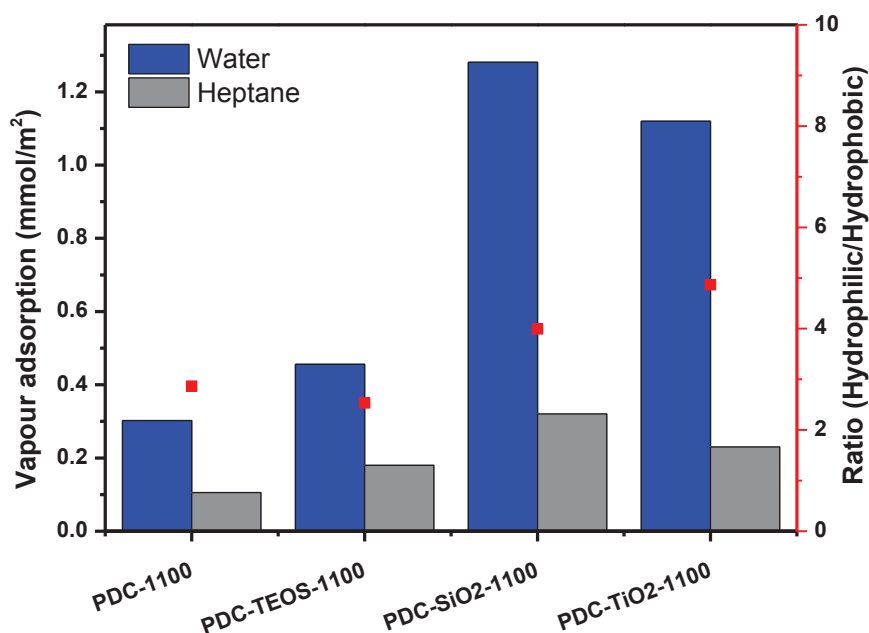


Figure 51. Water and n-heptane vapor adsorption for as prepared membrane materials at 1100 °C.

Ion exchange capacity

The IEC values of the ceramic membranes show a slightly increases with the addition of hygroscopic filler to the PDC matrix, as shown in Figure 52. This is mainly due to the surface interaction of hydronium ion and the hygroscopic filler materials. Moreover, the addition of TiO₂ to the PDC matrix increases the IEC by a factor of 2 for the ceramic membranes. Ion transfer in the ceramic membrane occurs by means of migration and convection through the porous structures of the PDC composite membranes. Meanwhile, the hygroscopic filler materials facilitate membrane proton transfer by the charged ions present in their structures.

8. Polysiloxane derived ceramic membrane composite with TiO₂ and SiO₂ filler material for Microbial fuel cell (MFC) and membrane bioreactor (MBR)

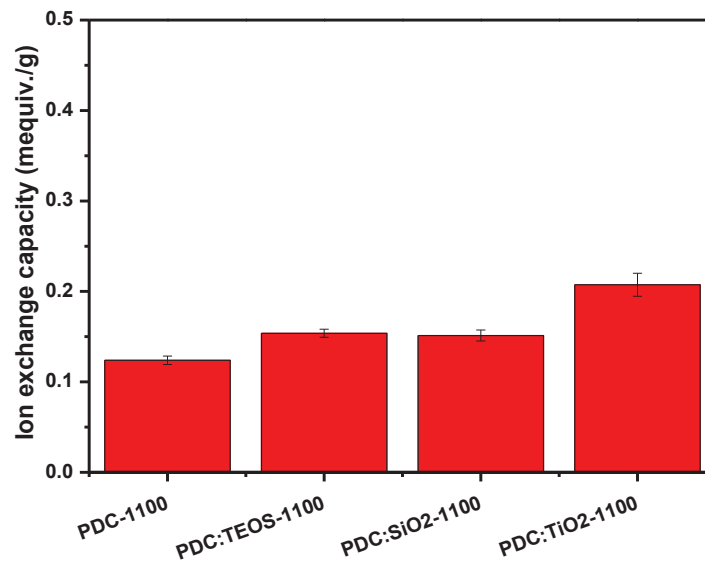


Figure 52. Ion exchange capacity of the membranes.

Oxygen diffusion coefficient

The membrane in an MFC is intended to prevent the diffusion of dissolved oxygen (DO) from the aerobic cathode chamber to the anaerobic anode chamber. The oxygen diffusion coefficients of the membranes are shown in Figure 53; oxygen diffusion is controlled by the pore structure of the ceramic membrane. Li *et al.* reported that the pore structure and open porosity of the membrane significantly affected the control of the diffusion of DO in porous-membrane MFC systems [28] [111] Here, the pure PDC membrane shows an average pore size of 768 nm and a higher oxygen mass transfer coefficient of 8.45×10^{-4} cm/s. The addition of 15% SiO₂ decreases the oxygen mass transfer coefficient to 4.97×10^{-4} cm²/s. This is mainly because of the reduced average pore size of 392 nm in the SiO₂ containing SiOC matrix. Furthermore, with the addition of 15% TiO₂, the PDC membrane shows the minimal oxygen mass transfer coefficient of 4.58×10^{-4} cm²/s and a reduced average pore size of 348 nm, while retaining 37% open porosity in the PDC:TiO₂-1100 membrane. Moreover, the minimal DO diffusion coefficient is observed for the PDC:TiO₂-1100 membrane compared to PDC-1100 membrane, because the PDC membrane is comparatively less hydrophilic and causes a higher oxygen permeability in the ceramic membrane.

8. Polysiloxane derived ceramic membrane composite with TiO₂ and SiO₂ filler material for Microbial fuel cell (MFC) and membrane bioreactor (MBR)

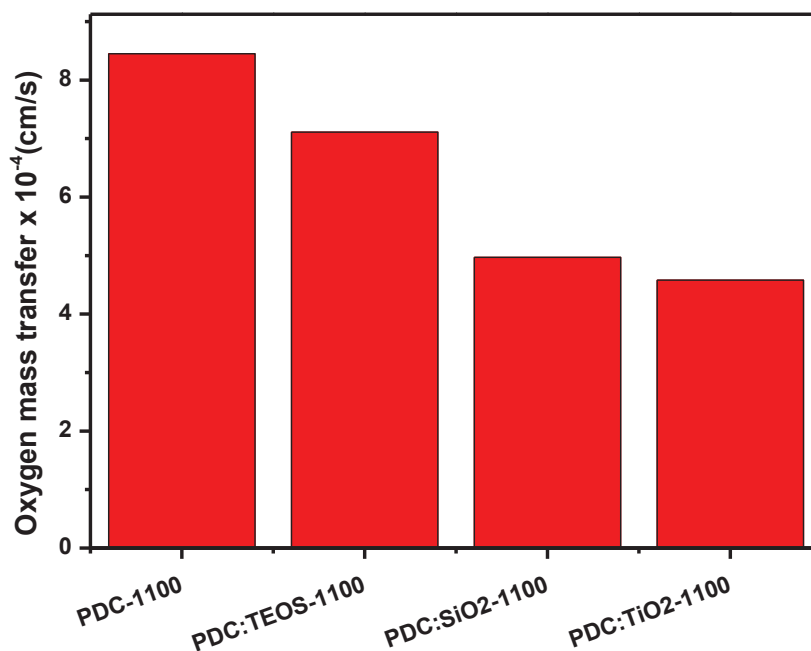


Figure 53. Oxygen mass transfer coefficient of the membranes.

MFC performance

The MFC performance were studied by Mr. Gourav Dhar Bhowmik and Prof. Dr. Makarand M. Ghangrekar from Indian Institute of Technology, Kharagpur, India. The MFC performances were evaluated in terms of the voltage generation, using the as-synthesized ceramic membranes as separator materials for MFCs in this study. The voltage generation was observed by measuring the open voltage (OV) and open-circuit voltage (OCV) from the day following MFC start-up, confirming the presence of active exoelectrogenic bacteria in the wastewater. The operating voltage was measured over a 100 Ω external resistance. Five MFCs with PDC-1100, PDC:TiO₂-1100, PDC:TEOS-1100, PDC:SiO₂-1000, and Nafion were labeled as MFC-1, MFC-2, MFC-3, MFC-4, and MFC-5, respectively using the reactor shown in Figure A6 (appendix). Firstly, for the MFC-1 with PDC-1100 ceramic membranes, the average OV of 171 mV was achieved under steady-state operating conditions. Secondly, for the MFC-2 using PDC:TiO₂-1100 as the membrane material, which has the OV value of 230 mV. This value was higher when compared to MFC-1 with PDC-1100 and also higher than the performance of MFC-5 with a polymeric Nafion membrane (181.80 mV). Polarization experiments were

8. Polysiloxane derived ceramic membrane composite with TiO₂ and SiO₂ filler material for Microbial fuel cell (MFC) and membrane bioreactor (MBR)

conducted for MFCs having different PDC membranes to compare performance in terms of their overall volumetric power densities and are shown in Figure 54. MFC-2 showed the best performance among ceramic membranes, having the maximum power density of 4978.28 W m⁻³. Secondly, the observed maximum power density of 3715.7 W m⁻³ was achieved for MFC-3 using PDC:SiO₂-1100 as the membrane material. This values were 4.5 % higher than the MFC-1 with PDC-1100. However, MFC-2 with PDC:TiO₂-1100 membrane power density is comparably lower than the one received for the MFC operated with polymeric nafion membrane. The overall trend of power densities in the MFCs is as follows: MFC-5 > MFC-2 > MFC-4 > MFC-1 > MFC-3 (Figure 54). The physical characteristics of the membrane materials, such as IEC, cation transport number, and oxygen diffusion coefficient, as discussed in previous, are well correlated with the results observed from the polarization data.

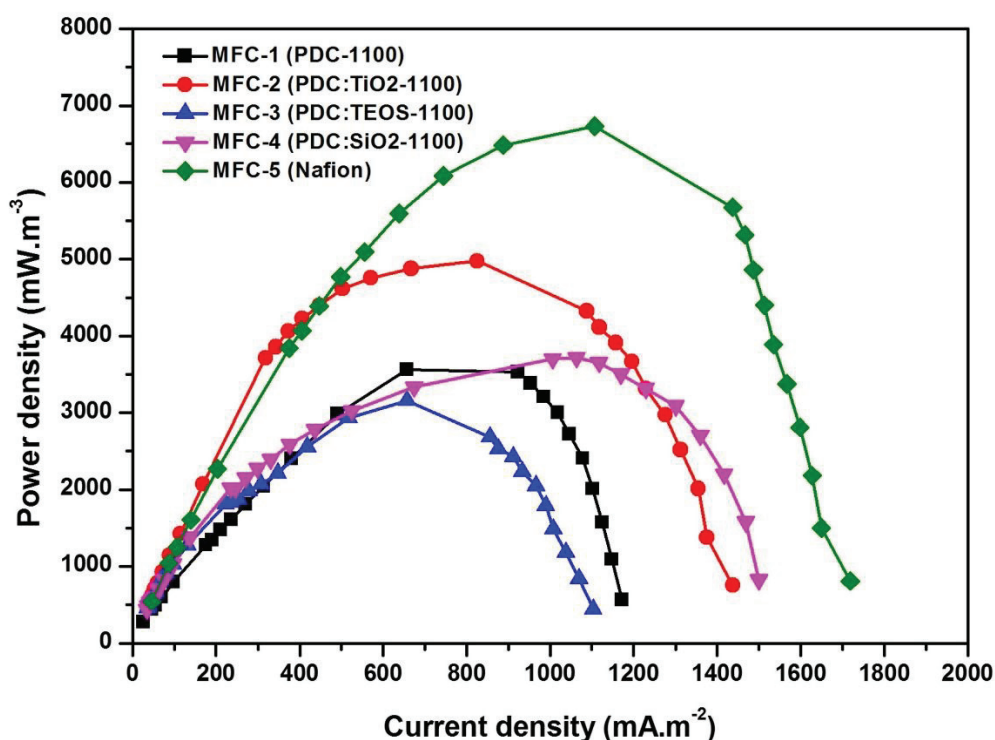


Figure 54. Polarization curves of MFCs using different membranes.

The internal resistance of the MFC system arises from overpotential losses occurring in the anode and cathode, as well as the ohmic resistance observed from the membrane–electrolyte

8. Polysiloxane derived ceramic membrane composite with TiO₂ and SiO₂ filler material for Microbial fuel cell (MFC) and membrane bioreactor (MBR)

interface in the MFC system. The internal resistance was determined from the slope of the straight line portion of the voltage–current curve. Among all tested MFCs, MFC-2 shows the lowest internal resistance of 132 Ω , followed by MFC-3 (215 Ω) and MFC-1 (186 Ω), which are nearly similar. A possible explanation for the power generation of MFC-2 is that the PDC:TiO₂-1100 ceramic membrane have high hydrophilic ratio, open porosity and low pore size that inhibits water diffusion from the anode chamber and consequently prevents the hydration of the cathode. Once the sufficient water molecules are produced on the cathode chamber, a subsequent increase in proton diffusion occurs because of the electro-osmotic drag mechanism from the transfer of water molecules, which drags H⁺ from the anolyte to the cathode surface. The table 7 shows the detailed electrochemical analysis data of all MFCs.

Wastewater treatment efficiency of MFCs

Wastewater contains complex macromolecules, which are easily degraded with the presence of various bacteria in the anaerobic inoculum. The electrogenesis step is preceded by fermentation, wherein complex macromolecules such as polysaccharides undergo degradation and are reduced to simpler carbon-chain compounds. The simpler carbon compounds then undergo electrogenesis. Some of the reduced substrates are utilized by microbes for life-supporting functions; the rest is converted into electrons and protons, yielding power generation by the MFC. In addition to power generation, organic matter removal from wastewater is necessary in determining the performance of an MFC system. The initial COD concentration (3000 mg L⁻¹) of the synthetic wastewater used here was measured over the experimental period. The synthetic wastewater was introduced to the anodic chambers of the MFCs as the fuel source. During the stable phase of operation, all MFCs show similar COD removal efficiencies of 80 – 90 %. The specific COD removal efficiency values of 78 ± 1.08 %, 87 ± 1.05 %, 81.3 ± 1.88 %, 83.8 ± 0.78 %, and 90.8 ± 1.86 % are achieved by MFC-1, MFC-2, MFC-3, MFC-4, and MFC-5, respectively (Figure 55). MFC-2 shows the highest COD removal efficiency of the MFCs used in this study, other than MFC-5 with Nafion. This is because the PDC:TiO₂-1100 ceramic membrane has a high IEC value, pore size distribution, and other physical characteristics, which maintain the anaerobic environment in the anode by promoting the scavenging of electrons and protons from the anode to cathode chambers in the MFC system.

8. Polysiloxane derived ceramic membrane composite with TiO₂ and SiO₂ filler material for Microbial fuel cell (MFC) and membrane bioreactor (MBR)

The coulombic efficiency (CE) of MFC-2 is also substantially higher, with an average CE of 27.06 ± 0.53 %, than those of all other MFCs in this study (Figure 56). This indicates that more organic matter is effectively utilized by the anodic microorganisms in MFC-2 for oxidation than by those in MFC-1 using the PDC-1100 membrane. This may be attributed to the superior ceramic membrane performance because of its porous structure and enhanced physical properties of IEC, cation transfer number, and oxygen permeability. Overall, the MFC-2 with the PDC:TiO₂-1100 ceramic membrane shows the highest power generation while demonstrating better organic matter removal efficiency compared to the other MFCs using ceramic membrane in this study.

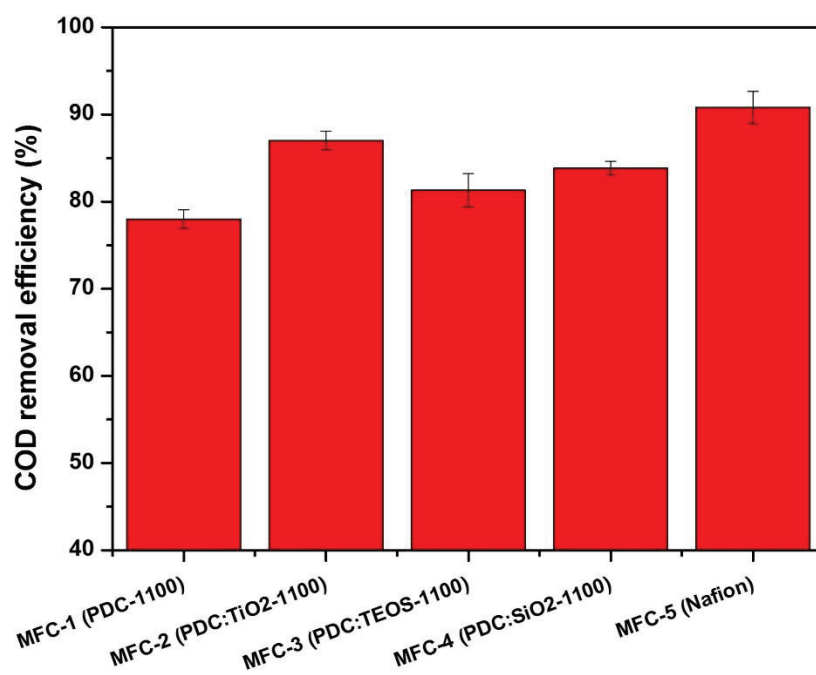


Figure 55. COD removal efficiency of MFCs

8. Polysiloxane derived ceramic membrane composite with TiO₂ and SiO₂ filler material for Microbial fuel cell (MFC) and membrane bioreactor (MBR)

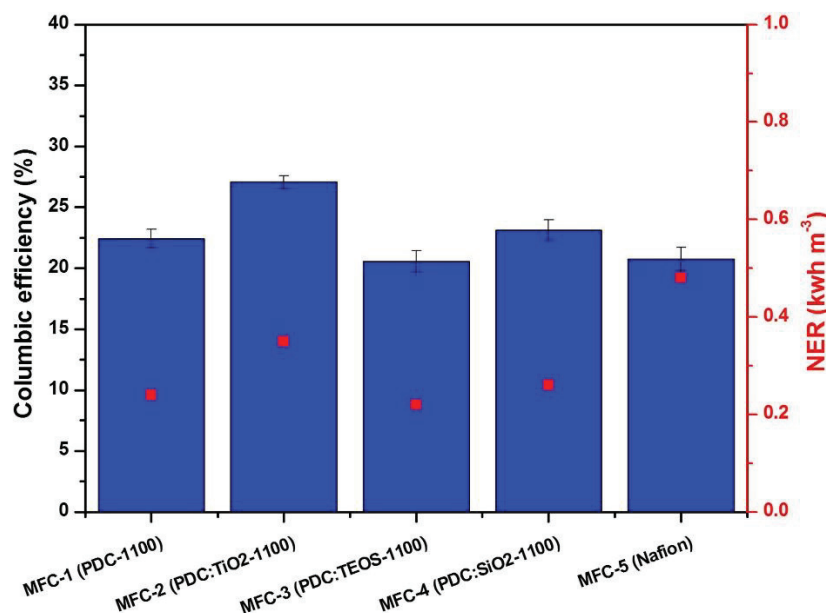


Figure 56. Columbic efficiency and Normalized energy recovery of MFCs.

Ultrafiltration membrane for MBR

The water permeability is a crucial factor related to MBR which affects the fluxes with activated sludge as a feed. The water permeability were measured as a function of time at different pressures (2, 3, 4, and 5 bar). It observed that the water flux through the optimized microfiltration membrane stabilizes for 15 min of water filtration. Moreover, the water flux of the membrane depends on the applied pressure. The obtained water permeability results of the membrane are shown in Figure 57 a. It shown that water fluxes are linear for the PDC membranes pyrolysed at 1100 °C. The values of water permeability were calculated from slope of the linear graphs and were found to be 51.32, 569, 113 and 14.06 L/h.m² bar for PDC-1100, PDC:TiO₂-1100, PDC:SiO₂-1100 and PDC:TEOS-1100 composite membranes, respectively (Figure 57 b).

The hydrophilicity of the membrane affects the permeability and the biomass attachment on the membrane [19]. As presented in Figure 51, the water and heptane ratio value increased from 2.86 to 4.86 with the addition of various amounts of hygroscopic filler. The addition of TiO₂ increased the hydrophilic nature of the PDC membranes compared with the bare PDC membrane. The significant improvement in hydrophilicity could be due to the reduced interfacial energy of the PDC membrane affected by the polar nature of TiO₂ [59].

8. Polysiloxane derived ceramic membrane composite with TiO₂ and SiO₂ filler material for Microbial fuel cell (MFC) and membrane bioreactor (MBR)

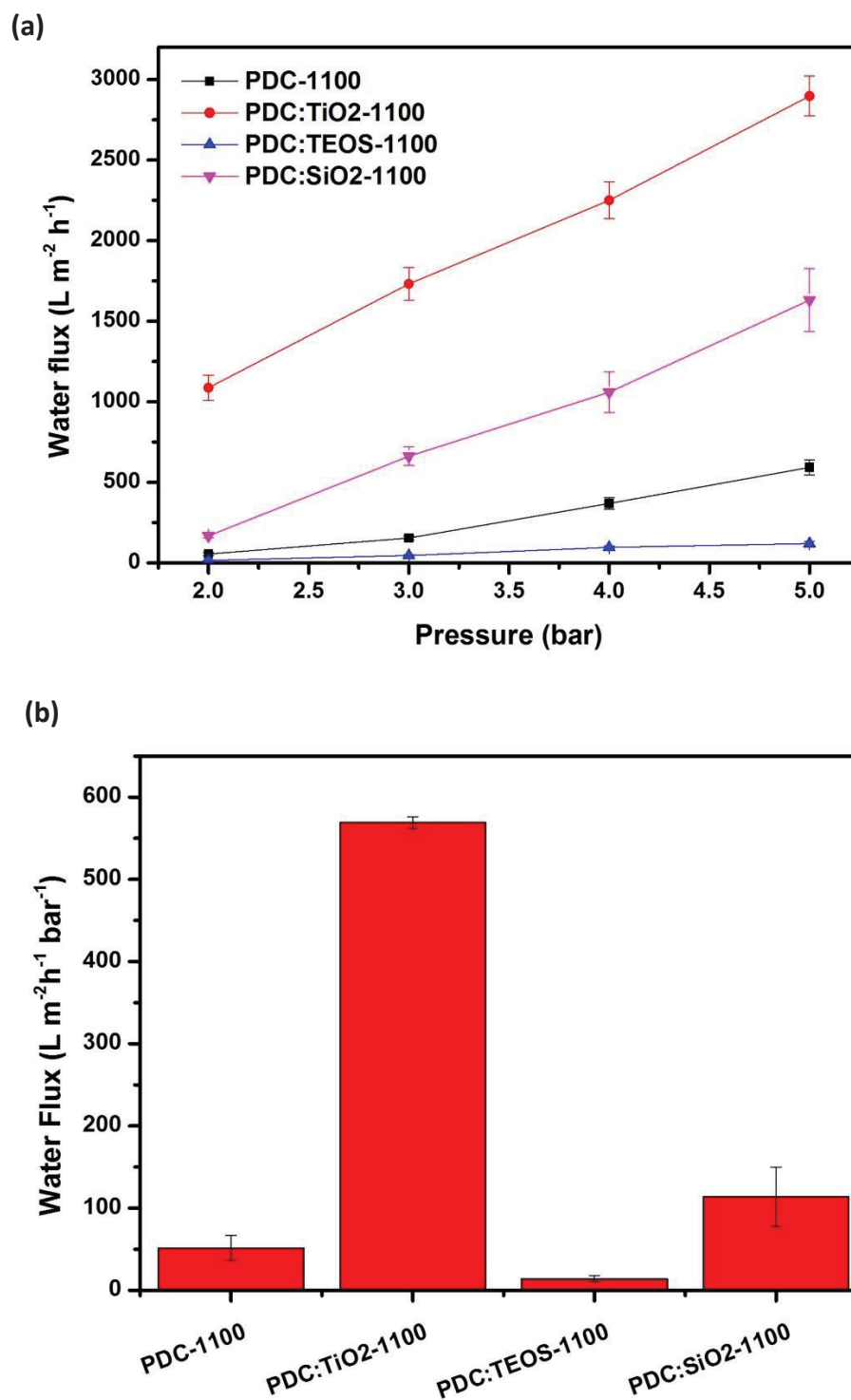


Figure 57. (a) Water permeate of prepared membranes as a function of applied pressure

(b) Water permeability per unit bar.

8. Polysiloxane derived ceramic membrane composite with TiO₂ and SiO₂ filler material for Microbial fuel cell (MFC) and membrane bioreactor (MBR)

The permeability of membranes increased remarkably from 51.32 to 569 about 10 fold the original permeability for membrane PDC-1100 and PDC:TiO₂-1100, respectively which significantly emphasized the significant role of hydrophilic TiO₂ in the membrane for increasing the water permeability. The steep increment in water permeability was most probably due to the reason of the high water retention capacity of the membrane and the facile water transport through the membrane as a result of strong hydrophilic properties. Besides that, the membrane porosity is one of the vital factors that affect the water permeability behaviour of membrane for MBR application. As shown in Figure 50, the membrane porosity increased from 27% to 37% with the addition of hygroscopic filler like TiO₂ along with PDC.

Table 7. Electrochemical analysis data for all the MFCs and water permeability for MBR.

Parameters	PDC-1100	PDC:TiO ₂ -1100	PDC:TEO S-1100	PDC:SiO ₂ -1100	Nafion
OV (mV)	171 ± 2.4	230.1 ± 2.9	163.2 ± 6.5	189.3 ± 6.4	181.80 ± 3.5
OCV(mV)	568.30 ± 3.47	617.5 ± 7.5	557.8 ± 5.00	580.7 ± 4.08	586.70 ± 2.66
MPD (mW m ⁻³)	3563	4978.28	3162	3715.7	6733
COD removal efficiency (%)	78 ± 1.08	87.00 ± 1.05	81.30 ± 1.88	83.8 ± 0.788	90.80 ± 1.86
CE (%)	22.42 ± 0.73	27.06 ± 0.53	20.54 ± 0.88	23.11 ± 0.86	20.48 ± 0.64
NER (kWh m ⁻³)	0.24	0.35	0.22	0.26	0.48
Water Flux (L m ⁻² h ⁻¹ bar ⁻¹)	51.32 ± 15.25	569 ± 7.29	14.06 ± 4.06	113.69 ± 36	-

8. Polysiloxane derived ceramic membrane composite with TiO₂ and SiO₂ filler material for Microbial fuel cell (MFC) and membrane bioreactor (MBR)

Summary

Composite ceramic membranes were developed using PDCs with the hygroscopic fillers TiO₂, SiO₂ (derived from TEOS) and SiO₂ (as particle). The best properties were obtained from the PDC:TiO₂-1100 ceramic membrane, with a substantially higher IEC value, higher hydrophilic ratio, and lower oxygen permeability compared to all other tested membranes, mainly because of the high porosity and small average pore size distribution. Firstly the MFC with the PDC:TiO₂-1100 ceramic membrane generated the maximum power density and columbic efficiency of 4.97 W m⁻³ and 27.06 ± 0.53%, which were higher than those from the MFC with a commercial polymeric Nafion membrane. Secondly, for the MBR system, the results showed that the optimum membrane performance was exhibited by PDC:TiO₂-1100. This membrane exhibited significant enhancement in terms of permeability, hydrophilicity and porosity properties. The membrane water/heptanes ratio decreased from 2.27 (PDC1-1100) to 4.27 (PDC1:TiO₂-1100) while membrane permeability increased from 51.32 (PDC1-1100) to 569 (PDC1:TiO₂-1100) L.m⁻². h⁻¹. bar⁻¹. The membrane porosity improved from 27% for PDC-1100 to 37% for PDC1:TiO₂-1100 membrane. These results suggest that the polysiloxane-derived ceramic composite membranes could be potential candidates as proton-exchange membranes and ultrafiltration membrane for integrated MBR and MFC system.

9. Polysiloxane derived ceramic membrane for pilot scale model integrated microbial fuel cell-membrane bioreactor (MFC-MBR)

9. Polysiloxane derived ceramic membrane for pilot scale model integrated microbial fuel cell-membrane bioreactor (MFC-MBR)

Objective

In this study, we designed an integrated single-chambered MFC-MBR that generate electricity and treat wastewater effectively. for wastewater aeration, electricity generation and wastewater treatment. The system consist of membrane that act as proton conducting membrane as well as ultrafiltraion membrane for bioelectricity generation, and as a membrane for wastewater filtration. We used bare PDC membrane prepared at 1000 °C as denoted by PDC-1000. The membrane material characterizations were shown in chapter 5.

Design of Pilot-scale Integrated MFC-MBR system

The study was carried out in pilot scale integrated MFC-MBR made of acrylic sheet with a working volume of 20 L (Figure 58). The integrated system were designed by Prof. Dr. Makarand M. Ghangrekar and his research scholar Mr. Gourav Dhar Bhowmik from Indian Institue of Technology, Kharagpur, India. Anodes are made of graphite felt material attached to the inner surface of proton exchange membrane (PEM) fabricated with PDC-1000 membrane. Cathodes were fabricated with graphite felt and sticked on the outer surface of PEM of integrated MFC-MBR to make suitable contact between the PEM and the cathode. Anodes and cathodes were connected by plastic insulated copper wire, and connections were made water resistant using araldite glue. Operating voltage was measured across 100 Ω of external resistance. Integrated MFC-MBR was inoculated with anaerobic sludge collected from septic tank bottom (volatile suspended solids of 19.95 g L⁻¹ and total suspended solids of 30.22 g L⁻¹), respectively. Synthetic wastewater, with sucrose as a carbon source having ~ 3 g L⁻¹ of chemical oxygen demand (COD), was used as a carbon source.

9. Polysiloxane derived ceramic membrane for pilot scale model integrated microbial fuel cell-membrane bioreactor (MFC-MBR)

MFC model:

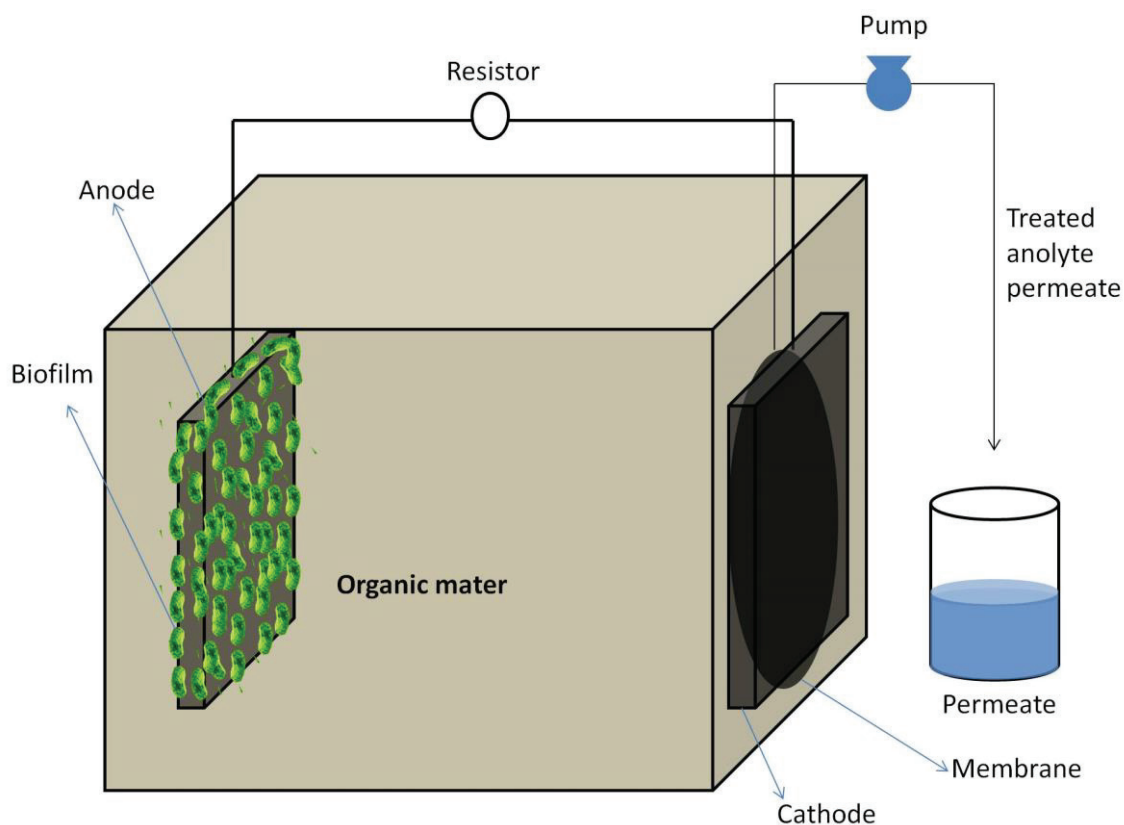


Figure 58. Schematic view of pilot scale integrated MFC-MBR system.

Results

The integrated system were running continuously for 60 days and biofilm were developing day by day on the surface of anode material. Once the wastewater from MFC setup were treated and followed by filtration through the membrane. The result obtained so far from the integrated MFC-MBR system is shown in Table 7. The observed open voltage of 102 ± 10 after 60 days of operation and this could increases with respect to build up of biofilm layer on the anode material. The experiment is currently ongoing. The detailed results will publish in Indian counterpart research scholar's dissertation (Indian Institute of Technology, Khargpur-India).

9. Polysiloxane derived ceramic membrane for pilot scale model integrated microbial fuel cell-membrane bioreactor (MFC-MBR)

Table 7. Electrochemical and wastewater treatment analysis data for the integrated MFC-MBR system.

Parameters	MFC-MBR
OV (mV)	102 ± 10
OCV (mV)	539 ± 24
Sustainable power density (mW m ⁻²)	115.6
COD removal efficiency (%)	69 ± 4
Maximum CE (%)	3.59

10. Conclusion

Porous polymer derived ceramic membranes were successfully fabricated by a polymer derived ceramic route, using the simple uni-axial hydraulic pressing technique. Tailorable porous structure and surface characteristics enhance the proton diffusion with minimal oxygen permeability, these properties are beneficial for membrane in integrated MFC- MBR system.

Porous polymer derived composite membranes were fabricated from polysiloxane precursor mixed with different filler materials, and their surface characteristics, porous structure, mechanical stability, IEC values, oxygen mass transfer coefficients, and diffusion coefficients were determined, and the MFCs performance was studied using PDC composite membranes.

The first approach involved tailoring the surface characteristics and porous structure by varying pyrolysis temperature and adding cation exchange filler materials. The surface characteristics of the PDC membrane could be altered from hydrophobic to hydrophilic by tuning the pyrolysis temperature. Furthermore, the addition of fillers to the PDC material increases the hydrophilic characteristics even at low pyrolysis temperature, and simultaneously incorporates micro-/meso-/macro porous structure. For that, a series of polymer derived ceramic membranes tailored based on pyrolysis temperature (400 °C – 1000 °C) and cation exchange filler like montmorillonite and $\text{H}_3\text{PMo}_{12}\text{O}_{40}/\text{SiO}_2$ was fabricated. The maximum power density of MFC with polymer derived ceramic membrane pyrolysed at 400 °C modified with 20 wt.% montmorillonite and 10 wt. % $\text{H}_3\text{PMo}_{12}\text{O}_{40}/\text{SiO}_2$ reached a value of 5.66 W m^{-3} , which was 4 times higher than that with non-modified polysiloxane derived ceramic membrane. In contrast, MFC with polymer derived ceramic membrane pyrolysed at 1000 °C modified with 20 wt.% montmorillonite delivers 1.2 times lower power density (4.20 W m^{-3}) than that with non-modified macroporous Polymer derived ceramic membrane pyrolysed at 1000 °C. This is due to low hydrophilic nature and absence of micro-/mesoporous structure. Hence, the findings demonstrated that tailoring the hydrophilic and porous structure of the ceramic membrane is a new and promising approach to enhance the performance of MFC.

The second approach was using PDC composite with graphitic filler material at high pyrolyzing temperature. The chemical compositions of the membranes were altered by adding carbon allotrope fillers including graphene oxide (GO) and multiwall carbon nanotubes into the polymer matrix as filler materials. The membrane ion exchange capacity and mechanical stability was significantly improved; after adding 0.5 wt. % of GO. The ion exchange capacity increased drastically corresponding to an increment of 9 fold with respect to that of the non-

modified ceramic membrane, respectively. The MFC operated with this membrane exhibited a maximum power density of 7.23 W m^{-3} with a coulombic efficiency of 28.8%, which was significantly higher than the value obtained during the use of a polymeric Nafion membrane.

Beside this promising bioelectrical performance, the resulting mechanical stability was suitable for microbial fuel cells but not for membrane bioreactors, due to their high operating pressure. The third approach was to further improve the mechanical stability of the membrane without compromising the hydrophilic nature, open porosity, or pore size for use in MFCs and MBRs. PDC membranes with 15 wt% hygroscopic fillers like SiO_2 , TEOS (SiO_2 derived from TEOS), and TiO_2 at $1100 \text{ }^\circ\text{C}$ were fabricated. The water permeability and maximum power density of MFC (with PDC functionalized with TiO_2) reached values of 4.97 W m^{-3} and $569 \text{ L m}^{-2} \text{ h}^{-1} \text{ bar}^{-1}$, respectively, which were much higher than those with bare PDC membrane.

Overall, for pilot scale studies without compromising on membrane cost and performance, the PDC-1000 membrane as the best proton conducting membrane and ultrafiltration membrane was chosen for a 20 liter pilot scale integrated MFC-MBR system. The so far results showed that the integrated MFC-MBR system using PDC membranes was able to produce bioelectricity with open circuit voltage of $539 \pm 24 \text{ mV}$ and simultaneous wastewater treatment with COD removal efficiency of $69 \pm 4\%$.

11. Outlook

PDC materials were identified within this work to be potentially applicable as a membrane material for integrated MFC-MBR system to generate bioelectricity with simultaneous wastewater treatment. PDC membranes have satisfactory ion exchange capacity, pore structure, hydrophilic characteristics, unique mechanical, chemical stability and low cost which is suitable for scaling up of MFC-MBR system using this membrane. However, high oxygen and substrate diffusion in porous membranes limited their overall efficiency. To overcome these drawbacks, PDC ceramic membranes need to be prepared with well-aligned hierarchical porous structure and surface coatings like phosphoric acid functionalized polysiloxane on the sides of the ceramic membrane. Atwater *et al* reported that the hydrophilic polymeric membrane have low oxygen permeable than porous ceramic membrane [301]. The presence of phosphoric acid functionalized polysiloxane surface coating in the ceramic membrane will minimize the oxygen diffusion from cathode to anode chamber. M. Jeske *et al* claimed that the phosphoric acid functionalized polysiloxane membrane act as a good proton conducting membrane in high temperature fuel cell [245]. The phosphoric acid group in the polymeric coating enable the proton to diffuse from the outer region of the membrane to inner ceramic structure. Furthermore, the well-aligned uniform pore structure in the ceramic membrane will aid to diffuse the proton from anode to cathode chamber in the shortest path. Secondly, these surface coating are hydrophilic nature on the PDC ceramic membrane will produce a smooth surface. The surface roughness factor of material plays a major role in the formation of biofilm on the surface of the membrane. The thin film coating on the PDC ceramic membrane hugely prevent biofouling and crossover of organic and bacterial substrate.

The preparation of precursor with sacrificial template method and followed by hot pressing of the green body will be a suitable approach for creating well-aligned porous structure. The sacrificial template method comprises of synthesizing two phase composite material made up of a ceramic precursor and a sacrificial polymeric phase which distributed uniformly throughout the matrix and is ultimately used to generate pores within the membrane structure. PDC material porosity is engineered by employing sacrificial polymeric template as polymer microbeads and silica microspheres. These sacrificial templates are often extracted by applying long thermal pyrolysis or by a chemical etching method. Further, the thin polymeric film coating on the ceramic membrane will either done by spin coating or spray coating.

The polymeric thin layer coated PDC ceramic membrane with well-aligned porous ceramic structure will give a new scope of research in membrane technology for the application of integrated MFC-MBR system.

References

1. Chu, S., Y. Cui, and N. Liu, The path towards sustainable energy. *Nature Materials*, 2016. **16**: p. 16.
2. Hey, T., N. Bajraktari, Å. Davidsson, J. Vogel, H.T. Madsen, C. Hélix-Nielsen, J.I.C. Jansen, and K. Jönsson, Evaluation of direct membrane filtration and direct forward osmosis as concepts for compact and energy-positive municipal wastewater treatment. *Environmental Technology*, 2018. **39**(3): p. 264.
3. Santoro, C., C. Arbizzani, B. Erable, and I. Ieropoulos, Microbial fuel cells: From fundamentals to applications. A review. *Journal of Power Sources*, 2017. **356**: p. 225.
4. Trapero, J.R., L. Horcajada, J.J. Linares, and J. Lobato, Is microbial fuel cell technology ready? An economic answer towards industrial commercialization. *Applied Energy*, 2017. **185**: p. 698.
5. Palanisamy, G., H.-Y. Jung, T. Sadhasivam, M.D. Kurkuri, S.C. Kim, and S.-H. Roh, A comprehensive review on microbial fuel cell technologies: Processes, utilization, and advanced developments in electrodes and membranes. *Journal of Cleaner Production*, 2019. **221**: p. 598.
6. Wang, Z., C. Cao, Y. Zheng, S. Chen, and F. Zhao, Abiotic Oxygen Reduction Reaction Catalysts Used in Microbial Fuel Cells. *ChemElectroChem*, 2014. **1**(11): p. 1813.
7. Mateo-Ramírez, F., H. Addi, F.J. Hernández-Fernández, C. Godínez, A. Pérez de los Ríos, E.M. Lotfi, M. El Mahi, and L.J. Lozano Blanco, Air breathing cathode-microbial fuel cell with separator based on ionic liquid applied to slaughterhouse wastewater treatment and bio-energy production. *Journal of Chemical Technology & Biotechnology*, 2017. **92**(3): p. 642.
8. Ghadge, A.N. and M. Ghangrekar, Development of low cost ceramic separator using mineral cation exchanger to enhance performance of microbial fuel cells. *Electrochimica Acta*, 2015. **166**: p. 320.
9. Dharmalingam, S., V. Kugarajah, and M. Sugumar, Chapter 1.7 - Membranes for Microbial Fuel Cells, in *Microbial Electrochemical Technology*, S.V. Mohan, S. Varjani, and A. Pandey, Editors. 2019, Elsevier. p. 143.
10. Achilli, A., T.Y. Cath, E.A. Marchand, and A.E. Childress, The forward osmosis membrane bioreactor: A low fouling alternative to MBR processes. *Desalination*, 2009. **239**(1): p. 10.
11. Nah, Y.M., K.H. Ahn, and I.T. Yeom, Nitrogen Removal in Household Wastewater Treatment Using an Intermittently Aerated Membrane Bioreactor. *Environmental Technology*, 2000. **21**(1): p. 107.
12. Drews, A., Membrane fouling in membrane bioreactors—Characterisation, contradictions, cause and cures. *Journal of Membrane Science*, 2010. **363**(1): p. 1.
13. Zhi-Guo, M., Y. Feng-lin, and Z. Xing-wen, MBR focus: do nonwovens offer a cheaper option? *Filtration & Separation*, 2005. **42**(5): p. 28.
14. Zhao, C., X. Xu, J. Chen, G. Wang, and F. Yang, Highly effective antifouling performance of PVDF/graphene oxide composite membrane in membrane bioreactor (MBR) system. *Desalination*, 2014. **340**: p. 59.
15. Khalid, A., A. Abdel-Karim, M. Ali Atieh, S. Javed, and G. McKay, PEG-CNTs nanocomposite PSU membranes for wastewater treatment by membrane bioreactor. *Separation and Purification Technology*, 2018. **190**: p. 165.
16. Hernández-Flores, G., A. Andrio, V. Compañ, O. Solorza-Feria, and H.M. Poggi-Varaldo, Synthesis and characterization of organic agar-based membranes for microbial fuel cells. *Journal of Power Sources*, 2019. **435**: p. 226772.

17. Yusuf, H., M.S.M. Anuar, S.M.D. Syed Mohamed, and R. Subramaniam, Medium-chain-length poly-3-hydroxyalkanoates-carbon nanotubes composite as proton exchange membrane in microbial fuel cell. *Chemical Engineering Communications*, 2019. **206**(6): p. 731.
18. Miyoshi, T., T.P. Nguyen, T. Tsumuraya, H. Tanaka, T. Morita, H. Itokawa, and T. Hashimoto, Energy reduction of a submerged membrane bioreactor using a polytetrafluoroethylene (PTFE) hollow-fiber membrane. *Frontiers of Environmental Science & Engineering*, 2018. **12**(3): p. 1.
19. Potter, M.C. and D. Waller Augustus, Electrical effects accompanying the decomposition of organic compounds. *Proceedings of the Royal Society of London. Series B, Containing Papers of a Biological Character*, 1911. **84**(571): p. 260.
20. Thirty-second Annual Meeting of the Society of American Bacteriologists. *Journal of bacteriology*, 1931. **21**(1): p. 1.
21. Rinaldi, A., B. Mecheri, V. Garavaglia, S. Licocchia, P. Di Nardo, and E. Traversa, Engineering materials and biology to boost performance of microbial fuel cells: a critical review. *Energy & Environmental Science*, 2008. **1**(4): p. 417.
22. Habermann, W. and E.H. Pommer, Biological fuel cells with sulphide storage capacity. *Applied Microbiology and Biotechnology*, 1991. **35**(1): p. 128.
23. Logan, B.E., Scaling up microbial fuel cells and other bioelectrochemical systems. *Applied Microbiology and Biotechnology*, 2010. **85**(6): p. 1665.
24. Ieropoulos, I., J. Greenman, C. Melhuish, and J. Hart, Energy accumulation and improved performance in microbial fuel cells. *Journal of Power Sources*, 2005. **145**(2): p. 253.
25. Liu, W.-f. and S.-a. Cheng, Microbial fuel cells for energy production from wastewaters: the way toward practical application. *Journal of Zhejiang University SCIENCE A*, 2014. **15**(11): p. 841.
26. Mamais, D., D. Jenkins, and P. Prrr, A rapid physical-chemical method for the determination of readily biodegradable soluble COD in municipal wastewater. *Water Research*, 1993. **27**(1): p. 195.
27. Venkata Mohan, S., G. Mohanakrishna, G. Velvizhi, V.L. Babu, and P.N. Sarma, Bio-catalyzed electrochemical treatment of real field dairy wastewater with simultaneous power generation. *Biochemical Engineering Journal*, 2010. **51**(1): p. 32.
28. Watanabe, K., Recent Developments in Microbial Fuel Cell Technologies for Sustainable Bioenergy. *Journal of Bioscience and Bioengineering*, 2008. **106**(6): p. 528.
29. Martin, E., O. Savadogo, S.R. Guiot, and B. Tartakovsky, The influence of operational conditions on the performance of a microbial fuel cell seeded with mesophilic anaerobic sludge. *Biochemical Engineering Journal*, 2010. **51**(3): p. 132.
30. Rahimnejad, M., A. Adhami, S. Darvari, A. Zirepour, and S.-E. Oh, Microbial fuel cell as new technology for bioelectricity generation: A review. *Alexandria Engineering Journal*, 2015. **54**(3): p. 745.
31. Harnisch, F. and U. Schröder, Selectivity versus Mobility: Separation of Anode and Cathode in Microbial Bioelectrochemical Systems. *ChemSusChem*, 2009. **2**(10): p. 921.
32. Ben Liew, K., W.R.W. Daud, M. Ghasemi, J.X. Leong, S. Su Lim, and M. Ismail, Non-Pt catalyst as oxygen reduction reaction in microbial fuel cells: A review. *International Journal of Hydrogen Energy*, 2014. **39**(10): p. 4870.
33. Erable, B., D. Féron, and A. Bergel, Microbial Catalysis of the Oxygen Reduction Reaction for Microbial Fuel Cells: A Review. *ChemSusChem*, 2012. **5**(6): p. 975.
34. Song, C. and J. Zhang, Electrocatalytic Oxygen Reduction Reaction, in *PEM Fuel Cell Electrocatalysts and Catalyst Layers: Fundamentals and Applications*, J. Zhang, Editor. 2008, Springer London: London. p. 89.

35. Ahilan, V., G.D. Bhowmick, M.M. Ghangrekar, M. Wilhelm, and K. Rezwani, Tailoring hydrophilic and porous nature of polysiloxane derived ceramer and ceramic membranes for enhanced bioelectricity generation in microbial fuel cell. *Ionics*, 2019.
36. Xie, X., C. Criddle, and Y. Cui, Design and fabrication of bioelectrodes for microbial bioelectrochemical systems. *Energy & Environmental Science*, 2015. **8**(12): p. 3418.
37. Zhang, Y., G. Mo, X. Li, W. Zhang, J. Zhang, J. Ye, X. Huang, and C. Yu, A graphene modified anode to improve the performance of microbial fuel cells. *Journal of Power Sources*, 2011. **196**(13): p. 5402.
38. Cao, Y., H. Mu, W. Liu, R. Zhang, J. Guo, M. Xian, and H. Liu, Electricigens in the anode of microbial fuel cells: pure cultures versus mixed communities. *Microbial Cell Factories*, 2019. **18**(1): p. 39.
39. Reguera, G., K.D. McCarthy, T. Mehta, J.S. Nicoll, M.T. Tuominen, and D.R. Lovley, Extracellular electron transfer via microbial nanowires. *Nature*, 2005. **435**(7045): p. 1098.
40. Malvankar, N.S. and D.R. Lovley, Microbial nanowires for bioenergy applications. *Current Opinion in Biotechnology*, 2014. **27**: p. 88.
41. Gorby, Y.A., S. Yanina, J.S. McLean, K.M. Rosso, D. Moyles, A. Dohnalkova, T.J. Beveridge, I.S. Chang, B.H. Kim, K.S. Kim, D.E. Culley, S.B. Reed, M.F. Romine, D.A. Saffarini, E.A. Hill, L. Shi, D.A. Elias, D.W. Kennedy, G. Pinchuk, K. Watanabe, S.i. Ishii, B. Logan, K.H. Nealson, and J.K. Fredrickson, Electrically conductive bacterial nanowires produced by *Shewanella oneidensis* strain MR-1 and other microorganisms. *Proceedings of the National Academy of Sciences*, 2006. **103**(30): p. 11358.
42. He, L., P. Du, Y. Chen, H. Lu, X. Cheng, B. Chang, and Z. Wang, Advances in microbial fuel cells for wastewater treatment. *Renewable and Sustainable Energy Reviews*, 2017. **71**: p. 388.
43. Peng, H., P. Zhang, M. Bilal, W. Wang, H. Hu, and X. Zhang, Enhanced biosynthesis of phenazine-1-carboxamide by engineered *Pseudomonas chlororaphis* HT66. *Microbial Cell Factories*, 2018. **17**(1): p. 117.
44. Rahimnejad, M., G.D. Najafpour, A.A. Ghoreyshi, F. Talebnia, G.C. Premier, G. Bakeri, J.R. Kim, and S.-E. Oh, Thionine increases electricity generation from microbial fuel cell using *Saccharomyces cerevisiae* and exoelectrogenic mixed culture. *Journal of Microbiology*, 2012. **50**(4): p. 575.
45. Park, D.H., M. Laivenieks, M.V. Guettler, M.K. Jain, and J.G. Zeikus, Microbial Utilization of Electrically Reduced Neutral Red as the Sole Electron Donor for Growth and Metabolite Production. *Applied and Environmental Microbiology*, 1999. **65**(7): p. 2912.
46. Thygesen, A., F.W. Poulsen, B. Min, I. Angelidaki, and A.B. Thomsen, The effect of different substrates and humic acid on power generation in microbial fuel cell operation. *Bioresource Technology*, 2009. **100**(3): p. 1186.
47. Zhang, E., Y. Cai, Y. Luo, and Z. Piao, Riboflavin-shuttled extracellular electron transfer from *Enterococcus faecalis* to electrodes in microbial fuel cells. *Canadian Journal of Microbiology*, 2014. **60**(11): p. 753.
48. Rahimnejad, M., G.D. Najafpour, A.A. Ghoreyshi, M. Shakeri, and H. Zare, Methylene blue as electron promoters in microbial fuel cell. *International Journal of Hydrogen Energy*, 2011. **36**(20): p. 13335.
49. Liu, J., Y. Qiao, C.X. Guo, S. Lim, H. Song, and C.M. Li, Graphene/carbon cloth anode for high-performance mediatorless microbial fuel cells. *Bioresource Technology*, 2012. **114**: p. 275.

-
50. Chang, S.-H., B.-Y. Huang, T.-H. Wan, J.-Z. Chen, and B.-Y. Chen, Surface modification of carbon cloth anodes for microbial fuel cells using atmospheric-pressure plasma jet processed reduced graphene oxides. *RSC Advances*, 2017. **7**(89): p. 56433.
 51. Cheng, S. and B.E. Logan, Ammonia treatment of carbon cloth anodes to enhance power generation of microbial fuel cells. *Electrochemistry Communications*, 2007. **9**(3): p. 492.
 52. Ahn, Y. and B.E. Logan, Effectiveness of domestic wastewater treatment using microbial fuel cells at ambient and mesophilic temperatures. *Bioresource Technology*, 2010. **101**(2): p. 469.
 53. Wang, X., Y.J. Feng, and H. Lee, Electricity production from beer brewery wastewater using single chamber microbial fuel cell. *Water Science and Technology*, 2008. **57**(7): p. 1117.
 54. Zhao, F., F. Harnisch, U. Schröder, F. Scholz, P. Bogdanoff, and I. Herrmann, Application of pyrolysed iron(II) phthalocyanine and CoTMPP based oxygen reduction catalysts as cathode materials in microbial fuel cells. *Electrochemistry Communications*, 2005. **7**(12): p. 1405.
 55. Phansroy, N., W. Khawdas, K. Watanabe, Y. Aso, and H. Ohara, Microbial fuel cells equipped with an iron-plated carbon-felt anode and *Shewanella oneidensis* MR-1 with corn steep liquor as a fuel. *Journal of Bioscience and Bioengineering*, 2018. **126**(4): p. 514.
 56. Karthikeyan, R., N. Krishnaraj, A. Selvam, J.W.-C. Wong, P.K.H. Lee, M.K.H. Leung, and S. Berchmans, Effect of composites based nickel foam anode in microbial fuel cell using *Acetobacter acetii* and *Gluconobacter roseus* as a biocatalysts. *Bioresource Technology*, 2016. **217**: p. 113.
 57. Hindatu, Y., M.S.M. Anuar, R. Subramaniam, and A.M. Gumel, Medium-chain-length poly-3-hydroxyalkanoates-carbon nanotubes composite anode enhances the performance of microbial fuel cell. *Bioprocess and Biosystems Engineering*, 2017. **40**(6): p. 919.
 58. Yong, Y.-C., X.-C. Dong, M.B. Chan-Park, H. Song, and P. Chen, Macroporous and Monolithic Anode Based on Polyaniline Hybridized Three-Dimensional Graphene for High-Performance Microbial Fuel Cells. *ACS Nano*, 2012. **6**(3): p. 2394.
 59. Dumitru, A. and K. Scott, 4 - Anode materials for microbial fuel cells, in *Microbial Electrochemical and Fuel Cells*, K. Scott and E.H. Yu, Editors. 2016, Woodhead Publishing: Boston. p. 117.
 60. Khilari, S. and D. Pradhan, Role of Cathode Catalyst in Microbial Fuel Cell, in *Microbial Fuel Cell: A Bioelectrochemical System that Converts Waste to Watts*, D. Das, Editor. 2018, Springer International Publishing: Cham. p. 141.
 61. Kumar, R., L. Singh, Z.A. Wahid, D.M. Mahapatra, and H. Liu, Novel mesoporous MnCo₂O₄ nanorods as oxygen reduction catalyst at neutral pH in microbial fuel cells. *Bioresource Technology*, 2018. **254**: p. 1.
 62. Chiodoni, A., G.P. Salvador, G. Massaglia, L. Delmondo, J.A. Muñoz-Tabares, A. Sacco, N. Garino, M. Castellino, V. Margaria, D. Ahmed, C.F. Pirri, and M. Quaglio, MnxOy- based cathodes for oxygen reduction reaction catalysis in microbial fuel cells. *International Journal of Hydrogen Energy*, 2019. **44**(9): p. 4432.
 63. Dong, H., X. Liu, T. Xu, Q. Wang, X. Chen, S. Chen, H. Zhang, P. Liang, X. Huang, and X. Zhang, Hydrogen peroxide generation in microbial fuel cells using graphene-based air-cathodes. *Bioresource Technology*, 2018. **247**: p. 684.
 64. Albarbar, A. and M. Alrweq, Proton Exchange Membrane Fuel Cells: Review, in *Proton Exchange Membrane Fuel Cells: Design, Modelling and Performance Assessment Techniques*, A. Albarbar and M. Alrweq, Editors. 2018, Springer International Publishing: Cham. p. 9.

-
65. Li, S., Y. Hu, Q. Xu, J. Sun, B. Hou, and Y. Zhang, Iron- and nitrogen-functionalized graphene as a non-precious metal catalyst for enhanced oxygen reduction in an air-cathode microbial fuel cell. *Journal of Power Sources*, 2012. **213**: p. 265.
 66. Schaetzle, O., F. Barrière, and U. Schröder, An improved microbial fuel cell with laccase as the oxygen reduction catalyst. *Energy & Environmental Science*, 2009. **2**(1): p. 96.
 67. Ghasemi, M., W.R.W. Daud, S.H.A. Hassan, S.-E. Oh, M. Ismail, M. Rahimnejad, and J.M. Jahim, Nano-structured carbon as electrode material in microbial fuel cells: A comprehensive review. *Journal of Alloys and Compounds*, 2013. **580**: p. 245.
 68. Moon, H., I.S. Chang, and B.H. Kim, Continuous electricity production from artificial wastewater using a mediator-less microbial fuel cell. *Bioresource Technology*, 2006. **97**(4): p. 621.
 69. Call, D.F., M.D. Merrill, and B.E. Logan, High Surface Area Stainless Steel Brushes as Cathodes in Microbial Electrolysis Cells. *Environmental Science & Technology*, 2009. **43**(6): p. 2179.
 70. Gnana kumar, G., Z. Awan, K. Suk Nahm, and J. Stanley Xavier, Nanotubular MnO₂/graphene oxide composites for the application of open air-breathing cathode microbial fuel cells. *Biosensors and Bioelectronics*, 2014. **53**: p. 528.
 71. Ge, B., K. Li, Z. Fu, L. Pu, and X. Zhang, The addition of ortho-hexagon nano spinel Co₃O₄ to improve the performance of activated carbon air cathode microbial fuel cell. *Bioresource Technology*, 2015. **195**: p. 180.
 72. Ge, B., K. Li, Z. Fu, L. Pu, X. Zhang, Z. Liu, and K. Huang, The performance of nano urchin-like NiCo₂O₄ modified activated carbon as air cathode for microbial fuel cell. *Journal of Power Sources*, 2016. **303**: p. 325.
 73. Deng, K., T. Guo, J. Su, D. Guo, X. Liu, L. Liu, X. Chen, and Z. Wang, Full hyperfine frequency modulation in the implementation of coherent population trapping atomic clocks. *Physics Letters, Section A: General, Atomic and Solid State Physics*, 2009. **373**(12-13): p. 1130.
 74. ter Heijne, A., H.V.M. Hamelers, V. de Wilde, R.A. Rozendal, and C.J.N. Buisman, A Bipolar Membrane Combined with Ferric Iron Reduction as an Efficient Cathode System in Microbial Fuel Cells. *Environmental Science & Technology*, 2006. **40**(17): p. 5200.
 75. Pant, D., G. Van Bogaert, M. De Smet, L. Diels, and K. Vanbroekhoven, Use of novel permeable membrane and air cathodes in acetate microbial fuel cells. *Electrochimica Acta*, 2010. **55**(26): p. 7710.
 76. Di Palma, L., I. Bavasso, F. Sarasini, J. Tirillò, D. Puglia, F. Dominici, and L. Torre, Synthesis, characterization and performance evaluation of Fe₃O₄/PES nano composite membranes for microbial fuel cell. *European Polymer Journal*, 2018. **99**: p. 222.
 77. Shahgaldi, S., M. Ghasemi, W.R. Wan Daud, Z. Yaakob, M. Sedighi, J. Alam, and A.F. Ismail, Performance enhancement of microbial fuel cell by PVDF/Nafion nanofibre composite proton exchange membrane. *Fuel Processing Technology*, 2014. **124**: p. 290.
 78. Liu, H., R. Ramnarayanan, and B.E. Logan, Production of Electricity during Wastewater Treatment Using a Single Chamber Microbial Fuel Cell. *Environmental Science & Technology*, 2004. **38**(7): p. 2281.
 79. Cheng, S., H. Liu, and B.E. Logan, Increased performance of single-chamber microbial fuel cells using an improved cathode structure. *Electrochemistry Communications*, 2006. **8**(3): p. 489.
 80. Chae, K.J., M. Choi, F.F. Ajayi, W. Park, I.S. Chang, and I.S. Kim, Mass Transport through a Proton Exchange Membrane (Nafion) in Microbial Fuel Cells. *Energy & Fuels*, 2008. **22**(1): p. 169.

-
81. Williams, M.V., H.R. Kunz, and J.M. Fenton, Operation of Nafion®-based PEM fuel cells with no external humidification: influence of operating conditions and gas diffusion layers. *Journal of Power Sources*, 2004. **135**(1): p. 122.
 82. Liang, Z., W. Chen, J. Liu, S. Wang, Z. Zhou, W. Li, G. Sun, and Q. Xin, FT-IR study of the microstructure of Nafion® membrane. *Journal of Membrane Science*, 2004. **233**(1): p. 39.
 83. Daud, S.M., B.H. Kim, M. Ghasemi, and W.R.W. Daud, Separators used in microbial electrochemical technologies: Current status and future prospects. *Bioresource Technology*, 2015. **195**: p. 170.
 84. Huang, D., B.-Y. Song, Y.-L. He, Q. Ren, and S. Yao, Cations Diffusion in Nafion117 Membrane of Microbial fuel cells. *Electrochimica Acta*, 2017. **245**: p. 654.
 85. MW, S.J.a.M., Matlab Source Code for Species Transport through Nafion Membranes in Direct Ethanol, Direct Methanol, and Direct Glucose Fuel Cells *Journal of Physical Mathematics*, 2016. **7**(4).
 86. Urbain, V., R. Benoit, and J. Manem, Membrane bioreactor: a new treatment tool. *Journal - American Water Works Association*, 1996. **88**(5): p. 75.
 87. Ng, A.N.L. and A.S. Kim, A mini-review of modeling studies on membrane bioreactor (MBR) treatment for municipal wastewaters. *Desalination*, 2007. **212**(1): p. 261.
 88. Wang, Y., X. Huang, and Q. Yuan, Nitrogen and carbon removals from food processing wastewater by an anoxic/aerobic membrane bioreactor. *Process Biochemistry*, 2005. **40**(5): p. 1733.
 89. Min-chao Chang, W.-Y.T., Shou Hwa Chuang, Wang-kuan Chang. Application of Non-woven fabric material in Membrane bioreactor Processes for Industrial Wastewater Treatment. in Conference proceedings. 2003.
 90. Dvořák, L., J. Svojitka, J. Wanner, and T. Wintgens, Nitrification performance in a membrane bioreactor treating industrial wastewater. *Water Research*, 2013. **47**(13): p. 4412.
 91. Rosenberger, S., U. Krüger, R. Witzig, W. Manz, U. Szewzyk, and M. Kraume, Performance of a bioreactor with submerged membranes for aerobic treatment of municipal waste water. *Water Research*, 2002. **36**(2): p. 413.
 92. Dvořák, L., M. Gómez, J. Dolina, and A. Černín, Anaerobic membrane bioreactors—a mini review with emphasis on industrial wastewater treatment: applications, limitations and perspectives. *Desalination and Water Treatment*, 2016. **57**(41): p. 19062.
 93. Lin, H., W. Peng, M. Zhang, J. Chen, H. Hong, and Y. Zhang, A review on anaerobic membrane bioreactors: Applications, membrane fouling and future perspectives. *Desalination*, 2013. **314**: p. 169.
 94. Skouteris, G., D. Hermosilla, P. López, C. Negro, and Á. Blanco, Anaerobic membrane bioreactors for wastewater treatment: A review. *Chemical Engineering Journal*, 2012. **198-199**: p. 138.
 95. Lin, H., J. Chen, F. Wang, L. Ding, and H. Hong, Feasibility evaluation of submerged anaerobic membrane bioreactor for municipal secondary wastewater treatment. *Desalination*, 2011. **280**(1): p. 120.
 96. He, Y., P. Xu, C. Li, and B. Zhang, High-concentration food wastewater treatment by an anaerobic membrane bioreactor. *Water Research*, 2005. **39**(17): p. 4110.
 97. Smith, A.L., S.J. Skerlos, and L. Raskin, Psychrophilic anaerobic membrane bioreactor treatment of domestic wastewater. *Water Research*, 2013. **47**(4): p. 1655.
 98. van der Marel, P., A. Zwijnenburg, A. Kemperman, M. Wessling, H. Temmink, and W. van der Meer, Influence of membrane properties on fouling in submerged membrane bioreactors. *Journal of Membrane Science*, 2010. **348**(1): p. 66.

-
99. Xiao, K., J. Sun, Y. Mo, Z. Fang, P. Liang, X. Huang, J. Ma, and B. Ma, Effect of membrane pore morphology on microfiltration organic fouling: PTFE/PVDF blend membranes compared with PVDF membranes. *Desalination*, 2014. **343**: p. 217.
 100. Le-Clech, P., Membrane bioreactors and their uses in wastewater treatments. *Applied Microbiology and Biotechnology*, 2010. **88**(6): p. 1253.
 101. Zhang, M., B.-q. Liao, X. Zhou, Y. He, H. Hong, H. Lin, and J. Chen, Effects of hydrophilicity/hydrophobicity of membrane on membrane fouling in a submerged membrane bioreactor. *Bioresource Technology*, 2015. **175**: p. 59.
 102. Wang, Y. and F. Caruso, Macroporous Zeolitic Membrane Bioreactors. *Advanced Functional Materials*, 2004. **14**(10): p. 1012.
 103. Amini, M., H. Etemadi, A. Akbarzadeh, and R. Yegani, Preparation and performance evaluation of high-density polyethylene/silica nanocomposite membranes in membrane bioreactor system. *Biochemical Engineering Journal*, 2017. **127**: p. 196.
 104. Abdel-Karim, A., T.A. Gad-Allah, A.S. El-Kalliny, S.I.A. Ahmed, E.R. Souaya, M.I. Badawy, and M. Ulbricht, Fabrication of modified polyethersulfone membranes for wastewater treatment by submerged membrane bioreactor. *Separation and Purification Technology*, 2017. **175**: p. 36.
 105. Cicek, N., D. Dionysiou, M.T. Suidan, P. Ginestet, and J.M. Audic, Performance deterioration and structural changes of a ceramic membrane bioreactor due to inorganic abrasion. *Journal of Membrane Science*, 1999. **163**(1): p. 19.
 106. Grossman, A.D., Y. Yang, U. Yogev, D.C. Camarena, G. Oron, and R. Bernstein, Effect of ultrafiltration membrane material on fouling dynamics in a submerged anaerobic membrane bioreactor treating domestic wastewater. *Environmental Science: Water Research & Technology*, 2019. **5**(6): p. 1145.
 107. Lee, W., S. Kang, and H. Shin, Sludge characteristics and their contribution to microfiltration in submerged membrane bioreactors. *Journal of Membrane Science*, 2003. **216**(1): p. 217.
 108. Bae, T.-H. and T.-M. Tak, Interpretation of fouling characteristics of ultrafiltration membranes during the filtration of membrane bioreactor mixed liquor. *Journal of Membrane Science*, 2005. **264**(1): p. 151.
 109. Yang, Y., P. Wang, and Q. Zheng, Preparation and properties of polysulfone/TiO₂ composite ultrafiltration membranes. *Journal of Polymer Science Part B: Polymer Physics*, 2006. **44**(5): p. 879.
 110. Cha, J., S. Choi, H. Yu, H. Kim, and C. Kim, Directly applicable microbial fuel cells in aeration tank for wastewater treatment. *Bioelectrochemistry*, 2010. **78**(1): p. 72.
 111. Liu, X.W., Y.P. Wang, Y.X. Huang, X.F. Sun, G.P. Sheng, R.J. Zeng, F. Li, F. Dong, S.G. Wang, and Z.H. Tong, Integration of a microbial fuel cell with activated sludge process for energy-saving wastewater treatment: Taking a sequencing batch reactor as an example. *Biotechnology and bioengineering*, 2011. **108**(6): p. 1260.
 112. Wang, Y.-P., X.-W. Liu, W.-W. Li, F. Li, Y.-K. Wang, G.-P. Sheng, R.J. Zeng, and H.-Q. Yu, A microbial fuel cell–membrane bioreactor integrated system for cost-effective wastewater treatment. *Applied Energy*, 2012. **98**: p. 230.
 113. Ren, L., Y. Ahn, and B.E. Logan, A Two-Stage Microbial Fuel Cell and Anaerobic Fluidized Bed Membrane Bioreactor (MFC-AFMBR) System for Effective Domestic Wastewater Treatment. *Environmental Science & Technology*, 2014. **48**(7): p. 4199.
 114. Malaeb, L., K.P. Katuri, B.E. Logan, H. Maab, S.P. Nunes, and P.E. Saikaly, A Hybrid Microbial Fuel Cell Membrane Bioreactor with a Conductive Ultrafiltration Membrane Biocathode for Wastewater Treatment. *Environmental Science & Technology*, 2013. **47**(20): p. 11821.

115. Oh, S.-E. and B.E. Logan, Proton exchange membrane and electrode surface areas as factors that affect power generation in microbial fuel cells. *Applied Microbiology and Biotechnology*, 2006. **70**(2): p. 162.
116. ElMekawy, A., H.M. Hegab, X. Dominguez-Benetton, and D. Pant, Internal resistance of microfluidic microbial fuel cell: Challenges and potential opportunities. *Bioresource Technology*, 2013. **142**: p. 672.
117. Ayyaru, S. and S. Dharmalingam, Improved performance of microbial fuel cells using sulfonated polyether ether ketone (SPEEK) TiO₂-SO₃H nanocomposite membrane. *RSC Advances*, 2013. **3**(47): p. 25243.
118. Fan, Y., E. Sharbrough, and H. Liu, Quantification of the Internal Resistance Distribution of Microbial Fuel Cells. *Environmental Science & Technology*, 2008. **42**(21): p. 8101.
119. Logan, B.E., C. Murano, K. Scott, N.D. Gray, and I.M. Head, Electricity generation from cysteine in a microbial fuel cell. *Water Research*, 2005. **39**(5): p. 942.
120. Ayyaru, S. and S. Dharmalingam, Enhanced response of microbial fuel cell using sulfonated poly ether ether ketone membrane as a biochemical oxygen demand sensor. *Analytica Chimica Acta*, 2014. **818**: p. 15.
121. Yousefi, V., D. Mohebbi-Kalhari, and A. Samimi, Application of layer-by-layer assembled chitosan/montmorillonite nanocomposite as oxygen barrier film over the ceramic separator of the microbial fuel cell. *Electrochimica Acta*, 2018. **283**: p. 234.
122. Du, Z., Q. Li, M. Tong, S. Li, and H. Li, Electricity Generation Using Membrane-less Microbial Fuel Cell during Wastewater Treatment. *Chinese Journal of Chemical Engineering*, 2008. **16**(5): p. 772.
123. Huang, D., B.-Y. Song, M.-J. Li, and X.-Y. Li, Oxygen diffusion in cation-form Nafion membrane of microbial fuel cells. *Electrochimica Acta*, 2018. **276**: p. 268.
124. Lee, H.-S., C.I. Torres, and B.E. Rittmann, Effects of Substrate Diffusion and Anode Potential on Kinetic Parameters for Anode-Respiring Bacteria. *Environmental Science & Technology*, 2009. **43**(19): p. 7571.
125. Kim, J.R., S. Cheng, S.-E. Oh, and B.E. Logan, Power Generation Using Different Cation, Anion, and Ultrafiltration Membranes in Microbial Fuel Cells. *Environmental Science & Technology*, 2007. **41**(3): p. 1004.
126. Chen, S., S.A. Patil, and U. Schröder, Substrate Crossover Effect and Performance Regeneration of the Biofouled Rotating Air-Cathode in Microbial Fuel Cell. *Frontiers in Energy Research*, 2018. **6**(85).
127. Harnisch, F., S. Wirth, and U. Schröder, Effects of substrate and metabolite crossover on the cathodic oxygen reduction reaction in microbial fuel cells: Platinum vs. iron(II) phthalocyanine based electrodes. *Electrochemistry Communications*, 2009. **11**(11): p. 2253.
128. Prabhu, N.V. and D. Sangeetha, Characterization and performance study of sulfonated poly ether ether ketone/Fe₃O₄ nano composite membrane as electrolyte for microbial fuel cell. *Chemical Engineering Journal*, 2014. **243**: p. 564.
129. Flimban, S.G., S.H. Hassan, M.M. Rahman, and S.-E. Oh, The effect of Nafion membrane fouling on the power generation of a microbial fuel cell. *International Journal of Hydrogen Energy*, 2018.
130. Miskan, M., M. Ismail, M. Ghasemi, J. Md Jahim, D. Nordin, and M.H. Abu Bakar, Characterization of membrane biofouling and its effect on the performance of microbial fuel cell. *International Journal of Hydrogen Energy*, 2016. **41**(1): p. 543.
131. Kim, B.H., I.S. Chang, and G.M. Gadd, Challenges in microbial fuel cell development and operation. *Applied Microbiology and Biotechnology*, 2007. **76**(3): p. 485.

-
132. Xu, J., G.-P. Sheng, H.-W. Luo, W.-W. Li, L.-F. Wang, and H.-Q. Yu, Fouling of proton exchange membrane (PEM) deteriorates the performance of microbial fuel cell. *Water Research*, 2012. **46**(6): p. 1817.
 133. Ghasemi, M., W.R. Wan Daud, M. Ismail, M. Rahimnejad, A.F. Ismail, J.X. Leong, M. Miskan, and K. Ben Liew, Effect of pre-treatment and biofouling of proton exchange membrane on microbial fuel cell performance. *International Journal of Hydrogen Energy*, 2013. **38**(13): p. 5480.
 134. Liu, C.X., D.R. Zhang, Y. He, X.S. Zhao, and R. Bai, Modification of membrane surface for anti-biofouling performance: Effect of anti-adhesion and anti-bacteria approaches. *Journal of Membrane Science*, 2010. **346**(1): p. 121.
 135. Wang, L., C. Hu, and L. Shao, The antimicrobial activity of nanoparticles: present situation and prospects for the future. *International journal of nanomedicine*, 2017. **12**: p. 1227.
 136. Yang, E., K.-J. Chae, A.B. Alayande, K.-Y. Kim, and I.S. Kim, Concurrent performance improvement and biofouling mitigation in osmotic microbial fuel cells using a silver nanoparticle-polydopamine coated forward osmosis membrane. *Journal of Membrane Science*, 2016. **513**: p. 217.
 137. Pandit, S., S. Khilari, K. Bera, D. Pradhan, and D. Das, Application of PVA–PDDA polymer electrolyte composite anion exchange membrane separator for improved bioelectricity production in a single chambered microbial fuel cell. *Chemical Engineering Journal*, 2014. **257**: p. 138.
 138. Kim, K.-Y., E. Yang, M.-Y. Lee, K.-J. Chae, C.-M. Kim, and I.S. Kim, Polydopamine coating effects on ultrafiltration membrane to enhance power density and mitigate biofouling of ultrafiltration microbial fuel cells (UF-MFCs). *Water Research*, 2014. **54**: p. 62.
 139. Sun, C., J. Miao, J. Yan, K. Yang, C. Mao, J. Ju, and J. Shen, Applications of antibiofouling PEG-coating in electrochemical biosensors for determination of glucose in whole blood. *Electrochimica Acta*, 2013. **89**: p. 549.
 140. Roosjen, A., W. Norde, H.C. van der Mei, and H.J. Busscher. The Use of Positively Charged or Low Surface Free Energy Coatings versus Polymer Brushes in Controlling Biofilm Formation. in *Characterization of Polymer Surfaces and Thin Films*. 2006. Berlin, Heidelberg: Springer Berlin Heidelberg.
 141. Trogadas, P. and V. Ramani, Membrane and MEA Development in Polymer Electrolyte Fuel Cells, in *Polymer Membranes for Fuel Cells*, S.M.J. Zaidi and T. Matsuura, Editors. 2009, Springer US: Boston, MA. p. 253.
 142. Lee, H., M. Yanilmaz, O. Toprakci, K. Fu, and X. Zhang, A review of recent developments in membrane separators for rechargeable lithium-ion batteries. *Energy & Environmental Science*, 2014. **7**(12): p. 3857.
 143. Rahimnejad, M., G. Bakeri, M. Ghasemi, and A. Zirepour, A review on the role of proton exchange membrane on the performance of microbial fuel cell. *Polymers for Advanced Technologies*, 2014. **25**(12): p. 1426.
 144. Tanimura, S. and T. Matsuoka, Proton transfer in nafion membrane by quantum chemistry calculation. *Journal of Polymer Science Part B: Polymer Physics*, 2004. **42**(10): p. 1905.
 145. Ghasemi, M., W.R.W. Daud, A.F. Ismail, Y. Jafari, M. Ismail, A. Mayahi, and J. Othman, Simultaneous wastewater treatment and electricity generation by microbial fuel cell: Performance comparison and cost investigation of using Nafion 117 and SPEEK as separators. *Desalination*, 2013. **325**: p. 1.
 146. Jie, Z., T. Haolin, and P. Mu, Fabrication and characterization of self-assembled Nafion–SiO₂–ePTFE composite membrane of PEM fuel cell. *Journal of Membrane Science*, 2008. **312**(1): p. 41.

147. Saccà, A., A. Carbone, E. Passalacqua, A. D'Epifanio, S. Licocchia, E. Traversa, E. Sala, F. Traini, and R. Ornelas, Nafion–TiO₂ hybrid membranes for medium temperature polymer electrolyte fuel cells (PEFCs). *Journal of Power Sources*, 2005. **152**: p. 16.
148. Chien, H.-C., L.-D. Tsai, C.-P. Huang, C.-y. Kang, J.-N. Lin, and F.-C. Chang, Sulfonated graphene oxide/Nafion composite membranes for high-performance direct methanol fuel cells. *International Journal of Hydrogen Energy*, 2013. **38**(31): p. 13792.
149. Lim, S.S., W.R.W. Daud, J. Md Jahim, M. Ghasemi, P.S. Chong, and M. Ismail, Sulfonated poly(ether ether ketone)/poly(ether sulfone) composite membranes as an alternative proton exchange membrane in microbial fuel cells. *International Journal of Hydrogen Energy*, 2012. **37**(15): p. 11409.
150. Sivasankaran, A. and D. Sangeetha, Influence of sulfonated SiO₂ in sulfonated polyether ether ketone nanocomposite membrane in microbial fuel cell. *Fuel*, 2015. **159**: p. 689.
151. Choi, T.H., Y.-B. Won, J.-W. Lee, D.W. Shin, Y.M. Lee, M. Kim, and H.B. Park, Electrochemical performance of microbial fuel cells based on disulfonated poly(arylene ether sulfone) membranes. *Journal of Power Sources*, 2012. **220**: p. 269.
152. Ayyaru, S., P. Letchoumanane, S. Dharmalingam, and A.R. Stanislaus, Performance of sulfonated polystyrene–ethylene–butylene–polystyrene membrane in microbial fuel cell for bioelectricity production. *Journal of Power Sources*, 2012. **217**: p. 204.
153. Rudra, R., V. Kumar, N. Pramanik, and P.P. Kundu, Graphite oxide incorporated crosslinked polyvinyl alcohol and sulfonated styrene nanocomposite membrane as separating barrier in single chambered microbial fuel cell. *Journal of Power Sources*, 2017. **341**: p. 285.
154. Rudra, R., V. Kumar, and P.P. Kundu, Acid catalysed cross-linking of poly vinyl alcohol (PVA) by glutaraldehyde: effect of crosslink density on the characteristics of PVA membranes used in single chambered microbial fuel cells. *RSC Advances*, 2015. **5**(101): p. 83436.
155. Khilari, S., S. Pandit, M.M. Ghangrekar, D. Pradhan, and D. Das, Graphene oxide-impregnated PVA–STA composite polymer electrolyte membrane separator for power generation in a single-chambered microbial fuel cell. *Industrial & Engineering Chemistry Research*, 2013. **52**(33): p. 11597.
156. Sivasankaran, A., D. Sangeetha, and Y.-H. Ahn, Nanocomposite membranes based on sulfonated polystyrene ethylene butylene polystyrene (SSEBS) and sulfonated SiO₂ for microbial fuel cell application. *Chemical Engineering Journal*, 2016. **289**: p. 442.
157. Merle, G., M. Wessling, and K. Nijmeijer, Anion exchange membranes for alkaline fuel cells: A review. *Journal of Membrane Science*, 2011. **377**(1): p. 1.
158. Vincent, I. and D. Bessarabov, Low cost hydrogen production by anion exchange membrane electrolysis: A review. *Renewable and Sustainable Energy Reviews*, 2018. **81**: p. 1690.
159. Li, X., H. Zhang, Z. Mai, H. Zhang, and I. Vankelecom, Ion exchange membranes for vanadium redox flow battery (VRB) applications. *Energy & Environmental Science*, 2011. **4**(4): p. 1147.
160. Danks, T.N., R.C.T. Slade, and J.R. Varcoe, Alkaline anion-exchange radiation-grafted membranes for possible electrochemical application in fuel cells. *Journal of Materials Chemistry*, 2003. **13**(4): p. 712.
161. Li, N., M.D. Guiver, and W.H. Binder, Towards High Conductivity in Anion-Exchange Membranes for Alkaline Fuel Cells. *ChemSusChem*, 2013. **6**(8): p. 1376.
162. Han, J., H. Peng, J. Pan, L. Wei, G. Li, C. Chen, L. Xiao, J. Lu, and L. Zhuang, Highly Stable Alkaline Polymer Electrolyte Based on a Poly(ether ether ketone) Backbone. *ACS Applied Materials & Interfaces*, 2013. **5**(24): p. 13405.

-
163. Cao, Y.-C., X. Wu, and K. Scott, A quaternary ammonium grafted poly vinyl benzyl chloride membrane for alkaline anion exchange membrane water electrolyzers with noble-metal catalysts. *International Journal of Hydrogen Energy*, 2012. **37**(12): p. 9524.
164. Xiong, Y., J. Fang, Q.H. Zeng, and Q.L. Liu, Preparation and characterization of cross-linked quaternized poly(vinyl alcohol) membranes for anion exchange membrane fuel cells. *Journal of Membrane Science*, 2008. **311**(1): p. 319.
165. Lu, W., Z.-G. Shao, G. Zhang, Y. Zhao, J. Li, and B. Yi, Preparation and characterization of imidazolium-functionalized poly (ether sulfone) as anion exchange membrane and ionomer for fuel cell application. *International Journal of Hydrogen Energy*, 2013. **38**(22): p. 9285.
166. Noonan, K.J.T., K.M. Hugar, H.A. Kostalik, E.B. Lobkovsky, H.D. Abruña, and G.W. Coates, Phosphonium-Functionalized Polyethylene: A New Class of Base-Stable Alkaline Anion Exchange Membranes. *Journal of the American Chemical Society*, 2012. **134**(44): p. 18161.
167. Gu, F., H. Dong, Y. Li, Z. Si, and F. Yan, Highly Stable N3-Substituted Imidazolium-Based Alkaline Anion Exchange Membranes: Experimental Studies and Theoretical Calculations. *Macromolecules*, 2014. **47**(1): p. 208.
168. Deavin, O.I., S. Murphy, A.L. Ong, S.D. Poynton, R. Zeng, H. Herman, and J.R. Varcoe, Anion-exchange membranes for alkaline polymer electrolyte fuel cells: comparison of pendent benzyltrimethylammonium- and benzylmethylimidazolium-head-groups. *Energy & Environmental Science*, 2012. **5**(9): p. 8584.
169. Cheng, J., G. He, and F. Zhang, A mini-review on anion exchange membranes for fuel cell applications: Stability issue and addressing strategies. *International Journal of Hydrogen Energy*, 2015. **40**(23): p. 7348.
170. Ren, X., S.C. Price, A.C. Jackson, N. Pomerantz, and F.L. Beyer, Highly Conductive Anion Exchange Membrane for High Power Density Fuel-Cell Performance. *ACS Applied Materials & Interfaces*, 2014. **6**(16): p. 13330.
171. Kruusenberg, I., L. Matisen, Q. Shah, A.M. Kannan, and K. Tammeveski, Non-platinum cathode catalysts for alkaline membrane fuel cells. *International Journal of Hydrogen Energy*, 2012. **37**(5): p. 4406.
172. Vega, J.A. and W.E. Mustain, Effect of CO₂, HCO₃⁻ and CO₃⁻² on oxygen reduction in anion exchange membrane fuel cells. *Electrochimica Acta*, 2010. **55**(5): p. 1638.
173. Pandit, S., S. Ghosh, M.M. Ghangrekar, and D. Das, Performance of an anion exchange membrane in association with cathodic parameters in a dual chamber microbial fuel cell. *International Journal of Hydrogen Energy*, 2012. **37**(11): p. 9383.
174. Elangovan, M. and S. Dharmalingam, Preparation and performance evaluation of poly (ether-imide) based anion exchange polymer membrane electrolyte for microbial fuel cell. *International Journal of Hydrogen Energy*, 2016. **41**(20): p. 8595.
175. Studart, A.R., U.T. Gonzenbach, E. Tervoort, and L.J. Gauckler, Processing Routes to Macroporous Ceramics: A Review. *Journal of the American Ceramic Society*, 2006. **89**(6): p. 1771.
176. Li, Y., Z. Rui, C. Xia, M. Anderson, and Y.S. Lin, Performance of ionic-conducting ceramic/carbonate composite material as solid oxide fuel cell electrolyte and CO₂ permeation membrane. *Catalysis Today*, 2009. **148**(3): p. 303.
177. Evans, A., A. Bieberle-Hütter, J.L.M. Rupp, and L.J. Gauckler, Review on microfabricated micro-solid oxide fuel cell membranes. *Journal of Power Sources*, 2009. **194**(1): p. 119.
178. Yousefi, V., D. Mohebbi-Kalhari, and A. Samimi, Ceramic-based microbial fuel cells (MFCs): A review. *International Journal of Hydrogen Energy*, 2017. **42**(3): p. 1672.
179. Richerson, D.W., *Modern Ceramic Engineering Properties, Processing, and Use in Design*, Third Edition. Taylor and Francis Group, 2005.

-
180. PAMELA B. VANDIVER, O.S., BOHUSLAV KLIMA³, JIŘI SVOBODA, The Origins of Ceramic Technology at Dolni Věstonice, Czechoslovakia. *Science*, 1989. **246**(4933).
 181. Kraft, A., Electrochemical Water Disinfection: A Short Review. *Johnson Matthey, Platinum Metals Review*, 2008. **52**: p. 177.
 182. Kim, J.H., S.S. Shin, H.S. Noh, J.-W. Son, M. Choi, and H. Kim, Tailoring ceramic membrane structures of solid oxide fuel cells via polymer-assisted electrospray deposition. *Journal of Membrane Science*, 2017. **544**: p. 234.
 183. Winfield, J., I. Gajda, J. Greenman, and I. Ieropoulos, A review into the use of ceramics in microbial fuel cells. *Bioresource Technology*, 2016. **215**: p. 296.
 184. Ortiz-Martínez, V.M., I. Gajda, M.J. Salar-García, J. Greenman, F.J. Hernández-Fernández, and I. Ieropoulos, Study of the effects of ionic liquid-modified cathodes and ceramic separators on MFC performance. *Chemical Engineering Journal*, 2016. **291**: p. 317.
 185. Behera, M., P.S. Jana, and M.M. Ghangrekar, Performance evaluation of low cost microbial fuel cell fabricated using earthen pot with biotic and abiotic cathode. *Bioresource Technology*, 2010. **101**(4): p. 1183.
 186. Behera, M., P.S. Jana, T.T. More, and M.M. Ghangrekar, Rice mill wastewater treatment in microbial fuel cells fabricated using proton exchange membrane and earthen pot at different pH. *Bioelectrochemistry*, 2010. **79**(2): p. 228.
 187. Ajayi, F.F. and P.R. Weigele, A terracotta bio-battery. *Bioresource Technology*, 2012. **116**: p. 86.
 188. Behera, M. and M.M. Ghangrekar, Electricity generation in low cost microbial fuel cell made up of earthenware of different thickness. *Water Science and Technology*, 2011. **64**(12): p. 2468.
 189. Ghadge, A.N., M. Sreemannarayana, N. Duteanu, and M.M. Ghangrekar, Influence of ceramic separator's characteristics on microbial fuel cell performance. *J. Electrochem. Sci. Eng.*, 2014. **4**(4): p. 315.
 190. Gajda, I., A. Stinchcombe, I. Merino-Jimenez, G. Pasternak, D. Sanchez-Herranz, J. Greenman, and I.A. Ieropoulos, Miniaturized Ceramic-Based Microbial Fuel Cell for Efficient Power Generation From Urine and Stack Development. *Frontiers in Energy Research*, 2018. **6**(84).
 191. Jana, P.S., M. Behera, and M.M. Ghangrekar, Performance comparison of up-flow microbial fuel cells fabricated using proton exchange membrane and earthen cylinder. *International Journal of Hydrogen Energy*, 2010. **35**(11): p. 5681.
 192. Winfield, J., J. Greenman, D. Huson, and I. Ieropoulos, Comparing terracotta and earthenware for multiple functionalities in microbial fuel cells. *Bioprocess and Biosystems Engineering*, 2013. **36**(12): p. 1913.
 193. Jadhav, D.A., A.N. Ghadge, D. Mondal, and M.M. Ghangrekar, Comparison of oxygen and hypochlorite as cathodic electron acceptor in microbial fuel cells. *Bioresource Technology*, 2014. **154**: p. 330.
 194. Chatterjee, P. and M.M. Ghangrekar, Design of Clayware Separator-Electrode Assembly for Treatment of Wastewater in Microbial Fuel Cells. *Applied Biochemistry and Biotechnology*, 2014. **173**(2): p. 378.
 195. Ghadge, A.N. and M.M. Ghangrekar, Performance of low cost scalable air-cathode microbial fuel cell made from clayware separator using multiple electrodes. *Bioresource Technology*, 2015. **182**: p. 373.
 196. Jadhav, D.A., A.N. Ghadge, and M.M. Ghangrekar, Enhancing the power generation in microbial fuel cells with effective utilization of goethite recovered from mining mud as anodic catalyst. *Bioresource Technology*, 2015. **191**: p. 110.

-
197. Pasternak, G., J. Greenman, and I. Ieropoulos, Comprehensive Study on Ceramic Membranes for Low-Cost Microbial Fuel Cells. *ChemSusChem*, 2016. **9**(1): p. 88.
 198. Walter, X.A., S. Forbes, J. Greenman, and I.A. Ieropoulos, From single MFC to cascade configuration: The relationship between size, hydraulic retention time and power density. *Sustainable Energy Technologies and Assessments*, 2016. **14**: p. 74.
 199. Iwahara, H., Proton conducting ceramics and their applications. *Solid State Ionics*, 1996. **86-88**: p. 9.
 200. You, S., B. Liu, Y. Gao, Y. Wang, C.Y. Tang, Y. Huang, and N. Ren, Monolithic Porous Magnéli-phase Ti₄O₇ for Electro-oxidation Treatment of Industrial Wastewater. *Electrochimica Acta*, 2016. **214**: p. 326.
 201. Manicone, P.F., P. Rossi Iommitti, and L. Raffaelli, An overview of zirconia ceramics: Basic properties and clinical applications. *Journal of Dentistry*, 2007. **35**(11): p. 819.
 202. Benfer, S., P. Árki, and G. Tomandl, Ceramic Membranes for Filtration Applications — Preparation and Characterization. *Advanced Engineering Materials*, 2004. **6**(7): p. 495.
 203. Kharton, V.V. and F.M.B. Marques, Mixed ionic–electronic conductors: effects of ceramic microstructure on transport properties. *Current Opinion in Solid State and Materials Science*, 2002. **6**(3): p. 261.
 204. Venkatesan, P.N. and S. Dharmalingam, Effect of cation transport of SPEEK – Rutile TiO₂ electrolyte on microbial fuel cell performance. *Journal of Membrane Science*, 2015. **492**: p. 518.
 205. Yang, E., K.-J. Chae, and I.S. Kim, Assessment of different ceramic filtration membranes as a separator in microbial fuel cells. *Desalination and Water Treatment*, 2016. **57**(58): p. 28077.
 206. Daud, S.M., W.R. Wan Daud, M.H. Abu Bakar, B.H. Kim, M.R. Somalu, J.M. Jahim, A. Muchtar, and M. Ghasemi, A comparison of long-term fouling performance by zirconia ceramic filter and cation exchange in microbial fuel cells. *International Biodeterioration & Biodegradation*, 2019. **136**: p. 63.
 207. Wei, J., Chapter 9 - Proton-Conducting Materials Used as Polymer Electrolyte Membranes in Fuel Cells, in *Polymer-Based Multifunctional Nanocomposites and Their Applications*, K. Song, C. Liu, and J.Z. Guo, Editors. 2019, Elsevier. p. 245.
 208. Miyake, T. and M. Rolandi, Grotthuss mechanisms: from proton transport in proton wires to bioprotonic devices. *Journal of Physics: Condensed Matter*, 2015. **28**(2): p. 023001.
 209. Kreuer, K.D., A. Rabenau, and W. Weppner, Vehicle mechanism, a new model for the interpretation of the conductivity of fast proton conductors. *Angewandte Chemie International Edition in English*, 1982. **21**(3): p. 208.
 210. Eikerling, M., A.A. Kornyshev, A.M. Kuznetsov, J. Ulstrup, and S. Walbran, Mechanisms of Proton Conductance in Polymer Electrolyte Membranes. *The Journal of Physical Chemistry B*, 2001. **105**(17): p. 3646.
 211. Petersen, M.K. and G.A. Voth, Characterization of the Solvation and Transport of the Hydrated Proton in the Perfluorosulfonic Acid Membrane Nafion. *The Journal of Physical Chemistry B*, 2006. **110**(37): p. 18594.
 212. Cai, K., F. Sun, X. Liang, C. Liu, N. Zhao, X. Zou, and G. Zhu, An acid-stable hexaphosphate ester based metal–organic framework and its polymer composite as proton exchange membrane. *Journal of Materials Chemistry A*, 2017. **5**(25): p. 12943.
 213. Kumar, P., R.P. Bharti, V. Kumar, and P.P. Kundu, Chapter 4 - Polymer Electrolyte Membranes for Microbial Fuel Cells: Part A. Nafion-Based Membranes, in *Progress and Recent Trends in Microbial Fuel Cells*, P.P. Kundu and K. Dutta, Editors. 2018, Elsevier. p. 47.

-
214. Colombo, P., G. Mera, R. Riedel, and G.D. Soraru, Polymer-derived ceramics: 40 years of research and innovation in advanced ceramics. *Journal of the American Ceramic Society*, 2010. **93**(7): p. 1805.
 215. Verbeek, W., Production of shaped articles of homogeneous mixtures of silicon carbide and nitride 1973: United states.
 216. Zhiwei Zhang, Chi-kyun Park, Lu Ying Sun, and C. Chai, Method of making an electrochemical cell by the application of polysiloxane onto at least one of the cell components 2002: United states.
 217. Arukalam, I.O., E.E. Oguzie, and Y. Li, Nanostructured superhydrophobic polysiloxane coating for high barrier and anticorrosion applications in marine environment. *Journal of Colloid and Interface Science*, 2018. **512**: p. 674.
 218. Bakumov, V., K. Gueinzus, C. Hermann, M. Schwarz, and E. Kroke, Polysilazane-derived antibacterial silver–ceramic nanocomposites. *Journal of the European Ceramic Society*, 2007. **27**(10): p. 3287.
 219. Mera, G., M. Gallei, S. Bernard, and E. Ionescu, Ceramic Nanocomposites from Tailor-Made Preceramic Polymers. *Nanomaterials (Basel, Switzerland)*, 2015. **5**(2): p. 468.
 220. Birot, M., J.-P. Pilot, and J. Dunogues, Comprehensive Chemistry of Polycarbosilanes, Polysilazanes, and Polycarbosilazanes as Precursors of Ceramics. *Chemical Reviews*, 1995. **95**(5): p. 1443.
 221. Riedel, R., A. Kienzle, W. Dressler, L. Ruwisch, J. Bill, and F. Aldinger, A silicoboron carbonitride ceramic stable to 2,000°C. *Nature*, 1996. **382**(6594): p. 796.
 222. Konegger, T., L.F. Williams, and R.K. Bordia, Planar, Polysilazane-Derived Porous Ceramic Supports for Membrane and Catalysis Applications. *Journal of the American Ceramic Society*, 2015. **98**(10): p. 3047.
 223. Bernardo, E., L. Fiocco, G. Parciannello, E. Storti, and P. Colombo, Advanced Ceramics from Preceramic Polymers Modified at the Nano-Scale: A Review. *Materials (Basel, Switzerland)*, 2014. **7**(3): p. 1927.
 224. Rivera, J.O.B., M.H. Talou, Y.M.X. Hung Hung, and M.A. Camerucci, Study of a silicon-based preceramic for the processing of polymer-derived ceramics. *Journal of Sol-Gel Science and Technology*, 2019. **91**(3): p. 446.
 225. Toreki, W., C.D. Batich, M.D. Sacks, M. Saleem, G.J. Choi, and A.A. Morrone, Polymer-derived silicon carbide fibers with low oxygen content and improved thermomechanical stability. *Composites Science and Technology*, 1994. **51**(2): p. 145.
 226. Li, H., L. Zhang, L. Cheng, Y. Wang, Z. Yu, M. Huang, H. Tu, and H. Xia, Polymer–ceramic conversion of a highly branched liquid polycarbosilane for SiC-based ceramics. *Journal of Materials Science*, 2008. **43**(8): p. 2806.
 227. Nedunchezian, S., R. Sujith, and R. Kumar, Processing and characterization of polymer precursor derived silicon oxycarbide ceramic foams and compacts. *Journal of Advanced Ceramics*, 2013. **2**(4): p. 318.
 228. Manoj Kumar, B.V. and Y.-W. Kim, Processing of polysiloxane-derived porous ceramics: a review. *Science and technology of advanced materials*, 2010. **11**(4): p. 044303.
 229. Schulz, M., Polymer derived ceramics in MEMS/NEMS – a review on production processes and application. *Advances in Applied Ceramics*, 2009. **108**(8): p. 454.
 230. Greil, P., Near Net Shape Manufacturing of Polymer Derived Ceramics. *Journal of the European Ceramic Society*, 1998. **18**(13): p. 1905.
 231. Mera, G., A. Navrotsky, S. Sen, H.-J. Kleebe, and R. Riedel, Polymer-derived SiCN and SiOC ceramics – structure and energetics at the nanoscale. *Journal of Materials Chemistry A*, 2013. **1**(12): p. 3826.

-
232. Esfahanian, M., R. Oberacker, T. Fett, and M.J. Hoffmann, Development of Dense Filler-Free Polymer-Derived SiOC Ceramics by Field-Assisted Sintering. *Journal of the American Ceramic Society*, 2008. **91**(11): p. 3803.
233. Mestre, S., A. Gozalbo, M.M. Lorente-Ayza, and E. Sánchez, Low-cost ceramic membranes: A research opportunity for industrial application. *Journal of the European Ceramic Society*, 2019.
234. Evans, J.W. and L.C. De Jonghe, Powder Compaction, in *The Production and Processing of Inorganic Materials*, J.W. Evans and L.C. De Jonghe, Editors. 2016, Springer International Publishing: Cham. p. 383.
235. Glass, S.J. and K.G. Ewsuk, Ceramic Powder Compaction. *MRS Bulletin*, 1997. **22**(12): p. 24.
236. Jiang, H., X.-H. Wang, W. Lei, G.-F. Fan, and W.-Z. Lu, Effects of two-step sintering on thermal and mechanical properties of aluminum nitride ceramics by impedance spectroscopy analysis. *Journal of the European Ceramic Society*, 2019. **39**(2): p. 249.
237. Ma, B., Y. Cao, Y. Zhu, X. Li, and Z. Cheng, Low-frequency dielectric dispersion in polymer-derived amorphous silicon carbonitride ceramics. *Journal of the American Ceramic Society*, 2019. **102**(6): p. 3547.
238. Liao, N., D. Jia, Z. Yang, and Y. Zhou, Enhanced mechanical properties and thermal shock resistance of Si₂BC₃N ceramics with SiC coated MWCNTs. *Journal of Advanced Ceramics*, 2019. **8**(1): p. 121.
239. Adam, M., C. Vakifahmetoglu, P. Colombo, M. Wilhelm, and G. Grathwohl, Polysiloxane-Derived Ceramics Containing Nanowires with Catalytically Active Tips. *Journal of the American Ceramic Society*, 2014. **97**(3): p. 959.
240. Parciannello, G., *Advanced ceramics from preceramic polymers and fillers*. 2012, Università degli Studi di Padova (IT).
241. Bouillon, E., F. Langlais, R. Paillet, R. Naslain, F. Cruege, P.V. Huong, J.C. Sarthou, A. Delpuech, C. Laffon, P. Lagarde, M. Monthieux, and A. Oberlin, Conversion mechanisms of a polycarbosilane precursor into an SiC-based ceramic material. *Journal of Materials Science*, 1991. **26**(5): p. 1333.
242. Rouxel, T., G.-D. Soraru, and J. Vicens, Creep Viscosity and Stress Relaxation of Gel-Derived Silicon Oxycarbide Glasses. *Journal of the American Ceramic Society*, 2001. **84**(5): p. 1052.
243. Rouxel, T., G. Massouras, and G.-D. Soraru, High Temperature Behavior of a Gel-Derived SiOC Glass: Elasticity and Viscosity. *Journal of Sol-Gel Science and Technology*, 1999. **14**(1): p. 87.
244. Narisawa, M., *Silicone Resin Applications for Ceramic Precursors and Composites*. Materials, 2010. **3**(6).
245. Jeske, M., C. Soltmann, C. Ellenberg, M. Wilhelm, D. Koch, and G. Grathwohl, Proton Conducting Membranes for the High Temperature-Polymer Electrolyte Membrane-Fuel Cell (HT-PEMFC) Based on Functionalized Polysiloxanes. *Fuel Cells*, 2007. **7**(1): p. 40.
246. Polmanteer, K.E. and M.J. Hunter, Polymer composition versus low-temperature characteristics of polysiloxane elastomers. *Journal of Applied Polymer Science*, 1959. **1**(1): p. 3.
247. Sorar, G.D., R. Campostrini, S. Maurina, and F. Babonneau, Gel Precursor to Silicon Oxycarbide Glasses with Ultrahigh Ceramic Yield. *Journal of the American Ceramic Society*, 1997. **80**(4): p. 999.
248. Cordelair, J. and P. Greil, Electrical conductivity measurements as a microprobe for structure transitions in polysiloxane derived Si-O-C ceramics. *Journal of the European Ceramic Society*, 2000. **20**(12): p. 1947.

-
249. Colombo, P., J.R. Hellmann, and D.L. Shelleman, Thermal Shock Behavior of Silicon Oxycarbide Foams. *Journal of the American Ceramic Society*, 2002. **85**(9): p. 2306.
250. Chang, I.-S., S.-O. Bag, and C.-H. Lee, Effects of membrane fouling on solute rejection during membrane filtration of activated sludge. *Process Biochemistry*, 2001. **36**(8): p. 855.
251. Liu, B., J. Chen, X. Du, and L. Xue, Poly (vinyl chloride)/montmorillonite hybrid membranes for total-heat recovery ventilation. *Journal of Membrane Science*, 2013. **443**: p. 83.
252. Titirici, M.-M. and M. Antonietti, Chemistry and materials options of sustainable carbon materials made by hydrothermal carbonization. *Chemical Society Reviews*, 2010. **39**(1): p. 103.
253. Tang, X. and X. Huang, Chapter 14 - Synthesis and Assembly Chemistry of Inorganic Polymers, in *Modern Inorganic Synthetic Chemistry*, R. Xu, W. Pang, and Q. Huo, Editors. 2011, Elsevier: Amsterdam. p. 295.
254. Pizon, D., L. Charpentier, R. Lucas, S. Foucaud, A. Maître, and M. Balat-Pichelin, Oxidation behavior of spark plasma sintered ZrC–SiC composites obtained from the polymer-derived ceramics route. *Ceramics International*, 2014. **40**(3): p. 5025.
255. Prenzel, T., T. Guedes, F. Schlüter, M. Wilhelm, and K. Rezwani, Tailoring surfaces of hybrid ceramics for gas adsorption—from alkanes to CO₂. *Separation and Purification Technology*, 2014. **129**: p. 80.
256. Zhang, H., P.D.A. Nunes, M. Wilhelm, and K. Rezwani, Hierarchically ordered micro/meso/macroporous polymer-derived ceramic monoliths fabricated by freeze-casting. *Journal of the European Ceramic Society*, 2016. **36**(1): p. 51.
257. Zdravkov, B.D., J.J. Čermák, M. Šefara, and J. Janků, Pore classification in the characterization of porous materials: A perspective. *Central European Journal of Chemistry*, 2007. **5**(2): p. 385.
258. Wilhelm, M., M. Adam, M. Bäumer, and G. Grathwohl, Synthesis and properties of porous hybrid materials containing metallic nanoparticles. *Advanced Engineering Materials*, 2008. **10**(3): p. 241.
259. Bois, L., J. Maquet, F. Babonneau, H. Mutin, and D. Bahloul, Structural Characterization of Sol-Gel Derived Oxycarbide Glasses. 1. Study of the Pyrolysis Process. *Chemistry of Materials*, 1994. **6**(6): p. 796.
260. Sorarù, G.D., H.-J. Kleebe, R. Ceccato, and L. Pederiva, Development of mullite-SiC nanocomposites by pyrolysis of filled polymethylsiloxane gels. *Journal of the European Ceramic Society*, 2000. **20**(14): p. 2509.
261. Xomeritakis, G., C.M. Braunbarth, B. Smarsly, N. Liu, R. Köhn, Z. Klipowicz, and C.J. Brinker, Aerosol-assisted deposition of surfactant-templated mesoporous silica membranes on porous ceramic supports. *Microporous and Mesoporous Materials*, 2003. **66**(1): p. 91.
262. Huo, Q., D.I. Margolese, and G.D. Stucky, Surfactant Control of Phases in the Synthesis of Mesoporous Silica-Based Materials. *Chemistry of Materials*, 1996. **8**(5): p. 1147.
263. Li, S., J. Zheng, W. Yang, and Y. Zhao, Preparation and Characterization of 3DOM H₃PMo₁₂O₄₀–SiO₂ with Keggin Structure. *Chemistry Letters*, 2007. **36**(6): p. 758.
264. Han, D.C., S. Son, Y.C. Choi, H.J. Shin, M.T. Kim, G. Kwak, and D.K. Lee, Chemical Surface Pre-treatment of Carbon Nanotube for Improving the Thermal Conductivity of Carbon Nanotube-Epoxy Composite. *Molecular Crystals and Liquid Crystals*, 2011. **551**(1): p. 228.
265. Misture, S.T. and R.L. Snyder, X-ray Diffraction, in *Encyclopedia of Materials: Science and Technology*, K.H.J. Buschow, et al., Editors. 2001, Elsevier: Oxford. p. 9799.
266. Warren, B.E., X-ray Diffraction. 1990: Addison Wesley publishing company.

-
267. Guinier, A., X-ray Diffraction in Crystals, Imperfect Crystals, and Amorphous Bodies. 1994: Dover Publication.
268. Scanning Electron Microscopy and X-Ray Microanalysis, ed. D.E.N. Joseph I. Goldstein, Joseph R. Michael, Nicholas W.M. Ritchie, John Henry J. Scott, David C. Joy. 2017: Springer.
269. Reimer, L., Scanning Electron Microscopy: Physics of Image Formation and Microanalysis. 2013: Springer.
270. Colthup, N., Introduction to Infrared and Raman Spectroscopy. 2nd edition. 1977: A Subsidiary of Harcourt Brace Jovanovich Publisher.
271. John R. Ferraro, K.N., Introductory Raman Spectroscopy. 2nd Edition. 2003: Elsevier.
272. McCreery, R.L., Raman Spectroscopy for Chemical Analysis. Vol. 157. 2005: Wiley Inter-science.
273. Peter R. Griffiths, J.A.D.H., Fourier Transform Infrared Spectrometry. 2nd edition. 2007: Wiley Interscience
274. Smith, B.C., Fundamentals of Fourier Transform Infrared Spectroscopy. **2nd edition**. 2011: Taylor and francis group
275. Naderi, M., Chapter Fourteen - Surface Area: Brunauer–Emmett–Teller (BET), in Progress in Filtration and Separation, S. Tarleton, Editor. 2015, Academic Press: Oxford. p. 585.
276. Whittemore, O.J., Mercury porosimetry of ceramics. Powder Technology, 1981. **29**(1): p. 167.
277. Müller, F.I., C.A. Ferreira, D.S. Azambuja, C. Alemán, and E. Armelin, Measuring the proton conductivity of ion-exchange membranes using electrochemical impedance spectroscopy and through-plane cell. The Journal of Physical Chemistry B, 2014. **118**(4): p. 1102.
278. Jadhav, G. and M. Ghangrekar, Performance of microbial fuel cell subjected to variation in pH, temperature, external load and substrate concentration. Bioresource Technology, 2009. **100**(2): p. 717.
279. Logan, B.E., Microbial fuel cells. 2008: John Wiley & Sons.
280. Association, A.P.H. and A.W.W. Association, Standard methods for the examination of water and wastewater. 1989: American public health association.
281. Ge, Z., J. Li, L. Xiao, Y. Tong, and Z. He, Recovery of electrical energy in microbial fuel cells: brief review. Environmental Science & Technology Letters, 2013. **1**(2): p. 137.
282. Hernández-Flores, G., H. Poggi-Varaldo, and O. Solorza-Feria, Comparison of alternative membranes to replace high cost Nafion ones in microbial fuel cells. International Journal of Hydrogen Energy, 2016. **41**(48): p. 23354.
283. Ahilan, V., M. Wilhelm, and K. Rezwani, Porous polymer derived ceramic (PDC)-montmorillonite-H3PMo12O40/SiO2 composite membranes for microbial fuel cell (MFC) application. Ceramics International, 2018. **44**(16): p. 19191.
284. Varadwaj, G.B.B., S. Rana, and K. Parida, Amine functionalized K10 montmorillonite: a solid acid–base catalyst for the Knoevenagel condensation reaction. Dalton Transactions, 2013. **42**(14): p. 5122.
285. Ng, S. and J. Plank, Interaction mechanisms between Na montmorillonite clay and MPEG-based polycarboxylate superplasticizers. Cement and concrete research, 2012. **42**(6): p. 847.
286. Vrankovic, D., K. Wissel, M. Graczyk-Zajac, and R. Riedel, Novel 3D Si/C/SiOC nanocomposites: Toward electrochemically stable lithium storage in silicon. Solid State Ionics, 2017. **302**: p. 66.

-
287. Martínez-Crespiera, S., E. Ionescu, H.-J. Kleebe, and R. Riedel, Pressureless synthesis of fully dense and crack-free SiOC bulk ceramics via photo-crosslinking and pyrolysis of a polysiloxane. *Journal of the European Ceramic Society*, 2011. **31**(5): p. 913.
288. Leenaars, A., K. Keizer, and A. Burggraaf, The preparation and characterization of alumina membranes with ultra-fine pores. *Journal of Materials Science*, 1984. **19**(4): p. 1077.
289. Colombo, P., Engineering porosity in polymer-derived ceramics. *Journal of the European Ceramic Society*, 2008. **28**(7): p. 1389.
290. Winfield, J., L.D. Chambers, J. Rossiter, and I. Ieropoulos, Comparing the short and long term stability of biodegradable, ceramic and cation exchange membranes in microbial fuel cells. *Bioresource technology*, 2013. **148**: p. 480.
291. Xu, H., S. Tao, and D. Jiang, Proton conduction in crystalline and porous covalent organic frameworks. *Nature materials*, 2016. **15**(7): p. 722.
292. Jheng, L.-C., S.L.-C. Hsu, T.-Y. Tsai, and W.J.-Y. Chang, A novel asymmetric polybenzimidazole membrane for high temperature proton exchange membrane fuel cells. *Journal of Materials Chemistry A*, 2014. **2**(12): p. 4225.
293. Prenzel, T., T. Guedes, F. Schlüter, M. Wilhelm, and K. Rezwani, Tailoring surfaces of hybrid ceramics for gas adsorption—From alkanes to CO₂. *Separation and Purification Technology*, 2014. **129**: p. 80.
294. Meera, K.M.S., R.M. Sankar, A. Murali, S.N. Jaisankar, and A.B. Mandal, Sol–gel network silica/modified montmorillonite clay hybrid nanocomposites for hydrophobic surface coatings. *Colloids and Surfaces B: Biointerfaces*, 2012. **90**: p. 204.
295. Rezaei-DashtArzhandi, M., A. Ismail, G. Bakeri, S. Hashemifard, and T. Matsuura, Effect of hydrophobic montmorillonite (MMT) on PVDF and PEI hollow fiber membranes in gas–liquid contacting process: a comparative study. *Rsc Advances*, 2015. **5**(126): p. 103811.
296. Lin, R.-Y., B.-S. Chen, G.-L. Chen, J.-Y. Wu, H.-C. Chiu, and S.-Y. Suen, Preparation of porous PMMA/Na⁺–montmorillonite cation-exchange membranes for cationic dye adsorption. *Journal of Membrane Science*, 2009. **326**(1): p. 117.
297. Wang, E., B. Li, B. Zhang, and Z. Wang, The proton conductivity of heteropoly compounds. *Transition Metal Chemistry*, 1997. **22**(1): p. 58.
298. Daiko, Y., T. Kasuga, and M. Nogami, Pore size effect on proton transfer in sol–gel porous silica glasses. *Microporous and mesoporous materials*, 2004. **69**(3): p. 149.
299. Xu, H., S. Tao, and D. Jiang, Proton conduction in crystalline and porous covalent organic frameworks. *Nature materials*, 2016. **15**(7): p. 722.
300. Li, W.-W., G.-P. Sheng, X.-W. Liu, and H.-Q. Yu, Recent advances in the separators for microbial fuel cells. *Bioresource technology*, 2011. **102**(1): p. 244.
301. Atwater, J.E. and J.R. Akse, Oxygen permeation through functionalized hydrophobic tubular ceramic membranes. *Journal of Membrane Science*, 2007. **301**(1-2): p. 76.
302. Angioni, S., L. Millia, G. Bruni, D. Ravelli, P. Mustarelli, and E. Quartarone, Novel composite polybenzimidazole-based proton exchange membranes as efficient and sustainable separators for microbial fuel cells. *Journal of Power Sources*, 2017. **348**: p. 57.
303. Jana, P.S., M. Behera, and M. Ghangrekar, Performance comparison of up-flow microbial fuel cells fabricated using proton exchange membrane and earthen cylinder. *International Journal of Hydrogen Energy*, 2010. **35**(11): p. 5681.
304. Neethu, B., G. Bhowmick, and M. Ghangrekar, Enhancement of bioelectricity generation and algal productivity in microbial carbon-capture cell using low cost coconut shell as membrane separator. *Biochemical Engineering Journal*, 2018. **133**: p. 205.

-
305. Ahilan, V., C.C. de Barros, G.D. Bhowmick, M.M. Ghangrekar, M.M. Murshed, M. Wilhelm, and K. Rezwani, Microbial fuel cell performance of graphitic carbon functionalized porous polysiloxane based ceramic membranes. *Bioelectrochemistry*, 2019. **129**: p. 259.
306. Kleebe, H.-J. and Y.D. Blum, SiOC ceramic with high excess free carbon. *Journal of the European Ceramic Society*, 2008. **28**(5): p. 1037.
307. Dobrzańska-Danikiewicz, A.D., W. Wolany, D. Łukowiec, K. Jurkiewicz, and P. Niedziałkowski, Characteristics of multiwalled carbon nanotubes-rhenium nanocomposites with varied rhenium mass fractions. *Nanomaterials and Nanotechnology*, 2017. **7**: p. 1847980417707173.
308. Zhang, J., H. Yang, G. Shen, P. Cheng, J. Zhang, and S. Guo, Reduction of graphene oxide via L-ascorbic acid. *Chemical Communications*, 2010. **46**(7): p. 1112.
309. King, A.A., B.R. Davies, N. Noorbehesht, P. Newman, T.L. Church, A.T. Harris, J.M. Razal, and A.I. Minett, A New Raman Metric for the Characterisation of Graphene oxide and its Derivatives. *Scientific reports*, 2016. **6**: p. 19491.
310. Fang, S., D. Huang, R. Lv, Y. Bai, Z.-H. Huang, J. Gu, and F. Kang, Three-dimensional reduced graphene oxide powder for efficient microwave absorption in the S-band (2–4 GHz). *Rsc Advances*, 2017. **7**(41): p. 25773.
311. Lou, Y., G. Liu, S. Liu, J. Shen, and W. Jin, A facile way to prepare ceramic-supported graphene oxide composite membrane via silane-graft modification. *Applied surface science*, 2014. **307**: p. 631.
312. Moni, P., M. Wilhelm, and K. Rezwani, The influence of carbon nanotubes and graphene oxide sheets on the morphology, porosity, surface characteristics and thermal and electrical properties of polysiloxane derived ceramics. *RSC Advances*, 2017. **7**(60): p. 37559.
313. Qian, D., E.C. Dickey, R. Andrews, and T. Rantell, Load transfer and deformation mechanisms in carbon nanotube-polystyrene composites, in *Applied Physics Letters*. 2000: Lexington. p. 2868.
314. Salvetat, J.-P., G.A.D. Briggs, J.-M. Bonard, R.R. Bacsa, A.J. Kulik, T. Stöckli, N.A. Burnham, and L. Forró, Elastic and Shear Moduli of Single-Walled Carbon Nanotube Ropes, in *Phys. Rev. Lett.* 1999. p. 944.
315. Reis, G.S.d., C.H. Sampaio, E. Lima, and M. Wilhelm, Preparation of novel adsorbents based on combinations of polysiloxanes and sewage sludge to remove pharmaceuticals from aqueous solutions, in *Colloids and Surfaces A: Physicochemical and Engineering Aspects*. 2016. p. 304.
316. Munavalli, B.B. and M.Y. Kariduraganavar, Development of novel sulfonic acid functionalized zeolites incorporated composite proton exchange membranes for fuel cell application. *Electrochimica Acta*, 2019. **296**: p. 294.
317. Naviroj, M., S. Miller, P. Colombo, and K. Faber, Directionally aligned macroporous SiOC via freeze casting of preceramic polymers. *Journal of the European Ceramic Society*, 2015. **35**(8): p. 2225.
318. Stankovich, S., D.A. Dikin, R.D. Piner, K.A. Kohlhaas, A. Kleinhammes, Y. Jia, Y. Wu, S.T. Nguyen, and R.S. Ruoff, Synthesis of graphene-based nanosheets via chemical reduction of exfoliated graphite oxide. *carbon*, 2007. **45**(7): p. 1558.
319. Karim, M.R., K. Hatakeyama, T. Matsui, H. Takehira, T. Taniguchi, M. Koinuma, Y. Matsumoto, T. Akutagawa, T. Nakamura, and S.-i. Noro, Graphene oxide nanosheet with high proton conductivity. *Journal of the American Chemical Society*, 2013. **135**(22): p. 8097.
320. Zhu, F. and K. Schulten, Water and proton conduction through carbon nanotubes as models for biological channels. *Biophysical journal*, 2003. **85**(1): p. 236.

321. Lee, K.J. and Y.H. Chu, Preparation of the graphene oxide (GO)/Nafion composite membrane for the vanadium redox flow battery (VRB) system. *Vacuum*, 2014. **107**: p. 269.
322. Mathuriya, A.S. and D. Pant, Assessment of expanded polystyrene as a separator in microbial fuel cell. *Environmental technology*, 2018: p. 1.
323. An, L., W. Xu, S. Rajagopalan, C. Wang, H. Wang, Y. Fan, L. Zhang, D. Jiang, J. Kapat, and L. Chow, Carbon-nanotube-reinforced polymer-derived ceramic composites. *Advanced Materials*, 2004. **16**(22): p. 2036.
324. Robert, T.M., D. Augustine, D. Mathew, and C.R. Nair, Graphene oxide induced fast curing of amino novolac phthalonitrile. *RSC Advances*, 2015. **5**(2): p. 1198.
325. Rahimnejad, M., G. Bakeri, G. Najafpour, M. Ghasemi, and S.-E. Oh, A review on the effect of proton exchange membranes in microbial fuel cells. *Biofuel Research Journal*, 2014. **1**(1): p. 7.
326. Rozendal, R.A., H.V.M. Hamelers, and C.J.N. Buisman, Effects of Membrane Cation Transport on pH and Microbial Fuel Cell Performance. *Environmental Science & Technology*, 2006. **40**(17): p. 5206.

Appendix

A.1 Additional Tables and figures

Table A1. Prepared membrane compositions with equal mole ratio of H44 and APTES and pyrolysed at 400 °C, 500 °C, 600 °C and 1000 °C.

Membranes	Montmorillonite M (wt %)	H ₃ PMo ₁₂ O ₄₀ /SiO ₂ PMA (wt %)
PDC	-	-
PDC:M10	10	-
PDC:M20	20	-
PDC:PMA10:M10	10	10
PDC:PMA10:M20	20	10

Table A2. Prepared membrane compositions with equal mole ratio of H44 and BisA and pyrolysed at 1100 °C

Membranes	Graphene oxide (wt %)	MWCNT (wt%)
PDC	-	-
PDC:0.5GO	0.5	-
PDC:2GO	2	-
PDC:0.5CNT	-	0.5
PDC:2CNT	-	2

Table A3. Prepared membrane compositions with equal mole ratio of H44 and APTES and pyrolysed at 1100 °C.

Membranes	TEOS (wt %)	SiO₂ (wt%)	TiO₂ (wt%)
PDC-1100	-	-	-
PDC:TEOS-1100	15	-	-
PDC:SiO ₂ -1100	-	15	-
PDC:TiO ₂ -1100	-	-	15

Table A4. Average particle size of material before pyrolysis.

Material	Particle size (µm)
PDC	5.8357
PDC:M10	3.8642
PDC:M20	3.6574
PDC:PMA10:M10	2.5328
PDC:PMA10:M20	2.2254

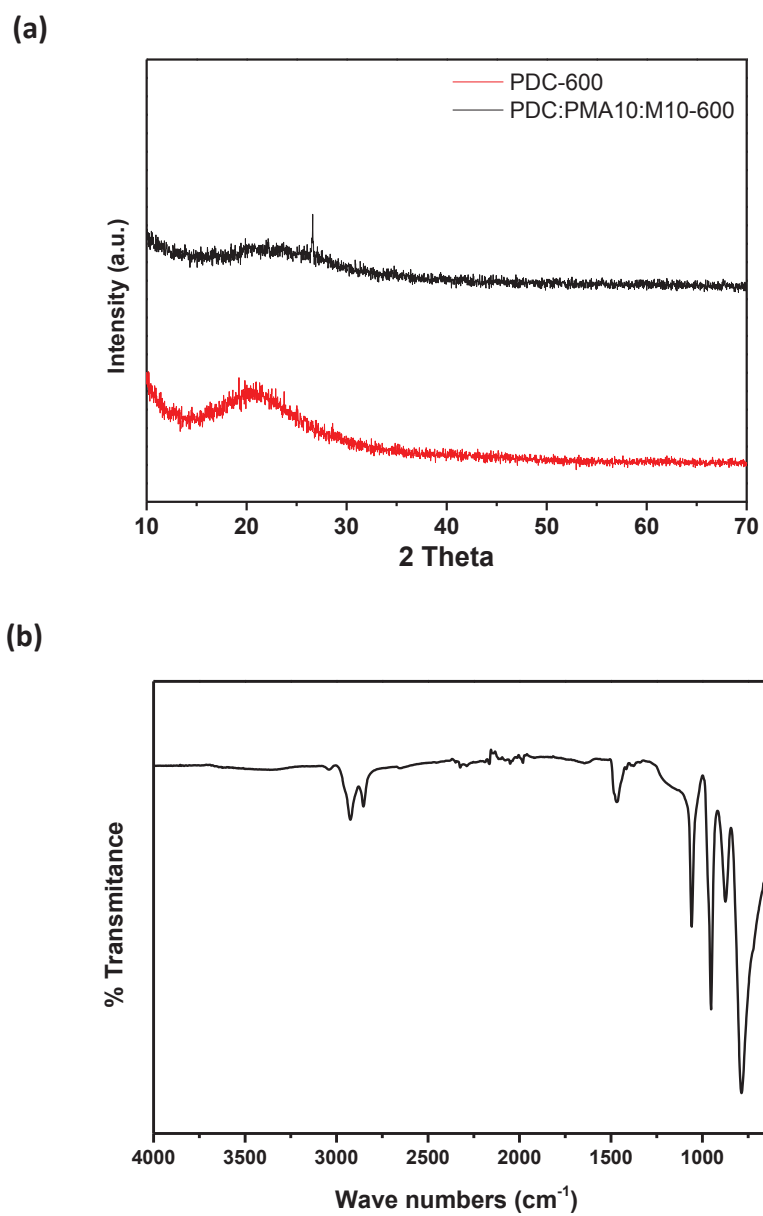


Figure A1. (a) XRD image of PDC-600 and PDC:PMA10:M10-600 membranes, (b) FTIR spectrum of $\text{H}_3\text{PMO}_{12}\text{O}_{40}/\text{SiO}_2$.

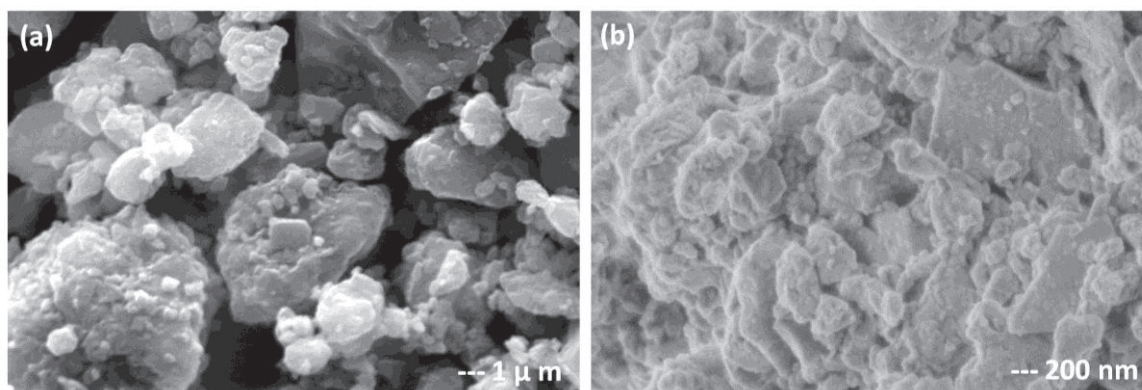


Figure A2. SEM image of PDC-1000 ceramic membrane.

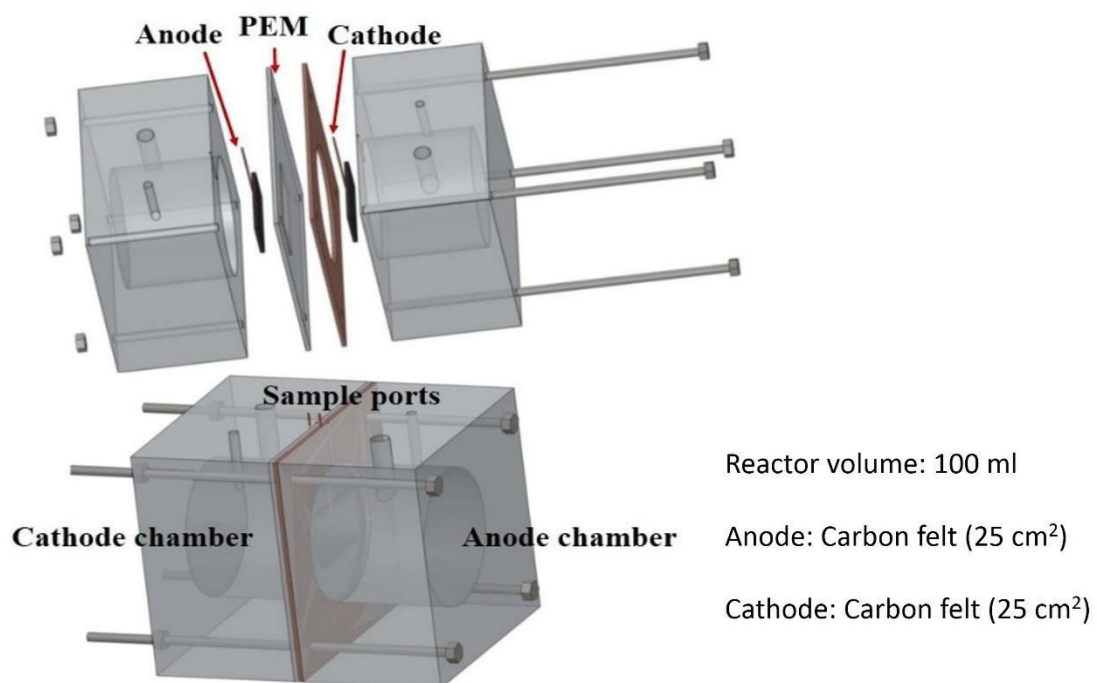


Figure A3. Schematic view of MFC reactor and parameter.

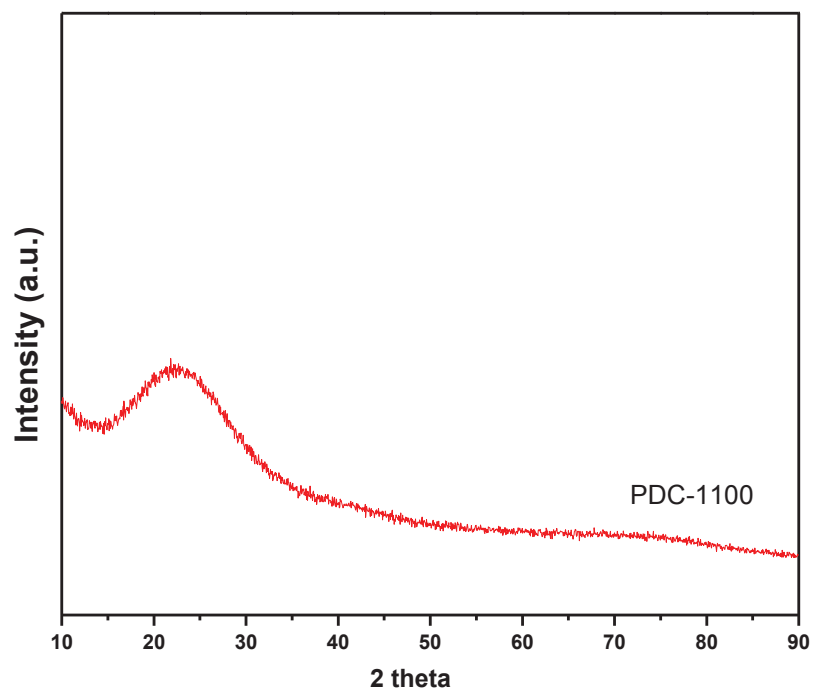


Figure A4. XRD pattern of PDC-1100 membrane.

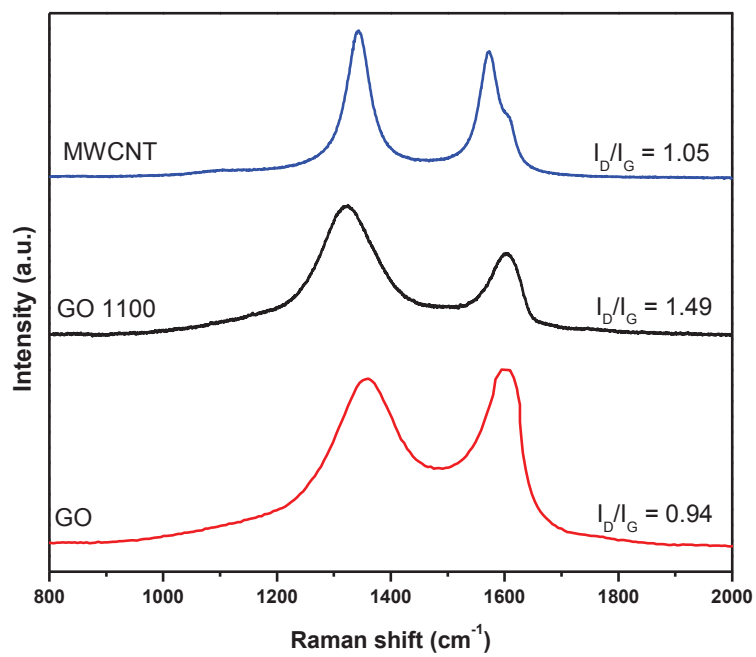


Figure A5. Raman spectroscopy of Graphene oxide and multiwall carbon nanotube.

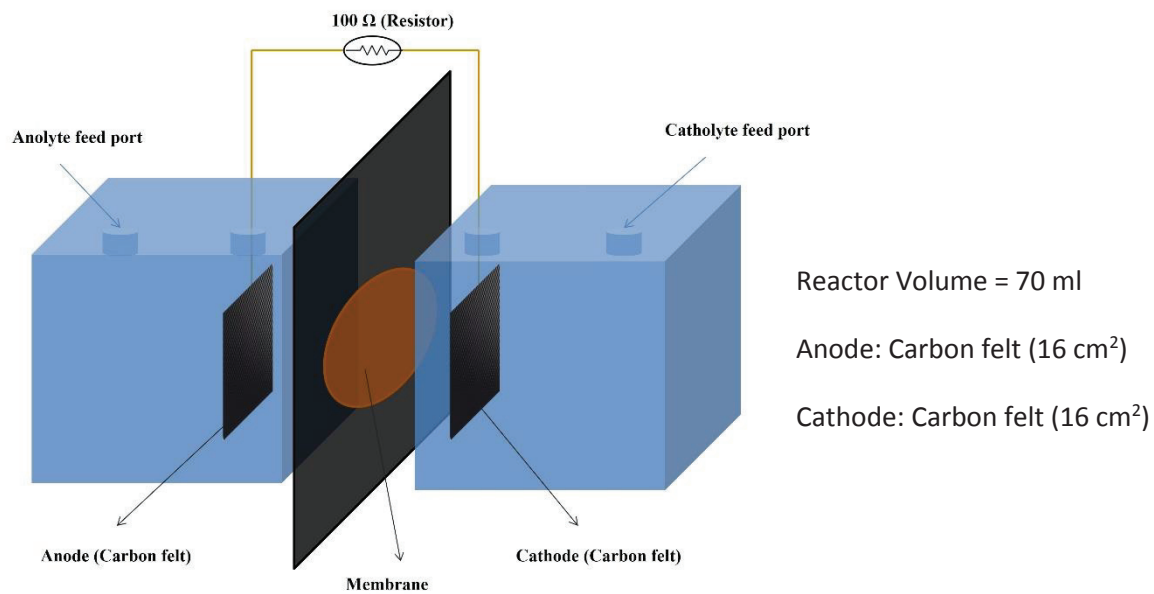


Figure A6. Scheme of MFC reactor and its parameter.

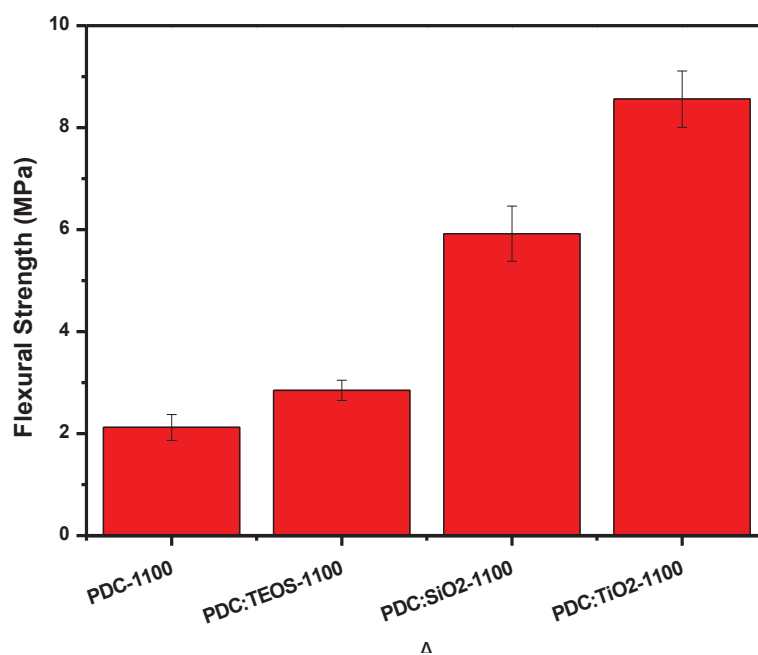


Figure A7. Flexural strength of PDC ceramic membrane.

A.2 Author contributions for the publications presented in this work**Chapter 5 published as**

Vignesh Ahilan, Michaela Wilhelm*, Kurosch Rezwan, Porous polymer derived ceramic (PDC)-montmorillonite- $\text{H}_3\text{PMo}_{12}\text{O}_{40}/\text{SiO}_2$ composite membranes for microbial fuel cell (MFC) application, *Ceramics International*, 2018 44(6): p.19191-19199. DOI: 10.1016/j.ceramint.2018.07.138

Author	Contribution
Vignesh Ahilan	Idea and planning of work, sample synthesis, samples preparation for characterizations, nitrogen adsorption/desorption measurements, XRD, FTIR, vapor adsorption measurements, data analysis and interpretation, manuscript preparation (writing and editing)
Michaela Wilhelm	Gave scientific input and conceptual advice, discussed data, edited manuscript
Kurosch Rezwan	Gave scientific input and conceptual advice, discussed data, edited manuscript

Chapter 6 published as

Vignesh Ahilan, Gourav Dhar Bhowmick, Makarand M. Ghangrekar, Michaela Wilhelm*, Kurosch Rezwan, Tailoring hydrophilic and porous nature of polysiloxane derived ceramer and ceramic membranes for enhanced bioelectricity generation in microbial fuel cell, *Ionics*, 2019, DOI:10.1007/s11581-019-03083-5

Author	Contribution
Vignesh Ahilan	Idea and planning of work, sample synthesis, samples preparation for characterizations, nitrogen adsorption/desorption measurements, XRD, FTIR, vapor adsorption measurements, data analysis and interpretation, manuscript preparation (writing and editing)
Gourav Dhar Bhowmick	MFC setup designing, polarization data measurements and analysis
Makarand M. Ghangrekar	Gave scientific input and conceptual advice, discussed data, edited manuscript
Michaela Wilhelm	Gave scientific input and conceptual advice, discussed data, edited manuscript
Kurosch Rezwan	Gave scientific input and conceptual advice, discussed data, edited manuscript

Chapter 7 published as

Vignesh Ahilan, Camila Cabral de Barros, Gourav Dhar Bhowmick, Makarand M. Ghangrekar, M. Mangir Murshed, Michaela Wilhelm*, Kurosch Rezwan, Microbial fuel cell performance of graphitic carbon functionalized porous polysiloxane based ceramic membranes, *Bioelectrochemistry*, 2019, 129: p. 259-269. DOI: 10.1016/j.bioelechem.2019.06.002

Author	Contribution
Vignesh Ahilan	Idea and planning of work, sample synthesis, samples preparation for characterizations, nitrogen adsorption/desorption measurements, XRD, FTIR, water and heptane adsorption measurements, data analysis and interpretation, manuscript preparation (writing and editing)
Camila Cabral de Barros	Sample synthesis and its characterizations
Gourav Dhar Bhowmick	MFC setup designing, polarization data measurements and analysis
Makarand M. Ghangrekar	Gave scientific input and conceptual advice, discussed data, edited manuscript
M. Mangir Murshed	Raman spectroscopy data measurement and its analysis
Michaela Wilhelm	Gave scientific input and conceptual advice, discussed data, edited manuscript
Kurosch Rezwan	Gave scientific input and conceptual advice, discussed data, edited manuscript

A.3. Supervised work of student

A.3.1 Supervised diploma/master thesis

- Luca Mazzeferro, Diploma thesis student “Polysiloxane based membrane material for microbial fuel cell-membrane bioreactor ” (03.10.2016 to 07.04.2017)
- Camila Cabral de Barros, Diploma thesis student “Graphitic carbon functionalized polymer Derived Ceramic (PDC) membranes for Microbial Fuel Cell (MFC)” (01.07.2017 to 31.12.2017)

A.4. Curriculum Vitae

Surname	Ahilan
First name	Vignesh
Date of birth	19.01.1992
Place of birth	Tamilnadu, India

Work Experience and Education

02/2016 – present	Ph.D student, Advanced Ceramics Institute, University of Bremen, Germany, Doctor Thesis: Porous polymer derived ceramic membranes for bioelectricity generation and wastewater treatment
02/2018 – 03/2018	Visiting Researcher, Indian Institute of Technology, India
03/2014 – 01/2016	M.Sc. in Energy systems Engineering, Daegu Gyeongbuk Institute of Science and Technology (DGIST), Republic of Korea, Master Thesis: Development of Air Cathode Materials for Metal-Air Batteries.
12/2014 – 01/2015	Research Intern, Waseda University Science and Engineering, Japan
08/2009 – 05/2013	B.Tech. in Chemical and Electrochemical Engineering, Central Electrochemical Research Institute, India, Bachelor Thesis: Electro dissolution of metal scrap anode for nickel removal from electroplating industrial effluent.

A. 5. List of Publications

A.5.1 Peer reviewed articles prepared within the frame work of this thesis

- **Vignesh Ahilan**, Michaela Wilhelm*, Kurosch Rezwan, Porous polymer derived ceramic (PDC)-montmorillonite- $\text{H}_3\text{PMo}_{12}\text{O}_{40}/\text{SiO}_2$ composite membranes for microbial fuel cell (MFC) application, *Ceramics International*, 2018, 44(6): p.19191-19199. DOI: 10.1016/j.ceramint.2018.07.138
- **Vignesh Ahilan**, Gourav Dhar Bhowmick, Makarand M. Ghangrekar, Michaela Wilhelm*, Kurosch Rezwan, Tailoring hydrophilic and porous nature of polysiloxane derived ceramer and ceramic membranes for enhanced bioelectricity generation in microbial fuel cell, *Ionics*, 2019, DOI:10.1007/s11581-019-03083-5
- **Vignesh Ahilan**, Camila Cabral de Barros, Gourav Dhar Bhowmick, Makarand M. Ghangrekar, M. Mangir Murshed, Michaela Wilhelm*, Kurosch Rezwan, Microbial fuel cell performance of graphitic carbon functionalized porous polysiloxane based ceramic membranes, *Bioelectrochemistry*, 2019, 129: p. 259-269. DOI: 10.1016/j.bioelechem.2019.06.002

A.5.2 Conferences contribution

- Oral Presentation: **Vignesh Ahilan**, Michaela Wilhelm, Kurosch Rezwan, Porous Ceramic Membranes for Integrated Microbial Fuel Cell-Membrane Bio Reactor (MFC-MBR), International Conference on Functional Electroceramics and Polymers (ICEP), India, 2016.
- Oral Presentation: **Vignesh Ahilan**, Gourav Dhar Bhowmik, Makarand. M. Ghangrekar, Michaela Wilhelm, Kurosch Rezwan, Porous polymer derived ceramic composite membranes for Microbial Fuel Cell (MFC), Inno-Indigo workshop, Indian Institute of Technology (Kharagpur), India, 2018.
- Oral Presentation: **Vignesh Ahilan**, Gourav Dhar Bhowmik, Makarand. M. Ghangrekar, Michaela Wilhelm, Kurosch Rezwan, A novel polymer derived ceramic composite membrane for high performance Microbial Fuel Cell (MFC), European - International Society for Microbial Electrochemistry and Technology, United Kingdom, 2018.
- Poster presentation: **Vignesh Ahilan**, Gourav Dhar Bhowmik, Makarand. M. Ghangrekar, Michaela Wilhelm, Kurosch Rezwan, Functionalized Polysiloxane

Derived Ceramic Membranes for Microbial Fuel Cell (MFC), International Society for Microbial Electrochemistry and Technology conference (ISMET), Portugal, 2017.

- Poster presentation: **Vignesh Ahilan**, Michaela Wilhelm, Kuroschi Rezwan, Porous Polymer Derived Ceramic (PDC) membrane as an Ion exchange separator for Microbial Fuel Cell (MFC) application, workshop on Ion exchange membranes for energy applications – EMEA, Germany, 2018.

A.5.3 Other publications

- M. Prabu, S. Hyun, **Vignesh Ahilan**, S. Shanmugam, Chrysanthemum flower like NiCo₂O₄ -nitrogen doped graphene oxide composite: An efficient electrocatalyst for Lithium-oxygen and Zinc-air batteries, *Chemical Communications*, 2017, 53:55.
- J. H. Park, P. Ramasamy, S. Kim, Y. K. Kim, **Vignesh Ahilan**, S. Shanmugam, J. S. Lee*, Hybrid metal-Cu₂S nanostructures as efficient co-catalysts for photocatalytic hydrogen generation, *Chemical Communication*, 2017,53:22.
- **Vignesh Ahilan**, M. Prabu, S. Shanmugam, Porous LaCo_{1-x}Ni_xO_{3-δ} Nanostructures as an Efficient Electrocatalyst for Water Oxidation and for a Zinc-air Battery, *ACS Applied Materials and Interfaces*, 2016, 2: 6019.
- S. Hyun, **Vignesh Ahilan**, H. Kim, S. Shanmugam*, The Influence of Co₃V₂O₈ Morphology on the Oxygen Evolution Reaction Activity and Stability, *Electrochemistry Communication*, 2016, 63: 44.
- S. Yuvaraj, **Vignesh Ahilan**, S. Shanmugam*, R. Kalai Selvan*, Nitrogen-doped multi-walled carbon nanotubes-MnCo₂O₄ microsphere as electrocatalyst for efficient oxygen reduction reaction, *International Journal of Hydrogen Energy* 2016,41: 15199.
- **Vignesh Ahilan**, A. S. Siddarth and B. R. Babu, Electro-dissolution of Metal Scrap Anodes for Nickel ion Removal from Metal Finishing Effluent, *Journal of Material Cycles and Waste Management*, 2015, 18: 1.
- **Vignesh Ahilan**, A. S. Siddarth, O.S. Gokul and B. R. Babu*, A Novel Approach to Methyl Orange Degradation by Fe, Zn Doped SnO₂/Ti Moving Anode, *International Journal of Environmental Science and Technology*, 2013, 11: 1669.